Compositional and lithological variation of the Platreef on the farm Nonnenwerth, northern lobe of the Bushveld Complex: Implications for the origin of Platinum-group elements (PGE) mineralization

By

Tawanda Darlington Manyeruke

Submitted in partial fulfillment of the requirements for the degree

DOCTOR OF PHILOSOPHY

In the Faculty of Natural & Agricultural Sciences

Geology Department

University of Pretoria

Pretoria

Supervisor: Prof. W.D. Maier

March 2007

Acknowledgements

I would like to thank first and foremost my supervisors Prof. W.D. Maier and Dr James Roberts for guiding me through this project. Dr. Thomas Oberthür and Dr. Frank Melcher are thanked for their help during PGM analyses in Hannover, Germany and for all the help and guidance during the review process and J. Lodziak for his enduring work on the microprobe during PGM analysis. I also thank P. Sibiya and M. Claassen (University of Pretoria) for thin section preparation, P. Gräser (University of Pretoria) for his help during microprobe analysis, M. Loubscher (University of Pretoria) for assistance with the XRF analysis, Patrice Gingras and Dany Savard (University of Quebec) for the PGE and REE analyses, and E.M. Ripley for performing S-isotope analysis.

This research was funded by the Centre for Research on Magmatic Ore Deposits (University of Pretoria). Pan Palladium and Impala Platinum Limited are thanked for providing the core material and for granting permission to publish the results. The PGM analyses were funded by the Federal Institute for Geosciences and Natural Resources, Hannover, Germany, the DAAD, and the University of Pretoria postgraduate study abroad bursary programme.

I shall always be grateful and deeply indebted to my parents, brothers Modling and Walter and the rest of the family, your strength and willpower was something I could always rely on. To my beautiful wife Trish and daughter Tinotenda Melody, thank you for bearing with me, on my every beg and call, thank you for having been there when

I had no one to turn to and giving me moral strength and support to go through each day.

However my greatest strength lies in the Lord, who has faithfully been with me throughout the project. Thank you Lord for the gift of life you have bestowed upon me.

TABLE OF CONTENTS

List of Tables

List of illustrations

with interstitial clinopyroxene (cpx), sample MO 20. (b, c and d) Orthopyroxene moderately altered to uralite along fractures, samples MO 63, MO 65 and MO 68, respectively. Note the patchy alteration to dark brown clays in plagioclase, the intercumulus nature of clinopyroxene, and the poikilitic nature of orthopyroxene and clinopyroxene. (e) Poikilitic orthopyroxene enclosing plagioclase. Clinopyroxene is interstitial and partially encloses orthopyroxene, sample MO 20. (f) Cumulus and intercumulus plagioclase intergrown with clinopyroxene that partially encloses orthopyroxene, sample MO 74. Transmitted cross polarised light.

Fig. 5.2: Norite**:** (a) Cumulus orthopyroxene (opx) intergrown with interstitial plagioclase (plag), and minor clinopyroxene (cpx), sample MO 67. (b) Orthopyroxene interstitial to plagioclase and containing anhedral inclusions of plagioclase, sample MO 19. (c) Cumulus orthopyroxene with intercumulus plagioclase and clinopyroxene. Note the small, subrounded orthopyroxene enclosed in clinopyroxene. Sample MO 18. (d) Cumulus plagioclase and orthopyroxene highly altered to amphibole and chlorite with interstitial sulphides rimmed by brown biotite, sample MO 75. Transmitted cross polarised light.

Fig. 5.3 Recrystallized gabbronorite (a and b) Recrystallized orthopyroxene (opx) and minor clinopyroxene (cpx) along deformed plagioclase grain boundaries, sample MO 70. (c and d) Recrystallized gabbronorite in contact with coarse clinopyroxene from medium to coarse grained gabbronorite, sample MO 66. Note the bent lamellae in clinopyroxene and plagioclase. (e and f) Recrystallized orthopyroxene and clinopyroxene along strained plagioclase margins and fractures, sample MO 12 and MO 70, respectively. Transmitted cross polarised light.

Fig. 5.3: Recrystallized norite**:** (g) Subrounded orthopyroxene intergrown with plagioclase and in places enclosed in plagioclase, sample MO 17. (h) Fine-grained recrystallized norite in contact with medium grained gabbronorite, sample MO 84.

Fig. 5.4. Anorthosite a) Plagioclase (plag) crystals patchily altered to dark brown clays, sample MO 8. (b and c) Plagioclase replaced by clinopyroxene (cpx) along cleavage planes and fractures. Also note the patchy alteration to dark brown clays, sample MO 68 and MO 73, respectively. (d) Clinopyroxene rimmed by orthopyroxene (opx) – plagioclase intergrowth when in contact with plagioclase, sample MO 27. Transmitted cross polarised light.

Fig. 5.5: Gabbro (a-d) Clinopyroxene with exsolved blebs and lamellae of orthopyroxene (opx) intergrown with plagioclase. Note the thin orthopyroxene corona around clinopyroxene when in contact with plagioclase in Fig. 5.4b.

Fig. 5.6: Serpentinized peridotite (a and b) Relict, partially serpentinised olivine and orthopyroxene, sample MO 26. Note the biotite flakes intergrown with serpentine in b. Transmitted cross polarised light.

Fig. 5.7 Gabbronorite (a) Deformed and recrystallized plagioclase showing 120^0 triple junctions and bent twin lamellae. Small corroded plagioclase grains are enclosed in orthopyroxene (opx), sample MO 4. (b) Interstitial clinopyroxene intergrown with cumulus plagioclase. Note the deformed twin lamellae in plagioclase; sample MO 50. (c) Orthopyroxene replacing clinopyroxene, sample MO 51. (d) Interstitial clinopyroxene and orthopyroxene intergrown with cumulus plagioclase that shows patchy alteration to dark brown clays. (e and f) Sub-poikilitic inverted pigeonite with two sets of exsolved augite lamellae, sample MO 2.

Fig. 6.1: CIPW normative compositions of Platreef samples from Nonnenwerth. gn = gabbronorite, rx = recrystallized gabbronorite, anor = anorthosite, Plag = plagioclase, Opx = orthopyroxene, Cpx = clinopyroxene, Ol =olivine. Note: Legend applies to Nonnenwerth samples only.

Fig. 6.2: Binary variation diagrams of (a and b) Al_2O_3 versus MgO, (c and d) CaO versus MgO and (e and f) Na_2O versus MgO in rocks from Nonnenwerth. Also plotted are compositional ranges of tholeiitic (B2/B3) Bushveld parental magma (Davies and Tredoux, 1985), and major rock forming minerals (shaded) in the Platreef on Nonnenwerth to determine which phases control the chemistry of the rocks. plag = plagioclase, cpx = clinopyroxene, opx = orthopyroxene, rx gn = recrystallized gabbronorite, gn = gabbronorite and mela-gn = mela-gabbronorite.

Fig. 6.2 (contd): Plot of Cr_2O_3 (m and n) versus MgO. Also plotted are major rock forming minerals (shaded). plag = plagioclase, cpx = clinopyroxene, opx = orthopyroxene, gn = gabbronorite, rx gn = recrystallized gabbronorite and mela-gn = mela-gabbronorite

Fig. 6.2 (contd): Binary variation diagrams of (g and h) SiO_2 versus MgO, (i and j) FeO versus MgO and (k and l) TiO_2 versus MgO in rocks from Nonnenwerth. Also plotted are compositional ranges of tholeiitic (B2/B3) Bushveld parental magma (Davies and Tredoux, 1985), and major rock-forming minerals (shaded) in the Platreef on Nonnenwerth. plag = plagioclase, cpx = clinopyroxene, opx = orthopyroxene, rx gn = recrystallized gabbronorite, gn = gabbronorite and mela-gn = mela-gabbronorite.

Fig. 6.3: Plot of (a and b) MgO versus depth, and Cr_2O_3 (c and d), in the Platreef at Nonnenwerth. gn = gabbronorite, rx gn = recrystallized gabbronorite and mela-gn = mela-gabbronorite

Fig. 6.4: Binary variation diagrams of (a and b) V versus MgO, (c and d) Zr vesus

(sample MOX10), (i & j) Pyrite in fractures within altered plagioclase (alt. plag). Disseminated chalcopyrite is intergrown with secondary silicates (sample MOX9 and 10, respectively). (k) Magnetite (mt) intergrown with ilmenite (ilm). Magnetite contains pyrrhotite along cleavage planes (sample MOX12). In reflected light, plane polarised light, i and j in air and g, h and k in oil.

Fig. 8.3: Photomicrographs of (a) Chalcopyrite intergrown with amphibole (am) laths along its margin, and enclosing subhedral zircon (sample MOX29). (b) Aggregate of pyrrhotite rimmed by chalcopyrite which is in turn rimmed by pyrite (sample MOX32). (c) Chalcopyrite intergrown with minor pentlandite at its margin and rimmed by pyrite. Note streaks of pyrite in adjacent altered plagioclase (Sample MOX32). (d) Pyrrhotite enclosing an intergrowth of pentlandite, pyrite and chalcopyrite. The corona around pyrrhotite consists of pyrite intergrown with minor chalcopyrite (sample MOX32). (e) Pyrrhotite enclosing vaguely round blebs of an intergrowth of pyrite and chalcopyrite. Chalcopyrite is concentrated towards the rims whereas pyrite is concentrated in the core. Pyrrhotite additionally contains flame-like exsolutions of pentlandite (sample MOX32). (f) Intergrowth of pyrrhotite (po) pyrite (py), minor chalcopyrite (cpy), and pentlandite (pn). (sample MOX27). opx = orthopyroxene. In reflected light, plane polarised light, in oil.

Fig. 8.3 continued: (g) Interstitial pentlandite intergrown with chalcopyrite. Disseminated chalcopyrite replaces adjacent altered plagioclase (alt. plag) along cleavage planes (sample MOX27). (h) Violarite (viol) rimming pentlandite and intergrown with pyrite and chalcopyrite sample (MOX29). (i) Violarite with minor relictic pentlandite is intergrown with pyrrhotite and chalcopyrite (sample MOX29). (j & k) Pyrite occurs interstitial to plagioclase and clinopyroxene (cpx) and replaces the silicates along fractures (sample MOX32). (l) Interstitial pyrite replaces clinopyroxene along cleavage planes (sample MOX 32). In reflected light, plane polarised light, in oil.

Fig. 8.4: Photomicrographs of (a) Chalcopyrite (cpy) and pyrite (py) intergrown with acicular amphibole actinolite (am) (sample P7). (b) An aggregate of intergrown anhedral magnetite (mt) and chalcopyrite in altered plagioclase (alt. plag) (sample P7). (c & d) Coarse pyrite intergrown with magnetite that encloses millerite (mil). Magnetite is also intergrown with anhedral, disseminated chalcopyrite (sample P7). (e & f) Coarse pyrite cut by veinlets of intergrown chalcopyrite and millerite (sample P7). In reflected light, in oil, (a, b & e) plane polarised light and (d & f) cross polarised light.

Fig. 8.4 continued: g & h) Chalcopyrite cut by covellite (cov) veins and rimmed by magnetite. Note minor pentlandite in h (sample P2). (i & j) Patches of violarite intergrown with pentlandite, minor chalcopyrite, covellite and cut by magnetite veinlets (sample P2). (k & l) Intergrowth of orthopyroxene (opx) and ilmenite, as well as granular, subhedral and anhedral ilmenite (ilm), orthopyroxene (opx) and minor anhedral hematite (hem) (sample P4). (m & n) Pentlandite and

chalcopyrite show extensive alteration to covellite and magnetite along irregular fractures (sample P2). In reflected light, plane polarised light except l, in oil.

Fig. 8.5: Photomicrographs of (a) Plagioclase (plag) containing vermicular network of pyrite. Pyrite also forms coronas around chalcopyrite (sample P19). (b) Skeletal pyrite and pyrite replacing plagioclase along cleavage planes (sample P19). (c) Pyrite cut by pentlandite-rich veins. Also note fine disseminated chalcopyrite in pyrite (sample P19). (d) Pentlandite replacing plagioclase along cleavage planes. Matrix is pyrrhotite with disseminated fine chalcopyrite (sample P19). (e) Pyrite enclosing millerite. Note fine disseminated chalcopyrite intergrown with pyrite (sample P15). (f & g) Millerite replacing chalcopyrite along fractures. Minor pyrite (py) grains occur at the contact between chalcopyrite and millerite, or are enclosed in millerite (sample P14). (h) Magnetite (mt) is intergrown with chalcopyrite, with minor chalcopyrite being remobilised into adjacent silicates (sample P11). In reflected light, cross polarised light, in oil.

Fig. 8.5 continued: (i) Anhedral chalcopyrite intergrown with anhedral pyrite (sample P11). (j) Massive, twinned, subhedral millerite (mil) intergrown with interstitial chalcopyrite (cpy) (sample P106). (k) Anhedral, twinned chalcopyrite intergrown with, and enclosing, vaguely round millerite (sample P106). (l & m) Fragmented pyrite intergrown with millerite and chalcopyrite (sample P15). (n) Subhedral magnetite with ilmenite lamellae (sample P15). (o & p) Radiating, skeletal ilmenite vaguely round chromite (cr) and enclosing an intergrowth of chalcopyrite and millerite (sample P15). In reflected light, plane polarised light (except i, l, n and o), in oil.

Fig. 8.6:Variation of a) Pd, b), Se with depth in pentlandite, and Se versus Pd. MP = Middle Platreef (from Townlands), anor = anorthosite, rx gn = recrystallized gabbronorite (both from Nonnenwerth).

Fig. 8.7a: Cr # versus Fe # of the analysed Cr-bearing spinels from serpentinised peridotite (MO 26) and from melagabbronorites (MO 27).

Fig. 8.8. fO2 vs fS2 (a) diagrams for the Fe-S-O system at 1270C, after Holland (1959). (b) fO2 vs fS2 diagram for the Fe-Ni-S-O system at about 1270C. Reaction boundaries for the Fe-S-O sub-system are shown as solid lines; others for which thermodynamic data are unavailable or unreliable are shown in dashed lines. (c) Approximate fO2 vs fS2 diagram for the Fe-Ni-S-O system under conditions of common hypogene equilibrium in altered ultramafic rocks, probably less than 2000C. Assemblages noted in the Platreef on Townlands are shown by circled numbers on the appropriate field of the boundary. Assemblage 1 is composed of pyrrhotite, chalcopyrite, pentlandite ± magnetite, assemblage 2 is characterized by pyrite, pentlandite, chalcopyrite and minor pyrrhotite and assemblage 3 is characterized by pyrite, millerite, chalcopyrite ± pentlandite ± galena, molybdenite and magnetite. Figures modified after Eckstrand (1975).

Fig. 9.1: Back-scattered electron images showing various textures and associations of PGM and gold. Rectangle (where present) represents area enlarged in the image to the immediate right. (a) PGM (in rectangle) enclosed in plagioclase (plag) that has been altered to amphibole (am), in the vicinity of chalcopyrite (cpy). The other highly reflective phase at the top of the image is Pb derived from polishing. Sample MOX9. (b) Enlarged rectangle from a). Anhedral moncheite (mon) is associated with disseminated anhedral kotulskite (kot) in amphibole (black). Sample MOX9. (c) Kotulskite and moncheite enclosed in altered portions of plagioclase. Moncheite is in contact with pyrite. orth = orthoclase, alb = albite. Sample MOX9. (d) Euhedral to subhedral kotulskite and moncheite. Altered plagioclase is shown in black. Sample MOX9. (e) Composite grain of pyrrhotite (po), pentlandite (pn) and chalcopyrite, with PGM (in rectangle) situated in the periphery of the grain. Sample MOX10. (f) Enlarged rectangle from e). Subhedral to anhedral moncheite and associated kotulskite occur included in altered plagioclase (black background). Sample MOX10. (g) A composite grain of kotulskite, gold (Au) and sperrylite in altered plagioclase (black background). Sample MOX9

Fig. 9.1 continued: Back-scattered electron images showing various textures and associations of PGM and gold. Rectangle (where present) represents area enlarged for image to the immediate right. (h) Chalcopyrite and PGM associated with quartz (qtz) and chlorite (chl), interstitial to plagioclase. Anhedral moncheite is highlighted by rectangle. The other PGM are subhedral kotulskites (kot) Sample MOX9. (i) Enlargement of rectangle from h). Anhedral moncheite is enclosed in chlorite (black background). Sample MOX9. (j) Subhedral moncheite forming a trail from the margin of chalcopyrite (cpy) into adjacent quartz and amphibole (after plagioclase). Sample MOX9. (k) Enlargement of rectangle from j. (l) Intergrown pyrrhotite and pentlandite, with braggite (in rectangle) occurring near margin of sulphide. Sample MOX10. (m) Enlargement of rectangle from l). Zoned subhedral grain of braggite. Increase in brightness corresponds to increase in Pt content. The numbers correspond to analyses e.g. 11 represents 11_MOX10 in Table 6 (Sample MOX10). (n) Grain of gold (Au) (in rectangle) located near fracture in orthopyroxene (opx). Sample MOX12. (o) Enlargement of rectangle from n). Subhedral grain of gold is partly corroded. Sample MOX12. (p) Gold (in rectangle) located at the contact between quartz (qtz) and chalcopyrite (cpy). Sample MOX9. (q) Enlargement of rectangle in p). Sample MOX9.

Fig. 9.2: Mineral chemistry of (Pt,Pd)-bismuthotellurides from Nonnenwerth and Townlands. a) Pd-dominated (Pt,Pd)-bismuthotellurides in the triangular plot (Pt+Pd)- (Bi+Sb)-Te (at. %). b) Pt-dominated (Pt,Pd)-bismuthotellurides in the triangular plot (Pd+Pt)-(Bi+Sb)-Te (at. %). c) (Pt,Pd)-bismuthotellurides in the triangular plot (Bi+Te+Sb)-Pt-Pd (at. %).

Fig. 9.3: Mineral chemistry of braggite from Nonnenwerth (sample MOX10).

Fig. 9.4: Back-scattered electron images showing various textures and associations of

PGM. (a) Merenskyite (mer) enclosed in pyrrhotite (po) and occurring as thin lamellae in chalcopyrite. Note also calcite enclosed in chalcopyrite. Sample MOX29. (b) Merenskyite lamellae in chalcopyrite. Sample MOX29. (c) Merenskyite (in rectangle) intergrown with amphibole, quartz and chalcopyrite within plagioclase. Sample MOX29. (d) Enlargement of rectangle in c). Subhedral merenskyite grains in amphibole and quartz after plagioclase. Sample MOX29. (e) Merenskyite (in rectangle) enclosed in chalcopyrite that is intergrown with acicular amphiboles (actinolite). Chalcopyrite also encloses subhedral zircons (zr). Sample MOX29. (f) Enlargement of rectangle in e). Subhedral merenskyite enclosed in chalcopyrite. Sample MOX29. (g) PGM (in rectangle) in amphibole peripheral to a composite grain of chalcopyrite, pyrrhotite and pentlandite. Sample MOX27. (h) Enlargement of rectangle in g) Anhedral moncheite and merenskyite in amphibole. Sample MOX27. (i) Back scattered electron image of kotulskite enclosed in chalcopyrite, close to a fracture. Sample MOX29.

Fig. 9.5: Back-scattered electron images of isomertieite and its textural setting. Isomertieite (iso) enclosed in chalcopyrite, near contact with pyrite. Sample P7. (b) Enlargement of isomertieite shown in a). Sample P7.

Fig. 9.6: Back-scattered electron images showing various textures and associations of PGM. Rectangle (where present) represents area enlarged for image to the immediate right. (a) PGM (in rectangle) enclosed in chalcopyrite (cpy) adjacent to the margin of the sulphide. Magnetite (mt) is also enriched in the border zone of the sulphide. po = pyrrhotite, pn = pentlandite, opx = orthopyroxene. Sample P13. (b) Enlargement of rectangle in a). Subrounded michenerite (mich) intergrown with merenskyite (mer). Sample P13. (c) Subrounded merenskyite enclosed in millerite. Sample P106. (d) A subrounded and an elongate merenskyite grain are enclosed in pyrite (py), associated with a fracture. Sample P15. (e) PGM (in rectangle) enclosed in pyrite along internal cracks. The PGM are associated with amphibole (am) that is intergrown with pyrite, also along cracks. Sample P15. (f) Enlargement of rectangle in e). Anhedral merenskyite intergrown with hessite (hes). Sample P15. (g) Kotulskite (kot) (in rectangle) enclosed in millerite (mil). Note chalcopyrite that is interstitial to millerite. Sample P106. (h) Enlargement of rectangle in g). Subrounded kotulskite enclosed in millerite. Sample P106.

Fig. 9.6 continued: Back scattered electron images showing various textures and associations of PGM and Bi-,Te- phases. Rectangle (where present) represents area enlarged for image to the immediate right. (i) Sperrylite (sp) (in rectangle) located at the contact between pyrrhotite and orthopyroxene (opx). Pyrrhotite is intergrown with pentlandite and also contains minor flame-like exsolutions of pentlandite. Sample P13. (j) Enlargement of rectangle in c). Subhedral sperrylite and smaller anhedral sperrylite at the contact between pyrrhotite and orthopyroxene. Sample P13. (k) Pyrite enclosing intergrowths of tetradymite-type (tet) minerals and chalcopyrite. Sample P15. (l) Pyrite enclosing a composite grain of chalcopyrite, pyrrhotite, pilsenite (pil), Fe-emplectite? (Fe-emp?) and the

unnamed phase UN 1133 with a calculated chemical formula [Bi_4Te_2Se]. Sample P15. (m) Altaite (alt) grains (in rectangle) are enclosed in secondary amphibole adjacent to pyrrhotite showing rims of magnetite. Sample P13. (n) Enlargement of rectangle in m). One grain of altaite is intergrown with galena (gal). Sample P13. (o) Gold (Au) grains (in rectangle) enclosed in pyrite or located near the contact between pyrite and enclosed chalcopyrite. Sample P106. (p) Enlargement of rectangle in o). Anhedral gold grains in pyrite. Sample P106.

Fig. 10.1: Regional geological map of the northern limb with results of S isotope analyses superimposed. Data from Townlands are from Manyeruke *et al*. (2005), data from Macalakaskop, Rietfontein and Turfspruit are from Sharman-Harris *et al*. (2005), data from Tweefontein are from Buchannan *et al*. (1981), data from Rooipoort are from Maier *et al*. (2007), data from Uitloop are from Tuovila (in preparation), data from Overysel are from Holwell *et al*. (2005) and data from Zwartfontein are from Liebenberg (1968). (Map modified after Ashwal *et al*., 2005).

Fig. 10.2: $d^{34}S$ values of sulphidic rocks and sulphides in selected mafic/ultramafic intrusions (modified from Ripley, 1999). Kabanga and Kunene data are from Maier (unpublished), Uitloop data are from Touvila, (personal communication) and Townlands data are from Manyeruke (2003).

ABSTRACT

The present study documents the nature of the Platreef on the farm Nonnenwerth, northern Bushveld Complex and compares the lithologies and composition of the mineralized interval to those on the farm Townlands. The Platreef on Townlands was the subject of a previous study (Manyeruke 2003, MSc thesis, University of Pretoria), but in the course of the present investigation, additional data were collected. Nonnenwerth is located more than 70 km to the north of the well characterized occurrences of the Platreef at Sandsloot, Overysel and Drenthe. At Nonnenwerth, the Platreef rests on Archaean granite gneiss floor rocks whereas at Townlands, the Platreef rests on pelitic rocks of the Transvaal Supergroup.

At Nonnenwerth, the basal rocks of the Bushveld Complex may be sub-divided into two lithologically and compositionally distinct units. At the base is a relatively heterogeneous sequence of gabbronorite with minor amounts of norite, anorthosite and igneous ultramafic rocks containing several calc-silicate xenoliths. It is some 110 m thick and is enriched in Platinum-group element (PGE)-Cu-Ni bearing sulphides (<ca. 3 modal %). Layering is mostly weekly defined and discontinuous. The mineralized interval is overlain by the Main Zone that is made up of some 170 m of relatively homogenous gabbronorite, containing several large dolomite xenoliths. The two units are separated by an up to 25m thick dolomite xenolith. In many aspects, the composition of the Platreef and the Main Zone broadly overlap ($Mg\#_{opx}$ 57 – 72, An_{plag} 40 – 75, $MgO_{whole\ rock}$

7 – 15 wt. %, similar incompatible trace element patterns). However, the Platreef has distinctly higher Cr contents ($Cr_{whole\ rock}$ up to 1813 ppm as opposed to 280 ppm in the Main Zone) as well as concentrations of chalcophile elements (Ni, Cu, PGE) and sulphur.

The Platreef and the Main Zone have relatively unfractionated REE patterns with Ce/Sm between 5.7 and 10.6 (averaging 8). This suggests that the Platreef on Nonnenwerth is genetically related to Bushveld tholeiitic magma (B2/B3 of Sharpe, 1981). In contrast, Platreef rocks on the farm Townlands, south of Mokopane, are more primitive in terms of mineral and whole rock composition (Mg# opx 77, An plag 68, presence of olivine) and have higher and more fractionated REE contents (Ce/Sm 8 – 14.2, averaging 11.6). They show certain similarities to Upper Critical Zone cumulates and appear to have crystallised either from B1 – B2 hybrid magmas, or from B2 magma contaminated with crust upon emplacement. This implies that Platreef PGE mineralization cannot be correlated with specific stratigraphic units or magma types, but that it formed in response to several different processes.

Platinum-group element (PGE) contents of Platreef samples from Nonnenwerth reach 10 ppm, whereas PGE contents in the Platreef at Townlands reach 4.4 ppm. PGE distribution patterns at Nonnenwerth are more fractionated than at Townlands, with Pd/Ir mostly >>100 at Nonnenwerth compared to < 100 at Townlands. At both localities, there is a broad positive correlation between the

concentrations of those PGE that could behave in a mobile manner (in particular Pd, Hsu *et al*. 1991) and those that are believed to be immobile under most conditions (e.g., Pt and Ir) and between individual PGE and S (for samples with > 0.1 % S), suggesting that sulphides were the primary PGE collector. At Nonnenwerth, this model is supported by a typical magmatic sulphide assemblage composed mostly of pyrrhotite, chalcopyrite and pentlandite and the close spatial relationship between platinum-group minerals (PGM) and base metal sulphides. However, at Townlands, the presence of pyrite and millerite attests to some secondary mobility of sulphur due to assimilation of floor rock shale.

Pd, Pt and Rh are below the detection limits of the electron microprobe in the sulphides analysed from Nonnenwerth and Townlands except for pentlandite from Nonnenwerth which hosts Pd in solid solution. Pd in pentlandites from Nonnenwerth constantly contain appreciable amounts of Pd (range from ~ 140 – 700 ppm). This finding is in accordance with literature data (e.g. Gervilla et al., 2004) that pentlandite may carry even up to some % of Pd (substituting for Ni) in its crystal lattice. Accordingly, the Pd contents in Nonnenwerth pentlandite probably reflect a primary magmatic signature. The lack of measurable Pd contents in pentlandite on Townlands may be due to (ii) mobilization of Pd-bearing PGM during replacement of 'primary' sulphides by pyrite dominated assemblages into the surrounding silicates (Prichard *et al*., 2001), (iii) syn- to

post-magmatic modification of the 'primary' sulphides or (iii) the results may not be representative as Pd in pentlandite was analysed in one sample only.

The platinum-group minerals (PGM) on Nonnenwerth are dominated by Pd-rich followed by Pt-rich bismuthotellurides and rare braggite and sperrylite. In contrast, mineral proportions of the PGM on Townlands are dominated by Pd-rich bismuthotellurides, minor sperrylite, rare stibiopalladinite and isomertieite. One obvious difference, however, is the wide compositional range of Pt-Pd bismuthotellurides and the presence of Pt-rich bismuthotellurides at Nonnenwerth only, whereas at Townlands, only Pd-rich bismuthotellurides are present. The significance of this finding cannot be evaluated conclusively. The variability may be related to local factors like different host rocks; footwall lithologies, down-temperature re-equilibration, activity of fluids, and other possible causes. The PGM at Nonnenwerth occur predominantly at the contact between sulphide (mostly chalcopyrite, minor pyrrhotite and rare pyrite) and secondary silicate (mostly chlorite and albite after plagioclase) or enclosed in sulphides. Importantly, Pd-rich PGM (Pd-bismuthotellurides) are mostly enclosed in silicates. However, even these PGM enclosed in silicates retain a strong spatial relationship with the base metal sulphides, mostly chalcopyrite, and are associated with secondary minerals (mostly chlorite and albite which replace plagioclase, or rarely amphibole which replaces orthopyroxene and base metal sulphides). The above observation may result from dissolution of the base metal sulphides hosting Pd, and leaving isolated insoluble Pd-PGM behind (Barnes *et*

al., 2007), or Pd may have been remobilized from the sulphides into the surrounding silicates. Based on textural evidence, the latter model is preferred. In contrast, on Townlands the PGM occur predominantly enclosed in sulphides (mostly pyrite and minor chalcopyrite and millerite), or locally at the contact between sulphide and secondary silicate (amphibole after orthopyroxene).

Sulphur isotopic ratios on Nonnenwerth range from $d^{34}S$ 0 to +2 ‰ suggesting that the sulphur in the Platreef is of mantle origin or that any S that may have been assimilated from the floor rocks was unfractionated. A similar value of $d^{34}S$ has been found by previous workers in the Platreef at Overysel which is equally located above granite gneiss. As both the basement granite and the Transvaal dolomites contain little sulphides, these results suggest that most of the S in the Platreef is of primary magmatic derivation. In contrast, Townlands sulphides have $d^{34}S$ between +4 and +8 ‰ suggesting addition of crustal sulphur. These data indicate that the formation of the PGE mineralisation in the Platreef was not controlled by assimilation of external sulphur. Instead, sulphide saturation may have been reached due to assimilation of dolomite, and/or due to differentiation and cooling of the magma upon emplacement. Subsequently, assimilation of S may have merely modified already existing sulphide melt particularly in areas where the floor rocks consisted of sulphidic shales e.g. at Townlands.

The study therefore indicates i) that contact-style PGE mineralization extends along most of the strike length of the northern lobe of the Bushveld Complex

despite variable floor rocks of different composition underlying the northern Bushveld Complex from south to north, ii) that contact-style PGE mineralization in the northern lobe of the Bushveld Complex cannot be correlated with specific stratigraphic units i.e. the Upper Critical Zone that hosts the Merensky Reef and the UG2 Reef or magma types, but that it formed due to several different processes, iii) that base metal sulphides were the primary PGE collector, iv) that Pd and Pt occur mostly as PGM with close spatial relationship with base metal sulphides. At Nonnenwerth, Pd additionally occur dissolved in pentlandite, v) that they was minimal S assimilation from floor rocks at Nonnenwerth compared to localities further south i.e. at Townlands, and vi) a dominant Bushveld B2/B3 magma source/lineage for the Platreef at Nonnenwerth.

CHAPTER ONE: INTRODUCTION

1.1 Statement of the problem

The Platreef represents the most important platinum-group element (PGE) mineralisation associated with the basal contact of the Bushveld Complex. It is still in its early stages of exploitation, with only two Anglo Platinum mines presently operating, namely Potgietersrust Platinums on the farms Sandsloot and Zwartfontein South. However, unpublished company reports indicate that the PGE mineralization extends along most of the strike of the northern limb, from Rooipoort in the south (www.caledoniamining.com) to Aurora and Nonnenwerth in the north (www.Pan Palladium).

Despite an enhanced exploration activity during the last decade, the genesis of the mineralisation in the Platreef remains enigmatic. Past workers have proposed that the sulphides formed in response to assimilation of the floor rocks by the magma (e.g. Buchanan *et al.*, 1981; Gain and Mostert, 1982; Buchanan and Rouse, 1984; Buchanan, 1988), a model that has been applied to the formation of many other examples of similar magmatic sulphide deposits elsewhere e.g. East Bull Lake (Peck *et al.*, 2002) and Portimo (Alapieti and Lahtinen, 2002). However, the Platreef overlies a variety of floor rocks, including quartzite, shale, iron formation, dolomite, and granite-gneiss. It is unclear which of these lithologies, if any, played an important role in magma contamination and sulphide saturation. For example, De Waal (1977) proposed that devolatization of dolomite may increase the O fugacity of the magma,

thereby decreasing the activity of Fe^{2+} and the sulphur solubility. Alternatively, sulphide segregation could have been triggered by assimilation of sulphur from the floor rocks, notably shales of the Timeball Hill and Duitschland formations which have been shown to contain up to several percent sulphides (Kinnaird, 2005). Lee (1996) proposed that the Platreef sulphides segregated in a staging chamber at depth followed by entrainment by the ascending silicate magma, and that *in situ* addition of sulphur merely modified the composition of the rocks. One of the reasons for the lack of consensus on a genetic model is the scarcity of compositional studies on the Platreef. Much of the exploration data is confined to a few elements (e.g. Pt, Pd, Ni, Cu) and few complete whole rock compositional analyses, including major elements, sulphur and PGE exist. The present study aims to improve this situation by conducting a detailed compositional study of two Platreef intersections that overlie granite gneiss in the northernmost portion of the northern limb of the Bushveld Complex. The data will be compared with the results of a previous study of the Platreef on the farm Townlands, in the southern part of the northern limb (Manyeruke, 2003) and at other localities, including Drenthe (Stevens, 2004) and Rooipoort (Maier *et al.*, 2007).

1.2 Aims of the study

The present study has two main aims. Firstly, I want to enlarge the database on the Platreef by providing

i) a detailed lithological and petrographic description of the Platreef on the farm Nonnenwerth 421 LR (see Fig. 2.3 and 3.1 for location),

ii) mineral compositional data, focusing on the major silicate minerals

(orthopyroxene, clinopyroxene, plagioclase) and the sulphides minerals. Some data on olivine from a serpentinized ultramafic rocks as well as micas and oxides will also be discussed,

iii) comprehensive major and trace element data, including the concentrations of the noble metals,

iii) additional lithophile trace element data from Townlands, in the south of the northern limb, to complement the study of Manyeruke (2003),

iv) a detailed mineralogical investigation of the platinum-group minerals (PGMs) on Townlands and Nonnenwerth 421 LR and a comparison of these data to published PGM data on the Platreef.

v) S- and O- isotopic data of the Platreef on Nonnenwerth 421 LR

Secondly, I will to use the lithophile trace element data to constrain the nature of the magma from which the Platreef crystallized S- and O-isotope data to evaluate the role of floor contamination in triggering sulfide segregation from the magma. In particular, I hope that a comparison of data from different localities, comprising deposits that overlie various types of floor rocks, allows determination of the relative importance of these floor rocks in triggering sulphide saturation. The mineralogical investigation of PGMs will Finally, I aim to place the Platreef mineralization into the broad lithostratigraphic framework of the Bushveld Complex.

1.3 Previous work

The occurrence of platinum in the northern limb of the Bushveld was first reported by a prospector named Adolf Erasmus in 1923. Erasmus panned ground from termite

mound on the farms Welgevonden and Rietfontein, 31 km southwest of Potgietersrus (White, 1994). The Pt was derived from mineralized quartz veins within the Rooiberg rhyolites. This was followed by the discovery of platinum by Dr. Hans Merensky on the farms Rietfontein and Tweefontein in January 1925 (White, 1994) which marks the beginning of the exploration history on the Platreef. Mining of the Platreef began in 1926 by Potgietersrus Platinums Limited. The first lithological descriptions of the Platreef were provided by Wagner (1929). He correlated the variably sulphide mineralized, composite rocks at the base of the northern limb of the Bushveld Complex with the Merensky Reef. Based on texture and mineral mode, Wagner distinguished three distinct mineralized layers, which Buchanan (1979) later referred to as the A, B and C reefs, from the base to the top (see section 2.2).

Several studies of the Platreef have emphasized the abundance of xenoliths of metasediments in the intrusive rocks. Buchanan *et al.* (1981) proposed that the Platreef mineralisation on Tweefontein formed as a result of assimilation of sulphur from anhydrite-bearing Malmani dolomite, banded ironstone, argillaceous sediments, and micronoritic sills by Bushveld magma. Buchanan *et al.* (1981) model is based partly on S isotopic studies of Platreef sulphides. In contrast, de Waal (1977) and Gain and Mostert (1982), prefer a mechanism whereby the Bushveld magma was oxidized in response to devolatization of the dolomite. The devolatization released CO_2 into the magma thereby increasing the O fugacity of the magma and, in response, decreasing the sulphur solubility and triggering sulphide supersaturation.

Regional trends in the platinum-group mineralogy of the Platreef where investigated

by Kinloch (1982). The author reported that on the farm Zwartfontein the main PGM in the Platreef are platinum-palladium tellurides, sperrylite ($PtAs_2$), platinum- palladium sulphides and palladium alloys. Compared to the Merensky reef and the UG-2 chromitite, the Platreef was shown to be relatively depleted in laurite (RuS_2). Laurite is mostly found in significant amounts in the chromitites-rich Bushveld ores, namely the thin chromitites stringers at the top and base of the Merensky Reef and throughout the UG2 chromitite layer (Kinloch, 1982). Kinloch (1982) attributed the paucity of laurite in the Platreef to the absence or scarcity of chromitites lenses. Alternatively, the Platreef's special emplacement conditions into dolomite of the Transvaal sequence may have played a part. Kinloch (1982) suggested that metamorphism of the dolomite floor rocks due to intrusion of hot Platreef magma released CO_2 from dolomite xenoliths into the Platreef magma resulting in volatization of Ru.

Cawthorn *et al.* (1985) presented major element, trace element and Sr isotope data of the Platreef on the farm Overysel showing a strong, but highly variable crustal component. At this locality, the immediate floor rocks to the Platreef consist of a suite of highly metamorphosed, banded tonalitic gneisses with leucotonalitic veins, which in turn are underlain by basement granite. Through isotope and trace element modeling, Cawthorn *et al.* (op.cit.) suggested that the most likely contaminant of the Platreef magma was a fluid derived from the granite.

White (1994) provided a description of the Platreef at several localities. He reported that the PGE grades in the Platreef are controlled by the nature of the floor rocks. Grades are relatively higher where the floor rocks consist of dolomite, but lower

where the floor rocks consist of granite, iron-formation or shale.

In situ formation of the Platreef sulphides was rejected by Lee (1996) who instead proposed that the sulphides segregated in a staging chamber at depth and were subsequently entrained by the ascending Platreef magma. *In situ* addition of S merely modified the composition of the rocks.

Viljoen and Schurmann (1998) produced a comprehensive review of the available data on the Platreef, including information on the geology, the mineralogy and theories of ore genesis.

Harris and Chaumba (2001) conducted a detailed major and trace element investigation as well as H and O isotopic study of the Platreef at Sandsloot. They found evidence for local contamination of Bushveld magma by dolomite, but in addition they suggest that contamination occurred in a staging chamber.

Armitage *et al.* (2002) studied the PGE mineralisation in the Platreef at Potgietersrust Platinums mine, Sandsloot pit, and provided some data on PGE and Au concentrations, and the nature of the PGM. Notably, at this locality, disseminated and vein-type PGE mineralisation is found up to several meters within the sedimentary floor rocks, below the basal contact of the intrusion. Based on scanning electron microscope (SEM) studies of four polished samples, Armitage *et al*. (2002) report the complete absence of PGE sulphides, but the existence of low-temperature semi-metallides and alloys and their high-temperature equivalents. Armitage *et al*. (2002)

also report that PGE ratios in the intrusion and its footwall are broadly similar pointing to similar processes controlling the final PGE distribution in the two packages. They go on to suggest that the PGE were initially concentrated by magmatic sulphides, but were subsequently remobilized by hydrothermal fluids.

Manyeruke (2003) and Manyeruke et al. (2005) conducted a detailed petrographic and geochemical investigation of a borehole core intersection through the Platreef on the farm Townlands. At this locality, the Platreef rests on metasedimentary rocks of the Silverton Formation of the Transvaal Supergroup, and is comprised of three medium-grained units of gabbronorite/feldspathic pyroxenite that are separated by hornfels interlayers. Manyeruke (2003) and Manyeruke et al. (2005) refer to the three platiniferous layers as the Lower, Middle and Upper Platreef. The Middle Platreef is the main mineralized layer, with total PGE contents up to 4 ppm. The Lower and Upper Platreefs are less well mineralized (up to 1.5 ppm). Trace element and S-isotope data show compositional breaks between the different platiniferous layers suggesting that they represent distinct sill-like intrusions of pyroxene and sulphide enriched crystal mushes. Their study also reveals a reversed differentiation trend of more primitive rocks towards the top of the succession, a pattern interpreted to reflect enhanced crustal contamination of the lower Platreef layers. All three Platreef layers are enriched in heavy S ($d^{34}S$ of 2.6 to 9.1 ‰) indicating addition of crustal sulphur, and they have elevated K, Ca, Zr and Y contents and high Zr/Y ratio relative to Critical Zone rocks from elsewhere in the Bushveld Complex, suggesting a model of crustal contamination in ore formation.

McDonald *et al.* (2005) suggested that the Platreef is related to the mixing of Main

Zone magma with differentiates of Lower Zone magma. They highlight that the Platreef has relatively low Pt/Pd and Pt/Au ratios compared to the Merensky Reef. They propose that the low Pt/Pd ratios are an inherent feature of the Platreef magma and that the Platreef and the Merensky Reef are not correlatable.

Ruiz *et al.* (2004) investigated the Re-Os isotopic composition of Platreef sulphides in three samples from a borehole located on the farm Turfspruit 241KR. This was done to constrain the age of the mineralisation and the source of osmium in the sulphides, and by inference, the origin of the PGE mineralisation. Ruiz *et al.* (2004) reported a Re-Os age of 2011 ± 50 Ma and an initial $^{187}Os/^{188}Os$ value of 0.226 ± 0.021. The initial osmium isotope ratio indicates a crustal component, but the fact that the three samples define a reasonable isochron suggests that this component may have been acquired prior to emplacement.

Holwell *et al.* (2005) studied the relationship between the Platreef and its Main Zone hangingwall at Sandsloot, Zwartfontein South and Overysel. Based on textural evidence such as xenoliths of reef pyroxenite in the Main Zone, they suggest that the hangingwall gabbronorites were emplaced after the Platreef and that there was a significant hiatus between the two intrusive events.

Hutchinson and Kinnaird (2005) investigated the Ni-Cu-PGE mineralisation of the southern Platreef on the farm Turfspruit. They report that S displays a good positive correlation with Ni and Cu, but that Pt and Pd show poor correlations with base metals. Hutchinson and Kinnaird (2005) attribute this to repeated modification of

primary sulphides by the introduction of As, Te, Bi and Sb during devolatization of the footwall hornfels and by percolating felsic melts resulting in redistribution of S, Cu and Ni. PGM were found in rims around orthopyroxenes, as discrete grains within secondary silicates and as grains adjacent to, or along the margins of, composite sulphides. More rarely they may occur as inclusions within sulphide minerals.

Kinnaird (2005) studied two borehole cores from the southern sector of the northern limb on the farm Turfspruit and suggested that the Platreef is a complex intrusive body comprising multiple pyroxenite and peridotite sills each with a distinctive chemistry.

Nex (2005) investigated the structural history of the Bushveld Complex in the northern limb by carrying out detailed mapping and structural investigations at Tweefontein Hill. The author suggested that there are two pre-Bushveld ductile deformation events which have resulted in a major south-west plunging fold at Tweefontein Hill. This fold structure primarily controlled the distribution of massive sulphide mineralisation at Tweefontein Hill, a feature unique to this locality.

Sharman-Harris *et al.* (2005) performed sulphur and oxygen isotope analysis on a range of Platreef and footwall rocks on the farm Turfspruit. Their study revealed that the Platreef sulphides at this locality contain a significant component of crustal S, which they propose to be derived from the adjacent shales of the Duitschland Formation. The heaviest S isotopic signatures occur closest to the footwall contact

whereas lighter signatures, more similar to that expected for magmatic sulphur, occur near the top of the Platreef.

A recent study by Holwell *et al.* (2006) on the PGM assemblage in the Platreef at Sandsloot mine revealed that the pyroxenites and pegmatites of the reef contain a PGM assemblage dominated by Pt and Pd tellurides (kotulskite and moncheite), electrum and some arsenides. Portions of the reef that have been replaced by olivine are characterised by the presence of Pt-Fe alloys, Pd-alloys and Pd-tellurides. The metamorphosed footwall rocks that contain PGE mineralisation are characterised by arsenides, bismuthides and antimonides. Holwell *et al.* (2006) suggest that the variety of PGM assemblages in the different Platreef rocks at Sandsloot reflects the late magmatic and hydrothermal processes which affected the Platreef during and after emplacement.

1.4 Methodology

The initial step of this investigation involved the examination and logging of two borehole cores (borehole 2121 and 2199) drilled in 1994 by Gencor on the farm Nonnenwerth. More than one hundred samples of the Platreef and its floor rocks were collected representing the different lithologies and mineralization. Seventy one quarter core samples, 10-30 cm in length, were selected for detailed study. Polished thin sections were prepared for all 71 samples. In relatively unaltered samples, the modal proportions of mineral phases were estimated by point counting. Thirty nine (39) samples were pulverised using a C-steel jaw-crusher and a C-steel milling vessel. The samples were analysed for major and trace elements by X-ray

fluorescence spectroscopy (XRF) at the University of Pretoria. The PGE concentrations were determined at the Université du Quebec à Chicoutimi, Canada, by Ni-sulphide fire assay followed by Instrumental Neutron Activation Analysis (INAA). Details of the method are given in Bédard and Barnes (2002). The compositions of selected minerals were determined by electron microprobe at the University of Pretoria, South Africa. S and O isotope analyses on selected samples were performed at Indiana University, Bloomington, USA. The compositions of few chromites from the serpentinised peridotite and magnesian gabbronorite were obtained using a CAMECA SX-100 electron probe micro-analyser at the University of Pretoria, South Africa. The analytical results were corrected for Fe^{3+} content using the method of Finger (1972). Twenty-five polished sections were investigated by reflected light microscopy and scanning electron microscopy at the Federal Institute for Geosciences and Natural Resources (BGR) in Hannover, Germany to investigate the nature of the platinum-group minerals, the host phases of Pd and Pt and the composition of the base metal sulphides. Quantitative electron microprobe analyses of sulphides and PGM were performed using a CAMECA SX 100 at the Federal Institute for Geosciences and Natural Resources in Hannover, Germany. All analytical details are given in Appendix 1e.

CHAPTER TWO: OVERVIEW OF THE BUSHVELD COMPLEX

2.1 General

The Bushveld Complex, ca. 2055 - 2060 Ma (Rb-Sr whole rock age, Walraven et al., 1990; U-Pb on zircons, Harmer and Armstrong, 2000; U-Pb titanite age, Buick et al., 2001), consists of at least two distinct phases, including the largest mafic-ultramafic layered intrusion on Earth (the Rustenburg Layered Suite (R.L.S), measuring ca. 65 000 km^2 in outcrop/sub-surface outcrop), and one of the largest A-type granites on Earth (the Lebowa Granite suite measuring ca. 60 000 km^2; Kleeman and Twist, 1989) (Fig. 2.1). Extrusive rhyolitic pyroclastics of the Rooiberg Group are broadly of the same age and may equally form part of the Bushveld event (Harmer and Armstrong, 2000). The Bushveld Complex is located in the northern portion of the Kaapvaal craton. It lies almost entirely within the bounds of the Transvaal sedimentary Supergroup. The latter represents a supracrustal volcanosedimentary sequence estimated to have a total stratigraphic thickness of >15 km (S.A.C.S, 1980). It consists, from the base to the top, of (a) the protobasinal Wolkberg and Buffelsfontein Groups, (b) the carbonaceous Chuniespoort Group, and (c) the largely pelitic Pretoria Group. The Transvaal Supergroup is underlain by Archaean greenstones and basement granite- gneiss. Both the intrusive and the sedimentary rocks possibly formed in response to intracratonic rifting (Eriksson et al. 1991). The mafic-ultramafic sequence contains approximately 80% of the world's resources of PGE (Morrissey, 1988), as well as abundant reserves of Cr and V. The felsic rocks of the Complex host some important Sn and F deposits (Bailie and Robb, 2004).

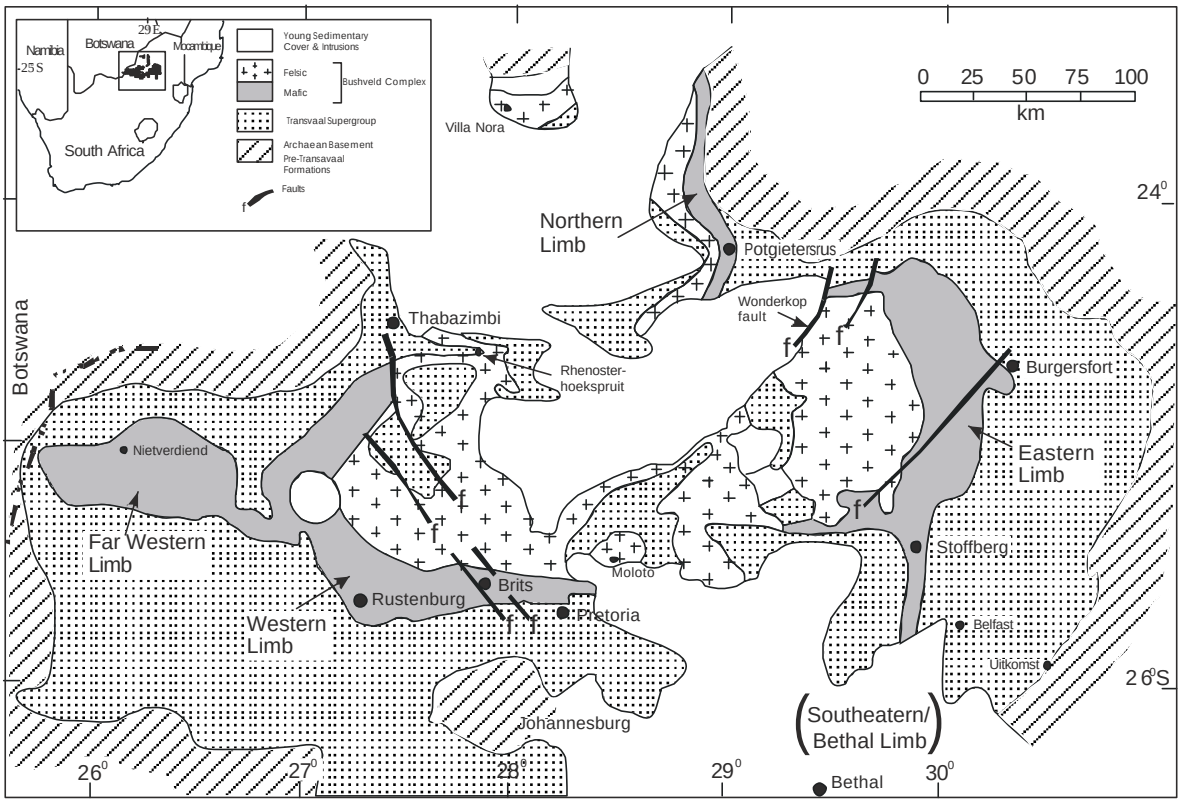

Fig. 2.1: Geologic map of the Bushveld Complex showing the different limbs (Modified after Reczko et al., 1995).

The R.L.S intruded the 2550 – 2060 Ma (Nelson et al., 1999) Transvaal Supergroup largely along an unconformity between the Magaliesberg quartzite of the Pretoria Group and the overlying Rooiberg felsites. However, in the eastern lobe of the Complex south of the Steelpoort fault the Complex transgressed upwards through more than 2 km of sediments. In the northern limb, the Complex intruded at the level of the Magaliesberg quartzite in the south, but transgressed progressively lower members of the Transvaal Supergroup towards the north, until the mafic rocks abut Achaean granitic gneiss (Eales and Cawthorn, 1996).

2.1.1 Rustenburg Layered Suite

The Rustenburg Layered Suite is an approximately 8 km thick succession of layered mafic and ultramafic rocks, exposed in five major lobes, i.e., the eastern-, western-, and far-western lobes, the northern or Potgietersrus - Villa Nora lobe, and the Bethal lobe. The latter is hidden below younger sedimentary cover. It was identified on the basis of a gravity high and is only known from borehole core (Buchanan, 1975). Drilling also established extensions of the western limb of the Complex at its northern end beneath the Bushveld granite, and of the eastern limb beneath the Karoo sedimentary cover to the west of the Wonderkop fault (Eales and Cawthorn, 1996).

There is still controversy as to whether the limbs are joined at depth. Such a model was initially proposed by Hall (1932) based on the lithological similarity between the lobes. However, gravity data collected in the 1950's showed that the centre of the Complex lacks a positive anomaly suggesting that the mafic-ultramafic rocks were not continuous at depth (Cousins, 1959). Cawthorn and Webb (2001) and Webb et al. (2004) reinterpreted the gravity data based on seismic evidence suggesting a thickened crust beneath the Bushveld Complex (James, et al., 2004). As a result the gravity data are consistent with a model of connectivity of the lobes at depth.

The mode of emplacement of the layered suite was one of repeated injections of magma. This is suggested by the frequent reversals in the trend of differentiation towards higher Mg# and Cr contents (Eales & Cawthorn, 1996), in the initial Sr – isotopic ratio towards more mantle-like values, and by textural evidence such as resorbed plagioclase inclusions in olivine and pyroxene (Eales et al. 1986).

The Rustenburg Layered Suite is generally sub-divided into five zones on the basis of mineralogical and petrological variations (Hall, 1932): at the base is the Marginal Zone which is overlain by the Lower Zone, the Critical Zone, the Main Zone, and the Upper Zone. A simplified stratigraphic column is shown in Fig. 2.2. The basal Marginal Zone consists of poorly layered, fine- to medium grained, heterogeneous gabbronoritic rocks. Marginal Zone rocks contain variable amounts of quartz and biotite, reflecting assimilation of the underlying shale. It varies in thickness between 0 and 250 m (western Bushveld Complex, Coertze, 1974). The rocks of the Marginal Zone are generally unmineralized (Viljoen and Schurmann, 1998). They may represent composite sills or rapidly cooled derivatives of the parental magmas to the Complex (Eales and Cawthorn, 1996). The Lower Zone reaches a thickness of approximately 800 m In the western limb, it comprises three main intervals. At the base occur interlayered olivine-rich and orthopyroxene-rich cumulates ca. 450 m, in the form of harzburgites and dunites (Eerlyl bronzitite of SACS, 1980). This is overlain by predominantly orthopyroxenite, ca. 100 m, (Makgope bronzitite of SACS, 1980), and at the top, some 300 m of mainly harzburgite and dunite (Groenfontein harzburgite of SACS, 1980). In the eastern limb, the Lower Zone is dominated by orthopyroxene-rich rocks (Eales and Cawthorn, 1996).

The Critical Zone is ca. 1.2 km thick and contains two economically important PGE-layers (the Merensky Reef and UG2 chromitite) and a total of 13 major chromite layers. The Critical Zone is sub-divided into two compositionally contrasting subzones, namely the Lower Critical Zone and the Upper Critical Zone (Cameron, 1980, 1982). The base of the Lower Critical Zone is characterised by an increase in

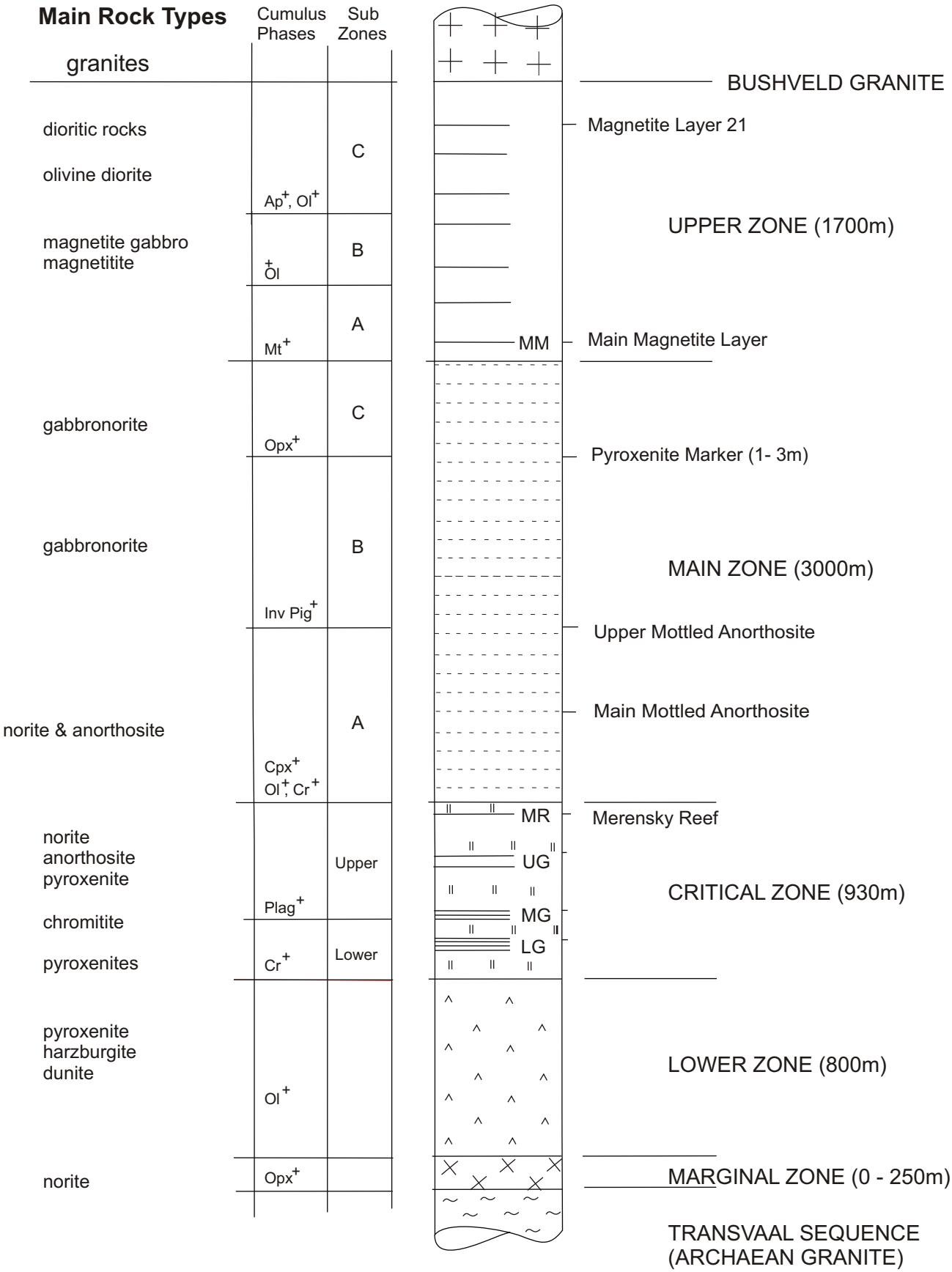

Fig. 2.2: Stratigraphy of the Rustenburg Layered Suite in the western Bushveld Complex (from Mithcell, 1990)

the proportion of interstitial plagioclase, from 2 to 6 % (Cameron, 1978). The boundary between the Lower Critical Zone and the Upper Critical Zone is defined by the appearance of cumulus plagioclase, forming an anorthosite layer between the MG2 and MG3 chromitites. The Upper Critical Zone is characterised by a number of cyclic units consisting of basal chromitite, overlain by harzburgite and/or pyroxenite, norite and anorthosite (Eales et al., 1986).

According to the most widely accepted subdivision, the base of the Main Zone may be placed at the top of the Giant Mottled Anorthosite with large oikocrysts of pyroxene at the top of the Bastard unit, although the exact position is somewhat controversial (Kruger, 1990; Mitchell and Scoon, 1991). The Main Zone is ca. 3000 m thick and consists mainly of norite in the basal and uppermost portions, but gabbronorite in the intervening central portion (Mitchell, 1990). Anorthosite constitutes some 5 % of the rocks, while pyroxenite is rare. The rocks are mostly poorly layered. Cumulus olivine and chromite are absent and magnetite occurs only near the top of the zone. The Main Zone onlaps the floor rocks to the south and the north where it is also the basal zone in the northern lobe

The position of the boundary between the Main Zone and the Upper Zone remains also controversial. Based on a reversal in Sr isotopic ratio and in the trend of iron enrichment (Von Gruenewaldt, 1973; Klemm et al., 1985), Kruger (1990) placed the boundary at the level of the Pyroxenite Marker, a prominent layer some 2.5 km above the base of the Main Zone. The more commonly used subdivision is that of Wager and Brown (1968) who defined the base of the Upper Zone by the first occurrence of

cumulus magnetite, some 660 m above the Pyroxenite Marker. The Upper Zone is a 2-3 km thick, well layered unit that consists of gabbronorite, gabbro, anorthosite, and quartz-bearing ferrodiorite. There are 24 layers of massive magnetite, up to 7 m thick that host the bulk of the world's V resources. Near the top of the Upper Zone occur highly differentiated rocks enriched in K-feldspar and quartz that may be termed granodiorite (Von Gruenewaldt, 1973).

2.1.2 Parental magmas

Based on the composition of the chilled marginal rocks, the Bushveld Complex is thought to have resulted from the intrusion into the Bushveld chamber of two or more chemically distinct parental magmas producing the layered succession of mafic rocks (Sharpe, 1981, 1985; Harmer and Sharpe, 1985). These are a high-Mg basaltic andesite (B1 of Sharpe, 1981; magnesian basaltic suite of Davies and Tredoux, 1985) and a tholeiitic basalt (B2/B3 of Davies and Tredoux, 1985). The Lower Zone is thought to have formed from the high-Mg andesite. Periodic mixing of the tholeiite and high-Mg andesite is considered to be responsible for the formation of the chromitite layers (Sharpe and Irvine, 1983; Hatton and von Gruenewaldt, 1987), the Merensky Reef (Kruger and Marsh, 1982, 1985; Naldrett et al., 1986; Hatton, 1989) and the liquation of immiscible sulphide melt (Naldrett and von Gruenewaldt, 1989). The Main Zone formed predominately from the tholeiitic basalt.

2.1.3 PGE-mineralization

The PGE-mineralization in the Rustenburg Layered Suite occurs in the form of:

a) stratiform sulphide-bearing layers including the Merensky Reef (Lee, 1983; Naldrett et al., 1986; Barnes and Maier, 2002), Platreef (Gain and Mostert, 1982; Van der Merwe, 1976), Bastard Reef (Lee, 1983), Pseudoreef and Tarentaal layers (Naldrett et al., 1986), and the footwall of the Main Magnetite Layer (Von Gruenewaldt, 1976).

b) chromitites (Gain, 1985; Von Gruenewaldt et al., 1986; Hiemstra, 1986; Lee and Parry, 1988; Teigler, 1990 a, b; Scoon and Teigler, 1994) and

c) discordant PGE-enriched pipes of mafic-ultramafic pegmatite and magnesian dunite in the Critical Zone of the eastern Bushveld Complex, at Mooihoek, Onverwacht and Driekop (Scoon and Mitchell, 1994)

For stratiform sulphides-bearing layers, two main genetic models are generally considered. Most workers believe that the PGE were concentrated by a sulphide liquid that segregated from the silicate magma after sulphide saturation was achieved. In the past, it was widely believed that sulphide saturation could be triggered by mixing of compositionally contrasting magmas, one being primitive, the other being more evolved (Naldrett and von Gruenewaldt, 1989; Irvine and Sharpe, 1986; Li et al., 2001a). Cawthorn (2002) suggested that this model is incorrect and that magma mixing cannot trigger sulphide supersaturation. However, Li & Ripley (2005) presented new data that support the original model. They argue that attainment of sulphide saturation after magma mixing is strongly dependent on the sulphur concentrations of the end-member magmas, mixing proportions, as well as pressure and temperature.

An alternative model (Boudreau et al. 1986) proposes that PGE in the basal portions of the intrusion partition into percolating late-magmatic fluids and are reprecipitated in sulphide-bearing layers at higher stratigraphic levels, but this model has been criticized by several authors, based mainly on the occurrence of PGE-enriched rocks throughout much of the Lower and Critical Zones of the Complex. Further, in terms of this model, the thickness of the silicate rocks underlying a mineralized layer ought to have had an influence on the grade of the PGE-mineralization in the layers. In reality, the grade of the reefs remains relatively constant along strike. Yet, the Merensky Reef is underlain by ~ 400 m of unmineralized pyroxenite, norites and anorthosite in the Winnaarshoek area, but by 60 - 120 m of unmineralized rocks at Impala mine in the Rustenburg area (www.implats.co.za).

Mineralization in the Merensky Reef is hosted by up to 3% base metal sulphides (pyrrhotite, pentlandite, pyrite, cubanite and rare sulpharsenides, galena and sphalerite) and accessory PGE-minerals interstitial to the silicates. The Precious metals of the Merensky Reef typically average 5-7g/t over hundreds of kilometers of strike, mainly within the eastern and western lobes of the Complex (Barnes and Maier 2002a, b; Cawthorn *et al*., 2002) and are in the proportions of 4.82 ppm Pt, 2.04 ppm Pd, 0.66 pp Ru, 0.24 ppm Rh, 0.08 ppm Ir, 0.26 ppm Au, and the Cu:Ni ratio is 0.61 (Lee, 1996). Interestingly, the extent and relative amount of PGE and base metal sulphides appears to be a function of reef thickness with the highest grades occurring where the reef is thin. This remarkably constant grade of the reef over extensive strike distances is not mirrored by the composition of the actual platinum group

mineralogy which is extremely variable even from mine to mine (Cawthorn et al., 2002b).

For S-poor chromitites, some workers have proposed that the PGE were initially concentrated by sulphides, but that much of the sulphur was subsequently lost during late magmatic processes, with the PGE remaining behind (e.g. Naldrett and Lehmann, 1988; von Gruenewaldt et al., 1989; Boudreau, 1998). Other authors have considered whether PGM can precipitate directly from the silicate magma, or were transported by the magma from the mantle source (Keays and Campbell, 1981; Barnes and Naldrett, 1987). The PGM could act as nuclei for crystallizing chromite or olivine. The weakness of this model is that it requires the magma to become saturated with PGM although it contains very low levels of these elements (10-20 ppb) (Mathez and Peach, 1997). As a possible alternative, Tredoux et al., 1995, proposed that PGE-ions in the melt tend to form clusters. When the clusters are destabilised in response to crystallisation of chromite or magnetite, PGM could crystallise directly from the magma. A criticism to this model is that most of the mineralized layers contain cumulus sulphide. It would not be possible to crystallize PGM from a magma that is at the same time segregating sulphide liquid. Thus, if the PGE are collected by PGM the sulphides must have been added to the rock after the formation of the PGM.

The UG2 chromitite has 60-90% chromite with an average Cr/Fe ratio between 1.26-1.4 and 43.5% Cr_2O_3. The PGE are interstitial to the chromite grains with the exception of laurite which is commonly found enclosed by chromite. PGE contents

are up to 10 ppm PGE+Au (3.6 ppm Pt, 3.81 ppm Pd, 0.3 ppm Rh). Base metal sulphides are accessory and Cu and Ni are low, generally less than 0.05% (Lee, 1996). The PGE distribution frequently displays two peaks (Hiemstra, 1985).

The PGE-mineralized discordant pipes consist of Fe-rich clinopyroxenite, Mg-dunite and hortonolite dunite (Wagner, 1929). The pipes contain a very unusual PGE-assemblage, dominated by Pt, suggesting that the mineralization is not of primary magmatic origin. Stumpfl (1993) has suggested that the PGE are the result of hydrothermal remobilisation from cumulates that host the pipes. The origin of the pipes remains unresolved. They may possibly represent ultramafic density flows crystallised from late magma injections (Viljoen and Schürmann, 1998).

2.2 General geology of the Platreef

The Platreef is a zone of mineralization developed mostly at or near the base of the northern limb of the Bushveld Complex (Fig. 2.3). It consists of a thick (up to 400 m; Kinnaird et al., 2005) package of texturally heterogeneous pyroxenite, norite and gabbronorite, containing numerous xenoliths of dolomite, calc-silicate, shale (graphitic in part), quartzite and Fe-formation derived from the floor rocks. The xenoliths range from several cm to 100s of metres in diameter. The Platreef rests on the Lower Zone in the southern part of the northern lobe (on the farms Grassvally and Rooipoort; Hulbert, 1983; Maier et al., 2007), on Transvaal Supergroup rocks between Rooipoort and Zwartfontein and on Archaean granite gneiss between Overysel and the northern edge of the lobe (Fig. 2.3). An up to 2000 m package of gabbro, magnetite gabbro and diorite belonging to the Main and Upper Zones of the Rustenburg Layered Suite

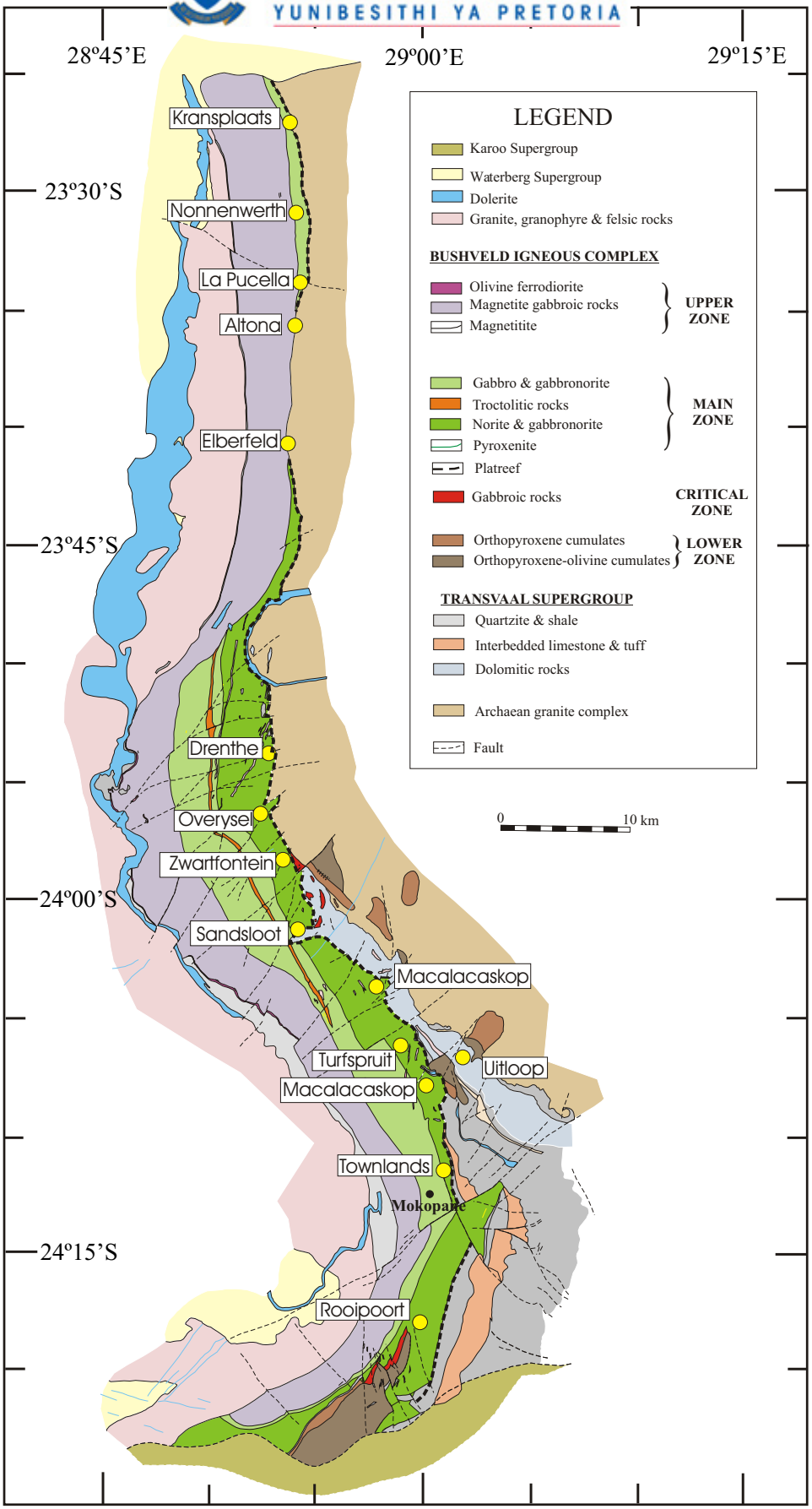

Fig. 2.3: Geological map of the Northern limb of the Bushveld Complex. (modified after Ashwal, et al., 2005).

overlies the Platreef. Between the farms Elberfeld and Altona, a ca. 10-km sector to the south of Nonnenwerth, the Main Zone and the Platreef are apparently not developed. In this area the Upper Zone has transgressed through the Main Zone and directly overlies the Archean basement which forms the floor of the intrusion (Fig. 2.3). The absence of sulfide mineralization in this area is indicated by a stream sediment survey conducted by the Geological Survey of South Africa. The survey failed to identify a pronounced positive Cu anomaly that is typical of the base of the remainder of the northern lobe. The implication here is that where Upper Critical Zone rocks overlie floor rocks, no basal contact-style PGE mineralization is developed, possibly because the parental magma to the Upper Critical Zone is too depleted in PGE to form a reef (Barnes *et al*, 2004).

The Platreef displays varying styles of mineralization in different sectors of the northern lobe. The PGE may be concentrated near the base of the layer e.g., at Tweefontein, near the top e.g., at Drenthe, or the PGE may be evenly distributed throughout the Platreef e.g., at Overysel (Kinnaird, 2005). Sulphide mineralization (up to 20%) may occur in the form of disseminated, net-textured, sub-massive or massive chalcopyrite, pentlandite and pyrrhotite, with minor galena and sphalerite with overall grades of 0.1-0.6% Cu and Ni. The mineralization may occur in norite, gabbronorite, anorthosite and pyroxenite. PGE grades are low and mostly <1–2 ppm, but higher grades are have been recorded in individual samples throughout the northern limb and, in particular, at Sandsloot and surrounding farms where average grades are ca. 4 ppm over 10 m (Vermaak 1995; Armitage et al., 2002). The PGE's occur as PtFe, Pt_3Sn and variable Pd or Pt-tellurides, bismuthides, arsenides, antimonides,

bismuthoantimonides and complex bismuthotellurides (Hutchinson and Kinnaird, 2005; Holwell *et al*., 2006). Pt:Pd ratio is ~1. PGM are rarely included in the sulphides. They occur as micron-sized satellite grains around interstitial sulphides and are common in serpentinised zones.

The correlation of the Platreef with the cumulate succession elsewhere in the Bushveld Complex remains unclear. In most of the northern lobe, the Platreef is overlain by the Main Zone and underlain by the sedimentary floor rocks. Together with the occassionally pegmatoidal textures of the Platreef, this has led several authors to correlate the Platreef with the Merensky Reef (Wagner, 1929; White, 1994). However, significant differences exist between the Platreef and the Merensky Reef as exposed in the western and eastern lobes of the Complex (e.g. Van der Merwe, 1976; Buchanan et al., 1981; Eales & Cawthorn, 1996). Firstly, the Merensky Reef tends to occur within the layered sequence, in many instances some 2 km above the floor of the Bushveld Complex, whereas in most cases the Platreef directly overlies the floor of the Complex or is separated from the later by a few 10's of meters (Fig. 2.4). Secondly, the mineralized interval is much thicker in the Platreef than in the Merensky reef (up to 400 m versus ca 1 m). Thirdly, there are important mineral- and whole rock compositional differences between the two layers, namely a relatively higher crustal component and lower metal tenors (e.g. Buchanan et al. 1981) in many Platreef intersections relative to the Merensky Reef (Barnes and Maier, 2002). The Platreef is also characterized by relative lower Pt/Pd ratios.

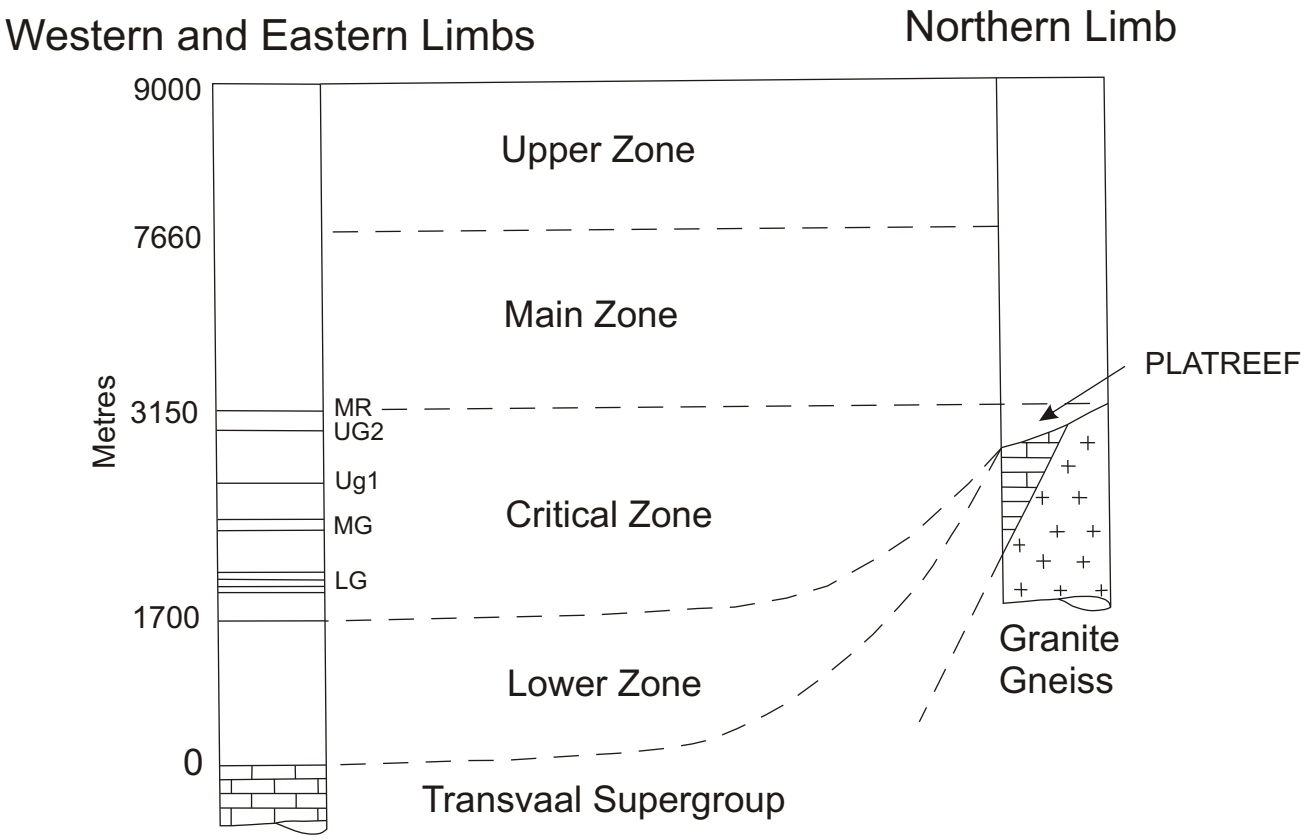

Fig. 2.4: Schematic section through the Rustenburg Layered Suite in different limbs of the Bushveld Complex (from Cawthorn *et al.*, 2002). Lateral correlation after Buchanan *et al*. (1981).

CHAPTER THREE: GEOLOGY OT THE PLATREEF ON NONNENWERTH

3.1 General

The farm Nonnenwerth 421 LR is located ca. 65 km north of Mokopane (Fig. 2.3). The area is generally covered by soil, thus little outcrop is present. The geology of the Platreef on Nonnenwerth 421 LR is known from boreholes drilled by Gencor and Pan Palladium, and from geophysical work. Two drill cores were investigated in this study. They were sampled by boreholes 2121 and 2199, located ca. 2 km apart (Fig. 3.1). Borehole 2121 was drilled to a depth of 342.85 m and borehole 2191 was drilled to a depth of 371.05 m. Both boreholes were collared (drilled) at an angle of 50^0 to the east, intersecting the Main Zone and the Platreef and terminating in granite gneiss floor rocks. The Platreef dips at approximately 40^0 in a westerly direction and is approximately 110 m meters thick. In the present work, it has been sub-divided into five sub-units that are mostly composed of medium to coarse-grained gabbronorite, norite and coarse-grained anorthosite which progressively become more leucocratic and coarser grained from the base upwards. Occasionally, pegmatoidal bands enriched in magnetite and phlogopite are developed. Two calc-silicate xenoliths, up to 25 m in thickness, are present.

The upper part of the intersected sequence, ca. 170 m, consists of homogenous medium-grained, unmineralized gabbronorite. Based on lithological and compositional grounds, this sequence is correlated with the Main Zone. The Platreef and the Main

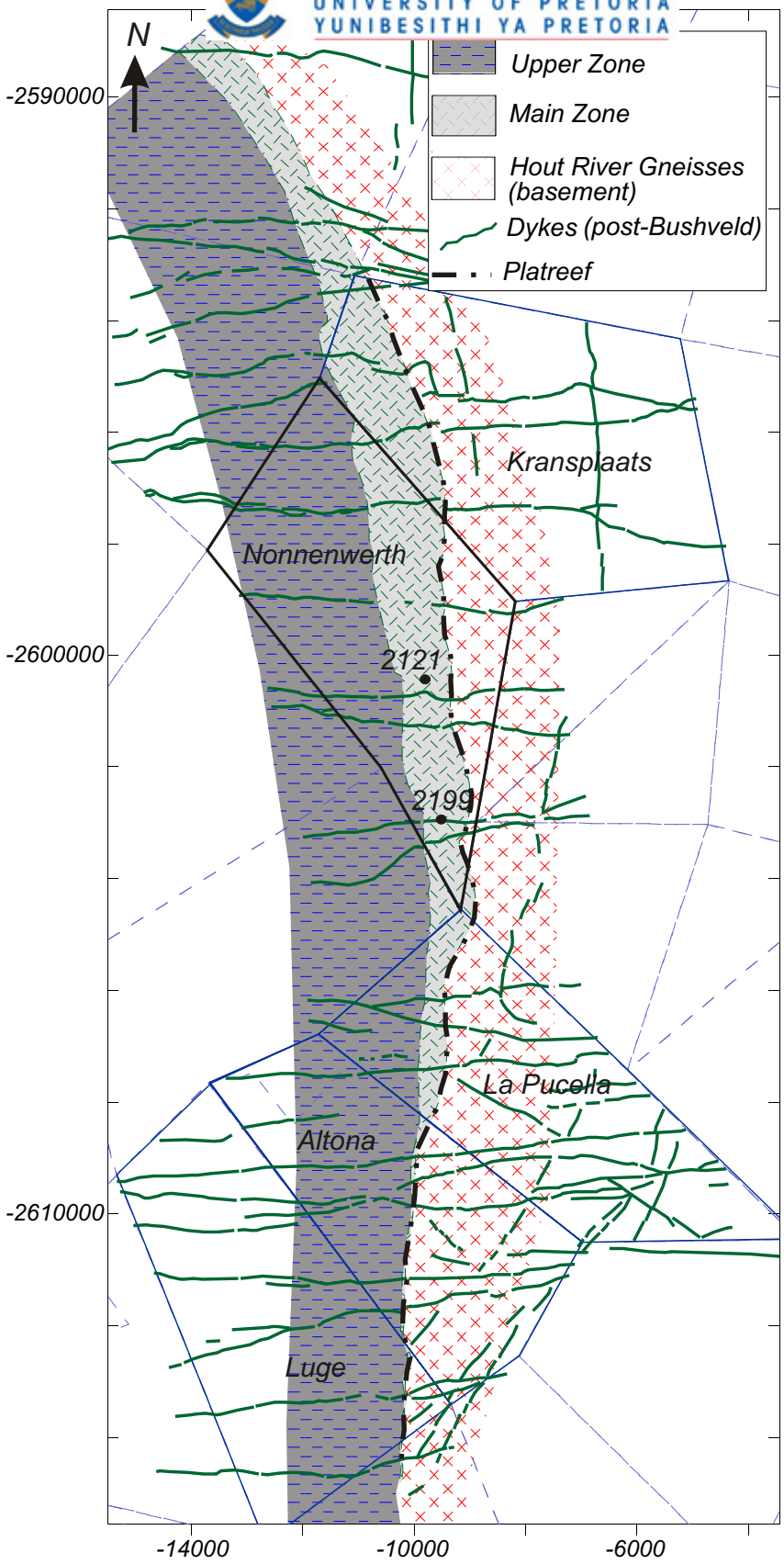

Fig. 3.1: Map of the northern sector of the Platreef (modified from www.panpalladium.com). Note the localities of boreholes 2121 and 2199.

Zone are separated by a dolomite xenolith that is ca. 25 m thick in borehole 2121 and 3 m in borehole 2199. A second dolomite xenolith or raft occurs within the Main Zone, at a depth of 51 – 65 m in borehole 2199 and 49 - 71.5 m in borehole 2121.

3.2 Borehole 2121

A simplified stratigraphic column of Borehole 2121 is given in Fig. 3.2. The footwall to the Platreef is composed of Archaean granite gneiss. This is a medium-grained, pinkish-grey, quartzo-feldspathic rock containing dark green, orthopyroxene-rich melanosomes that define rhythmic layering (Fig. 3.3). The contact between the granite gneiss and the overlying mafic rocks of the Rustenburg Layered Suite is sharp (Fig. 3.4).

3.2.1 Platreef

Sub-unit 1

The base of the Platreef is marked by a fine-grained norite, up to ca. 30 cm, possibly representing a chilled contact facies. This is overlain by a ca. 13.15 m thick, medium-grained melagabbronorite interlayered with several further layers (up to 20 cm) of fine- to medium-grained norite (Fig. 3.5 and 3.6). The contacts between the gabbronorite and norites are sharp (Fig. 3.5 and 3.6) possibly suggesting a hiatus between the intrusion of the norite and the gabbronorites. It is here acceptable that the distinction of layers from xenoliths in borehole intersections is difficult. However, from the two boreholes studied and further examination of more Platreef core from Nonnenwerth at Impala core shed in Springs, the norites seem to represent layers

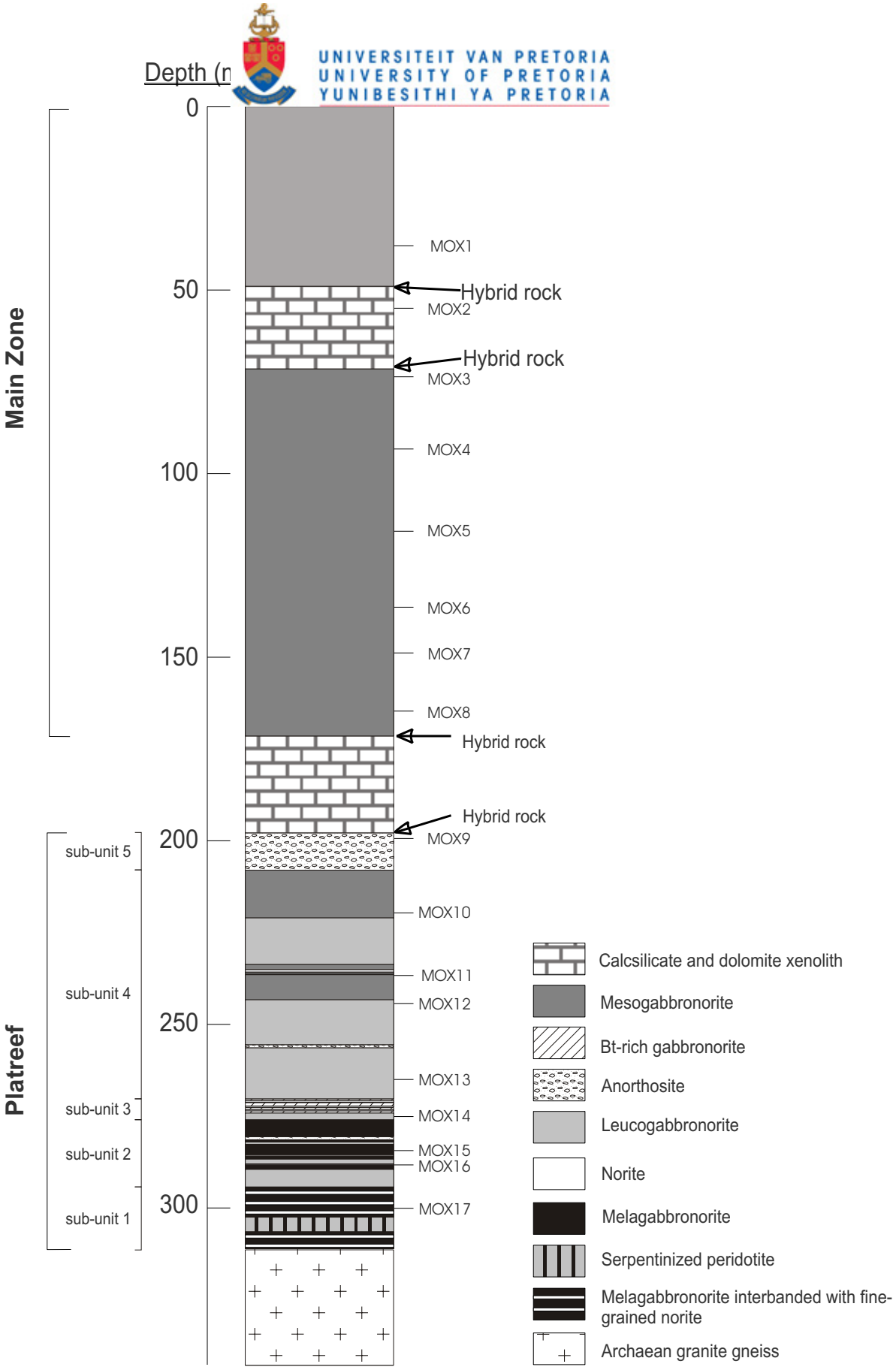

Fig. 3.2: Stratigraphic log of borehole 2121. Numbers on right side of log indicate samples that were analysed by XRF.

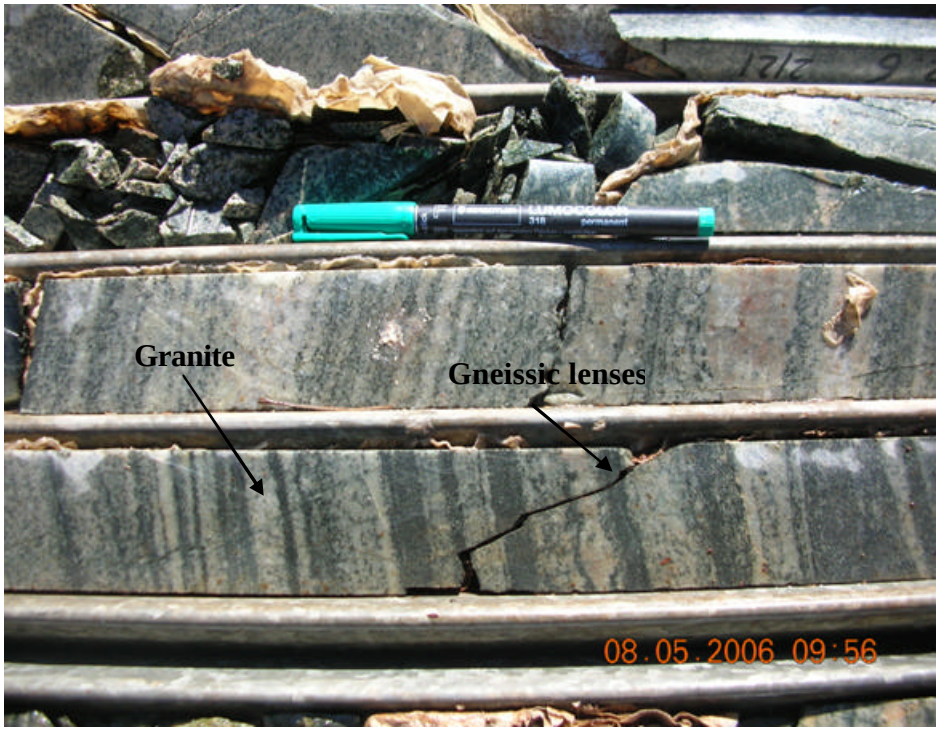

Fig. 3.3: Medium-grained, pinkish-grey granite gneiss containing dark green melanosomes that define rhythmic layering. 330m depth, borehole 2121. Pen is shown for scale.

Fig. 3.4: Sharp contact at 311.30m depth (indicated by stippled line) between granite gneiss (above) and fine-grained (chilled) norite (below). Pen is shown for scale. Borehole 2121.

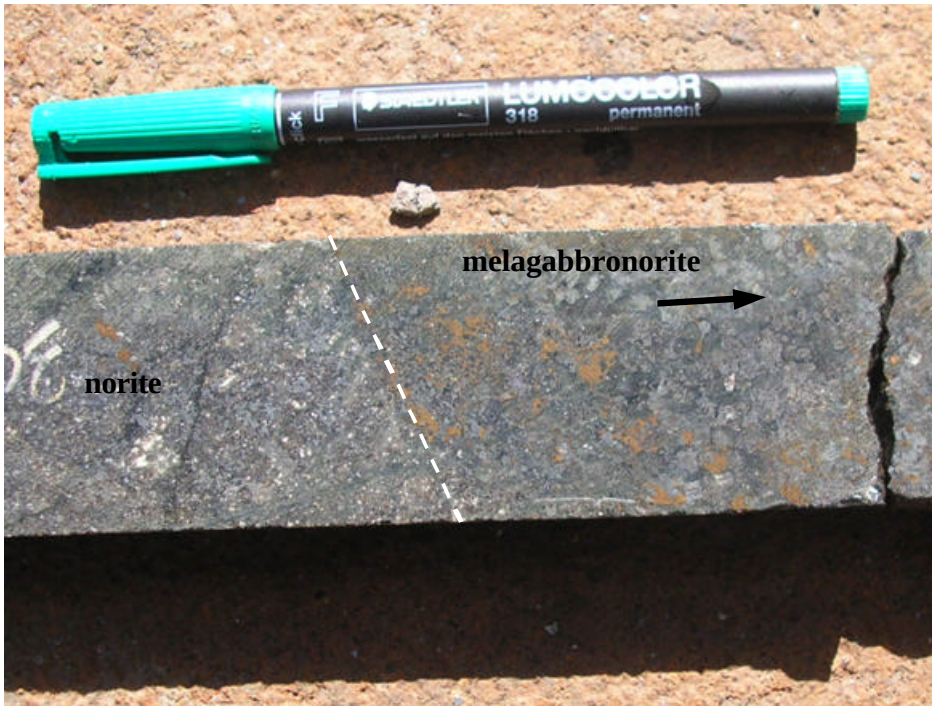

Fig. 3.5: Sharp contact (at 300.93m) between medium-grained, sulphide-bearing melagabbronorite and fine-grained, poorly mineralized to barren norite. Stippled line represents the contact. Arrow indicates stratigraphic up. Pen is shown for scale. Borehole 2121.

Fig. 3.6: Sharp contact (at 296.62 m and 296.50 m depth) between medium-grained, sulphide-bearing melagabbronorite and fine-grained, poorly mineralized to barren norite. Stippled lines represent the contact. Arrow indicates stratigraphic up. Pen is shown for scale. Borehole 2121.

Fig. 3.7: Medium-grained peridotite with serpentine veins at 305.50m depth, borehole 2121. Arrow indicates stratigraphic up. Pen is shown for scale.

rather than xenoliths. Within the succession is a pervasively serpentinised layer, ca. 3.6 m (Fig. 3.7). The composition of the rock, particularly its relatively low CaO (1.64 wt. %), high Fe_2O_3 (22.63 wt. %), Ni (2463 ppm) and Cr (3605 ppm) whole rock contents suggest that the rock is a serpentinized peridotites of igneous derivation. The contacts between the ultramafic rock and the gabbronorite-norite succession are sharp. The occurrence of this ultramafic rock is notable, as ultramafic rocks are less common in the northern portions of the northern lobe than in the southern to south-central portions of the northern lobe (Armitage *et al.*, 2002; Kinnaird, 2004). Holwell and McDonald (2006) report on the presence of several calc-silicate/dolomite xenoliths and serpentinites at Overysel where the floor rocks are Archean basement gneisses, but they do not mention any igneous ultramafic rocks. The contrast in

composition between the present ultramafic rock and its gabbronoritic host rocks could suggest that it represents a xenolith, but a similar ultramafic layer also occurs in borehole 2199, suggesting the rock represents an intrusion of primitive magma.

The melagabbronorite is composed of greenish brown to dark grey, anhedral and subhedral pyroxenes and mostly translucent feldspar crystals. The norite contains greenish to dark grey, anhedral and subhedral pyroxenes and white feldspar crystals giving the rock a “speckled” appearance. The white feldspars and the fine-grained nature clearly distinguish the norite from the melagabbronorite in hand specimen (Fig. 3.6). The feldspar to pyroxene ratio is approximately 30:70 in the melagabbronorite increasing to 50:50 in the norite. Phlogopite is an accessory phase in most samples from the melagabbronorite. The norite is poorly mineralized with generally < 0.1% sulphides, but in the medium-grained melagabbronorite sulphides locally reach up to 3 modal %. The sulphides occur as interstitial and net textured, intergrown grains of pyrrhotite, chalcopyrite and minor pentlandite.

Sub-unit 2

The contact between sub-unit 1 and 2 occurs at 294.35 m and is sharp. Sub-unit 2 is composed of repetitive sequences of interlayered medium to coarse-grained leucogabbronorite and fine to medium-grained melagabbronorite. The contacts between leucogabbronorite and melagabbronorite are sharp (Fig. 3.8). Sulphides (up to 2 modal %) occur as interstitial and net textured, intergrown grains of pyrrhotite, chalcopyrite and minor pentlandite in the melagabbronorite. No sulphides were identified in the leucogabbronorite. A fine-grained norite (from 288.30 to 288.00 m

and 282.05 to 281.42 m) and a coarse-grained anorthosite (from 281.42 to 280.62 m) (Fig. 3.9) occur with sharp contacts, within the interlayered leucogabbronorite and melagabbronorite sequence. The fine-grained norite is texturally similar to the ones described earlier and are not shown on the stratigraphic log. The anorthosite is composed of up to 1.5 cm wide, euhedral and subhedral, white and translucent feldspars intergrown with less than 10 % interstitial pyroxenes.

Sub-unit 3

Sub-unit 2 is overlain at a depth of 276.00 m by a sequence, ca. 5.70 m thick, of interlayered medium-grained leucogabbronorite and coarse-grained phlogopite-rich gabbronorite constituting sub-unit 3. The contacts between the lithologies are sharp (Fig. 3.10). Locally, pegmatoidal domains are developed in the phlogopite-rich melagabbronorite. The phlogopite-rich gabbronorite has dark green to grey, subhedral pyroxenes and white, anhedral to subhedral feldspar crystals. Phlogopite constitutes up to 5 modal % of the rock and sulphides less than 1 modal %. The sulphides occur as interstitial and net textured composite grains of pyrrhotite, chalcopyrite and minor pentlandite.

Sub-unit 4

At 270.30 m, sub-unit 3 is overlain with a sharp contact by coarse-grained, light grey leucogabbronorite of sub-unit 4 (Fig. 3.11). Pegmatoidal and medium-grained leucogabbronorite domains are locally developed. In the pegmatoidal domains, feldspar crystals may reach 3 cm in size. At 256.40 m, a coarse-grained anorthosite,

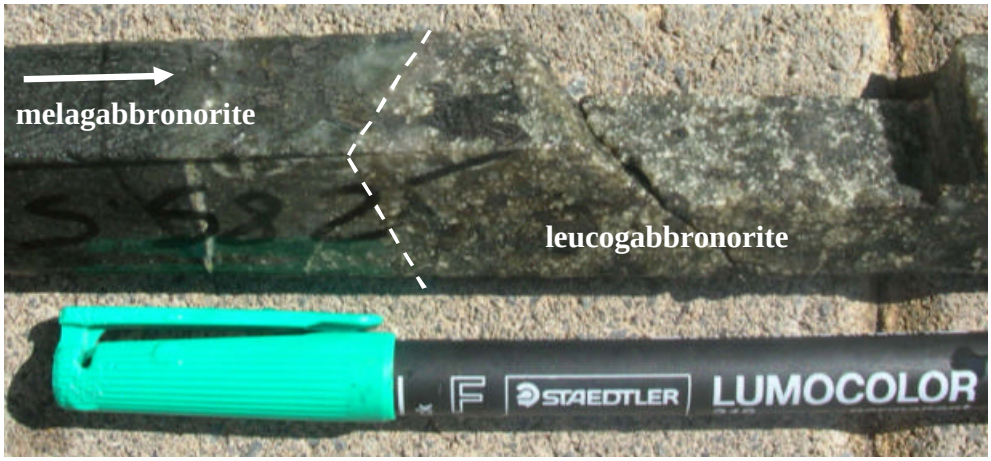

Fig. 3.8: Leucogabbronorite in contact (at 285.46m depth) with melagabbronorite. Arrow indicates stratigraphic up. Stippled line represents the contact. Pen is shown for scale. Borehole 2121.

Fig. 3.9: Anorthosite in contact (at 281.42m depth) with fine-grained melagabbronorite. Note the sharp contact between the two rock types. Arrow indicates stratigraphic up. Stippled line represents the contact. Pen is shown for scale. Borehole 2121.

Fig. 3.10: Phlogopite-rich gabbronorite in contact (at 274.15m depth) with leucogabbronorite. Note the sharp contact between the two rock types. Stippled line represents the contact. Arrow indicates stratigraphic up. Pen is shown for scale. Borehole 2121.

ca. 0.9 m, similar to the one described earlier occurs. From, 246.84 to 208.00 m, the coarse-grained leucogabbronorite is overlain by a sequence of medium to coarse-grained leucogabbronorite interlayered with coarse-grained, locally pegmatoidal mesogabbronorite. The feldspars in the rocks are pervasively altered, resulting in their white colour (Fig. 3.11). Pyroxenes are greenish to dark grey and anhedral or subhedral. The mesogabbronorite is composed of greenish brown to dark grey, anhedral and subhedral pyroxenes with mostly translucent feldspar crystals.

The mesogabbronorite has less than 2 % disseminated sulphides (Fig. 3.12) with the sulphide content increasing in pegmatoidal domains (up to 10 %). The sulphides consist of pyrrhotite and chalcopyrite in broadly equal proportions, with minor pentlandite. At 221.54 m, a melagabbronorite fragment/xenoliths, ca. 5 cm in size, occurs in leucogabbronorite (Fig. 3.13). This suggests that the leucogabbronorite intruded after the melagabbronorite.

Sub-unit 5

Sub-unit 5 consists of a coarse-grained mesocratic anorthosite, ca. 10.53 m, with a brownish grey colour. Euhedral white to translucent feldspars are intergrown with minor brownish-green anhedral pyroxenes. Disseminated pyrrhotite and chalcopyrite generally occur in abundances of <1 %, except for isolated patches where sulphides may reach up to 3 % of the rock.

The upper contact of the Platreef is marked by the occurrence of a calc-silicate xenolith, ca. 25.97 m (Fig. 3.14). The contact zone is marked by a, dark green to

Fig. 3.11: Coarse-grained leucogabbronorite. At 255.30m depth, borehole 2121. Pen included for scale.

Fig. 3.12: Medium-grained sulphide-bearing mesogabbronorite in medium-grained leucogabbronorite. 252.81m depth, borehole 2121. Arrow indicates stratigraphic up. Stippled lines represent the contact. Pen is shown for scale.

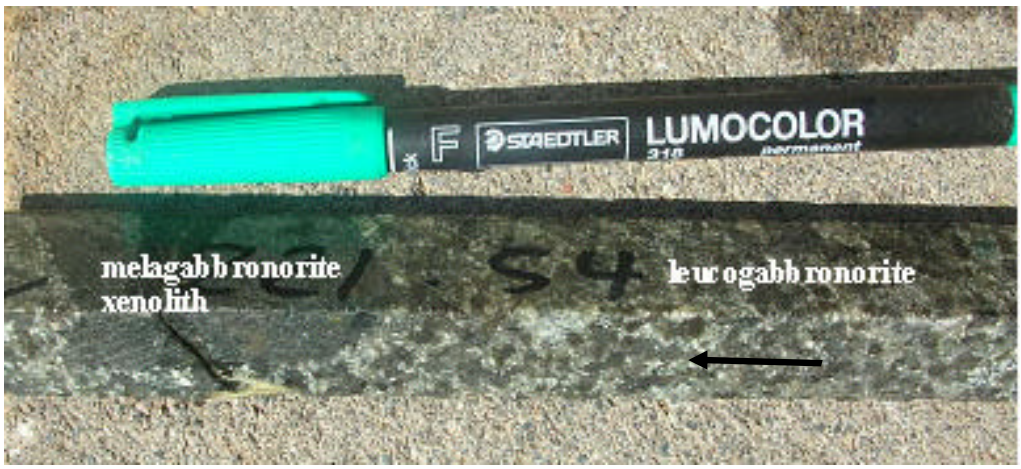

Fig. 3.13: Melagabbronorite xenolith in leucogabbronorite at 221.54m depth, borehole 2121. Arrow indicates stratigraphic up. Pen is shown for scale.

Fig. 3.14: Dolomite xenolith separating Platreef and Main Zone at 197.47m depth, borehole 2121. Pen is shown for scale.

black hybrid rock, ca. 1 m thick, consisting of gabbronorite and numerous small calc-silicate and dolomite fragments. The massive dolomite/calc-silicate xenolith is a leucocratic greyish green rock, with medium-grained, milky white to clear domains and patchy, fine-grained, greyish green clays (probably chlorite and kaolinite).

3.2.2 Main Zone

The Main Zone forms much of the upper portion of the drill core. It is underlain by a contact zone, ca. 1 m thick, that immediately overlies the calc-silicate xenolith. This contact zone consists of calc-silicate fragments in gabbronorite and is highly chloritised and serpentinised, suggesting increased hydrothermal activity. Disseminated sulphides associated with large magnetite crystals persist throughout this contact zone, but are absent in the xenolith proper.

The Main Zone consists of homogenous, medium-grained gabbronorite with a leucocratic base (Fig. 3.15a), except for numerous (5 - 50 cm) pyroxenite bands

particularly towards the top of the unit, and an interval of magnetite-bearing pegmatoidal mesogabbronorite a few metres above the basal contact. The latter rock contains patchy centimeter-scale feldspar-rich domains in coarse gabbronorite.

Magnetite (up to 1 cm) is interstitial to plagioclase and pyroxene (Fig. 3.15b). The bulk of the Main Zone gabbronorites are of medium grain size, with little or no sulphides and magnetite. Greyish-green to dark grey, medium-grained pyroxene occurs as subhedral to euhedral grains together with pale green to white, anhedral to subhedral, saussuritised feldspar. The pyroxene to feldspar ratio varies from 40:60 to55:45. The gabbronorite is cut by a quartz - epidote vein between 140.23 – 140.35 m. A light grey, gabbroic pegmatoid is developed at 71.47 m. It is composed of dark green, interstitial pyroxene grains up to 2 cm wide and light grey to pale green, subhedral saussuritised feldspar grains, up to 6 cm in size. The gabbroic pegmatoid grades into a 1.5 m leucogabbronorite overlain by a calc-silicate xenolith from 68.00 to 53.50 m. A dark green to black, “mottled” rock consisting of calc-silicate fragments in a gabbroic matrix is developed at the lower and upper contacts of the calc-silicate with the leucogabbronorite.

Close to the surface, the Main Zone is weathered and eventually gives way, at about 1.36 m depth, to red loamy soil. The weathered gabbronorite is of a khaki colour, and extremely friable with a 60 to 80% core recovery. Greenish brown, altered, subhe dral pyroxenes constitute 60% of the rock. Pale green to khaki feldspars occur as subhedral to euhedral grains and make up the rest of the rock.

Fig. 3.15a: leucocratic gabbronorite at the base of the Main Zone at 171.50m depth, borehole 2121. Stratigraphic up direction is towards the top of the page. Pen is shown for scale.

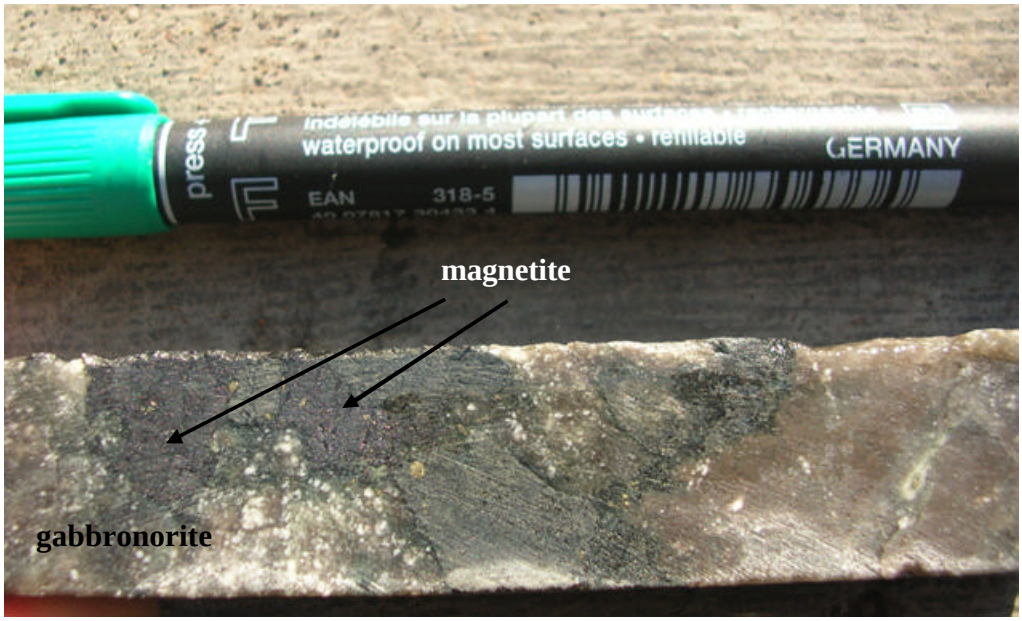

Fig. 3.15b: Coarse magnetite (at 161.60m depth) in Main Zone gabbronorite. Pen is shown for scale. Borehole 2121.

3.3 Borehole 2199

A simplified stratigraphic column of the sequence intersected by borehole 2199 is given in Fig. 3.16. As in borehole 2121, the Platreef is underlain by Archaean granite gneiss which has the same texture and appearance as the one described in borehole 2121 (Fig. 3.17). The stratigraphy of borehole 2199 is broadly similar to that of borehole 2121 despite differences in the thicknesses of correlatable units. Furthermore, sub-unit 5 is not developed in borehole 2199. Thus, sub-unit 1 consists of a basal fine-grained norite overlain by an interval of medium-grained melagabbronorite containing several further layers of fine-grained norite and containing a layer of pervasively serpentinised peridotite, ca. 4.50 m (from 342.50 to 338 m). Next is a sequence of interlayered medium to coarse-grained leucogabbronorite and medium-grained melagabbronorite with sharp contacts, also intruded by fine-grained norite (sub-unit 2). Two coarse-grained anorthosites, ca. 0.70 m and 3.4 m wide occur within the abovementioned sequence. The sequence is overlain by sub-unit 3 at ca. 204.20 m, composed of interlayered coarse-grained phlogopite-rich gabbronorite and medium-grained leucogabbronorite, with sharp contacts between the two rock types. Locally, pegmatoidal domains of the phlogopite-rich melagabbronorite are developed. Sub-unit 4, overlies sub-unit 3 with sharp contacts and consists of cycles of coarse to medium-grained mesogabbronorite interlayered with medium-grained leucogabbronorite. Note that the coarse-grained, leucogabbronorite that forms the base of sub-unit 4 in borehole 2121 is not developed here. Pegmatoidal domains in the leucogabbronorite with feldspar crystals up to 3 cm in size are locally developed.

The dolomite xenolith separating the Platreef and the Main Zone is 3 m thick, in contrast to the 26 m observed in borehole 2121. The Main Zone consists of similar medium-grained gabbronorite as in borehole 2121, and contains a further dolomite xenoliths, ca. 1.8 m, at a depth of 160.00 to 158.20 m.

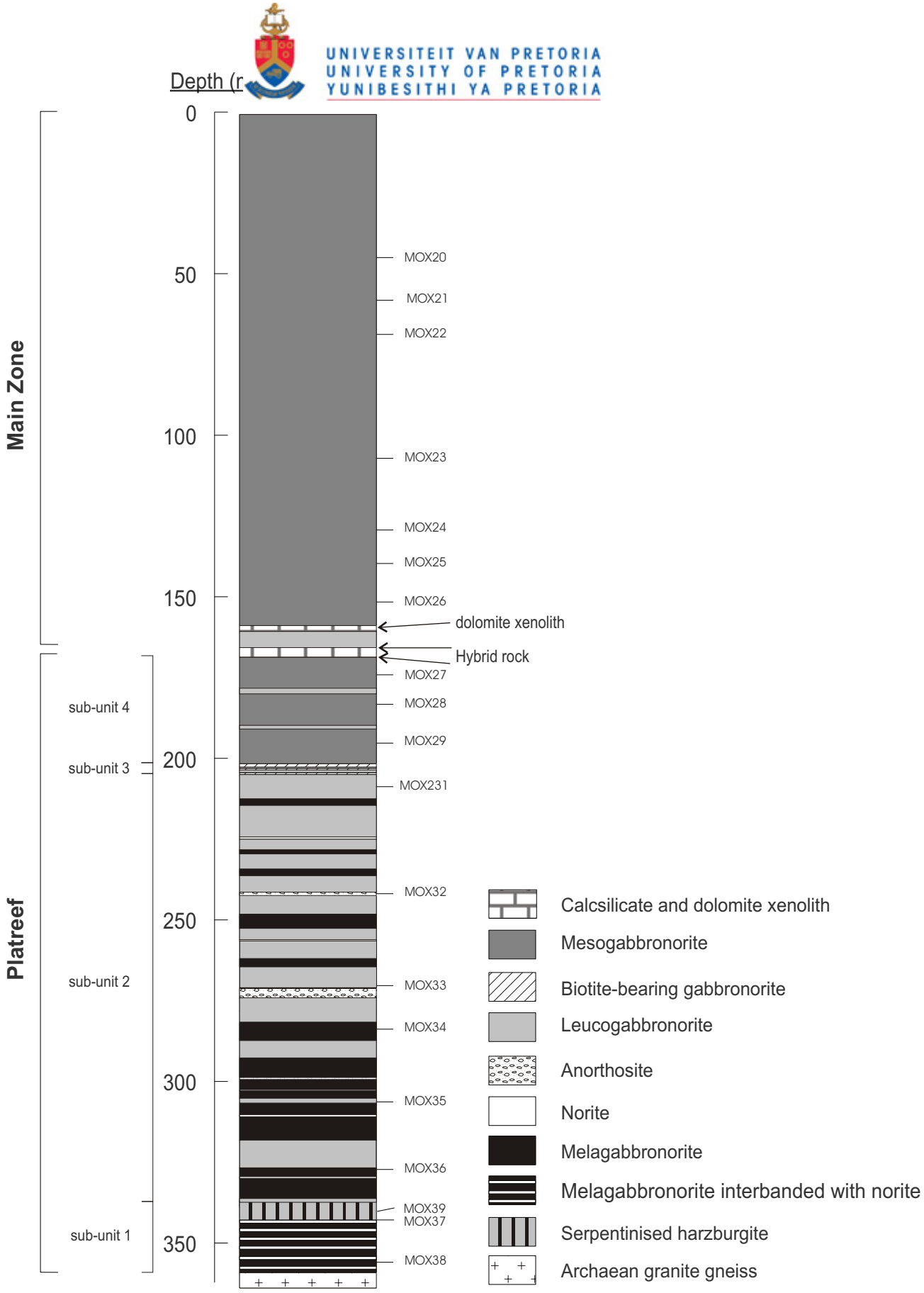

Fig. 3.16: Stratigraphic log of borehole 2199. Numbers on right side of log indicate samples that were analysed by XRF.

Fig. 3.17: Granite gneiss in sharp contact (at 359.00 m) with fine-grained (chilled) norite. Stippled line represents the contact. Pen included for scale. Borehole 2199.

CHAPTER FOUR: GEOLOGY OF THE PLATREEF ON TOWNLANDS

The farm Townlands hosts the town of Mokopane, formerly Potgietersrus (Fig. 4.1). A drillcore intersecting part of the Platreef has been investigated by Manyeruke (2003) and Manyeruke *et al.* (2005). Since the data generated during these studies will be compared to the data from Nonnenwerth, and since I have generated additional trace element data from Townlands during the present investigation, a short revision of the stratigraphy of the Platreef on Townlands is necessary. The examined drillcore comes from a borehole collared some 2 km to the NE of Mokopane. A simplified stratigraphic column of the Platreef and its floor rocks in the borehole is given in Fig. 4.2. At this locality, the floor rocks of the Platreef consist of hornfels, quartzite and calc-silicates probably belonging to the early Proterozoic Silverton Formation of the Pretoria Group, Transvaal Supergroup. The hornfels possibly formed by heating of the sedimentary floor rocks by hot Platreef magma. The sedimentary rocks are locally layered on a millimeter to centimeter scale with the layering defined by thin (1-2 mm), dark bands. They are intruded by numerous sill-like bodies of pyroxenites which show internal variation in grain size, from fine-grained margins to medium-grained central portions. The widths of the sills range from a few centimeters to several meters. The contacts between the pyroxenite sills and the sedimentary rocks are sharp and may be defined by thin (< 2 mm) reaction rims. Notably, no sills were observed within the Platreef. This may be a coincidence or could indicate that the sills are older than the Platreef. More information from other borehole intersections is necessary to constrain this question.

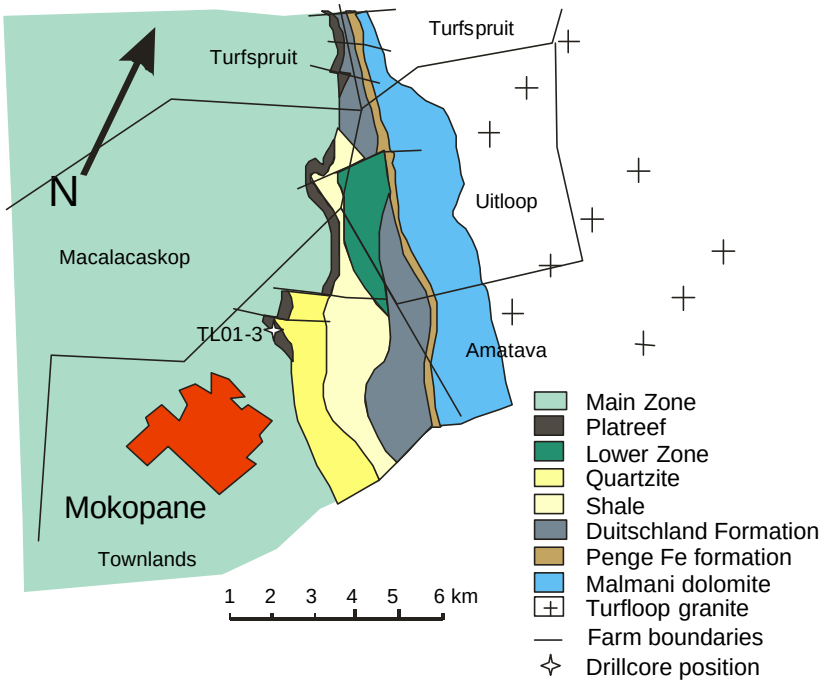

Fig. 4.1: Geological map of the Platreef on the farm Townlands and the location of borehole TL01-3. Map from Falconbridge Ventures of Africa (Pty) Ltd.

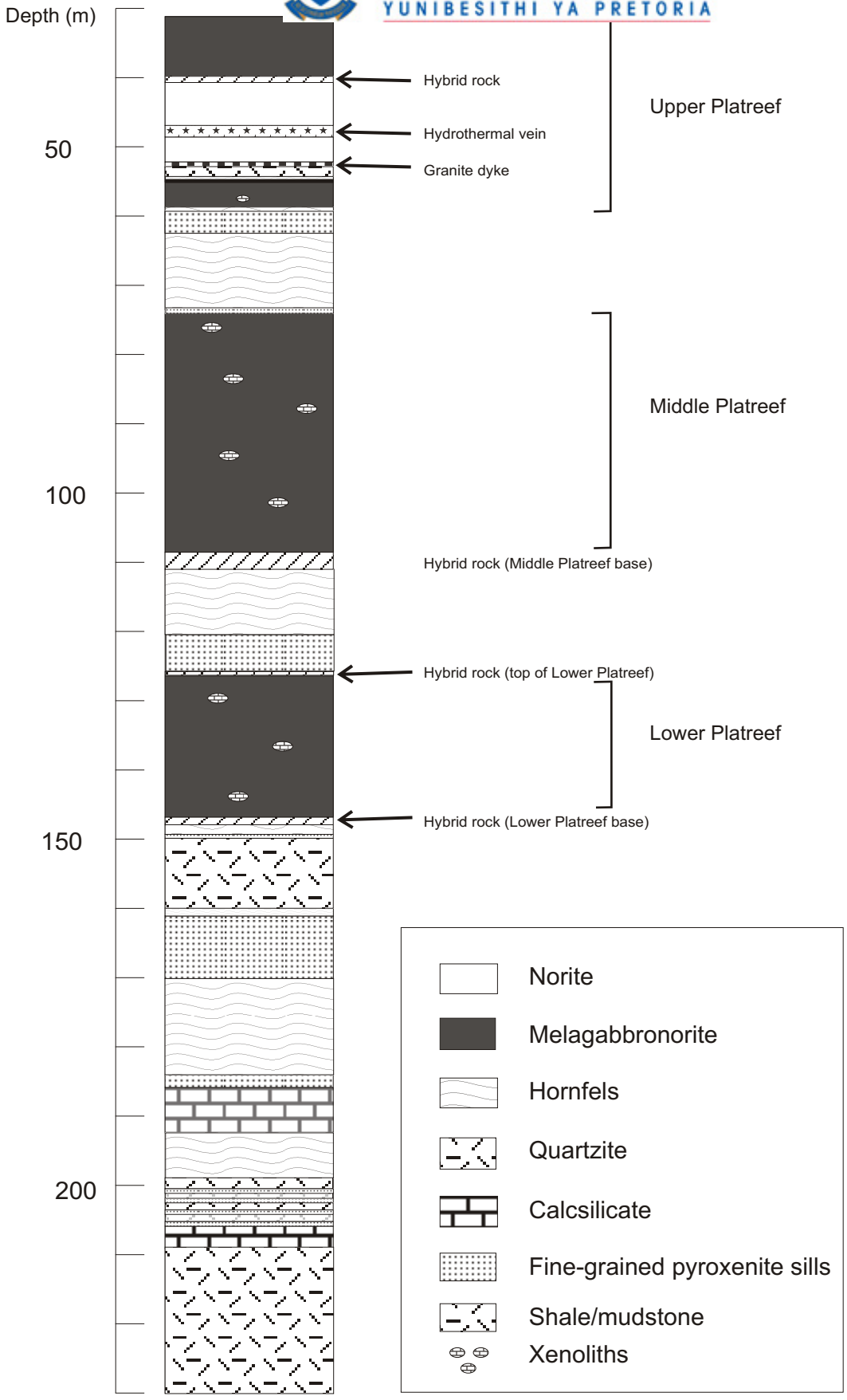

Fig. 4.2: Generalised stratigraphic column through the Platreef on the farm Townlands (from Manyeruke, 2003).

In general terms, the Platreef on Townlands consists of medium-grained gabbronorite and olivine melagabbronorite. Manyeruke (2003) distinguished three distinct units, a Lower, Middle and Upper Platreef (Fig. 4.2). The individual units are separated by thick (several 10s of meters) intervals consisting of hornfels and fine grained pyroxenite sills.

The Lower Platreef is noritic to gabbronoritic in composition, with minor pyroxenitic domains. The contact between the Lower Platreef and the quartzitic floor rocks is formed by a hybrid zone which consists of highly altered metasedimentary rocks apparently injected by medium grained, non-mineralized pyroxenite. Alternatively, the hybrid rock may represent pyroxenite containing a dense load of sedimentary xenoliths. A clear distinction between the two possibilities is not possible in the borehole core.

A ca ~18 m interlayer consisting of 1 m of hybrid rock, 6m of fine-grained pyroxenite overlain by ferruginous hornfels and ca 3 m of hybrid rock separates the Lower Platreef from the Middle Platreef. The hybrid rocks are similar in appearance to the ones described earlier. The fine-grained pyroxenite is interpreted to belong to the suite of sills described above. The Middle Platreef is approximately 35 m thick and consists mainly of a medium grained, olivine bearing, gabbronorite with a heterogeneous texture. Pegmatoidal patches are abundant and represent a local increase in modal proportion and grain size of feldspars intergrown with dark, altered olivine and greyish-green pyroxene. Coarse sulphides of up to 3 cm in size are preferably associated with the felsic pegmatoidal domains, whereas fine-grained

sulphides are found in the more even-textured gabbronorite. Xenoliths of metadolomite are not uncommon and are usually pervasively serpentinised. In the vicinity of the xenoliths, the igneous rocks show a progressive increase in the degree of serpentinisation and in modal olivine. Interaction between the xenoliths and the intrusive rocks is also evident by means of coarse-grained to pegmatoidal textures in the intrusives surrounding the xenoliths.

A hornfels interlayer, ca. 10 m (similar to the one between the Lower and Middle Platreef) overlain by a 3 m fine-grained pyroxenite sill barren of sulphide mineralization (59.55 – 62.83m) separates the Middle Platreef from the Upper Platreef. The lower and upper contacts of the sill are sharp and the Platreef rocks adjoining the contact are medium grained pyroxenites/gabbronorites, broadly similar in appearance to the Middle Platreef, but somewhat more melanocratic. As in the case of the Lower and Middle Platreef, there is no chilled margin developed at the contact of the Platreef with the hornfels. The pyroxenite/gabbronorite has about 12 % interstitial plagioclase in the upper portions decreasing to about 3 % in the lower portions. Sulphides are mainly present in the form of fine disseminations and irregular interstitial blebs of pyrrhotite and minor chalcopyrite. More massive sulphide patches (up to 3 cm) may also be developed locally. The Upper Platreef contains an intervening 13 m noritic package (41.44 to 54.62 m). The norite has a markedly different appearance to the Platreef pyroxenite/gabbronorite. It is medium grained and contains 50 – 60 % plagioclase and 40-50 % orthopyroxene. Minor (< 1 %) sulphides (chalcopyrite and pyrrhotite) occur as fine disseminations within the norite. The contact between the upper portion of the norite and the overlying

pyroxenite/gabbronorite of the Upper Platreef is defined by a ca 1.5 m fine-to medium grained hornfels layer grading into a hybrid zone similar to the ones at the contacts of the Lower and Middle Platreef. The hornfels is highly magnetic with magnetite reaching up to 50 modal %.

CHAPTER FIVE: PETROGRAPHY

This work follows the international standard nomenclature (IUGS) in naming the different Platreef rock types. It should be noted that new lithologies not described in chapter 3 (Geology of the Platreef on Nonnenwerth), e.g. recrystallized gabbronorite will be discussed in this chapter. It was not possible to pick up such lithologies on hand specimen as these rocks are relatively thin and occur at the interface between two different lithologies probably as a secondary feature i.e. recrystallization.

The modal abundances of major rock forming minerals are given below.

Rock type	Plag-ioclase (modal %)	Ortho-pyroxene (modal %)	Clino-pyroxene (modal %)	inverted pigeonite (modal %)	Minor phases
Platreef Gabbronorite and recrystallized	46-68	32-48	5-10	15-20	amphibole, biotite, magnetite, sericite and sulphides
norite	60 - 70	25-30	2-5		amphibole, sericite, chlorite, sulphides
Recrystallized norite	60-70	25-30	2-5		sulphides, sericite
Anorthosite	90-97	1-3	<1 - 7		sericite, amphibole, sulphides
Gabbro	58 - 62		38-42		sericite, chlorite, amphibole and spinel
Main Zone gabbronorite	55-65	10-15	8-10	5-10	amphibole, sericite, biotite, sulphides, clay

5.1 Platreef

5.1.1 Gabbronorite

Gabbronorites are the most abundant rocks at Nonnenwerth and constitute about 80 - 85 % of the Platreef. The gabbronorites are mostly medium grained, but finer grained varieties may occur in places. Plagioclase (48 - 65 modal %) occurs as subhedral, equant to prismatic, poorly twinned crystals (up to 4 mm) and as an interstitial phase. The crystals show evidence of minor deformation in the form of bent lamellae (Fig. 5.1a). Slight deuteric alteration to sericite (particularly along cracks and fractures) and to patchy, fine grained, brown clays is common (Figs. 5.1b, c and d).

Orthopyroxene (32 - 48 modal %) forms subhedral granular crystals and anhedral poikilitic crystals (up to 1.5 mm) enclosing anhedral plagioclase crystals that are mostly < 0.3 mm in size (Fig. 5.1e). Orthopyroxene typically contains irregular exsolution lamellae and blebs of clinopyroxene. Minor to moderate alteration of orthopyroxene to uralite along cleavage planes (Figs. 5.1b and c) and along grain margins to amphibole, biotite and oxides is common.

Clinopyroxene (5 – 10 modal %) forms anhedral and subhedral grains, reaching up to 7 mm in size that may form simple twins. Orthopyroxene exsolution lamellae are developed parallel to prismatic cleavages. They may coalesce to form blebs that are mostly altered to amphibole and sericite, with iron oxides forming along the cleavage planes. Clinopyroxene is commonly replaced by hydrothermal veinlets filled with uralite.

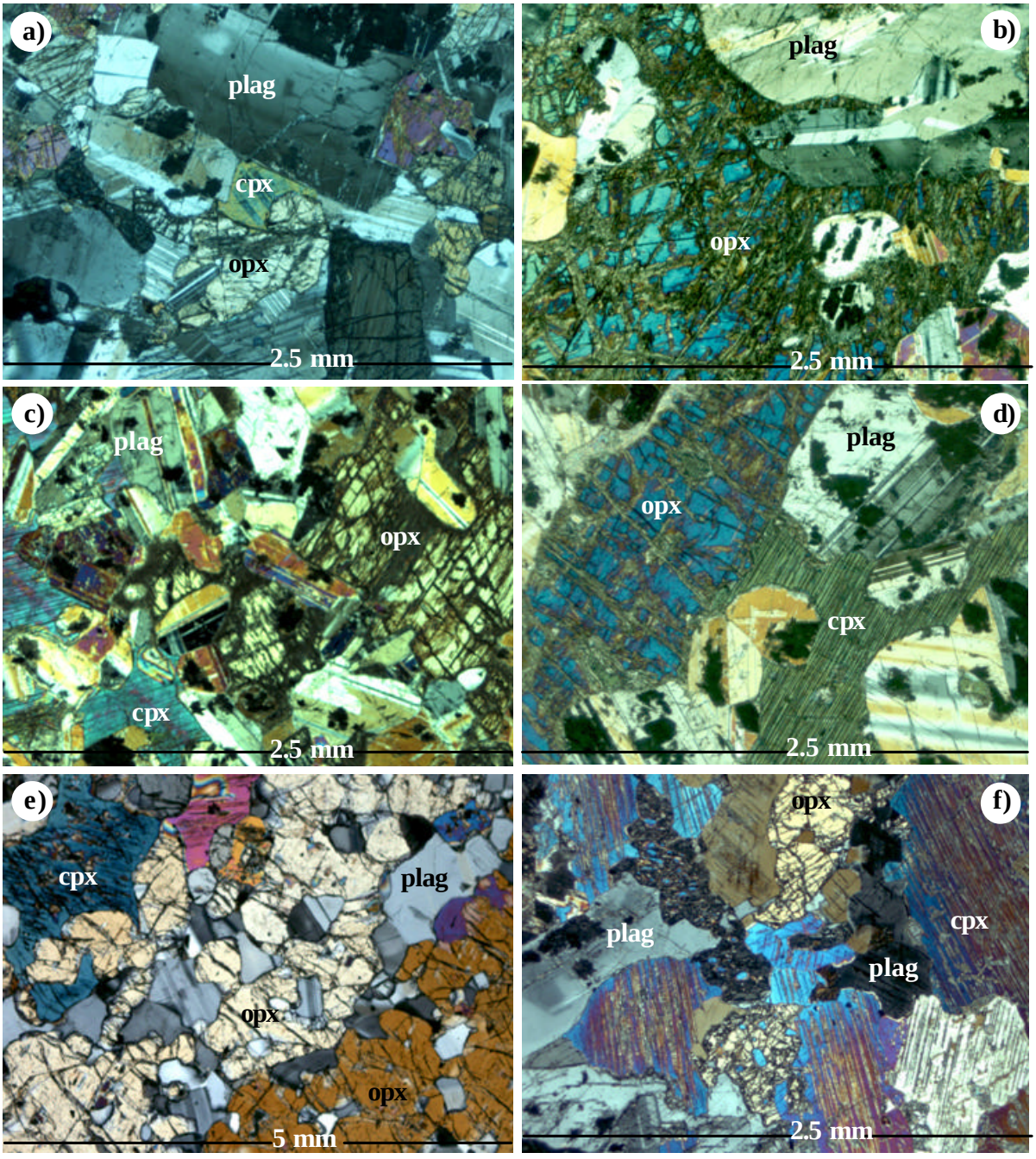

Fig. 5.1: **Platreef Gabbronorite** (a) Cumulus plagioclase (plag) and orthopyroxene (opx) with interstitial clinopyroxene (cpx), sample MO 20. (b, c and d) Orthopyroxene moderately altered to uralite along fractures, samples MO 63, MO 65 and MO 68, respectively. Note the patchy alteration to dark brown clays in plagioclase, the intercumulus nature of clinopyroxene, and the poikilitic nature of orthopyroxene and clinopyroxene. (e) Poikilitic orthopyroxene enclosing plagioclase. Clinopyroxene is interstitial and partially encloses orthopyroxene, sample MO 20. (f) Cumulus and intercumulus plagioclase intergrown with clinopyroxene that partially encloses orthopyroxene, sample MO 74. Transmitted cross polarised light.

Inverted pigeonite (15 - 20 modal %) is developed in places. This forms poikilitic, anhedral or subhedral crystals that enclose corroded plagioclase and, occasionally, clinopyroxene and orthopyroxene. Inverted pigeonite is characterised by thick, bleb-like lamellae of exsolved augite. Occasionally, two sets of augite exsolution lamellae are developed with the second set at about 74^0 to (100) in the zone of (010).

Minor phases are biotite, magnetite and sulphides. Biotite occurs around altered orthopyroxene where the latter is in contact with plagioclase or as flakes in orthopyroxene metamorphosed to amphibolite facies grade. The sulphides (< 1 modal %) consist of pyrrhotite, pentlandite, chalcopyrite and pyrite. Chalcopyrite and pyrrhotite occur intergrown in small interstitial blebs, or as fine disseminations in orthopyroxene altered to amphibole and chlorite. Pyrite forms veinlets, predominantly in plagioclase. Magnetite is interstitial and tends to be associated with the sulphides. In general, the rocks are poorly mineralized.

5.1.2 Norite

Norites constitute ca. 3 to 5 % of the Platreef rocks. Norites occur as medium grained rocks with no obvious mineral fabric. They are composed mostly of plagioclase and orthopyroxene with minor interstitial augite. Plagioclase (60 to 70 modal %) is mostly an intercumulus phase (Fig. 5.2a). It occurs as anhedral or subhedral, medium grained (up to 1.5 mm) oikocrysts as well as equant and lath-shaped crystals. Occasionally, polysynthetic twinning may be developed. Moderate to strong alteration of plagioclase to sericite and to patchy, dark brown, fine grained, clays is common.

Orthopyroxene (25 to 30 modal %) occurs as medium grained (< 2 mm) subhedral, equant to elongate, prismatic grains (Fig. 5.2a). Fine clinopyroxene exsolution lamellae are commonly developed in the orthopyroxene crystals. Orthopyroxene grains are occasionally altered along fractures. Alteration minerals are fine grained brown amphibole (uralite) and chlorite which may also partially replace adjacent plagioclase grains. Orthopyroxene may occasionally enclose a few plagioclase grains.

Augite is a minor interstitial phase constituting generally between 2 - 5 modal %, and forming anhedral grains that occasionally enclose small rounded orthopyroxene and plagioclase grains (Fig. 5.2c). Thin (100) lamellae of exsolved orthopyroxene are commonly developed. Augite may be altered to chlorite and amphibole, mostly along cleavage planes, with the alteration phases sometimes invading adjacent plagioclase. In places, norites may be biotite- and sulphide-rich (up to 5 modal %). Sulphides consist of chalcopyrite and pentlandite with minor pyrrhotite and secondary pyrite. Sulphides and biotite occur associated with each other in the interstitial space (Fig. 5.2d). Pyroxenes located adjacent to the biotite and sulphides tend to be highly altered to fine grained amphibole and chlorite.

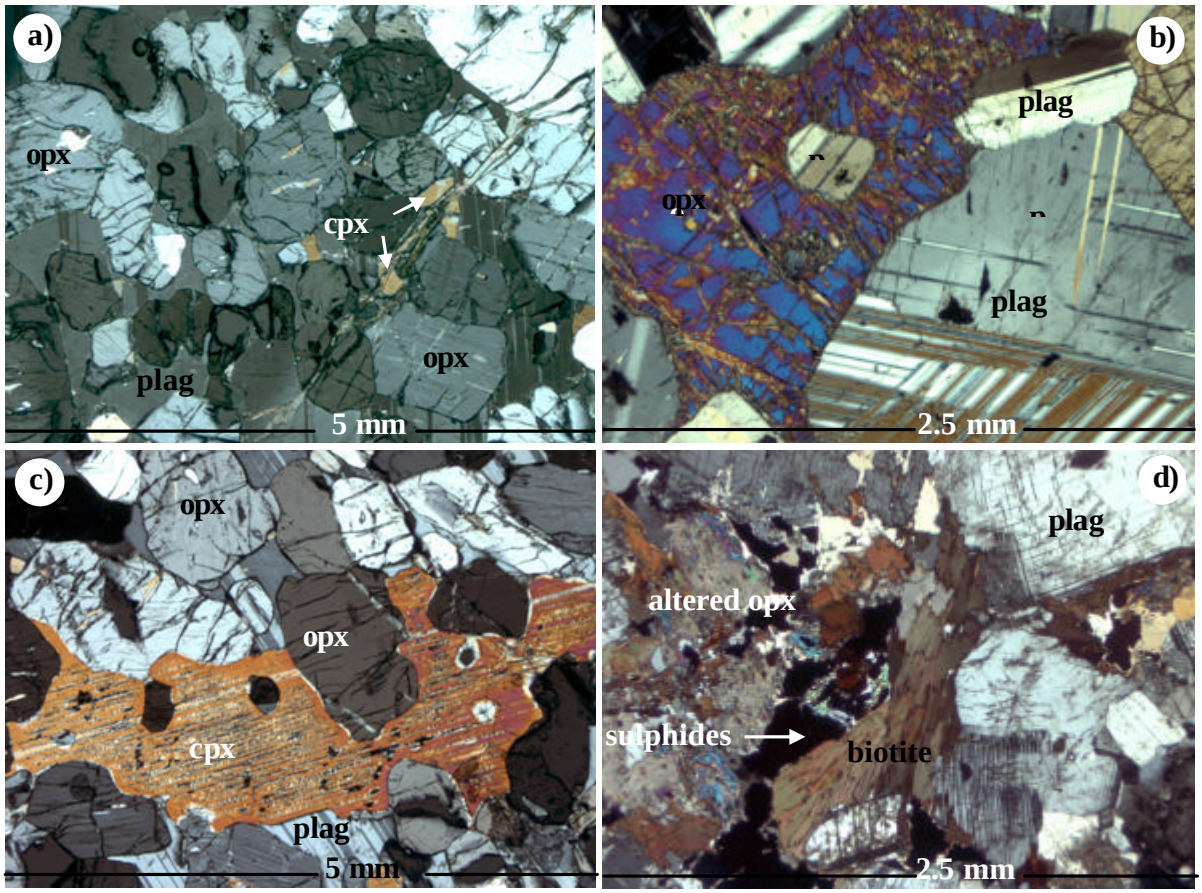

Fig. 5.2: **Norite:** (a) Cumulus orthopyroxene (opx) intergrown with interstitial plagioclase (plag), and minor clinopyroxene (cpx), sample MO 67. (b) Orthopyroxene interstitial to plagioclase and containing anhedral inclusions of plagioclase, sample MO 19. (c) Cumulus orthopyroxene with intercumulus plagioclase and clinopyroxene. Note the small, subrounded orthopyroxene enclosed in clinopyroxene. Sample MO 18. (d) Cumulus plagioclase and orthopyroxene highly altered to amphibole and chlorite with interstitial sulphides rimmed by brown biotite, sample MO 75. Transmitted cross polarised light.

5.1.3 Recrystallized gabbronorite and norite

5.1.3.1 Recrystallized gabbronorite

Recrystallized gabbronorites occur mostly towards the upper half of the Platreef where they form relatively thin layers at the contact between different rock types, possibly due to shearing during intrusion. They constitute ca. 4 - 6 % of the Platreef

rocks. The recrystallized gabbronorites are fine- to medium grained and characterised by clusters of small (up to 0.4 mm) orthopyroxene and plagioclase crystals that are situated between, and adjacent to, coarse plagioclase, orthopyroxene and clinopyroxene crystals (Fig. 5.3a and b). Modal proportions of the minerals are similar to those of other gabbronorites in the Platreef.

Plagioclase forms coarse (up to 6 mm) subhedral crystals that are polysynthetically twinned, or small (up to 0.4 mm) subrounded and recrystallized grains. The large plagioclase grains have bent twin lamellae and show undulose extinction (Fig. 5.3b). The lamellae may be tapered away from grain margins. Fine grained plagioclase occurs as interlocking grains with 120° triple junctions (Fig. 5.3a and b). The above features suggest deformation. Plagioclase is slightly to moderately altered to sericite and patchy dark brown clays.

Orthopyroxene may form coarse, anhedral (up to 5 mm) crystals enclosing plagioclase, or aggregates of small (< 0.3 mm) subhedral to subrounded crystals with 120^0 triple junctions (Fig. 5.3a and c). Orthopyroxene is commonly altered to uralite along fractures and cleavage planes. Clinopyroxene may occur as coarse, up to 10 mm, but more often less than 3 mm wide grains containing orthopyroxene exsolution lamellae and simple twins (Fig. 5.3b). The coarser grains are often deformed as evidenced by bent/curved orthopyroxene lamellae (Fig. 5.3c). Sulphides (up to 4 modal %) include pyrrhotite, subordinate chalcopyrite and pentlandite, and minor

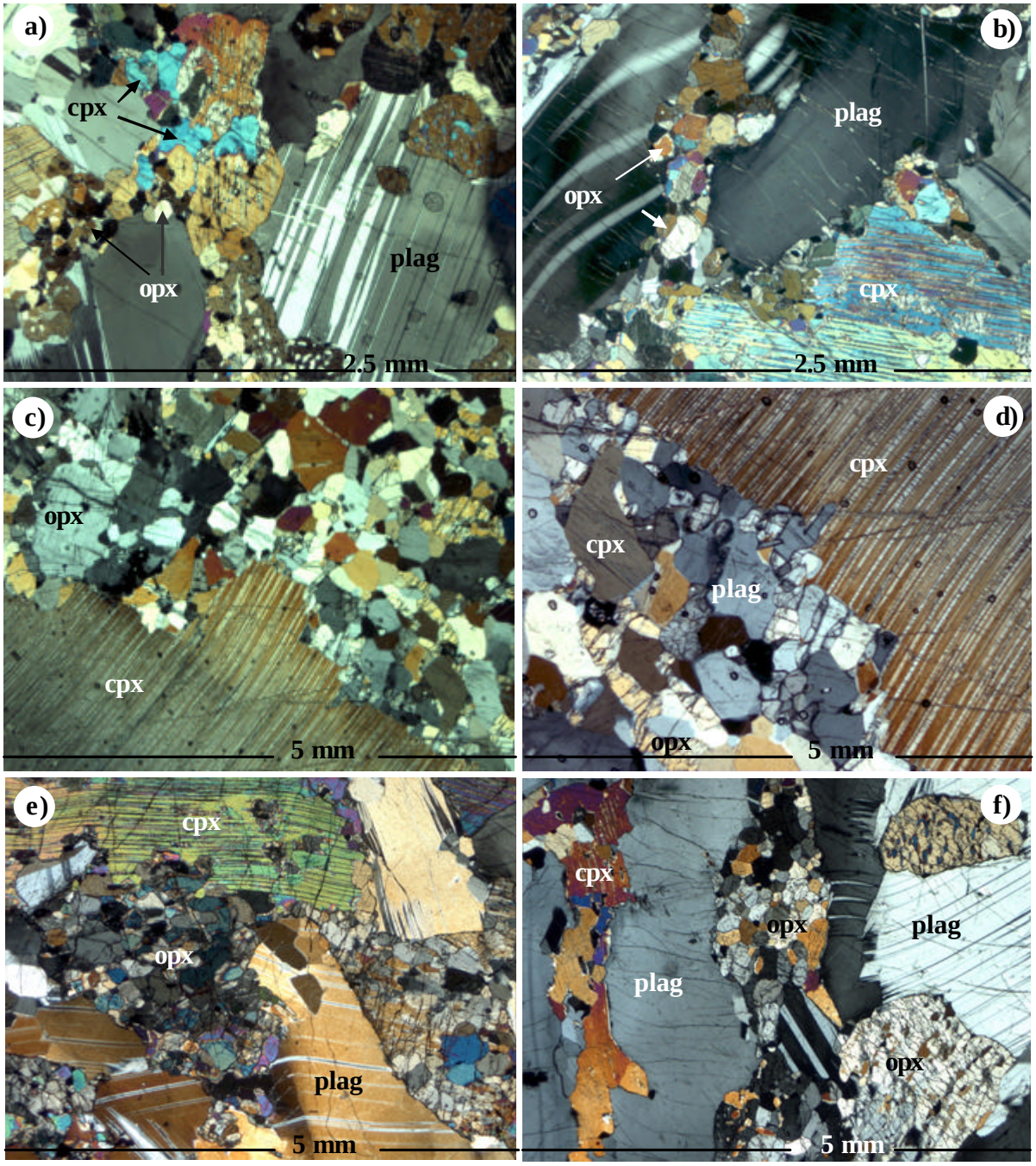

Fig. 5.3 **Recrystallized gabbronorite** (a and b) Recrystallized orthopyroxene (opx) and minor clinopyroxene (cpx) along deformed plagioclase grain boundaries, sample MO 70. (c and d) Recrystallized gabbronorite in contact with coarse clinopyroxene from medium to coarse grained gabbronorite, sample MO 66. Note the bent lamellae in clinopyroxene and plagioclase. (e and f) Recrystallized orthopyroxene and clinopyroxene along strained plagioclase margins and fractures, sample MO 12 and MO 70, respectively. Transmitted cross polarised light.

pyrite. Rare intergrown magnetite and ilmenite grains may be associated with recrystallized orthopyroxene grain boundaries or they may occasionally be intergrown with pyrrhotite.

It is notable that gabbronorite adjacent to the recrystallized domains tends to be extensively hydrothermally altered. As a result the pyroxenes are altered to amphibole and chlorite and cut by hydrothermal veinlets filled with fine grained amphibole. Plagioclase is chloritised and sericitised, particularly when in contact with interstitial sulphides. The fluids responsible for this alteration were probably derived from the recrystallized domains. Importantly, the recrystallized gabbronorite and the adjacent altered gabbronorite are among the best mineralized lithologies.

5.1.3.2 Recrystallized norite

Norites within the Platreef may also locally be recrystallized, constituting ca. 1 % of the Platreef. The rocks occur at and towards the base of the Platreef. They are fine grained and show no change in modal abundances relative to undeformed norites. Plagioclase (60 to 70 modal %), is anhedral or subhedral, lath-shaped and mostly of intercumulus habit (Fig. 5.3g). Occasionally, polysynthetic twinning may be developed and the plagioclase may enclose orthopyroxene (Fig. 5.3g).

Orthopyroxene (25 to 30 modal %) occurs as fine grained (< 0.5 mm) subhedral, equant to elongate or subrounded crystals (Fig. 5.3 g and h). Orthopyroxene may occasionally enclose plagioclase grains. Augite is a minor interstitial phase constituting generally between 2 - 5 modal % of the rock and forming anhedral grains

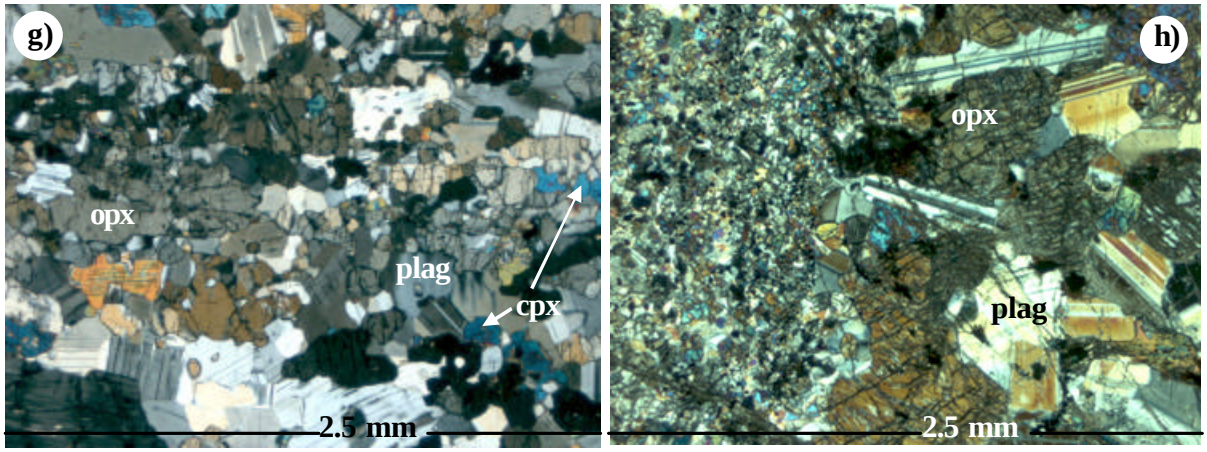

Fig. 5.3: **Recrystallized norite:** (g) Subrounded orthopyroxene intergrown with plagioclase and in places enclosed in plagioclase, sample MO 17. (h) Fine-grained recrystallized norite in contact with medium grained gabbronorite, sample MO 84.

that occasionally contain thin (100) lamellae of exsolved orthopyroxene. Recrystallized norite is generally barren containing only traces of chalcopyrite, pentlandite and pyrrhotite.

5.1.4 Anorthosite

Anorthosites constitute ca. 9 – 11 % of the Platreef rocks. The anorthosites are medium-grained or, locally, pegmatoidal. They contain between 1 and 7 modal % pyroxene. Plagioclase (90 - 97 modal %) occurs as randomly oriented, elongate, subhedral cumulus crystals (up to 25 mm long) forming an adcumulate texture (Fig. 5.4a). In pegmatoidal varieties, plagioclase may be replaced by clinopyroxene along cleavage planes (Fig. 5.4b and c.). Most plagioclase crystals have irregular margins but are mutually interlocking with each other. Patchy alteration to dark brown, fine grained clays is pronounced giving the thin section and hand specimen a white speckled appearance when viewed with the naked eye. Along grain boundaries with oxides, plagioclase may be altered to radiating chlorite, minor amphibole and biotite.

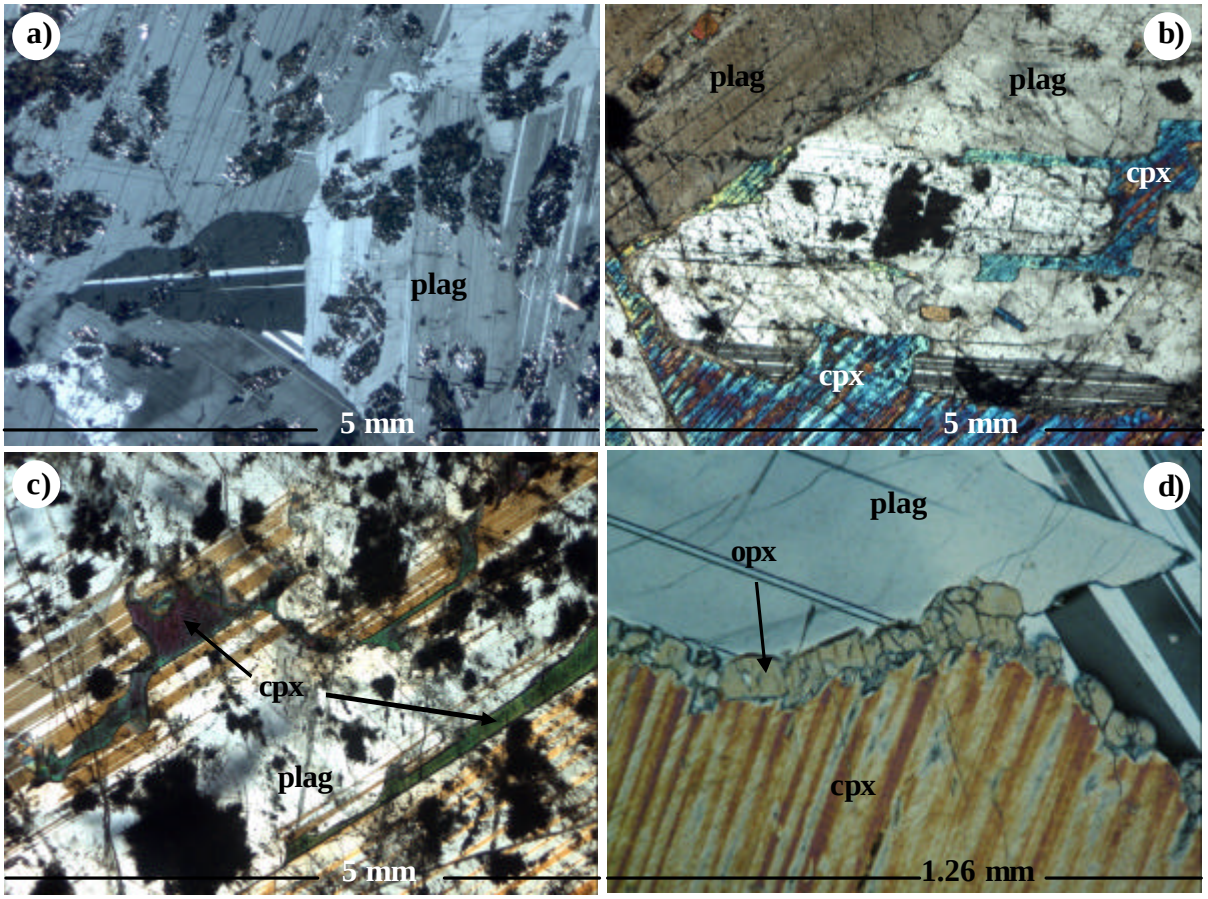

Fig. 5.4. **Anorthosite** a) Plagioclase (plag) crystals patchily altered to dark brown clays, sample MO 8. (b and c) Plagioclase replaced by clinopyroxene (cpx) along cleavage planes and fractures. Also note the patchy alteration to dark brown clays, sample MO 68 and MO 73, respectively. (d) Clinopyroxene rimmed by orthopyroxene (opx) – plagioclase intergrowth when in contact with plagioclase, sample MO 27. Transmitted cross polarised light.

In fractures, sericite alteration dominates.

Clinopyroxene (< 1 – 7 modal %) forms large interstitial crystals (up to 9 mm long) that contain orthopyroxene lamellae along the prismatic cleavage. Some portions of the grains are hydrothermally altered to tremolite and oxides. Clinopyroxene locally includes small plagioclase grains (~1 mm). When in contact with plagioclase, clinopyroxene is rimmed by coronas of orthopyroxene – plagioclase intergrowth (Fig.

5.4d) suggesting localized partial melting processes resulting from emplacement of the gabbronorites. Crystallization of the melt produced plagioclase and orthopyroxene at the expense of clinopyroxene. Orthopyroxene (1 – 3 modal %) forms coarse interstitial grains, up to 9 mm in size, containing fine clinopyroxene exsolution lamellae. The orthopyroxene crystals may be partially altered to green amphibole. Sulphides (~ 3 modal %) mostly occur interstitial to, or along, plagioclase fractures and include pyrrhotite, subordinate chalcopyrite and pentlandite, and minor pyrite.

5.1.5 Gabbro

Gabbros are rare in the Platreef and occur as thin lenses within gabbronorites. The gabbros are medium grained rocks consisting mostly of plagioclase (58 - 62 modal %) and clinopyroxene (38 – 42 modal %). Plagioclase occurs as elongate subhedral to euhedral laths which display polysynthetic twinning and have no preferred orientation. The crystals are mostly unaltered, although minor sericite alteration may occur along fractures. Fine grained dark brown clays may form patchy zones within the crystals.

Clinopyroxene forms large (up to 9 mm) cumulus or interstitial, anhedral or subhedral crystals, with orthopyroxene lamellae occurring along prismatic cleavage planes. The orthopyroxene lamellae may coalesce and form blebs (Fig. 5.5a and c). Some crystals are hydrothermally altered to chlorite, amphibole and minor green spinel. When in contact with plagioclase, clinopyroxene reacts to form orthopyroxene coronas (Fig. 5.5c). Orthopyroxene is a minor phase and occurs as cumulus or intercumulus crystals with abundant fine clinopyroxene exsolution lamellae. Orthopyroxene is moderately to intensely altered to fine grained uralite.

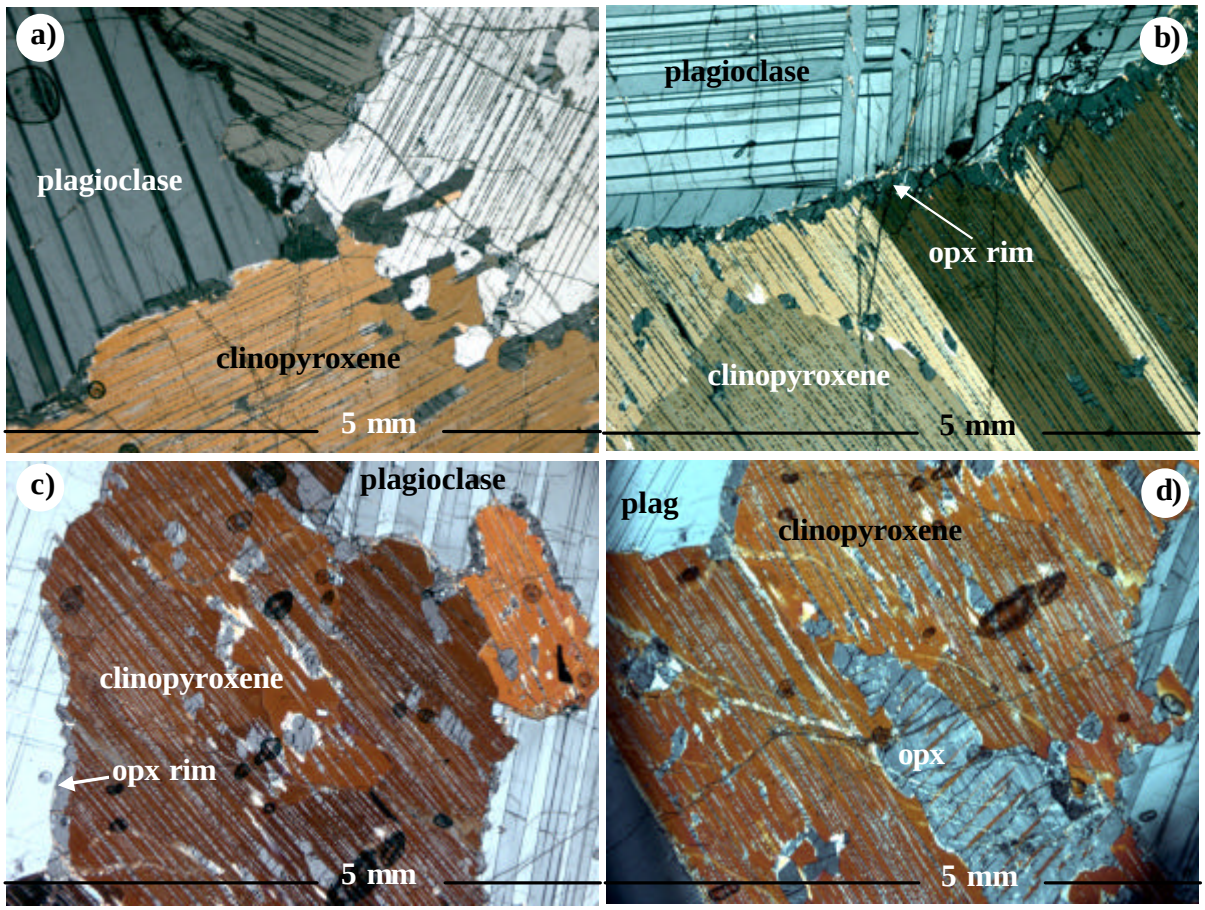

Fig. 5.5: **Gabbro** (a-d) Clinopyroxene with exsolved blebs and lamellae of orthopyroxene (opx) intergrown with plagioclase. Note the thin orthopyroxene corona around clinopyroxene when in contact with plagioclase in Fig. 5.4b.

5.1.6 Serpentinized peridotite

Serpentinites constitute les than 2 % of the Platreef rocks. These include some partially altered peridotites (Figs. 5.6a and b) occurring near the base of the sequence (Figs. 3.2 and 3.16). Serpentine occurs as veinlets and flakes replacing olivine with very high Fo contents (average 90). Subrounded and occasionally corroded orthopyroxene crystals are partially altered to green amphibole. Secondary hydrous minerals include biotite, chlorite and amphibole. Chlorite and amphibole are mostly found associated with the oxides.

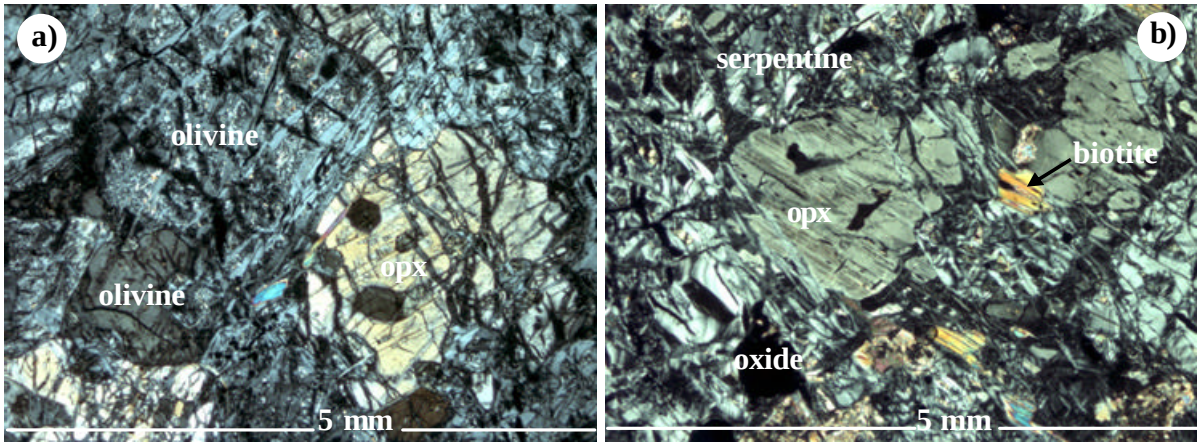

Fig. 5.6: **Serpentinized peridotite** (a and b) Relict, partially serpentinised olivine and orthopyroxene, sample MO 26. Note the biotite flakes intergrown with serpentine in b. Transmitted cross polarised light.

5.2 Main Zone

In the two boreholes examined, the Main Zone consists of medium grained gabbronorite characterised by plagioclase, orthopyroxene, inverted pigeonite and augite. The gabbronorite has an adcumulus to mesocumulate texture and exhibits a subtle mineral fabric defined by sub-parallel alignment of pyroxene and plagioclase laths (Fig. 5.7a).

Plagioclase (55 to 65 modal %) forms subhedral or euhedral, equant or lath-shaped, mostly medium-grained (up to 9 mm) cumulus grains. The grains show prominent polysynthetic twinning. Plagioclase shows evidence of increased deformation with depth, characterised by bent twin lamellae and undulous extinction (Fig. 5.7a and b). Alteration of plagioclase to patchy, fine grained dark brown clays and sericite is common.

Orthopyroxene (10 – 15 modal %) forms medium grained (0.5 to 8 mm), subhedral or anhedral, equant to prismatic, cumulus and intercumulus grains. The orthopyroxene grains are weakly pleochroic in pale yellowish-brown to pale green shades. Orthopyroxene may be subophitic, partially enclosing undeformed (< 1.5 mm) plagioclase laths, and has a single set of bleb-like augite exsolution lamellae parallel to the prismatic cleavage (100). Orthopyroxene is partially altered along fractures and grain boundaries to fine grained brown amphibole (uralite), disseminated iron oxides and minor biotite, but in some cases most of the grains may be altered to green amphibole. Biotite occurs as small < 1 mm brown flakes mostly associated with interstitial sulphides in contact with pyroxenes.

Inverted pigeonite (5 – 10 modal %) occurs as anhedral, sub-poikilitic to poikilitic crystals with thick bleb-like lamellae of exsolved augite (Figs. 5.7e). Occasionally, two sets of augite exsolution lamellae are developed with the second set at about 74^0 to (100) in the zone of (010) (Figs. 5.7f). This suggests that the orthopyroxene is an iron-rich hypersthene. Plagioclase crystals may occur ophitically enclosed in inverted pigeonite (Fig. 5.7f).

Augite (8-10 modal %) forms cumulus or interstitial, subhedral or anhedral grains (up to 4.3 mm wide). The grains may show simple twinning and thin (100) lamellae of exsolved orthopyroxene. The crystals are slightly altered to fine grained amphibole, mostly along cleavage planes and internal fractures.

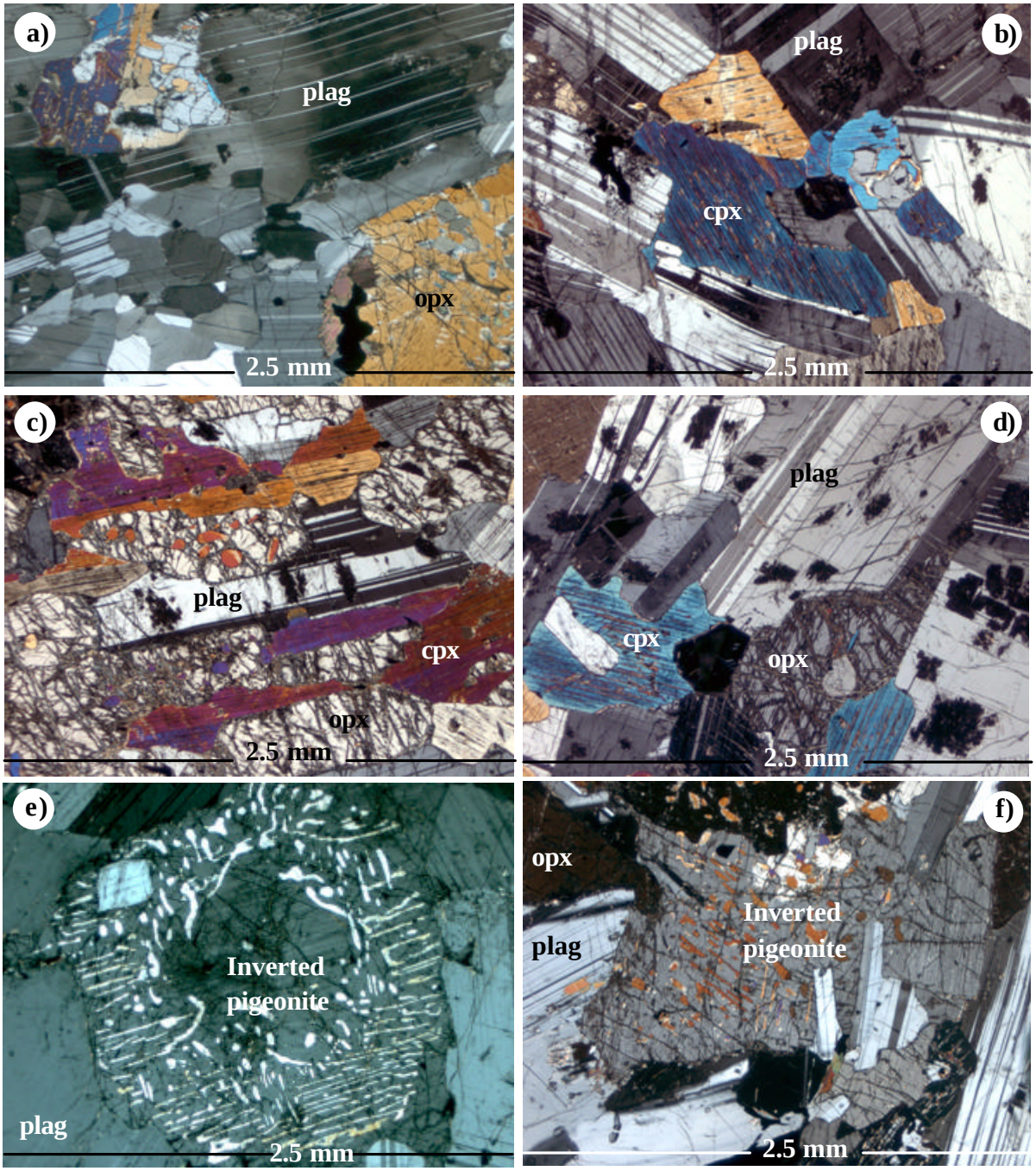

Fig. 5.7 **Gabbronorite** (a) Deformed and recrystallized plagioclase showing 120^0 triple junctions and bent twin lamellae. Small corroded plagioclase grains are enclosed in orthopyroxene (opx), sample MO 4. (b) Interstitial clinopyroxene intergrown with cumulus plagioclase. Note the deformed twin lamellae in plagioclase; sample MO 50. (c) Orthopyroxene replacing clinopyroxene, sample MO 51. (d) Interstitial clinopyroxene and orthopyroxene intergrown with cumulus plagioclase that shows patchy alteration to dark brown clays. (e and f) Sub-poikilitic inverted pigeonite with two sets of exsolved augite lamellae, sample MO 2.

CHAPTER SIX: WHOLE ROCK CHEMISTRY

6.1 CIPW norms

As the Platreef rocks from Nonnenwerth are relatively altered, I have calculated CIPW norms for the analysed samples (Fig. 6.1). The rocks are mostly gabbronorites and leucogabbronorites with normative orthopyroxene slightly dominating over clinopyroxene. This observation is in agreement with the petrographic data presented in chapter 4. However, what is notable is that the rocks also have a considerable normative olivine component. This is also observed in other Platreef intersections e.g. at Rooipoort and Townlands, but it is absent in most Upper Critical Zone rocks, e.g. the Merensky Reef from Impala mine (Barnes and Maier, 2002a). The enrichment in normative olivine in the Platreef could be explained in two contrasting ways: (i) Assimilation of a Si-poor and Mg-rich component derived from dolomite or calc-silicate as suggested by the abundance of dolomite xenoliths in the analysed sequence. (ii) Hydrothermal Si-loss of the rocks as suggested by the common alteration of the rocks, notably that of plagioclase to fine-grained clays.

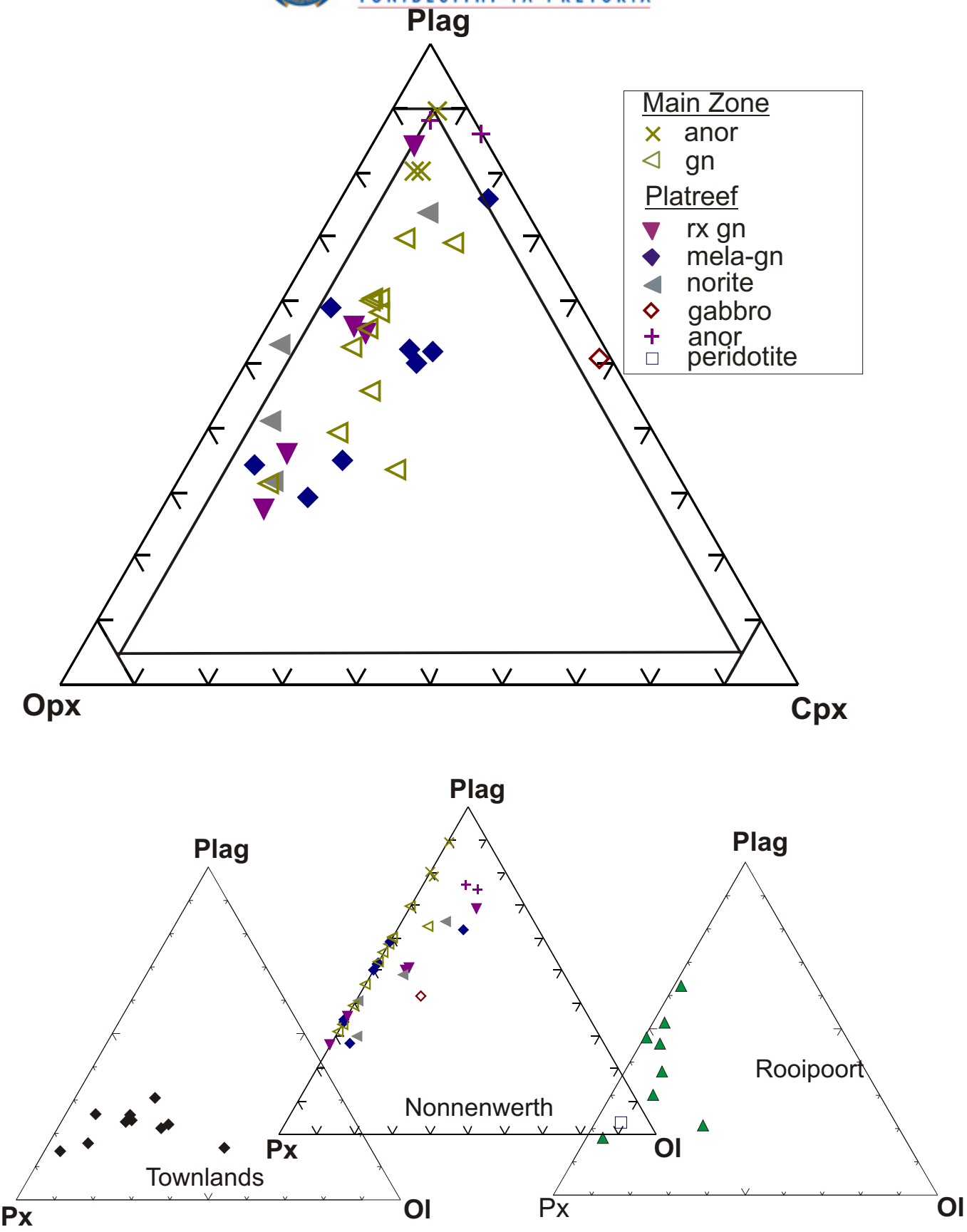

Fig. 6.1: CIPW normative compositions of Platreef samples from Nonnenwerth. gn = gabbronorite, rx = recrystallized gabbronorite, anor = anorthosite, Plag = plagioclase, Opx = orthopyroxene, Cpx = clinopyroxene, Ol =olivine. Note: Legend applies to Nonnenwerth samples only.

6.2 Lithophile geochemistry

6.2.1 Major and minor elements

Whole rock analytical results are given in Table 1. Selected major element data representing the different lithologies from the Platreef and the Main Zone at Nonnenwerth are shown in Fig. 6.2 and 6.3. The compositional fields of orthopyroxene, plagioclase and clinopyroxene, and tholeiitic (B2/B3) Bushveld parental magma (Davies and Tredoux, 1985) are also plotted. The data from both intervals (Platreef and Main Zone) essentially overlap. They define a negative correlation between MgO and Al_2O_3, CaO and Na_2O_3 (Fig. 6.2a - f) and a positive correlation between MgO and SiO_2, FeO, TiO_2 and Cr_2O_3 (Fig. 6.2g - l). Most samples plot near tielines joining plagioclase with orthopyroxene and clinopyroxene (except for the SiO_2 versus MgO plot) confirming that the chemistry of the rocks is controlled by the relative proportions of these phases and trapped melt. The data also show that plagioclase constitutes ca. 20 – 60 % of the rocks.

The relatively low SiO_2 contents of the samples are noteworthy (Fig. 6.2g and h). This may indicate the presence of calc-silicate component derived from dolomite or calc-silicate as suggested by the abundance of dolomite xenoliths in the analysed sequence, or alteration resulting in SiO_2-loss as suggested by the common alteration of the rocks, notably that of plagioclase to fine-grained clays.

Cr contents in most samples are controlled by the trapped melt and the cumulus phases i.e. clinopyroxene and orthopyroxene (Fig. 6.2m and n). However,

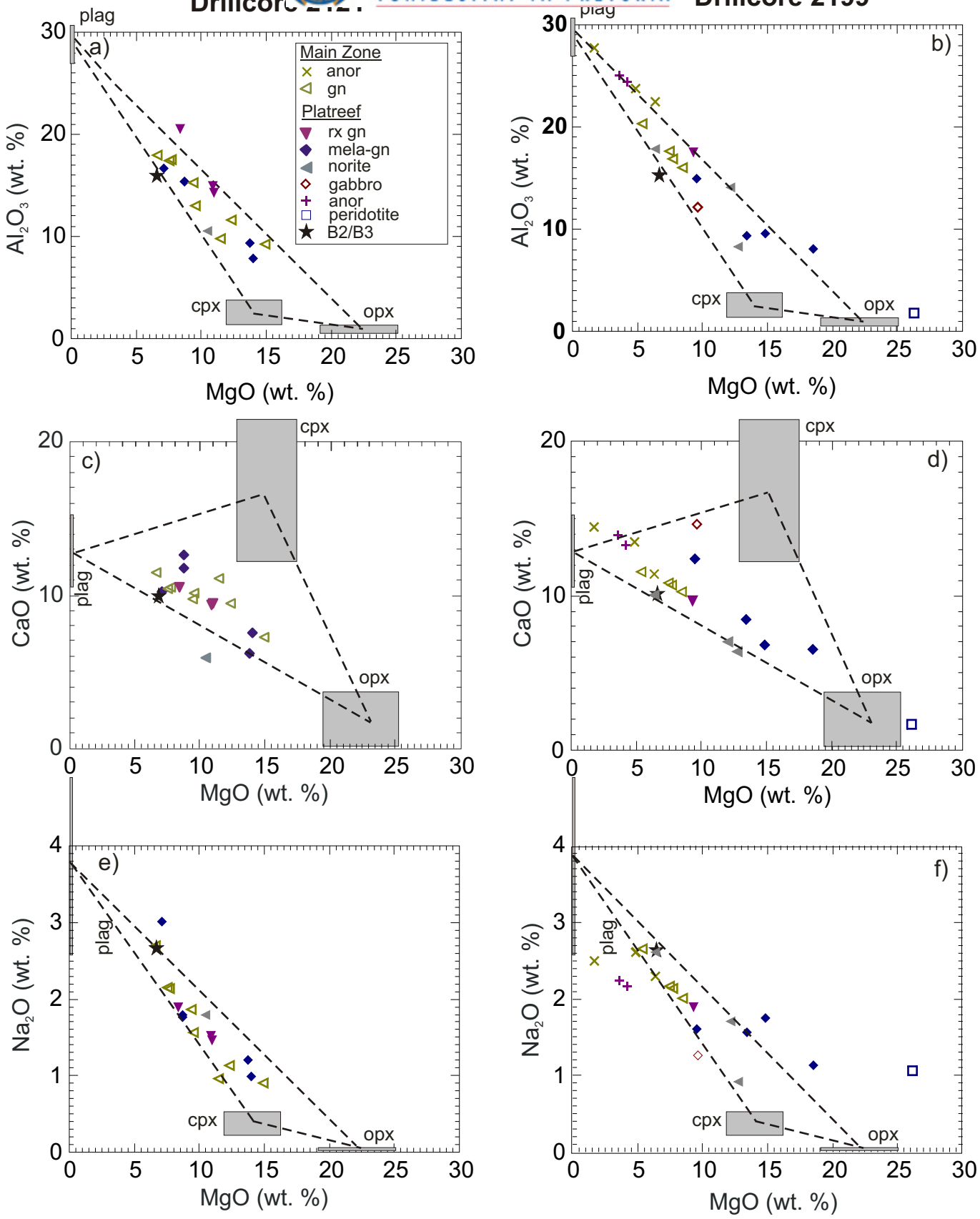

Fig. 6.2: Binary variation diagrams of (a and b) Al_2O_3 versus MgO, (c and d) CaO versus MgO and (e and f) Na_2O versus MgO in rocks from Nonnenwerth. Also plotted are compositional ranges of tholeiitic (B2/B3) Bushveld parental magma (Davies and Tredoux, 1985), and major rock forming minerals (shaded) in the Platreef on Nonnenwerth to determine which phases control the chemistry of the rocks. plag = plagioclase, cpx = clinopyroxene, opx = orthopyroxene, rx gn = recrystallided gabbronorite, gn = gabbronorite and mela-gn = mela-gabbronorite.

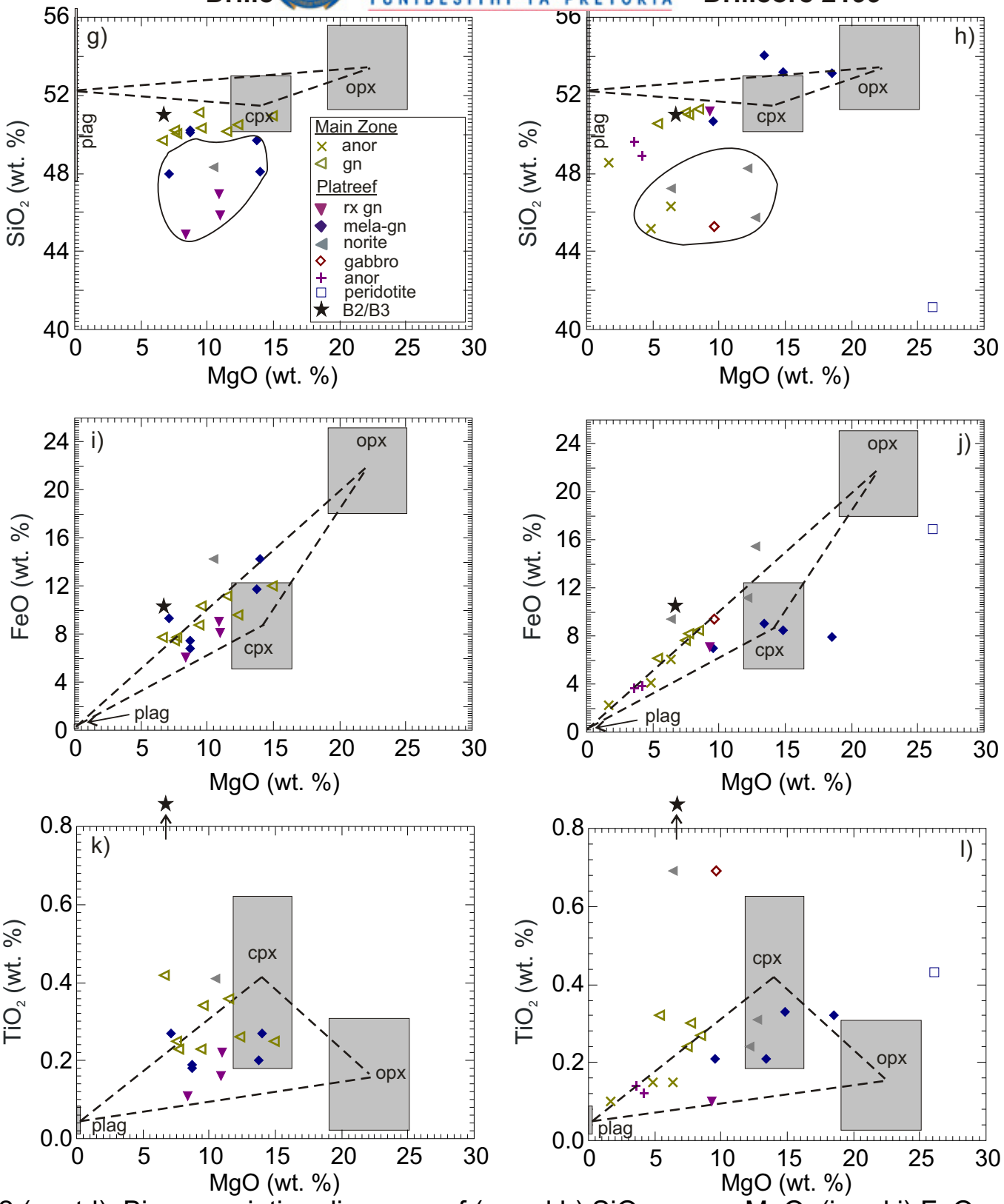

Fig. 6.2 (contd): Binary variation diagrams of (g and h) SiO_2 versus MgO, (i and j) FeO versus MgO and (k and l) TiO_2 versus MgO in rocks from Nonnenwerth. Also plotted are compositional ranges of tholeiitic (B2/B3) Bushveld parental magma (Davies and Tredoux, 1985), and major rock-forming minerals (shaded) in the Platreef on Nonnenwerth. plag = plagioclase, cpx = clinopyroxene, opx = orthopyroxene, rx gn = recrystallized gabbronorite, gn = gabbronorite and mela-gn = mela-gabbronorite.

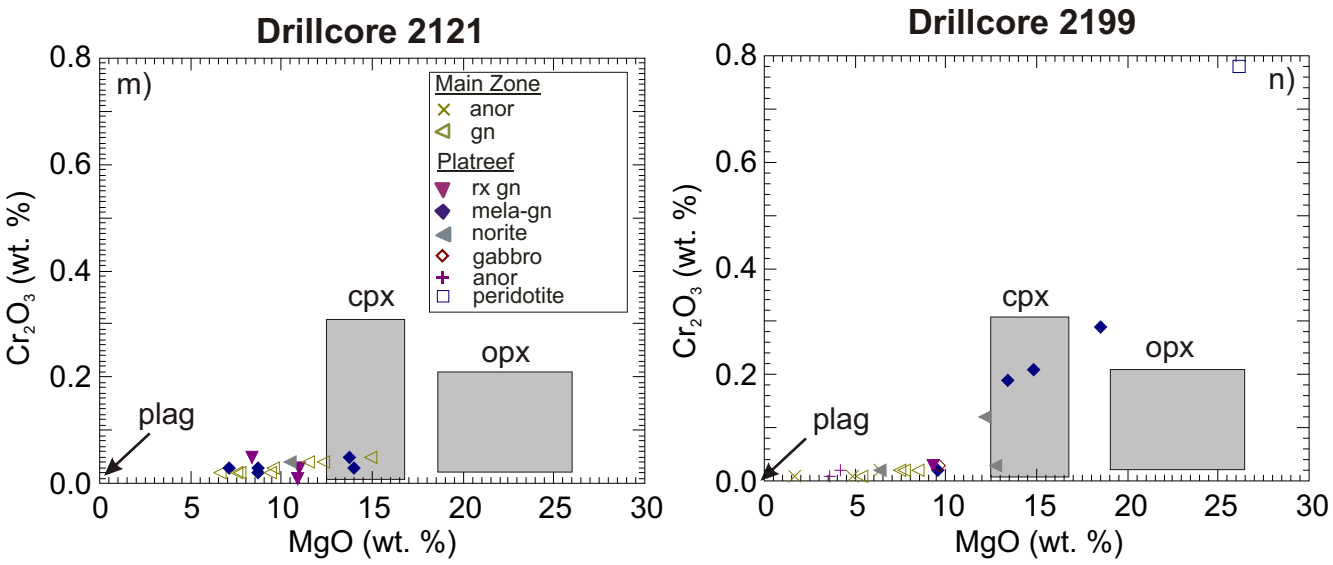

Fig. 6.2 (contd): Plot of Cr_2O_3 (m and n) versus MgO. Also plotted are major rock forming minerals (shaded). plag = plagioclase, cpx = clinopyroxene, opx = orthopyroxene, gn = gabbronorite, rx gn = recrystallized gabbronorite and mela- gn = mela-gabbronorite

serpentinised peridotite and some magnesian melagabbronorite samples from core 2199 contain cumulus chromite, as their Cr_2O_3 contents are too high to be explained by trapped melt and pyroxene alone.

MgO and Cr_2O_3 contents are plotted against depth in Fig. 6.3. The data show broadly similar MgO and Cr_2O_3 contents in the Platreef and the Main Zone, except for a distinct increase in MgO and Cr_2O_3 in some of the basal samples in drillcore 2199 with depth, and high Cr_2O_3 contents in gabbronorites towards the base of the Platreef. The data is consistent with lithological observations that the rocks become progressively more leucocratic with height.

6.2.2 Trace elements

Selected trace elements (V, Zr, Y, Sr and Sm) are plotted against MgO in Fig. 6.4. As the major rock forming minerals from the Platreef at Nonnenwerth were not analysed

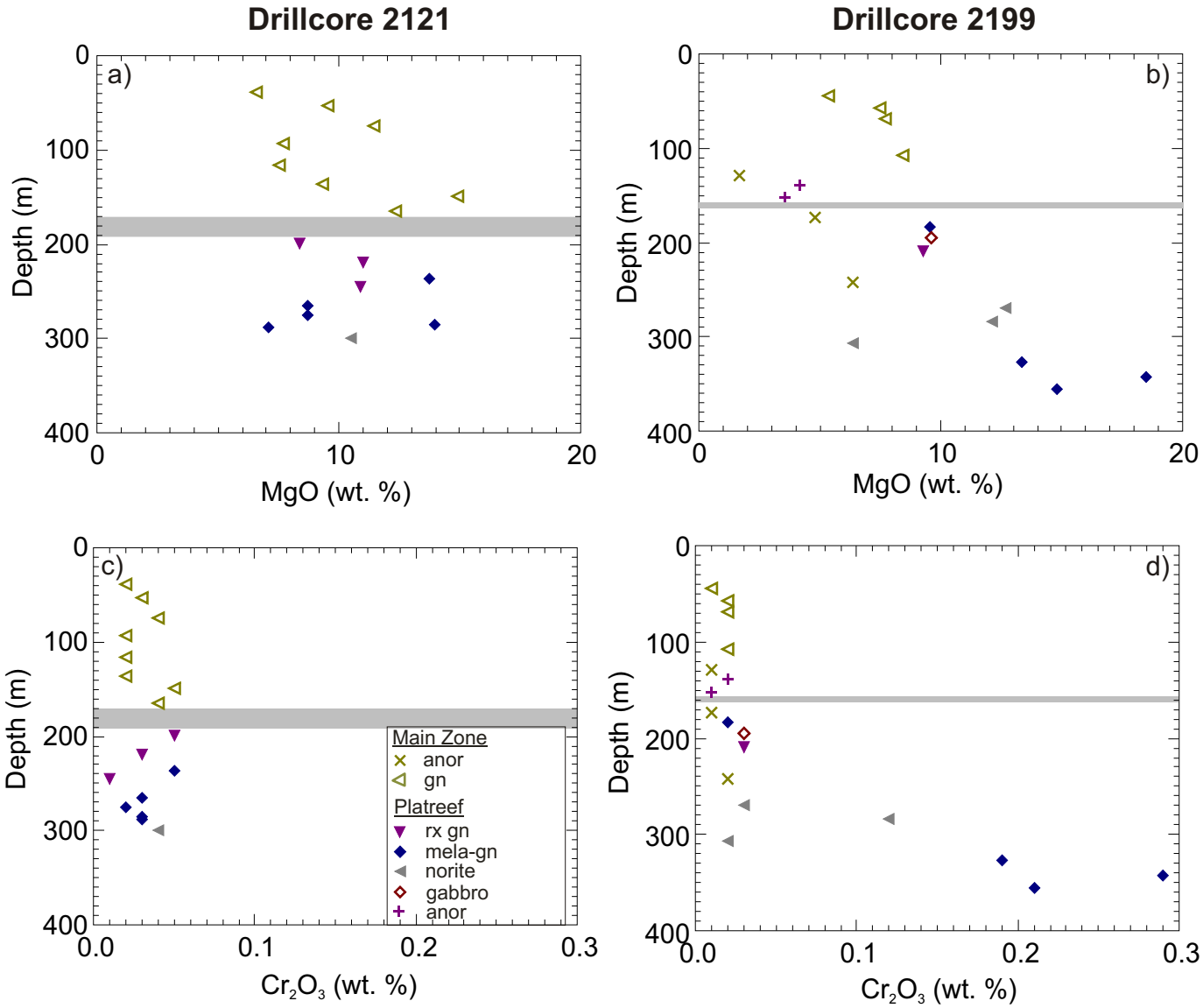

Fig. 6.3: Plot of (a and b) MgO versus depth, and Cr_2O_3 (c and d), in the Platreef at Nonnenwerth. gn = gabbronorite, rx gn = recrystallized gabbronorite and mela- gn = mela-gabbronorite

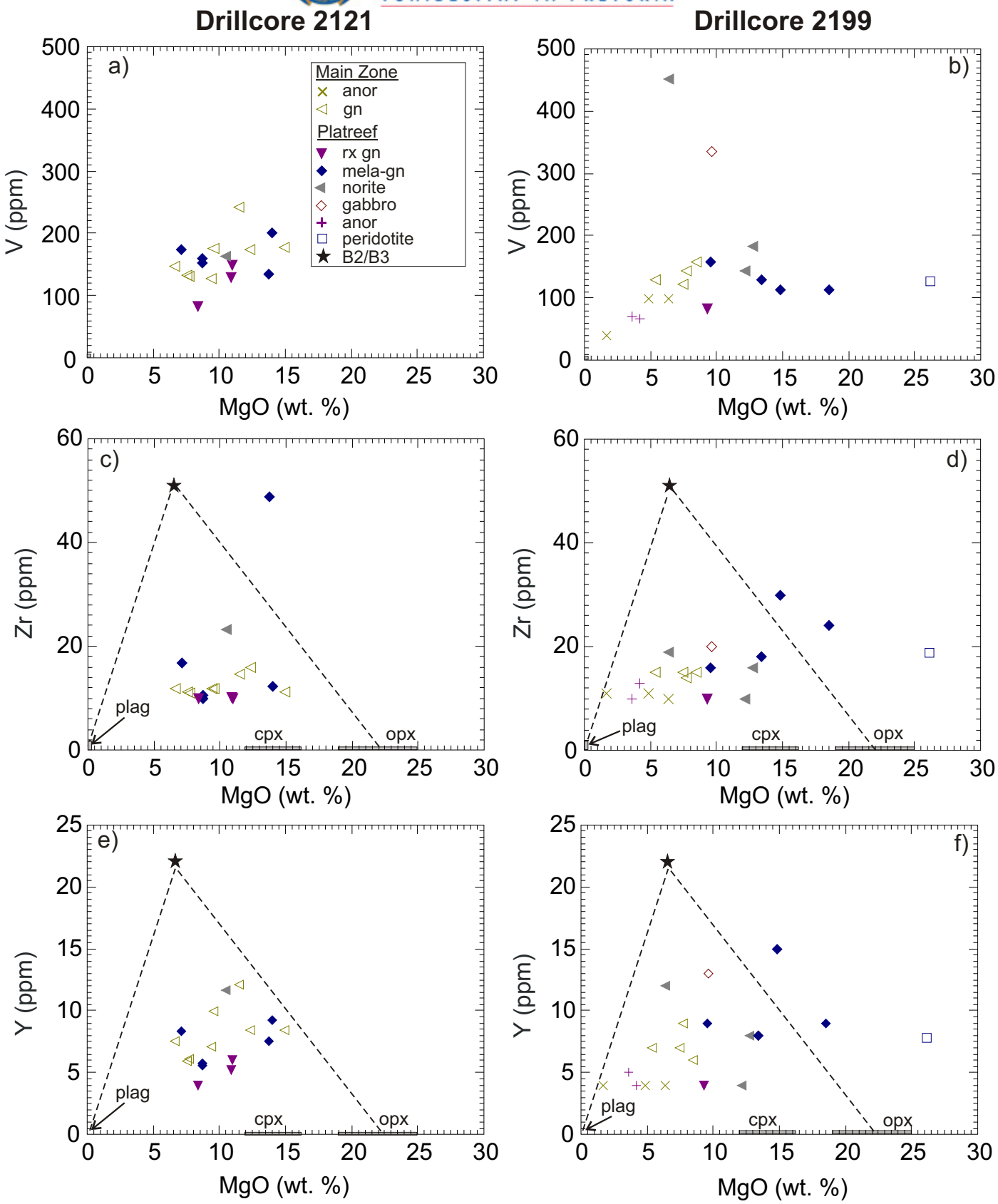

Fig. 6.4: Binary variation diagrams of (a and b) V versus MgO, (c and d) Zr vesus MgO and (e and f) Y Versus MgO in rocks from Nonnenwerth. Also plotted are compositional ranges of tholeiitic (B2/B3) Bushveld parental magma (Davies and Tredoux, 1985) and major rock forming minerals assuming they have 0 ppm incompatible trace elements. plag = plagioclase, cpx = clinopyroxene, opx = orthopyroxene, rx gn = recrystallized gabbronorite, gn = gabbronorite and mela-gn = mela-gabbronorite.

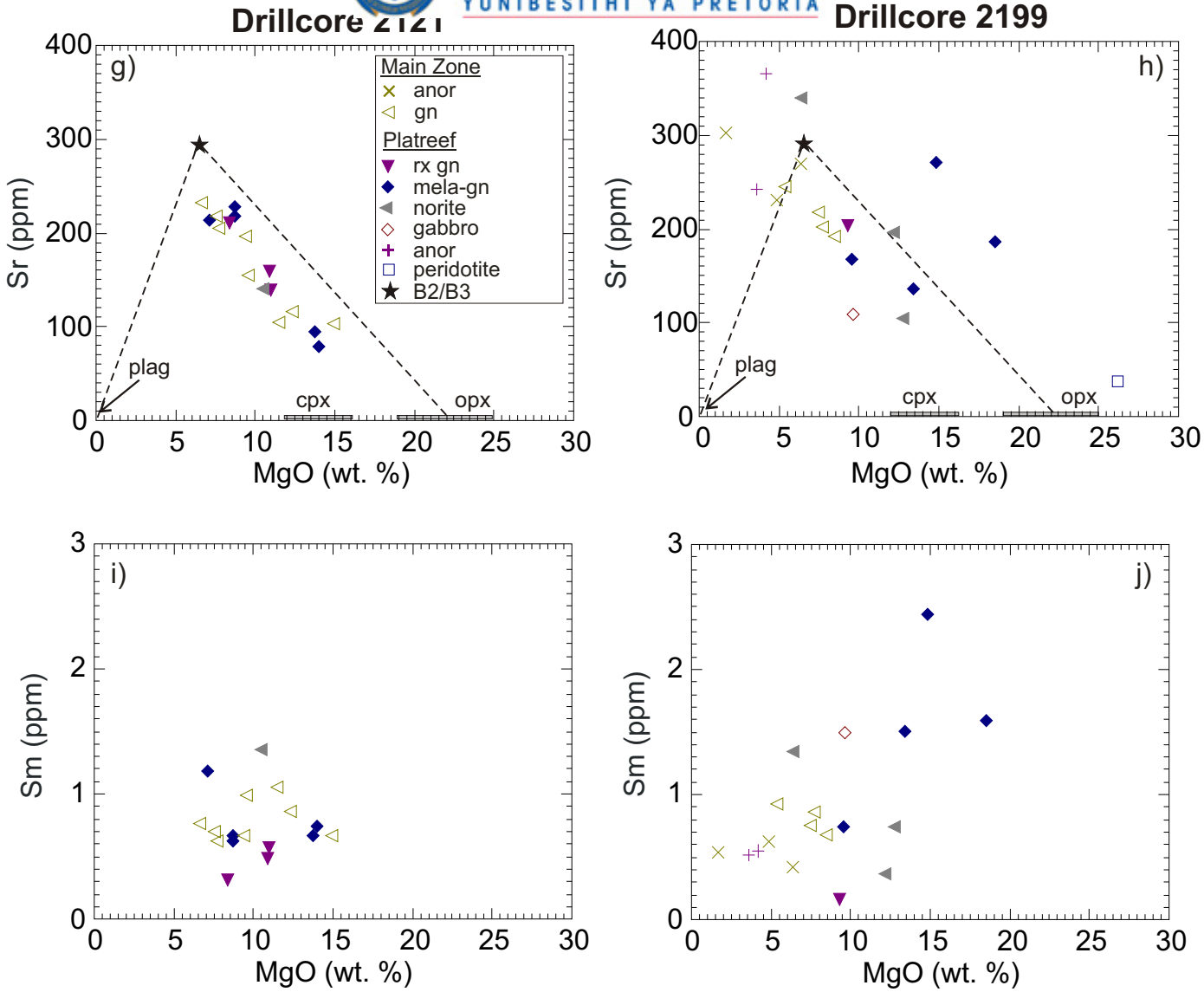

Fig. 6.4 (contd): Binary variation diagrams of (g and h) Sr versus MgO, (i and j) Sm versus MgO in rocks from Nonnenwerth. Also plotted are compositional ranges of tholeiitic (B2/B3) Bushveld parental magma (Davies and Tredoux, 1985) and major rock forming minerals assuming they have 0 ppm incompatible trace elements. plag = plagioclase, cpx = clinopyroxene, opx = orthopyroxene, rx gn = recrystallized gabbronorite, gn = gabbronorite and mela-gn = mela- gabbronorite.

for these elements, the minerals were not plotted onto the diagrams. It is evident that the concentrations of the elements show broad overlap in the Platreef and the Main Zone.

Vanadium shows a broadly positive correlation with MgO, suggesting that it is largely hosted by pyroxenes ($D_V^{opx/melt}$ = 0.6, $D_V^{cpx/melt}$ = 1.35; Rollinson, 1993). Two samples show markedly elevated V contents, suggesting they contain some cumulus magnetite.

The diagrams of Zr and Y against MgO show that Zr and Y apparently behave in a compatible manner. The trend may be due to the elements concentrations of the two elements being close to the detection limits (see Appendix 1b) except for one melagabbronorite (MOX11) which has 49ppm Zr (Fig. 6.4c) suggesting the presence of zircon. No zircon was identified in the sample. However, since Zr, Y and Sm are incompatible with regard to the major rock forming minerals, their concentration should thus be largely controlled by the trapped melt. Assuming that the Platreef largely crystallized from B2/B3 magma, as indicated by the compositional overlaps with the Main Zone (Chapter 6), one can estimate that the rocks contain ca. 20 – 30% trapped melt.

Strontium is compatible with regard to plagioclase ($D_{Sr}^{plag/melt}$ = 1.83; Rollinson, 1993) explaining the negative correlation between Sr and MgO seen in Fig. 6.3g and h.

Chondrite-normalized rare earth element patterns of the analysed rocks are considered in Fig. 6.5. In general, the analysed Platreef and Main Zone rocks have broadly similar patterns as the Main Zone of the western Bushveld Complex (Maier and Barnes, 1998). This suggests a genetic ink between the Platreef and the Main Zone.

One of the principal differences between the Platreef and the Main Zone is the less pronounced positive Eu anomaly in many of the Platreef rocks. This is particularly apparent in those samples with relatively high REE contents and probably reflects a relatively higher liquid component in the Platreef. The lowest REE concentrations occur in the recrystallized rocks, suggesting expulsion of the liquid component during recrystallization and explaining the positive Eu anomaly in the recrystallized rocks.

The REE patterns of the Platreef on Nonnenwerth are distinct from those of the Platreef on the farms Townlands and Rooipoort which show higher REE concentrations and more fractionated REE patterns (Fig. 6.5). Thus La/Lu_N ratios for the Platreef on Nonnenwerth are 0.82 – 6.26 (averaging 2.08) whereas the Platreef at Rooipoort has La/Lu_N 0.71 – 7.41 (averaging 3.96) and at Townlands it has 2.19 – 5.49 (averaging, 4.09). The contrasting concentration patterns of the REE at the individual localities may be due to variable contamination with different floor rocks. In the Mokopane area, the floor rocks consist of hornfels, quartzite and calc-silicates of the Pretoria Group (Manyeruke, 2003). In contrast, at Nonnenwerth the floor rocks are granitic gneisses, and probably included calc-silicate and dolomite. The latter lithologies contain low levels of incompatible trace elements (Klein and Beukes, 1989)

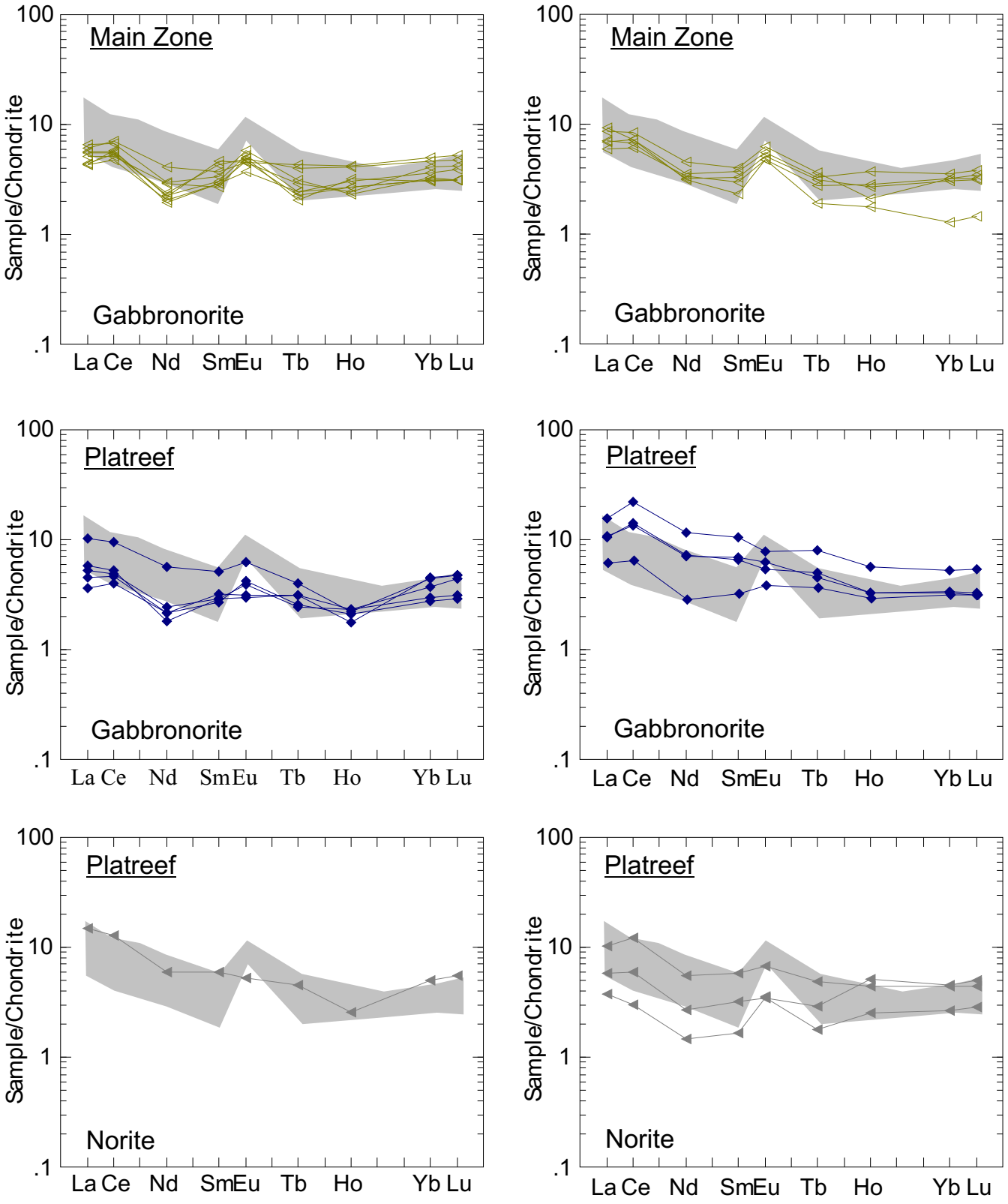

Fig. 6.5: Chondrite-normalized REE diagrams for Platreef lithologies on Nonnenwerth and from the Main Zone in the western Bushveld Complex (shaded; Maier and Barnes, 1998). Normalization values are from Taylor and McLennan (1985).

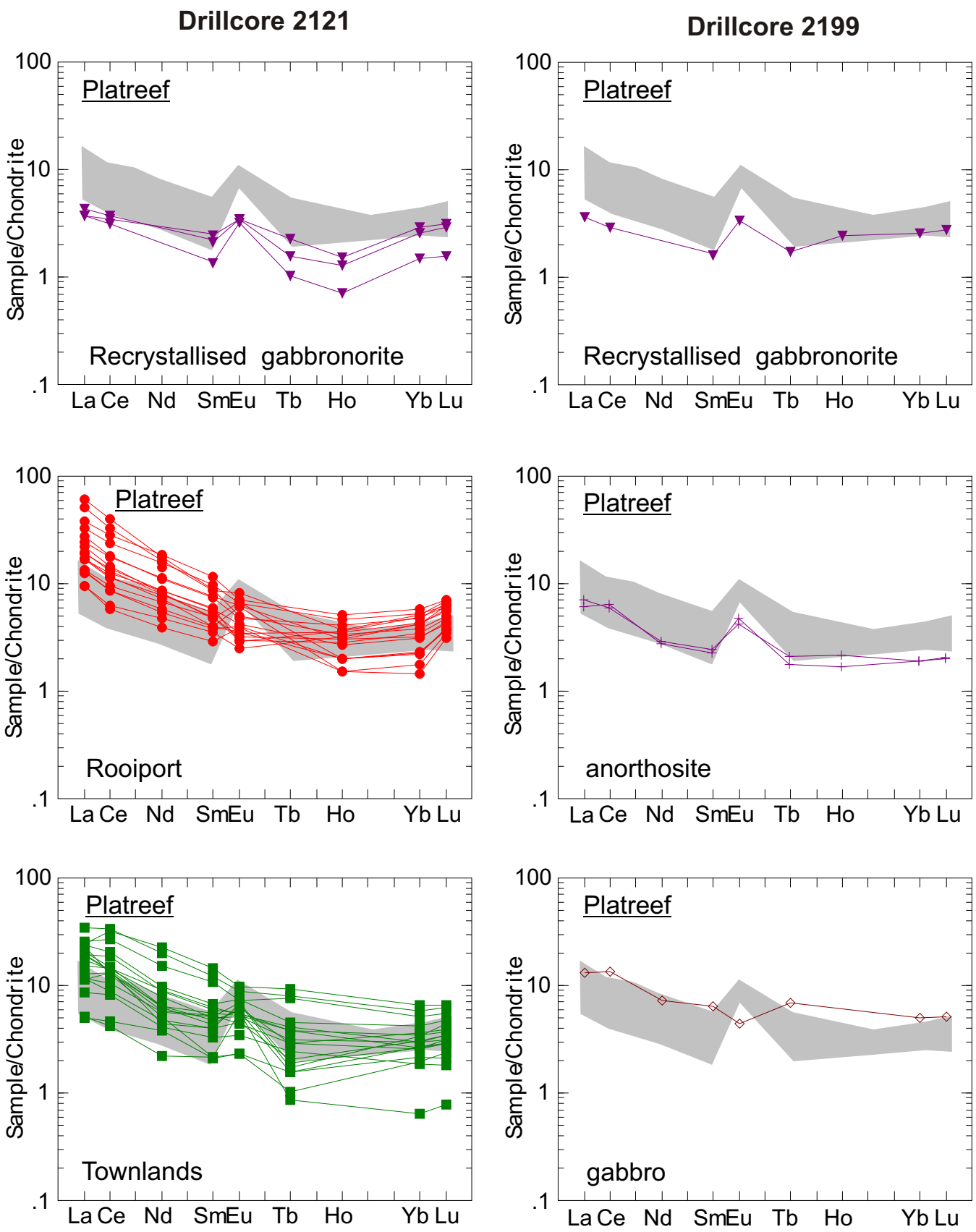

Fig. 6.5 contd: Chondrite-normalized REE patterns for Platreef lithologies on Nonnenwerth and from the Main Zone in the western Bushveld Complex (shaded; Maier and Barnes, 1998). Also shown are data from Townlands (Manyeruke et al, 2005) and Rooipoort (Maier et al., 2007). Normalization values are from Taylor and McLennan (1985).

(Fig. 6.5) and thus would not contribute significant amounts of these elements to the magma.

Mantle normalized trace element patterns on Nonnenwerth are weakly fractionated, but show negative Nb and Ti anomalies and strong positive Sr and Pb anomalies (Fig. 6.6). The positive Sr anomalies are due to the presence of cumulus plagioclase in most of the rocks, whereas the positive Pb suggests the presence of a crustal component. However, it remains unclear whether this crustal component is derived from contamination during emplacement or whether it reflects contamination of B2/B3 liquids prior to emplacement, in a staging chamber.

Mantle normalised trace element patterns for Platreef samples from Rooipoort and Townlands are more fractionated than those from Nonnenwerth, and show stronger positive Pb and negative Nb and Ti anomalies, suggesting a larger crustal component. This could be due to more enhanced crustal contamination in the southern portion of the northern lobe of the Bushveld Complex, or it could reflect a more important B1 liquid component.

In an attempt to better constrain the derivation of the crustal component, and the magmatic lineage of the rocks, the REE data have been plotted in binary variation diagrams (Fig. 6.7). It is evident that the Nonnenwerth rocks have Ce/Sm ratios similar to B2/B3 liquids (average 8.2 at Nonnenwerth, 7.9 in B2/B3 liquids; Curl, 2001) and that the influence of B1 liquid is minor. Furthermore, the rocks were evidently not significantly contaminated with shale, as shale has similar Ce/Sm ratios as B1

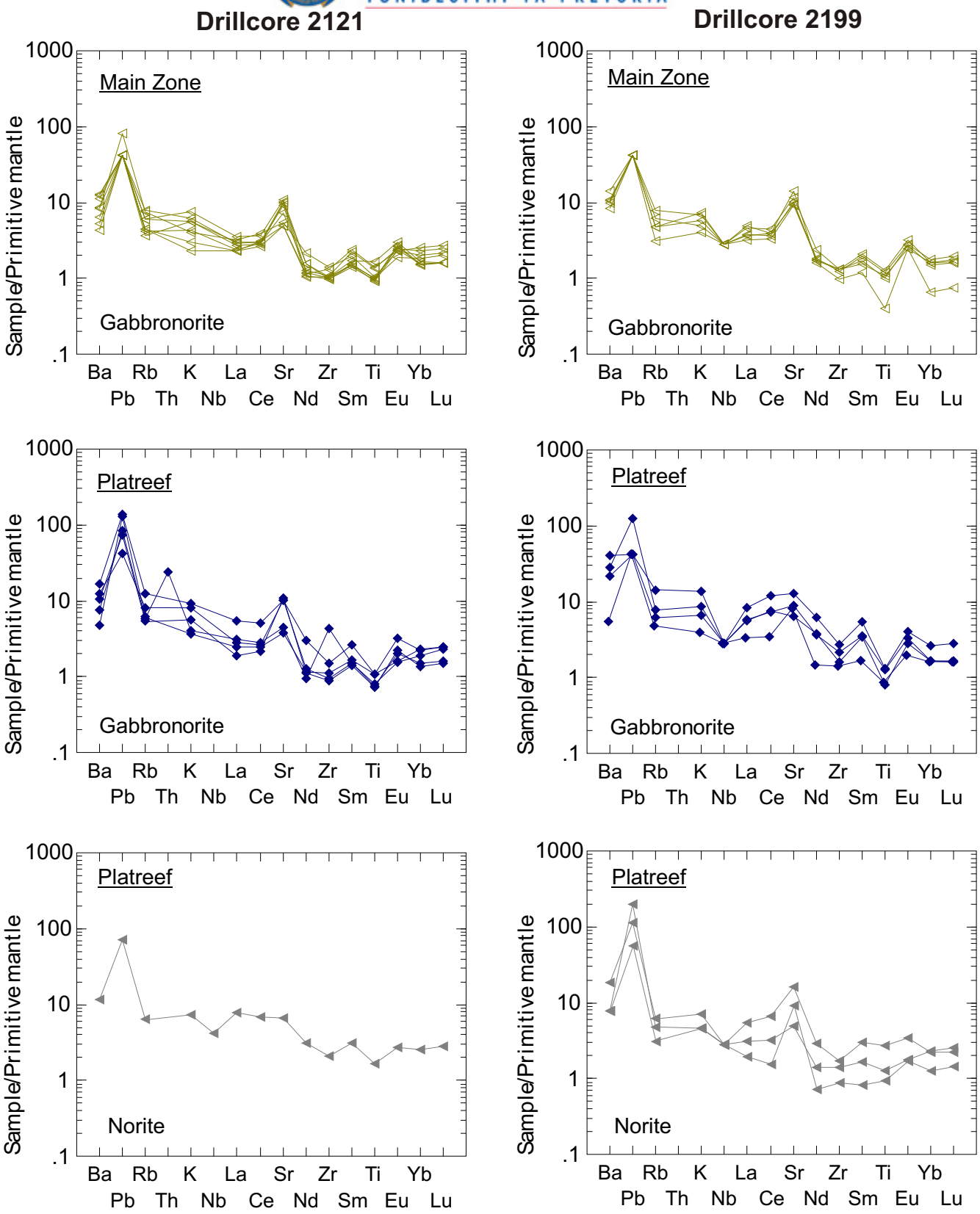

Fig.6.6: Primitive mantle normalized incompatible trace element patterns for Platreef rocks on Nonnenwerth (drillcores 2121and 2199). Normalization values are from Sun and McDonough (1989).

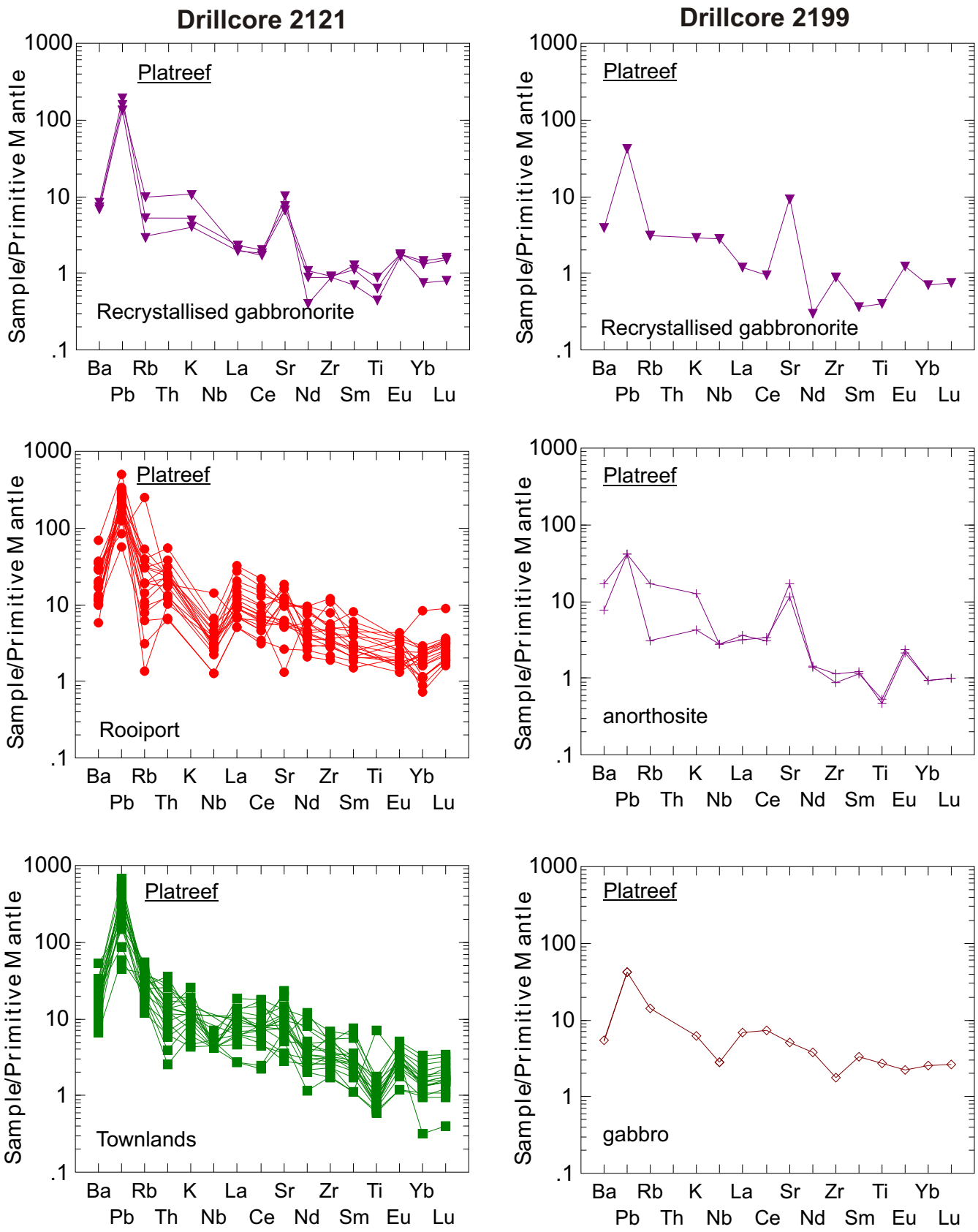

Fig. 6.6: contd: Primitive mantle normalized incompatible trace elements for Platreef rocks on Nonnenwerth from (2121and 2199). Also included are the patterns of Platreef rocks from Townlands (Manyeruke et al., 2005) and Rooipoort (Maier et al., 2007). Normalization values are from Sun and McDonough (1989).

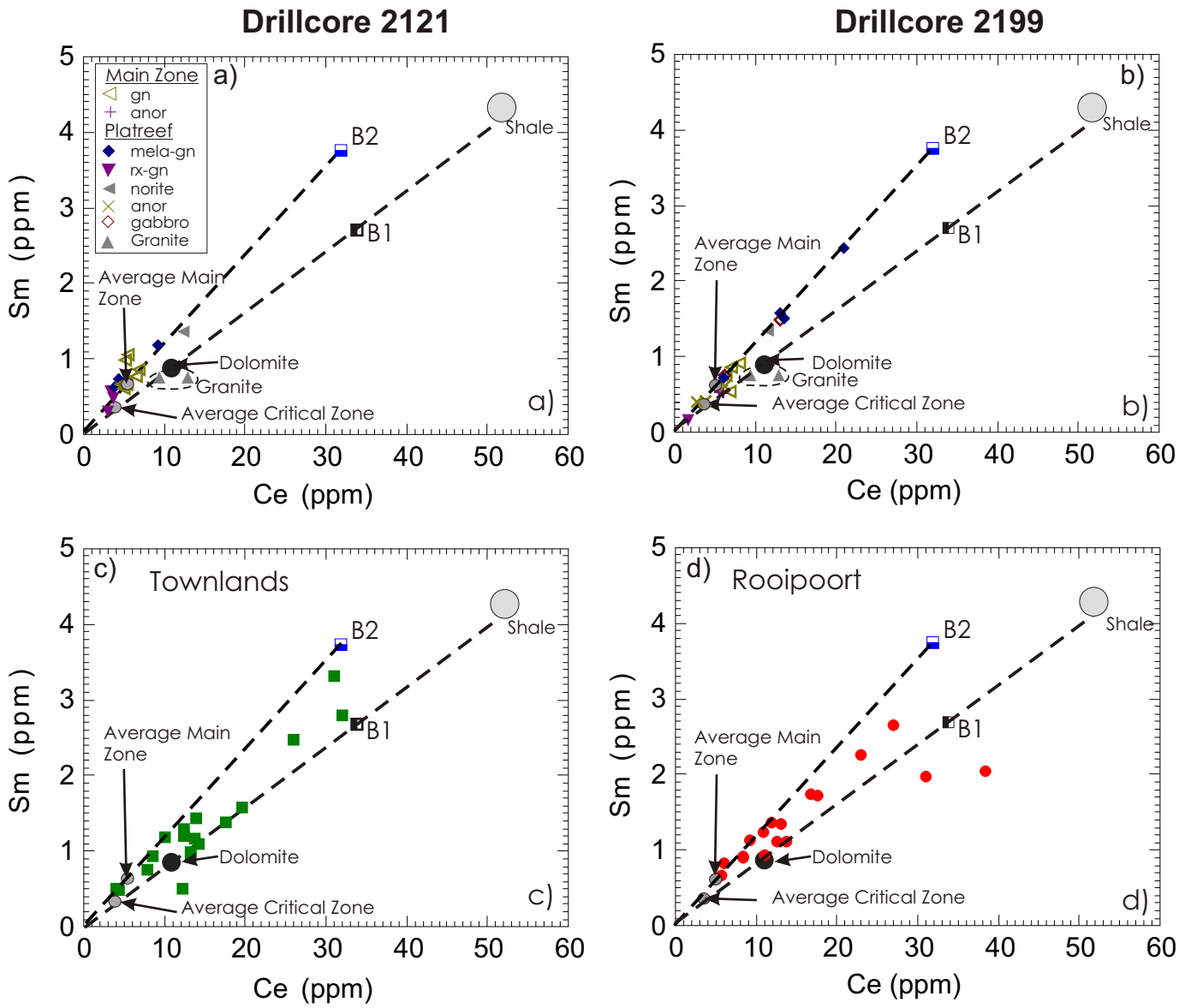

Fig. 6.7: Sm versus Ce for Platreef rocks on (a) Nonnenwerth, drillcore 2121. (b) Nonnenwerth, drillcore 2199. (c) Townlands (Manyeruke, 2003; Manyeruke et al., 2005). (d) Rooipoort (Maier et al., 2007). Also shown are the compositions of Bushveld B1 and B2 parental magmas (Curl, 2001), average Critical Zone and Main Zone rocks (Maier and Barnes, 1998), shales and dolomite (Klein and Buikes, 1989). gn = gabbronorite, anor = anorthosite, rx gn = recrystallized Gabbronorite, mela gn = melagabbronorite.

Bushveld parental magma, as well as high Ce and Sm contents. In contrast, contamination with dolomite cannot be excluded as dolomite has low concentrations of Ce and Sm as well as most other incompatible trace elements. Platreef rocks from Townlands and Rooipoort have Ce/Sm ratios between B2 and B1 liquids (Fig. 6.6). This could indicate a larger B1 component, but the trace element contents in many samples are too high to be solely explained by a trapped liquid component and require addition of a contaminant, most likely shale.

6.3 Concentrations of sulphur and chalcophile elements

Sulphur contents in the analysed rocks are plotted against MgO in Fig. 6.8. The tholeiitic (B2/B3) and Mg-basaltic (B1) parental magmas of the Bushveld Complex are plotted for comparison. The tholeiitic B2 magma has ca. 400 ppm S (Davies and Tredoux, 1985; Barnes and Maier, 2002b). Since S is an incompatible element, the S-saturation boundary would be around 400 ppm S. Platreef rocks (except one recrystallized gabbronorite sample and two melagabbronorite samples from drillcore 2199) have S contents mostly significantly above 400 ppm. This suggests that the Platreef rocks crystallized from a S- saturated magma and contain cumulus sulphides. The Main Zone rocks from Nonnenwerth have between 120 and 300 ppm S indicating that the Main Zone magma was probably S-undersaturated during crystallization of the rocks and is supported by the absence of sulphides in the Main Zone rocks.

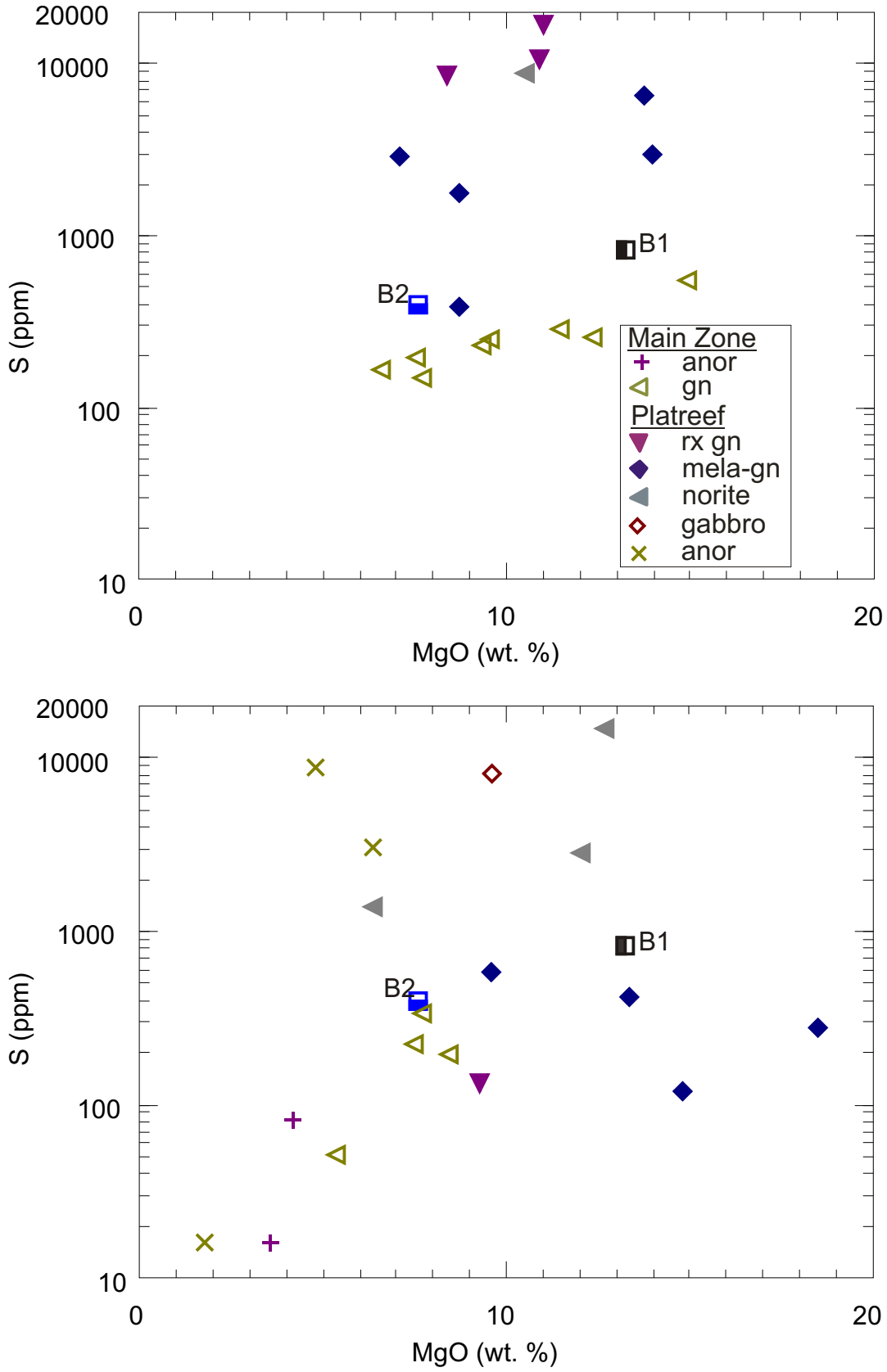

Fig. 6.8: Plot of MgO versus S in drillcore 2121 (top) and 2199 (bottom). Also plotted are compositions of Mg-basaltic and tholeiitic Bushveld parental magmas (Davies and Tredoux, 1985). gn = gabbronorite, rx gn = recrystallized gabbronorite, anor = anorthite, and mela-gn = mela-gabbronorite

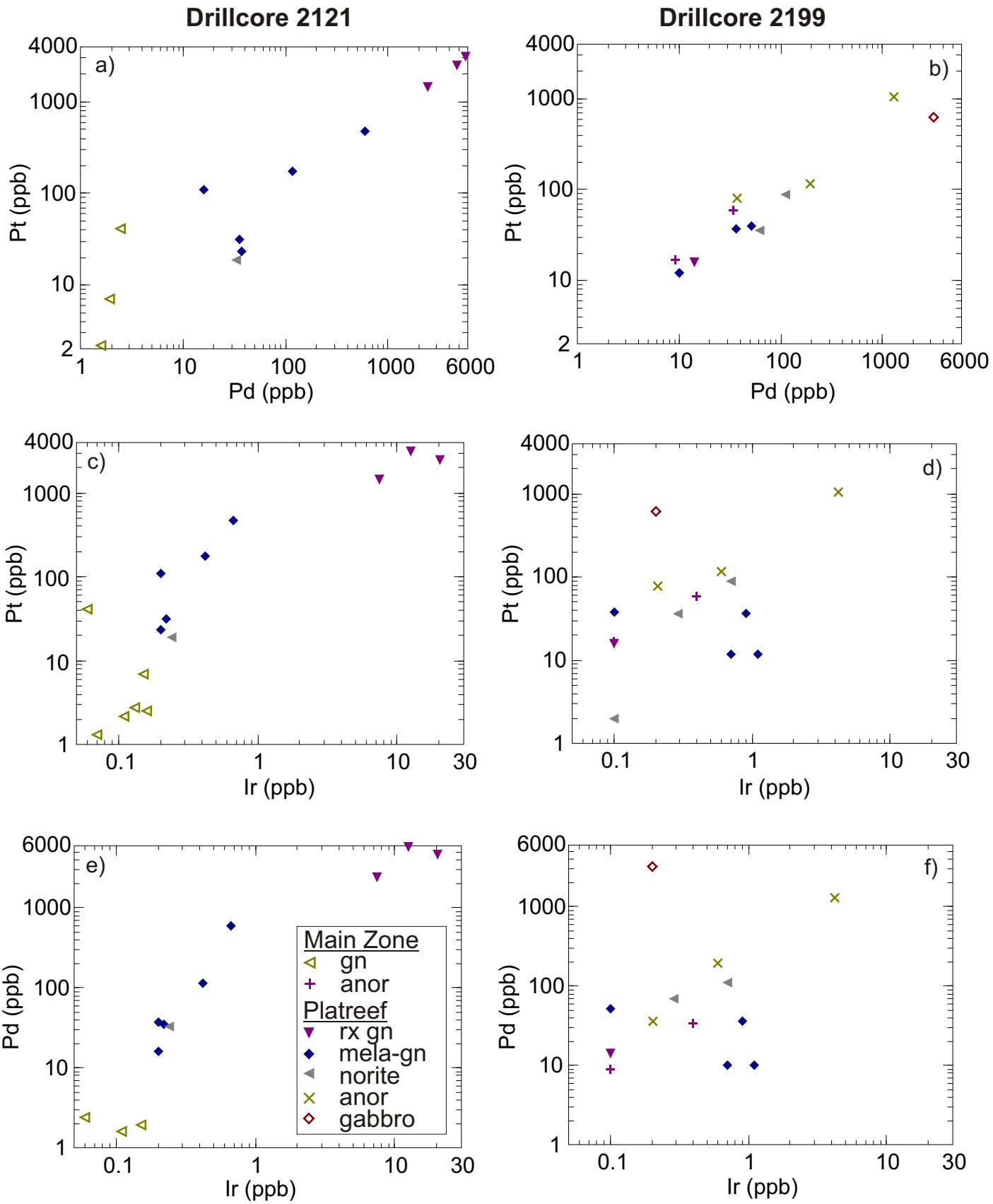

Fig. 6.9: PGE binary plots of the Platreef on the farm Nonnenwerth. rx gn = recrystallized gabbronorite, gn = gabbronorite, mela-gn = mela-gabbronorite, anor = anorthosite.

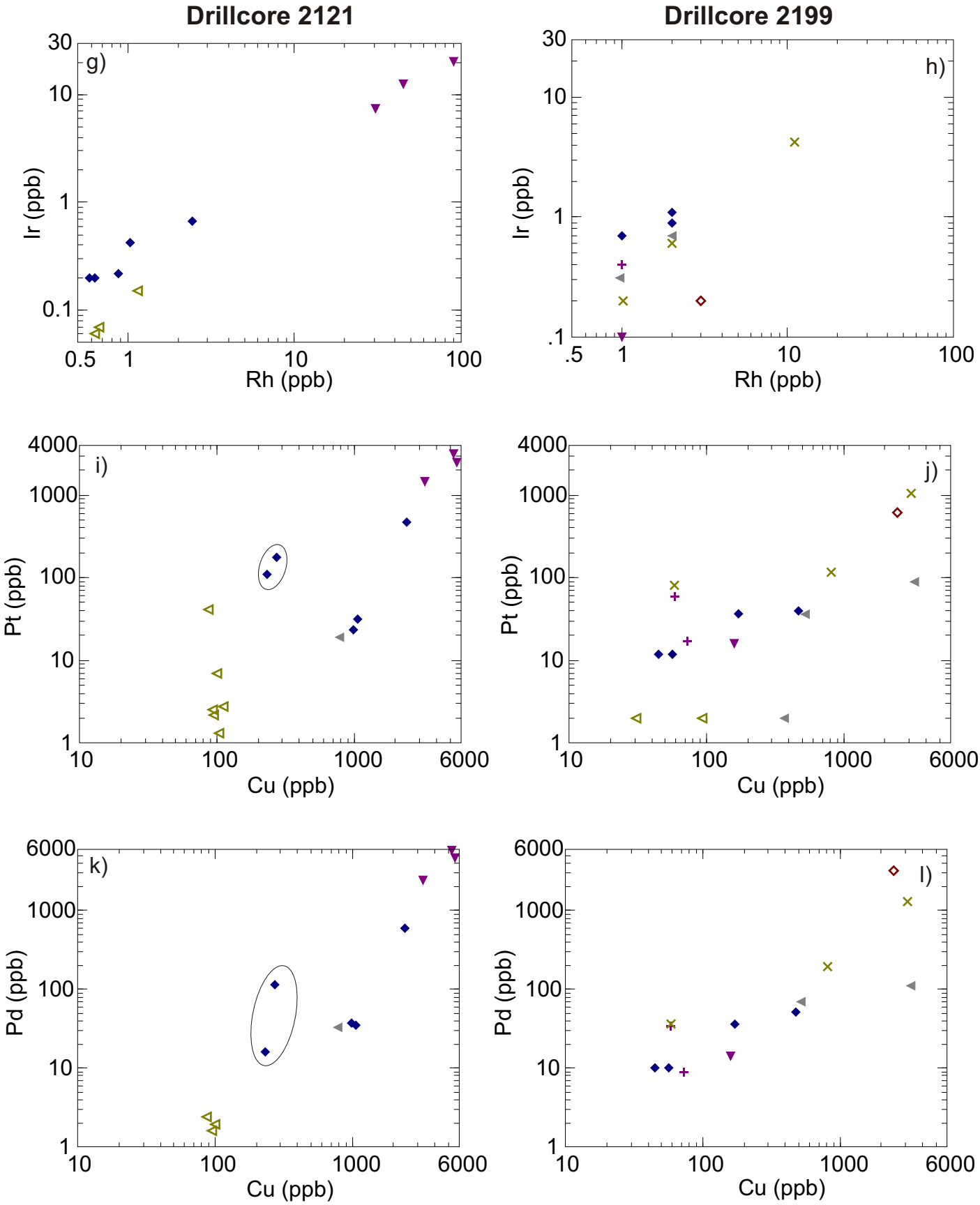

Fig. 6.9: (contd) PGE binary plots of the Platreef on the farm Nonnenwerth. rx gn = recrystallized gabbronorite, gn = gabbronorite, mela-gn = mela-gabbronorite, anor = anorthosite.

To assess the nature of the phases controlling the PGE, the PGE are plotted against each other in Fig. 6.9. In mafic–ultramafic igneous systems, the chalcophile metals are normally assumed to be mainly concentrated by magmatic sulfides. This model is supported by the broadly positive correlations between those PGE that could behave in a mobile manner (in particular Pd, Hsu *et al*. 1991) and those that are believed to be immobile under most conditions (e.g., Pt and Ir; Fig. 6.9b and e). The broad positive correlation between these elements thus suggests that in most samples the PGE were concentrated by magmatic sulphides. However, in drillhole 2199, the correlations between Pt and Pd on the one hand and Ir on the other hand are relatively poor, suggesting that in some samples from this locality Pt and Pd behaved in a mobile manner.

Further support for the model of primary sulphide control is shown by the broadly positive correlations between PGE, Ni and Cu with sulphur in samples containing > ca. 1000 ppm S (Fig. 6.10). By extending best- fit tie-lines through the data to 38 % S (i.e. the approximate S content of the sulphide), one can estimate the metal content of the sulphide at ca. 12 % Cu, 6 % Ni, 40 ppm Pt and 80 ppm Pd. These values are comparable to those of the Platreef on Townlands. Assuming D values between sulphide melt and silicate melt of ca. 1000 for Cu and 500 for Ni (Francis, 1990). The metal tenors suggest that the Platreef magma had ca. 120 ppm Cu and Ni, values that are normal for tholeiites but different to those of Mg-basaltic B1 magma which has ca. 70 ppm Cu and ca. 400 ppm Ni.

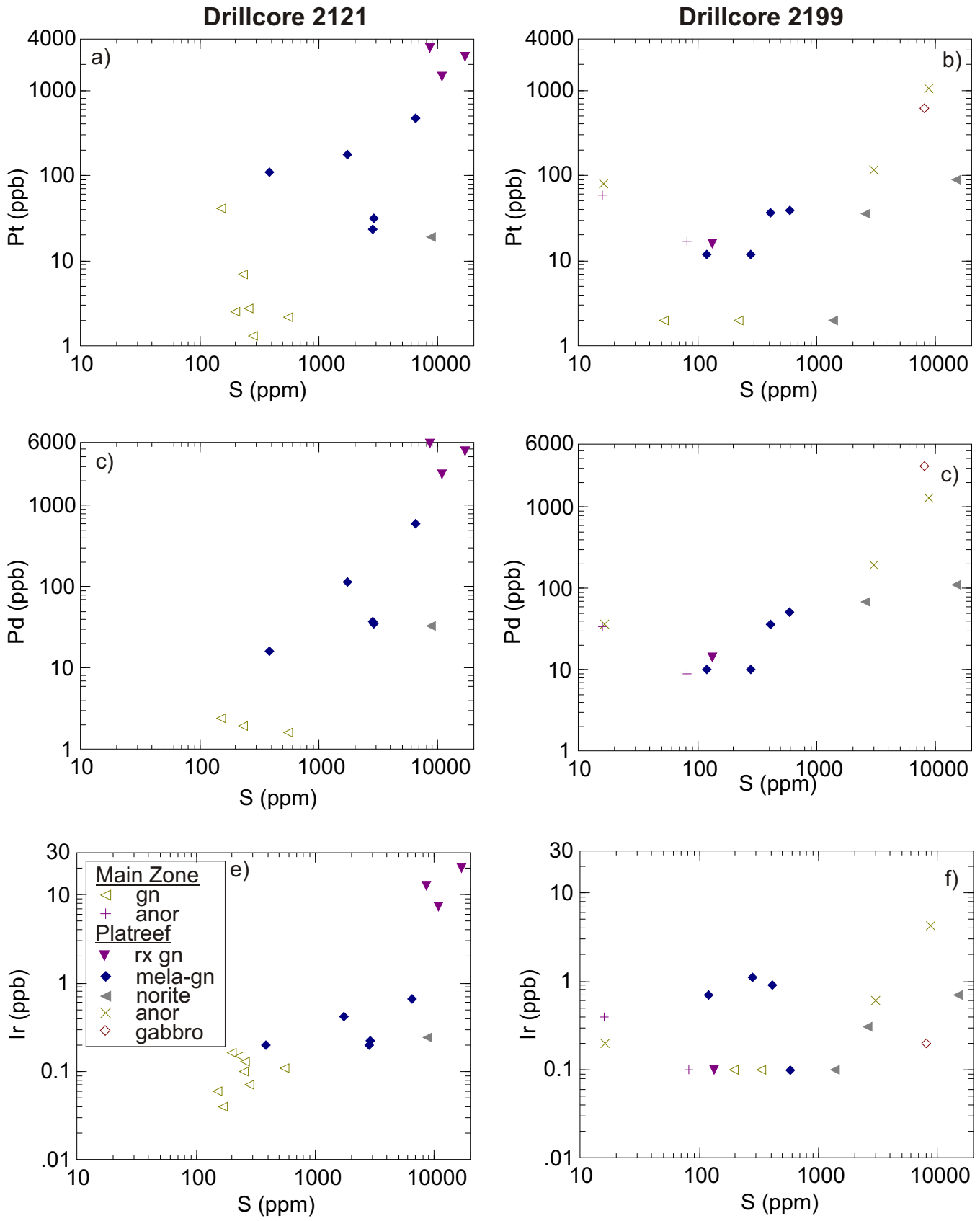

Fig. 6.10. Plots of a) Pt, b) Pd and c) Ir versus S. rx gn = recrystallized gabbronorite, gn = gabbronorite, mela-gn = mela-gabbronorite, anor = anorthosite.

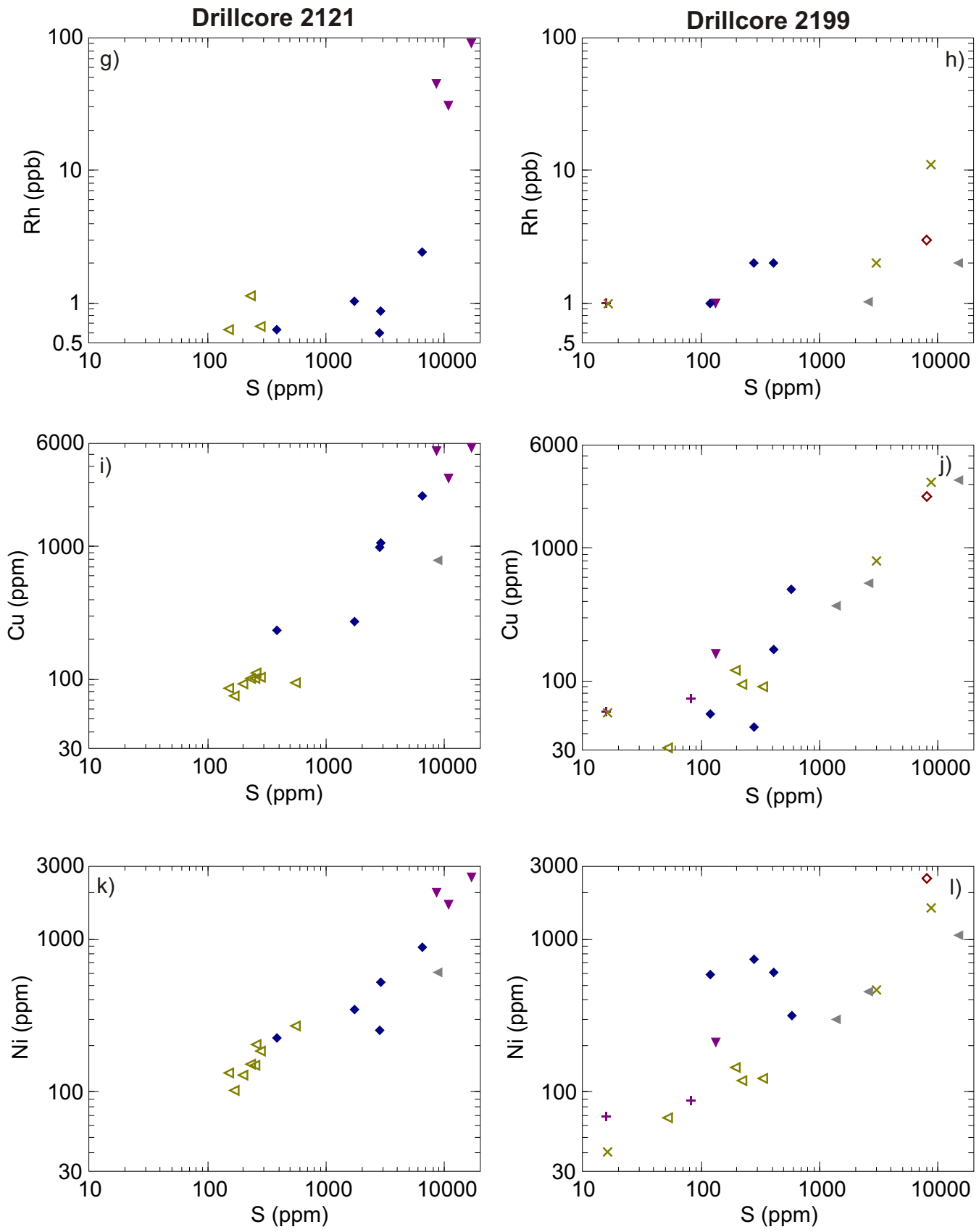

Fig. 6.10. (contd) Plots of d) Rh, e) Cu and f) Ni versus S. rx gn = recrystallized gabbronorite, gn = gabbronorite, mela-gn = mela-gabbronorite, anor = anorthosite.

In Fig. 6.11, the metals and S are plotted versus stratigraphic height. The sharp compositional break between the Platreef and the Main Zone that was evident in the mineral compositional data is again visible. The Platreef has relatively high PGE contents (between 0.002 and 8.865 ppm Pt + Pd) whereas the Main Zone mostly has PGE contents approaching the detection limit (< 0.2 ppb). In the Platreef, PGE and sulphur contents increase with height. This includes Ir which is normally separated from Pt and Pd during fractionation and crystallization of sulphide liquid (Kullerud et al., 1969; Naldrett, 1989). However, the observation that S also increases with stratigraphic height suggest a sulphide control for the PGE and that if Ir was fractionated from Pt and Pd, it was not transported far from the sulphide liquid (probably cm scale). The highest PGE concentrations occur in the recrystallized gabbronorite in drillcore 2121 (average 6.6 ppm Pt + Pd). In drillcore 2199, the highest concentrations occur in one anorthositic sample and a gabbro which have 2.3 and 3.8 ppb Pt + Pd, respectively. It is presently not known why the highest PGE values occur in different lithologies in the different boreholes. This may be due to the heterogeneity of the Platreef.

The noble metal concentrations have been normalised to primitive mantle and plotted in order of decreasing melting temperature in Fig. 6.12. Noble metal concentrations of the Merensky Reef and the Main Zone are shown for comparison. Ni is included in the plots to the left of Os, and Cu (as well as Au) to the right of Pd due to their broadly similar behaviour to Os and Pd, respectively, during fractionation (Barnes and Naldrett, 1987).

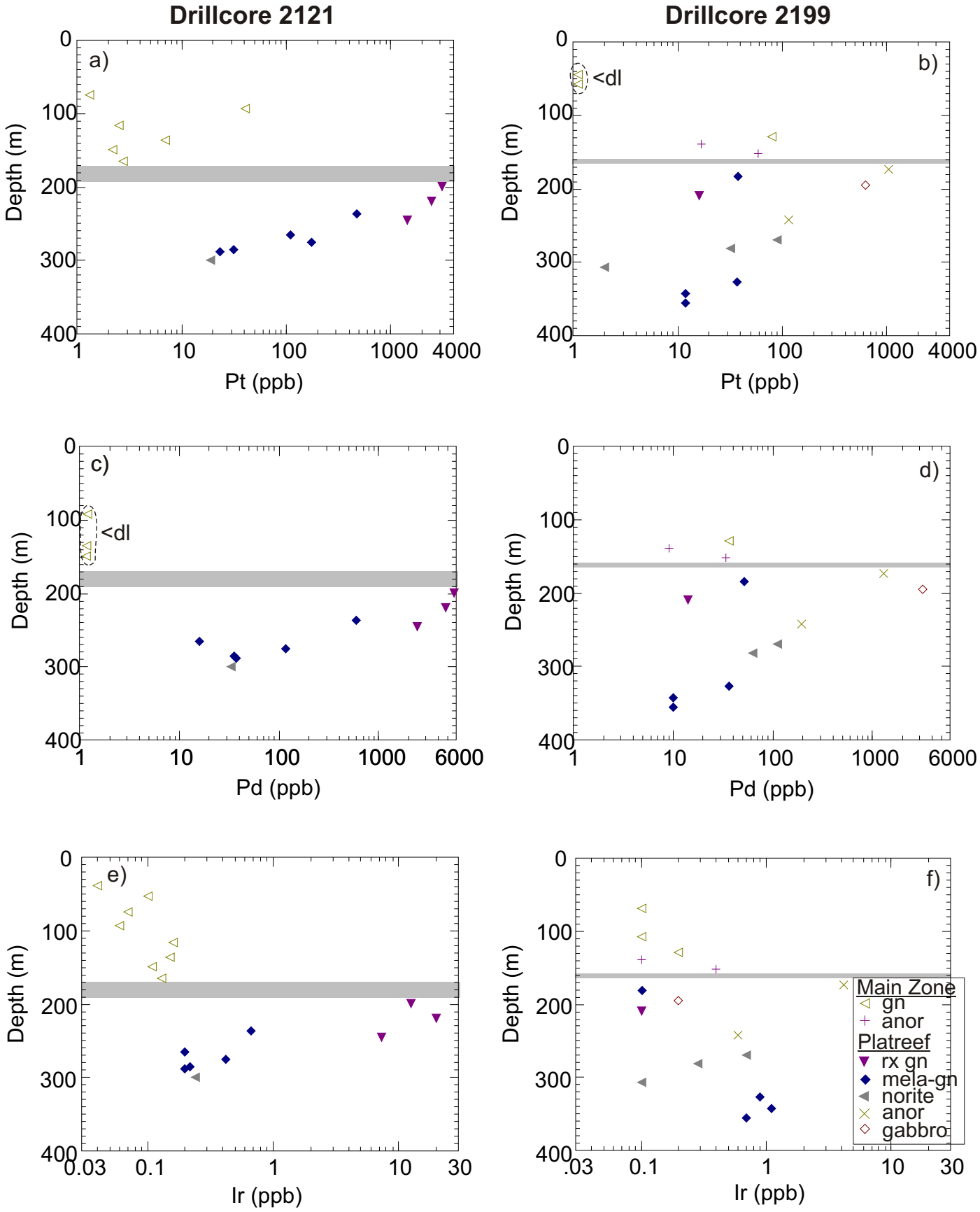

Fig. 6.11: Concentration of PGE and S in logarithmic scale plotted versus stratigraphic height (m). rx gn = recrystallized gabbronorite, gn = gabbronorite, mela-gn = mela-gabbronorite, anor = anorthosite, <dl = below detection limit. The shaded bar represents the boundary between Platreef and Main Zone.

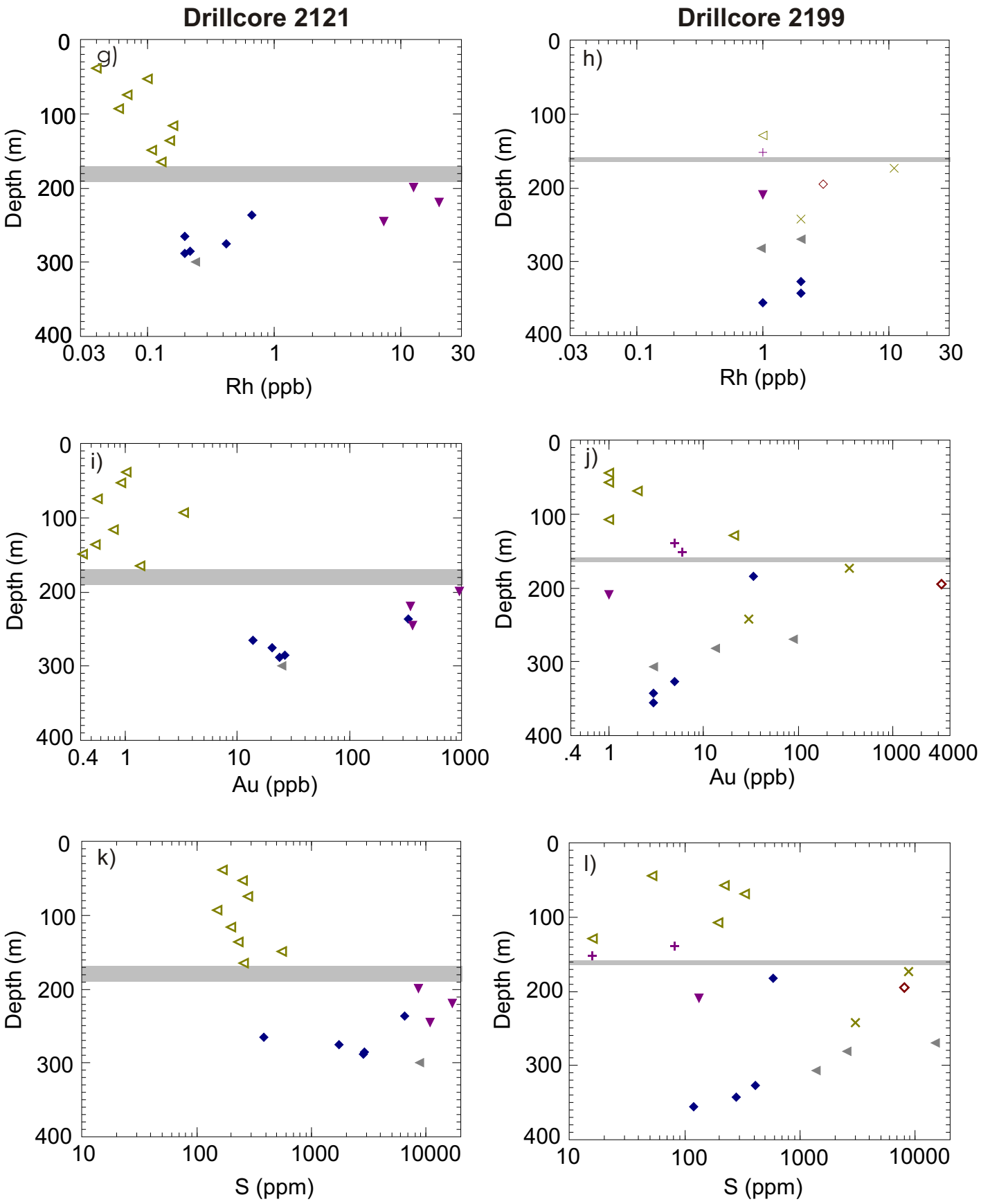

Fig. 6.11: (contd) Concentration of PGE and S in logarithmic scale plotted versus stratigraphic height (m). rx gn = recrystallized gabbronorite, gn = gabbronorite, mela-gn = mela- gabbronorite, anor = anorthosite. The shaded bar represents the boundary between Platreef and Main Zone.

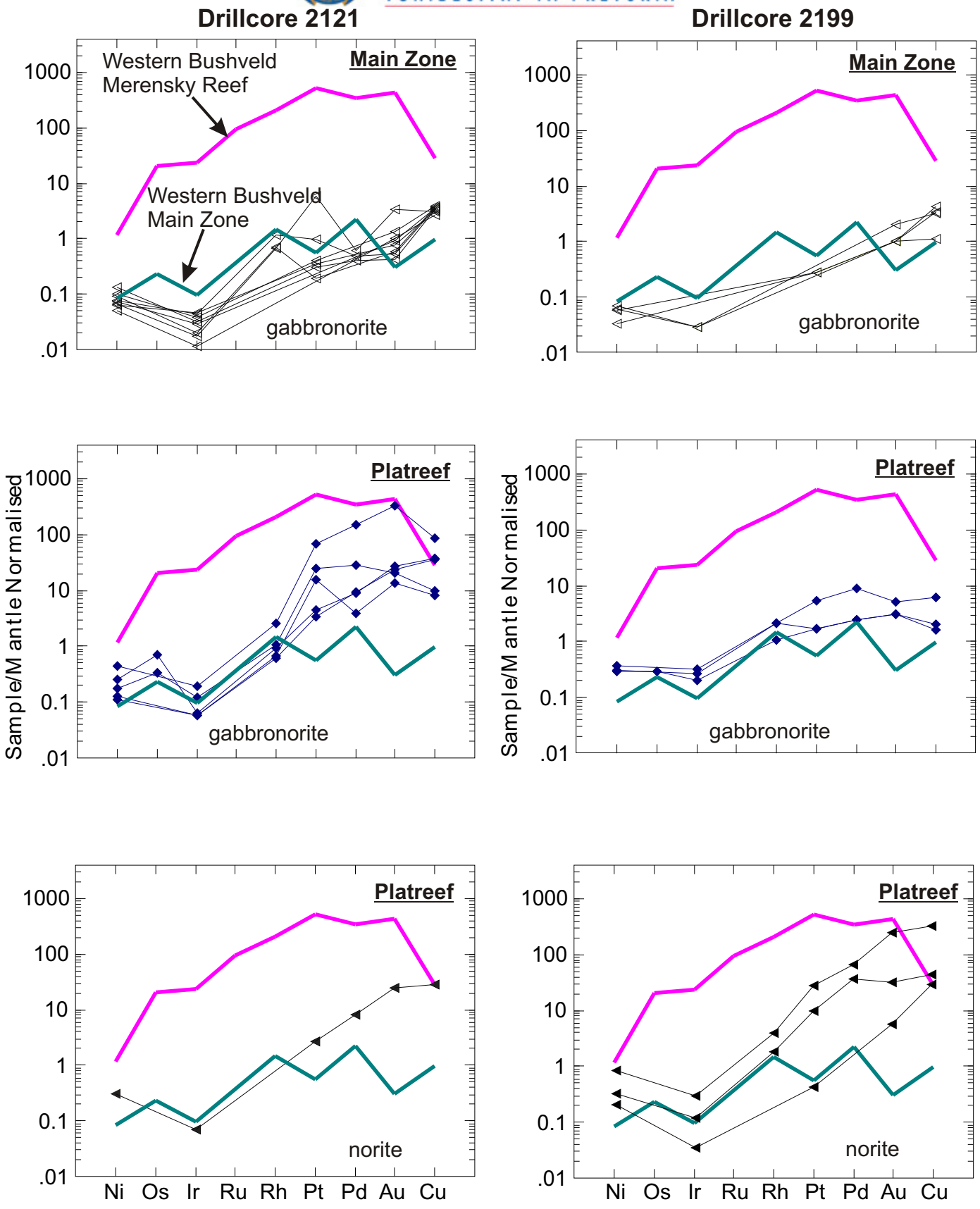

Fig. 6.12: Mantle-normalized PGE patterns for rocks from the Platreef and the Main Zone on the farm Nonnenwerth. Included are PGE concentrations for the Main Zone (Maier and Barnes, 1999 and the Merensky Reef (Barnes and Maier, 2002) in the western Bushveld Complex. (Normalization factors are from Barnes and Maier, 1999).

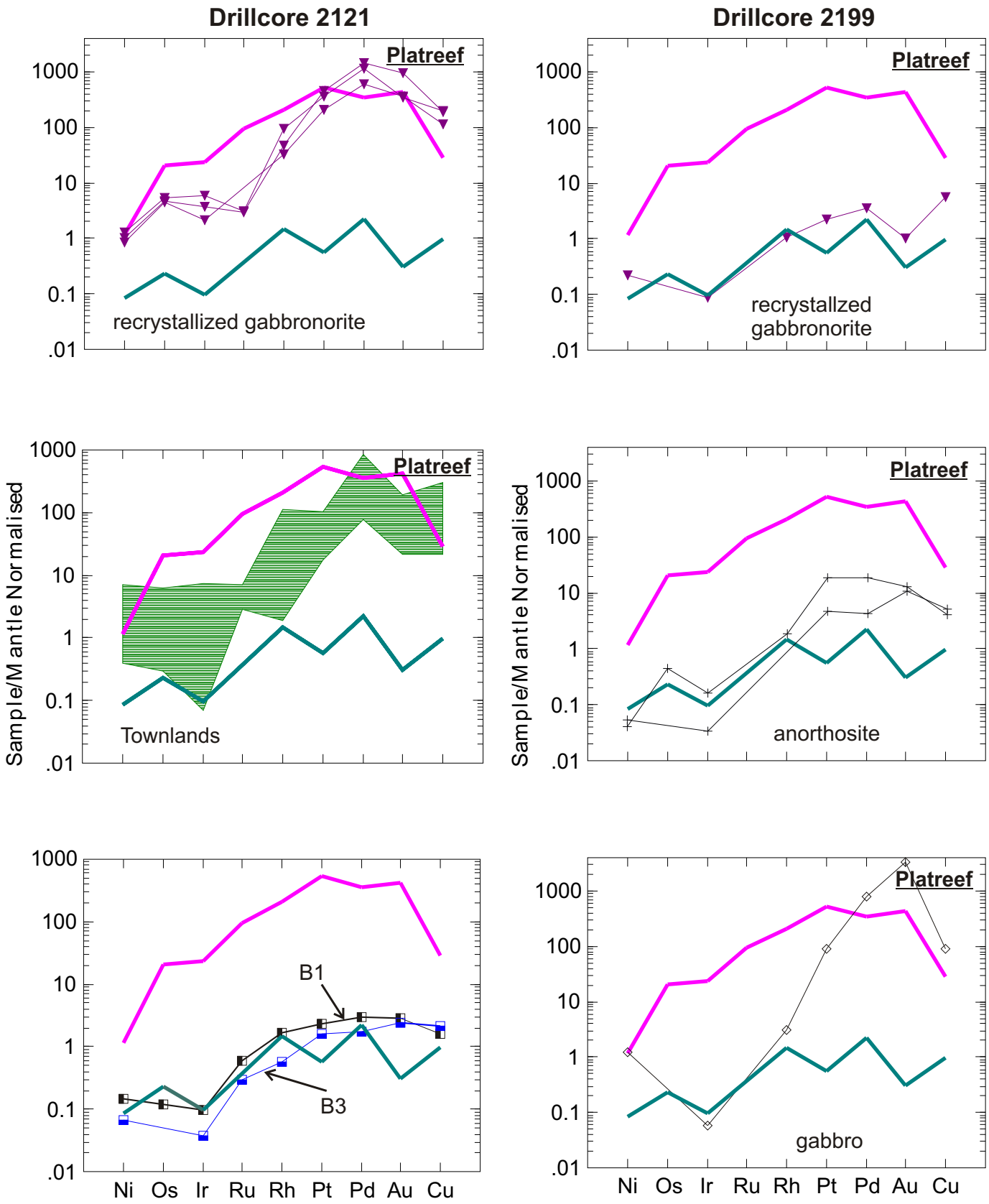

Fig. 6.12: (Contd) Mantle-normalized PGE patterns for rocks from the Platreef and the Main Zone on the farm Nonnenwerth, Townlands (Manyeruke and Maier, 2003) and B1 and B2 Bushveld parental magmas (Davies and Tredoux, 1985). Included are PGE concentrations for the Main Zone (Maier and Barnes, 1999 Merensky Reef (Barnes and Maier, 2002) in the western Bushveld Complex. (Normalization factors are from Barnes and Maier, 1999).

The diagrams highlight that Platreef rocks on Nonnenwerth have variable Pt and Pd contents, with some samples being as enriched as the Merensky Reef, but the shape of the metal patterns is different to that of the Merensky Reef due to a relative depletion in IPGE and, to a lesser degree, Rh. This results in more fractionated patterns with mostly steep slopes from Ir to Au (Pd/Ir >> 100). Ni/Ir_N is mostly > 1 whereas Cu/Pd_N is mostly at unity or < 1. This suggests that the sulphide melt segregated from a fertile magma in terms of PGE. The Main Zone gabbronorite has broadly similar metal patterns as the Main Zone elsewhere in the Bushveld Complex, with Cu/Pd_N > 1, suggesting that it crystallized from a magma that had experienced sulphide segregation prior to emplacement.

The patterns of most Platreef samples show a positive Pd anomaly, in contrast to the Merensky Reef which has a positive Pt anomaly. Pt/Pd ratios of samples with at least 0.1 wt. % S range from 0.2 to 1.5, averaging 0.7. For samples with less than 0.1 wt. % S, Pt/Pd ratios are mostly above unity and as high as 16.8. The variation of Pt/Pd ratio suggests that in the rocks with less than 0.1 wt. % S other phases besides sulphides exert some control on the PGE contents (e.g. silicates, oxides, PGM) or fractionation of the immiscible sulphide liquid during sulphide crystallization.

Metal patterns of Platreef samples at Townlands are also shown in Fig. 6.12. The patterns show broad similarities with the Platreef at Nonnenwerth, but Townlands has somewhat less fractionated patterns, resulting in lower Pd/Ir ratios (average 96).

6.4 Summary

Platreef samples from Nonnenwerth mostly plot near tielines joining plagioclase with orthopyroxene and clinopyroxene in most major element bivariate plots confirming that the chemistry of the rocks is controlled by the relative proportions of these phases and trapped melt. The data also show that plagioclase constitutes ca. 20 – 60 % of the rocks in agreement with the petrographic descriptions in chapter 5.

Trace element patterns at Nonnenwerth are unfractionated with Ce/Sm ratios between 5.7 and 10.6 (averaging 8) and show similarities to the Main Zone at Union Section. Major element data also overlap with central Main Zone. This suggests the Platreef has a B2/B3 magmatic lineage with little contamination or some dolomite contamination. At Townlands (Manyeruke *et al.*, 2005), the data indicate mixed B1-B2 signature i.e., higher and more fractionated REE contents (average Ce/Sm 12.6 at Townlands) more similar to Upper Critical Zone with relatively higher La/Yb_N. Moreover, the high concentration of the trace elements in some samples clearly indicates contamination with floor rock shale because the concentrations of the REE are too high to be explained by a trapped melt component of either B1 or B2 Bushveld lineage. It is possible that the entire crustal component is due to contamination with shale, and thus the importance of B1 is uncertain.

PGE at Nonnenwerth Platreef are more fractionated than elsewhere along the Platreef, with higher Pd/Ir ratios. This is in agreement with a more differentiated magma, suggested by the mineral and major elements chemistry and the absence of pyroxenite and chromitite. The present study has established a broad positive

correlation amongst the individual PGE and between individual PGE and S (for samples with > 0.1 % S), suggesting that magmatic sulphides were the primary PGE collector and that PGE are largely hosted by sulphides. However, there is also considerable scatter, notably in samples from borehole 2199, suggesting some secondary mobility of S, Cu, Pt and Pd. A similar pattern has been observed at Overysel (Holwell, *et al.*, 2005), Drenthe (Gain and Mostert, 1982) and at Townlands (Manyeruke, 2003; Manyeruke *et al.*, 2005).

CHAPTER SEVEN: COMPOSITION OF THE SILICATE MINERAL AT NONNENWERTH

The selected chemical compositions of the silicate minerals plagioclase, orthopyroxene and clinopyroxene are given in Tables 2a, b and c, respectively. Analytical details are given in Appendix 1c.

7.1 Plagioclase

The analysed plagioclase plots mostly in the labradorite field with only a few grains plotting in the bytownite and andesine fields (Fig. 7.1).There is no systematic compositional difference between plagioclase from the two drillcores. An (100 x cationic ratio of Ca / (Ca + Na + K)) contents in the Platreef tend to be similar to those in the Main Zone, but the spread in composition is much wider in the former i.e. An_{37-75} versus An_{60-76}, respectively (Fig. 7.2). Furthermore, plagioclase becomes more calcic with height in the Platreef, but more sodic with height in the Main Zone. The increase in An of plagioclase with height in the Platreef is opposite to what might be expected in an intrusion crystallizing from the base upwards, from progressively differentiating magma. However, similar basal reversals in differentiation trend have been observed in many layered intrusions, including the Bushveld Complex (Hulbert, 1983). A further important observation is the distinct compositional break across the dolomite xenoliths in borehole 2121 to consistent lower An contents, but the break to consistent lower An contents in borehole 2199 occurs within the Main Zone rocks well above the dolomite xenolith. The high An contents close to the dolomite may be due to sub-solidus reaction between the dolomite and plagioclase with plagioclase gaining Ca from dolomite hence the high An contents towards the dolomite xenoliths.

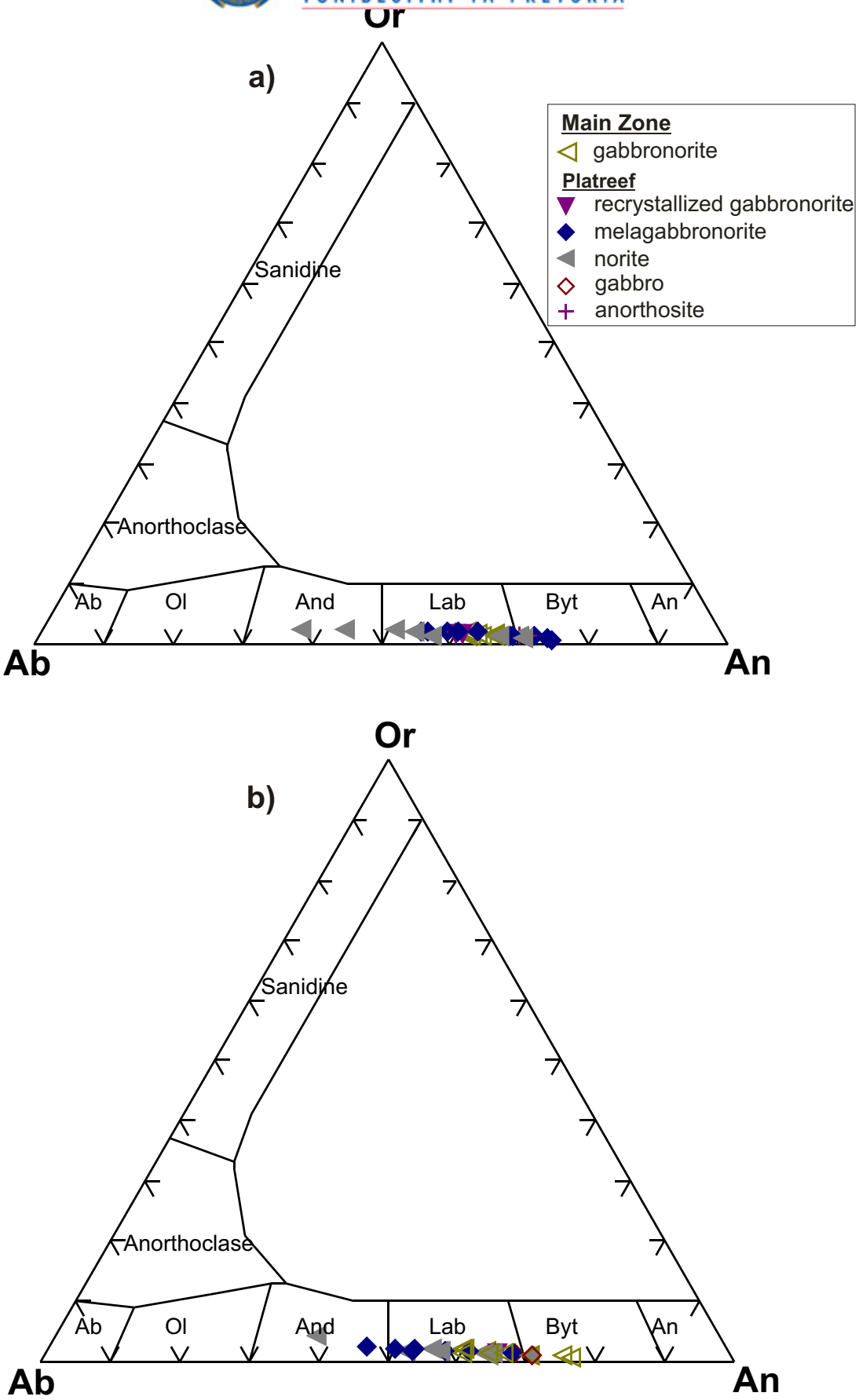

Fig. 7.1: Composition of plagioclase in Platreef and Main Zone rocks from Nonnenwerth a) drillcore 2121, b) drillcore 2199

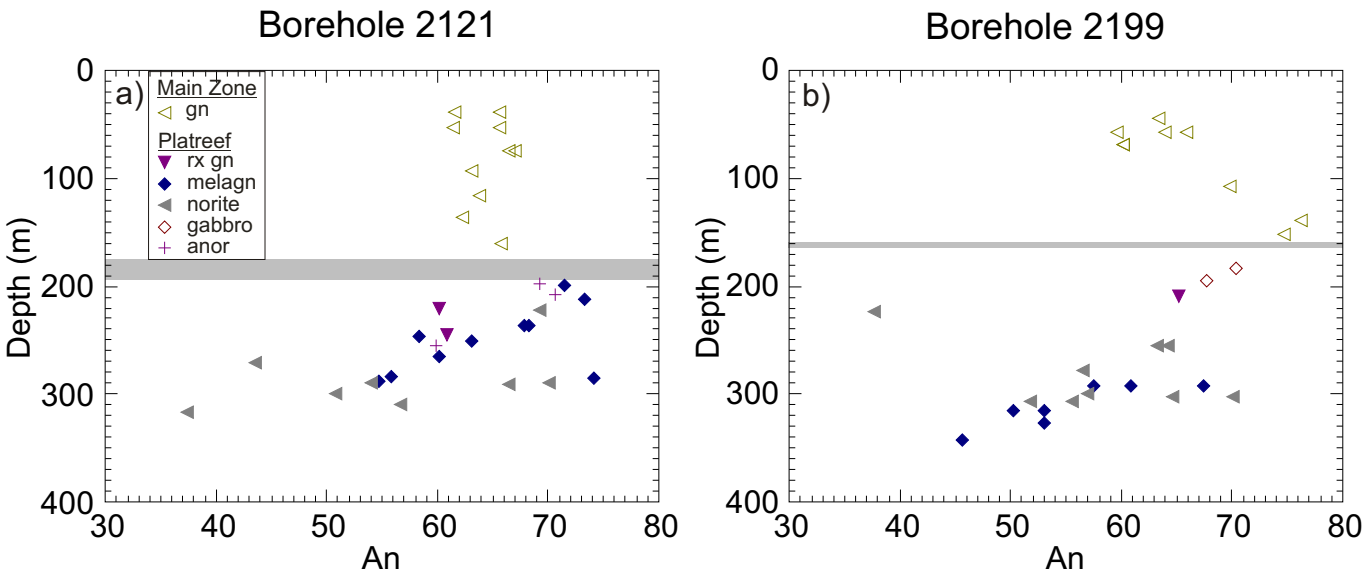

Fig. 7.2: (a and b) An content of plagioclase plotted versus depth. gn = gabbronorite, anor = anorthosite, melagn =melagabbronorite, rx = recrystallized gabbronorite. The shaded bar represents the dolomite layer defining the boundary between the Platreef and the Main Zone.

However, the plots of depth against An content shows different trends between the Main Zone and Platreef possibly suggesting that the rocks may have crystallized from distinct magma batches. It should also be noted that An values in the norites of both boreholes display an exceptionally wide range and the An contents of melagabbronorites are markedly different in the two boreholes. It is currently not known why this is so, but this may be attributed to localized effects and assimilation of xenoliths.

Plagioclase in the Platreef at Nonnenwerth is less An-rich than plagioclase on the farm Townlands (An_{54-85}; Manyeruke, 2003), where plagioclase is of broadly similar composition as plagioclase in the Upper Critical Zone (An_{68-85}; Cameron, 1982a; Naldrett *et al.*, 1986; Kruger and Marsh, 1985; Maier and Eales, 1997).

Inclusions of plagioclase within orthopyroxene in gabbronorite are more calcic than cumulus plagioclase (see Table 2a). Eales *et al.* (1994) noted a similar trend in the Upper Critical Zone at Union Section and attributed this to replenishment of the magma chamber with primitive magma leading to resorption of plagioclase phenocrysts suspended within the magma chamber.

7.2 Orthopyroxene

The orthopyroxenes at Nonnenwerth are mostly clinoenstatites with only three samples plotting in the pigeonite field (Fig. 7.3a and b). Enstatite contents vary between 70 and 56. Plots of Mg# (100 x cationic ratio of Mg^{2+} / (Mg^{2+} + Fe^{2+})), NiO

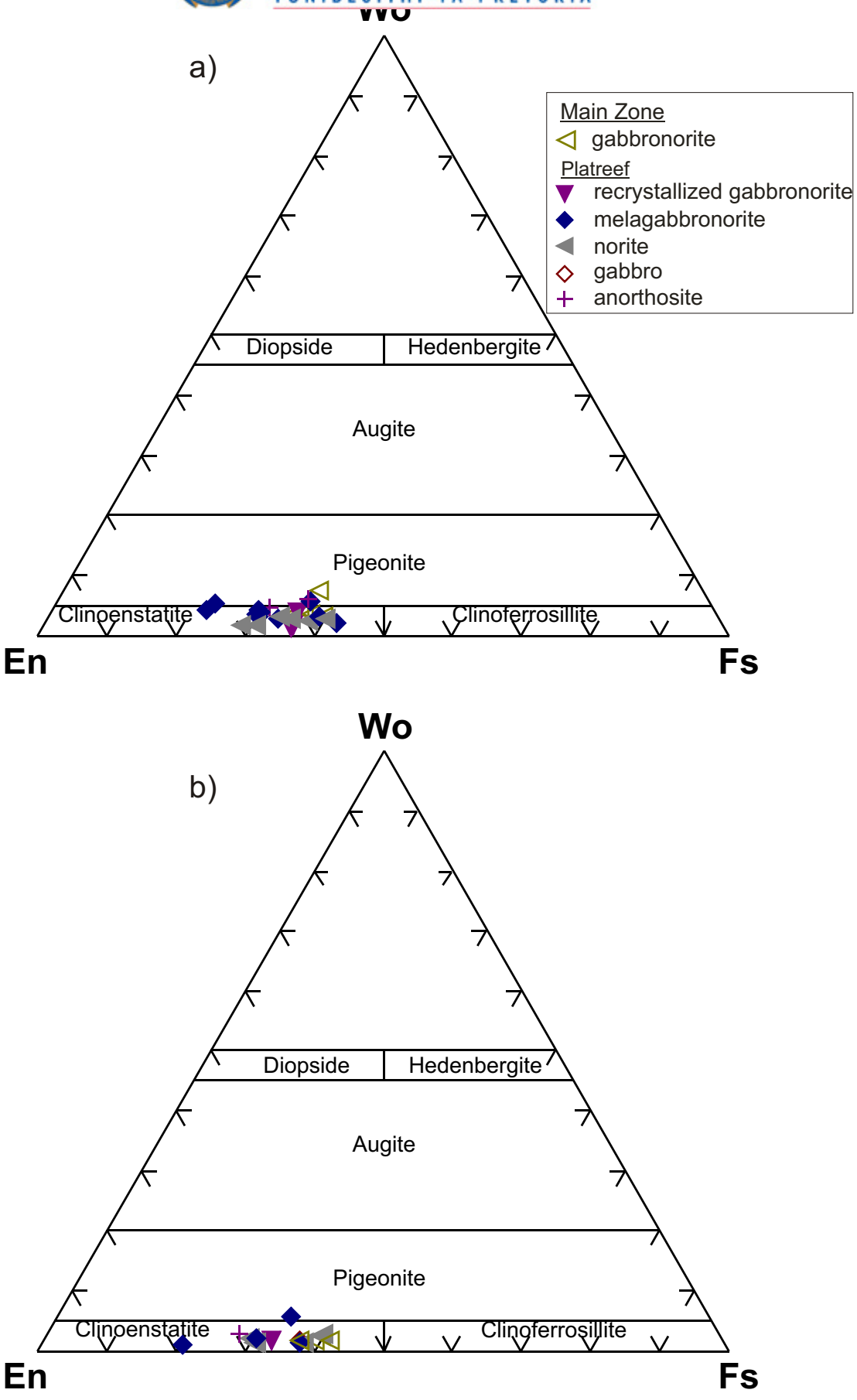

Fig. 7.3: Composition of orthopyroxene in Platreef and Main Zone rocks from Nonnenwerth a) drillcore 2121, b) drillcore 2199

and Cr_2O_3 against depth reveal an analogous compositional pattern as that observed in the case of plagioclase, i.e. a certain overlap in the composition of the Platreef and the Main Zone, but more compositional variation in the Platreef. Several Platreef samples have significantly higher Mg#, NiO and Cr_2O_3 contents than the Main Zone.

The plots of MnO and TiO_2 versus Mg# display an inverse linear relationship, except for TiO_2 versus Mg# in drillcore 2199 which does not show a clear trend (Fig. 7.5a and b). This indicates that Mn and Ti are incompatible in orthopyroxene and increase during differentiation. In contrast, Al_2O_3 increases with Mg# (Fig. 7.5c), indicating a simultaneous decrease in Mg and Al during differentiation. This pattern has also been described from the Upper Critical Zone of the Bushveld Complex (Eales *et al*., 1993) and may be explained by co-precipitation of orthopyroxene and plagioclase.

The compositions of orthopyroxenes in the Main Zone at Nonnenwerth are similar to those of orthopyroxene in the central Main Zone elsewhere in the Bushveld Complex (Mitchell, 1986). This suggests that the lower Main Zone is not developed in the studied area, a conclusion that is in agreement with the published geological maps.

The orthopyroxenes from the Platreef at Nonnenwerth are more difficult to correlate with other sequences in the northern lobe or elsewhere, partly because of their compositional variations. The orthopyroxenes are markedly less magnesian ($Mg\#_{57-72}$) than orthopyroxenes in the Platreef on the farms Townlands ($Mg\#_{68-82}$; Manyeruke, 2003), Tweefontein ($Mg\#_{74-78}$; Buchanan *et al.*, 1981) and Sandsloot ($Mg\#_{76-80}$ for the primary reef, McDonald *et al.*, 2005). However, Platreef

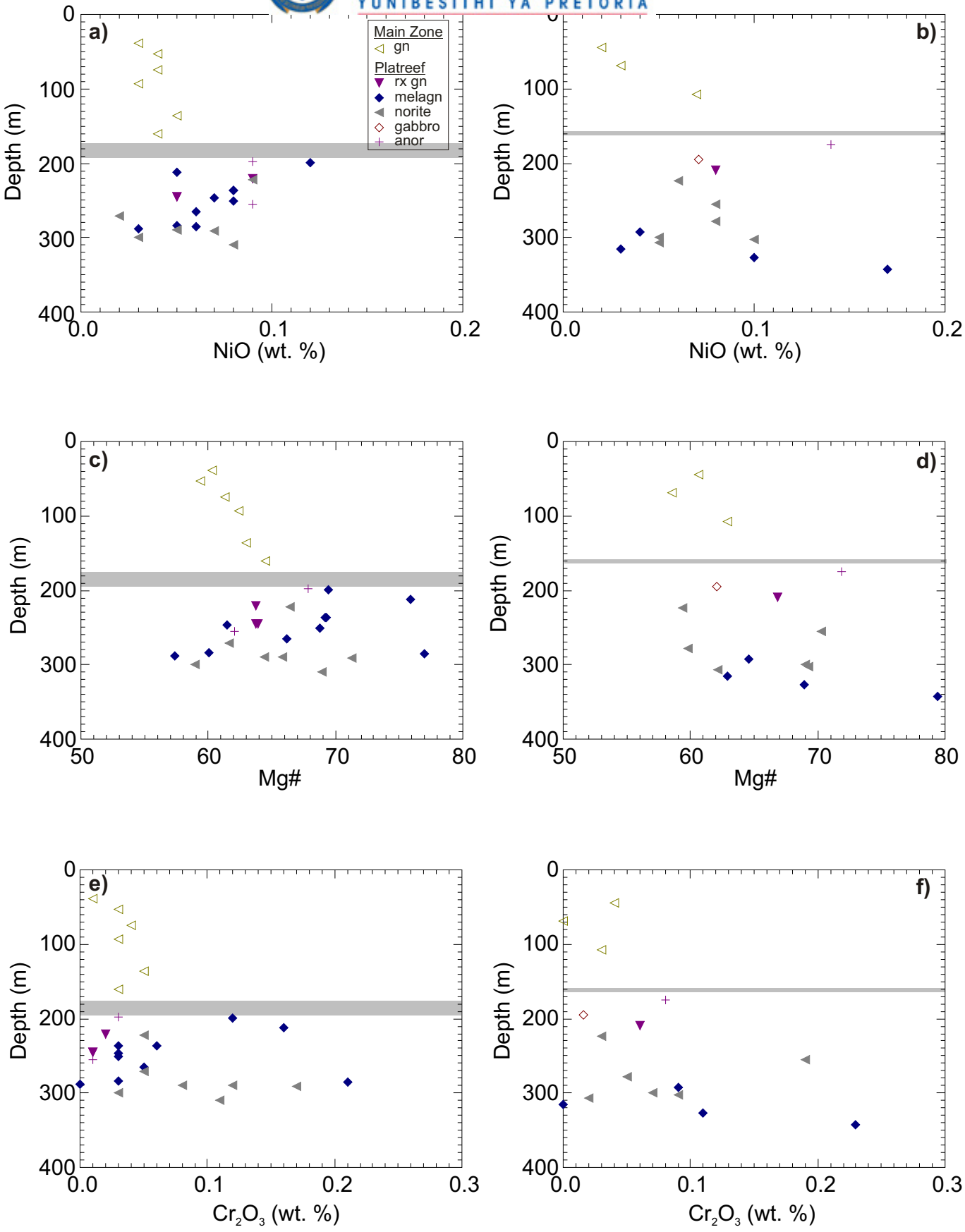

Fig. 7.4: Variation in orthopyroxene composition with depth at Nonnenwerth. (a and b): NiO. (c and d): Mg#. (e and f): Cr_2O_3. gn = gabbronorite, anor = anorthosite, melagn = melagabbronorite, rx gn = recrystallized gabbronorite. The shaded bar represents the boundary between the Platreef and the Main Zone.

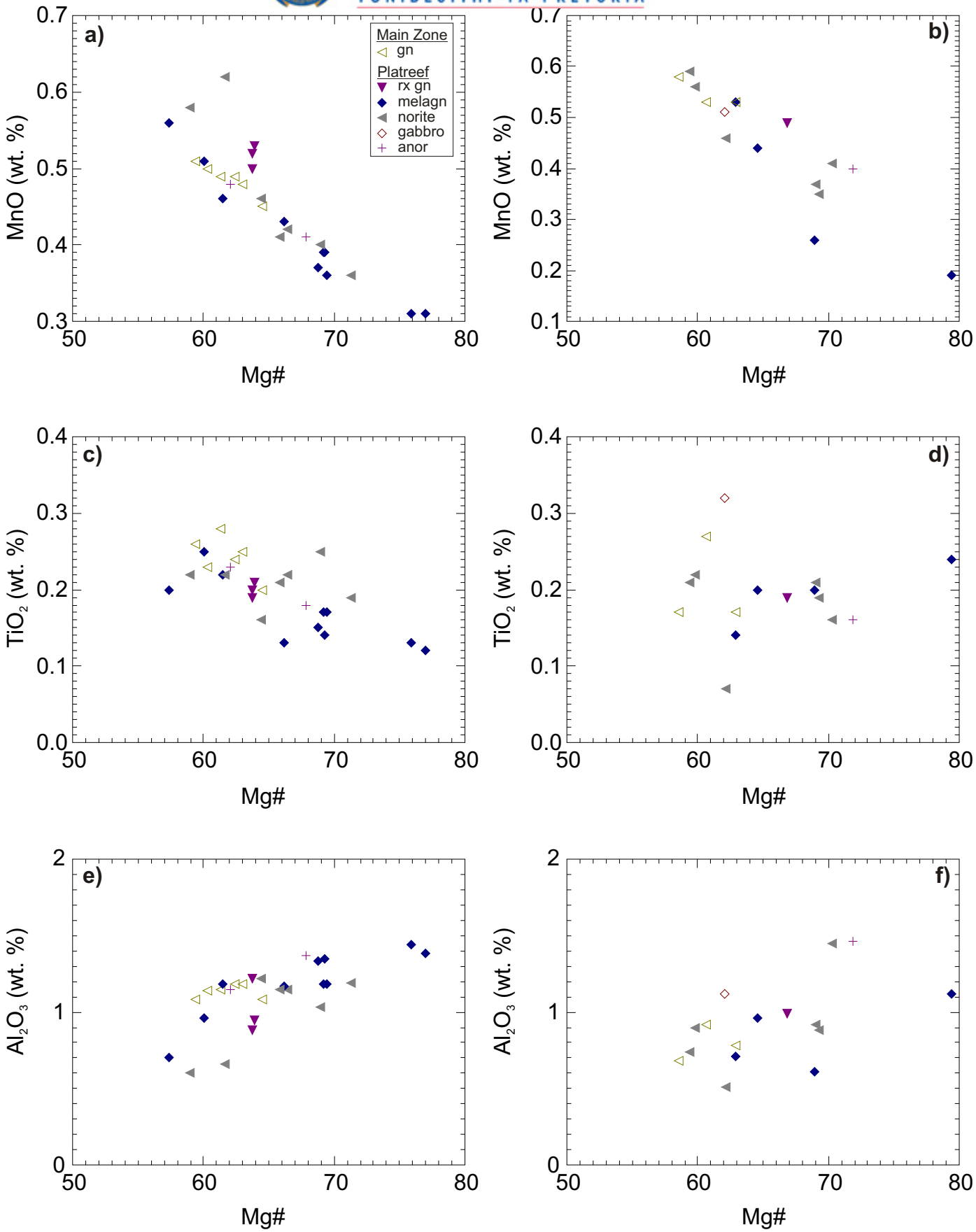

Fig. 7.5: Plots of (a and b) MnO versus Mg#, (c and d) TiO_2 versus Mg# and (e and f) Al_2O_3 versus Mg# in orthopyroxenes. gn = gabbronorite, anor = anorthosite, rx gn = recrystallized gabbronorite, melagn = mela- gabbronorite.

orthopyroxenes on Nonnenwerth have broadly similar maximum values of Mg# as orthopyroxenes on Drenthe and Overysel ($Mg\#_{65-77}$; Gain and Mostert, 1982; Cawthorn *et al.*, 1985), where the reef is equally underlain by granite-gneiss and dolomite. Thus there is a trend of the Platreef orthopyroxene becoming less magnesian towards the north. In the southern sectors, the orthopyroxene have broadly similar composition as the Upper Critical Zone ($Mg\#_{78 - 84}$; Cameron, 1982a; Naldrett *et al.*, 1986; Eales *et al.*, 1993; Maier and Eales, 1997; Cawthorn, 2002), whereas in the northern sectors, the composition of Platreef orthopyroxene overlaps with that of the lower to central Main Zone.

Cr_2O_3 contents in orthopyroxene of the Platreef on Nonnenwerth range from less than detection limit to 0.23 wt. % whereas those in the Main Zone are generally below 0.05 wt. % (Fig. 7.4e and f). The Cr_2O_3 contents in the Platreef orthopyroxenes are distinctively lower than those of typical Upper Critical Zone orthopyroxenes, which have Cr_2O_3 contents of 0.4 - 0.5 wt % (Eales and Cawthorn, 1996; Maier and Eales, 1997) and Townlands orthopyroxenes which have up to 0.41 wt. % Cr_2O_3 (Manyeruke, 2003; Manyeruke *et al.*, 2005). In contrast, the Cr_2O_3 contents of the Nonnenwerth orthopyroxene overlap with those of the lower to central Main Zone.

7.3 Clinopyroxene

Clinopyroxenes from the different lithologies mostly plot in the augite field of the pyroxene quadrilateral (Fig. 7.6), but several analyses plot in the diopside field. Mg# varies mostly between 64 – 80. The compositions are more ferric than those of

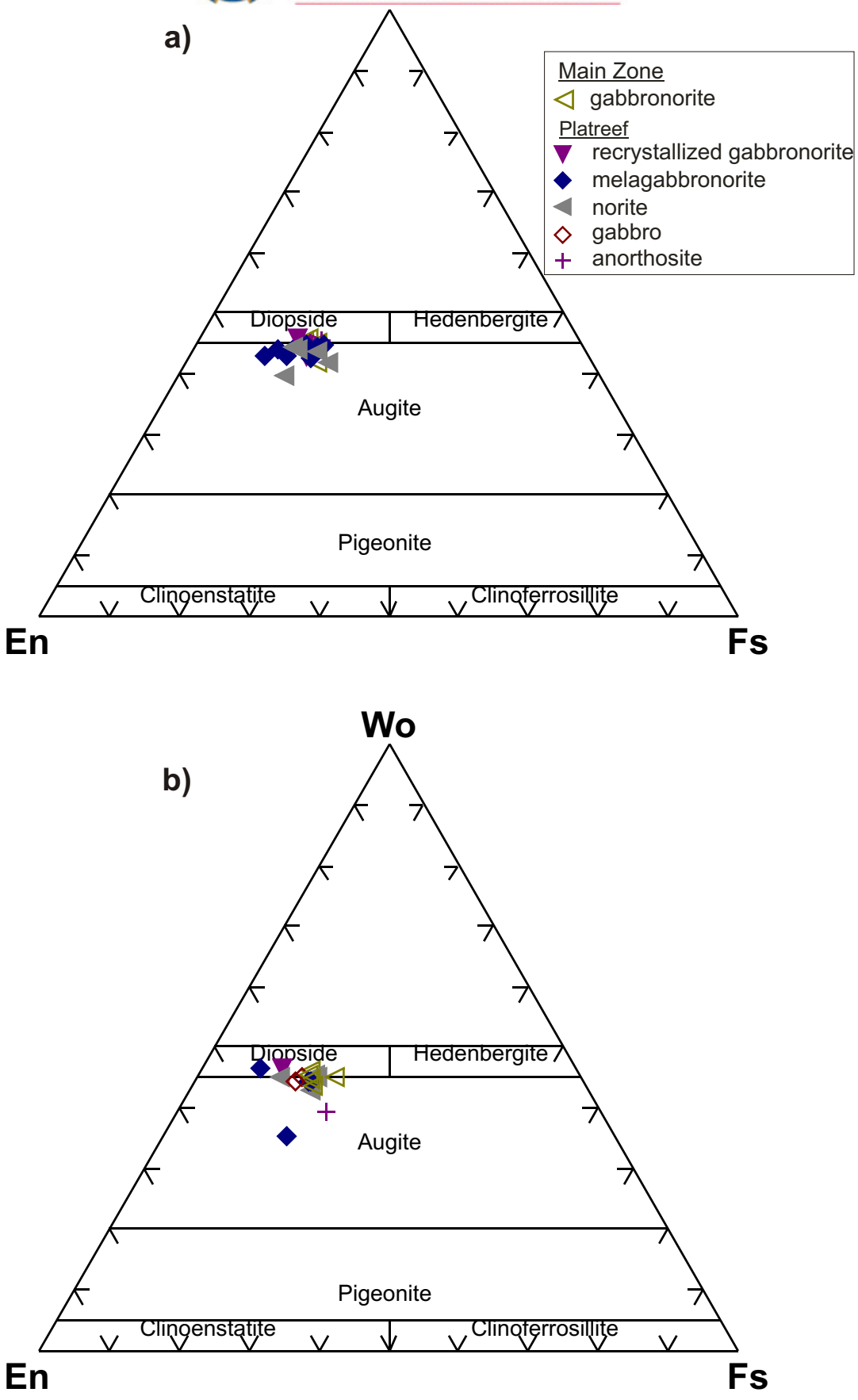

Fig. 7.6: Composition of clinopyroxene in Platreef and Main Zone rocks from Nonnenwerth. a) Borehole 2121, b) borehole 2199

clinopyroxenes in the Platreef on Townlands ($Mg\#_{76-91}$, Manyeruke, 2003; Manyeruke *et al.*, 2005) and Sandsloot (McDonald *et al.*, 2005), and clinopyroxenes from the Merensky Reef (Eales *et al.* 1993; Maier and Eales 1994; Cawthorn, 2002). However, clinopyroxene on Nonnenwerth shows similarities with that on Drenthe. Plots of NiO, TiO_2 and Mg# against depth reveal a broadly similar pattern as was observed in the plagioclase and orthopyroxene data, i.e. relatively more primitive compositions in some Platreef samples than in the Main Zone (Fig. 7.7a, c and e), a distinct break between the two intervals (Fig. 7.7a, c, d and e), a reverse differentiation trend with height in the Platreef (Fig. 7.7a) and normal differentiation with height in the Main Zone (Fig. 7.7c and e).

Borehole 2121 Borehole 2199

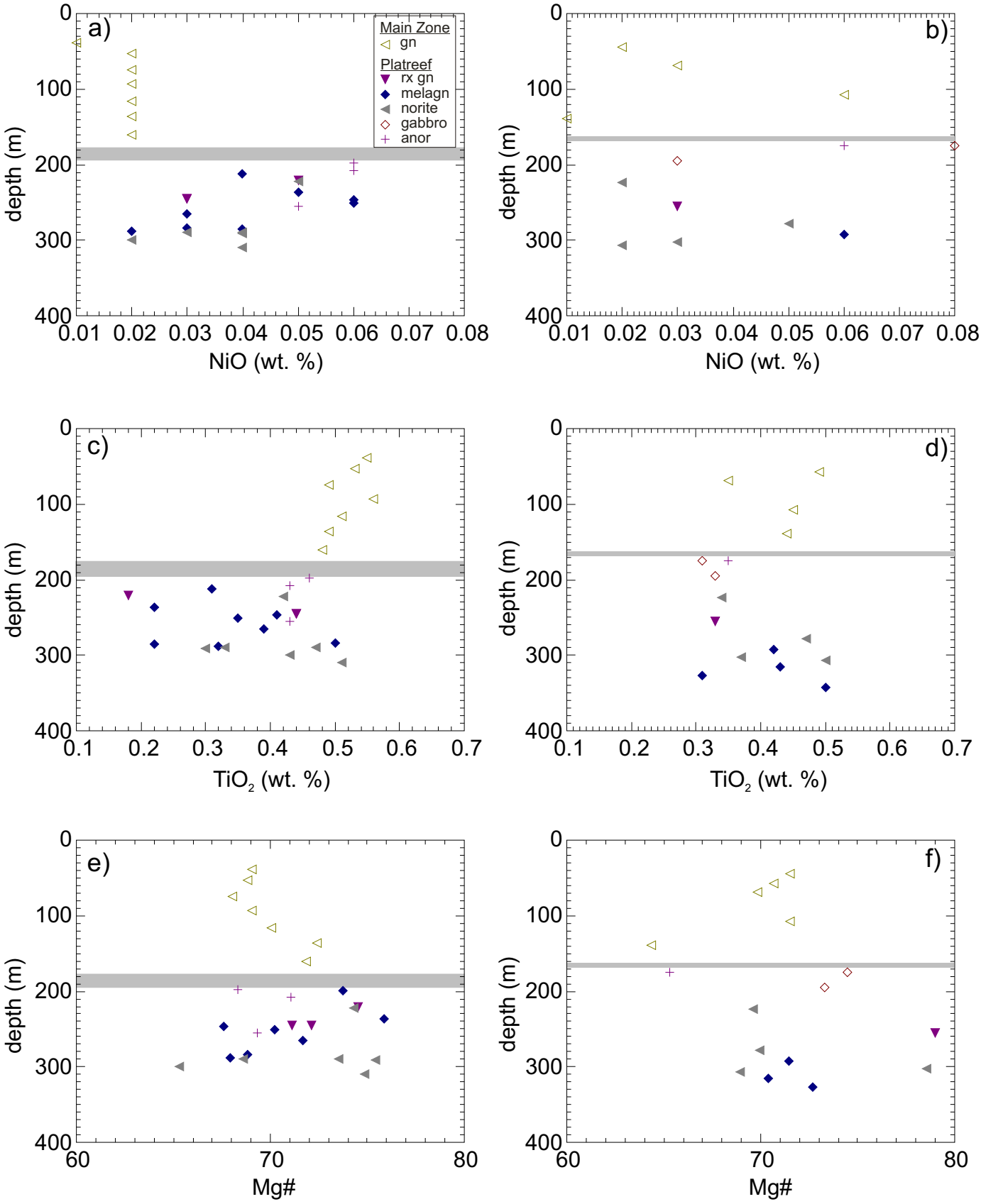

Fig. 7.7: Variation in clinopyroxene composition with depth at Nonnenwerth. NiO (a and b), TiO_2 (c and d) and Mg# (e and f). gn = gabbronorite, anor = anorthosite, rx gn = recrystallized gabbronorite, melagn = melagabbronorite. The shaded bar represents the boundary between Platreef and Main Zone.

7.4 Summary

Silicate minerals reveal a compositional break between the Platreef and Main Zone e.g. plagioclase becomes more calcic with height in the Platreef, but more sodic with height in the Main Zone. These compositional differences between the Platreef and the Main Zone suggest that the two units represent distinct influxes of magma. Although the composition of the two intervals overlap, the Platreef is more heterogeneous, with several samples having high Ni, Cr and Mg# in pyroxenes and An in plagioclase.

The orthopyroxenes at Nonnenwerth are markedly less magnesian ($Mg\#_{57-72}$) than orthopyroxenes in the Platreef on the farms Townlands ($Mg\#_{68-82}$; Manyeruke, 2003), Tweefontein ($Mg\#_{74-78}$; Buchanan *et al.*, 1981). Plagioclase in the Platreef at Townlands (An_{54-84}, average 71; Manyeruke *et al.*, 2005) is also more An-rich than plagioclase at Nonnenwerth (An_{47-75}, average 63). The former has a composition similar to plagioclase in the Upper Critical Zone (An_{68-85}; Cameron, 1982a; Naldrett *et al.*, 1986; Kruger and Marsh, 1985; Maier and Eales, 1997).

CHAPTER EIGHT: OCCURRENCE, DESCRIPTION AND CHEMICAL COMPOSITION OF THE OPAQUE MINERALS

In this chapter, the base metal sulphides, their occurrence and composition as well as the possible evolution of the sulphide assemblages at Nonnenwerth and Townlands will be described and discussed.

8.1 Sulphide and oxide minerals on Nonnenwerth

8.1.1 Platreef gabbronorite

The gabbronorite is generally barren or weakly mineralized and typically contains less than 1 vol. % sulphides (locally up to 4 vol. %) and up to 5 vol. % magnetite, chromite and ilmenite. The sulphides consist of pyrrhotite (50 – 70 %), chalcopyrite (10 – 40 %), pentlandite (5 – 10 %) and traces of pyrite, sphalerite and mackinawite. The sulphides occur as mm-sized, composite grains interstitial to or included in silicates, and as µm-sized disseminations in altered silicate minerals mostly forming aureoles around massive composite sulphides.

Pyrrhotite forms micron- to millimetre-sized grains that are often intergrown with chalcopyrite and pentlandite and may carry flame-like exsolution lamellae of the latter (Fig. 8.1a, b and c). The mineral rarely forms monomineralic grains. Chalcopyrite and pentlandite mostly occur along the margins of pyrrhotite grains (Figs 8.1c, d and e), or along fractures within pyrrhotite. Chalcopyrite also occurs as disseminations in aureoles around composite pyrrhotite, chalcopyrite and

pentlandite grains (Fig. 8.1b, d and e). The disseminated chalcopyrite is intergrown with secondary hydrosilicates adjacent to composite sulphide grains. Chalcopyrite often contains fine flame-like exsolutions of mackinawite and may include up to 10 µm wide disseminated sphalerite grains. In places, anhedral, micron-sized chalcopyrite occurs included in magnetite and may be intergrown with pentlandite (Fig. 8.1f).

Pentlandite occurs as polycrystalline fragmented grains along fractures in pyrrhotite or towards pyrrhotite grain margins (Fig. 8.1c and d), and as flame-like exsolution lamellae oriented along a single crystallographic axis (Fig. 8.1b). Only one grain of anhedral or subhedral pyrite enclosed in plagioclase was identified. Magnetite is anhedral or subhedral, commonly fractured (Fig. 8.1f) and occurs interstitial to silicates. It is often intergrown with ilmenite and in places encloses anhedral chalcopyrite and pentlandite grains (Fig. 8.1f). Ilmenite is internally homogenous. It is mostly intergrown with composite grains of pyrrhotite with minor pentlandite and chalcopyrite (Fig. 8.1d and e).

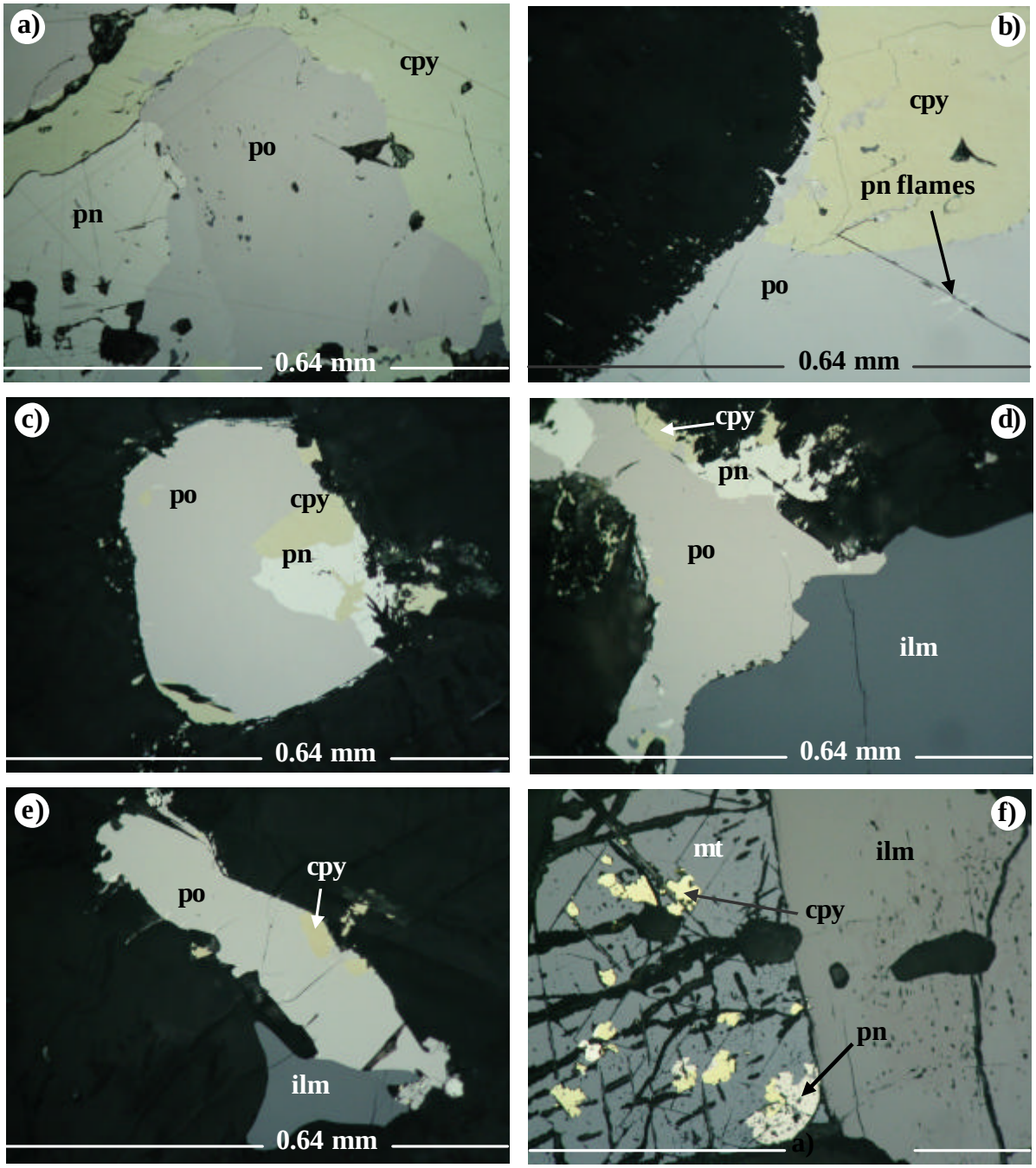

Fig. 8.1: Photomicrographs:
(a) Pyrrhotite (po) intergrown with pentlandite (pn) and chalcopyrite (cpy) (sample MOX11). b) Pyrrhotite and chalcopyrite intergrowth. Dark material is silicate. Note the pentlandite flames in pyrrhotite and the fine pyrrhotite injections into adjacent silicate (sample MOX15). (c) Pyrrhotite intergrown with minor pentlandite and chalcopyrite (sample MOX15). (d & e) Anhedral pyrrhotite intergrown with ilmenite (ilm). Minor chalcopyrite and pentlandite occur along the grain margin of pyrrhotite. Note the fine disseminations of chalcopyrite in adjacent silicates (sample MOX15). (f) Fractured magnetite (mt) intergrown with ilmenite. Magnetite encloses anhedral chalcopyrite intergrown with pentlandite (sample MOX14). In reflected light, plane polarised light, in oil.

8.1.2 Recrystallized gabbronorite

The unit is characterised by up to 5 vol. % sulphides and up to 4 vol. % of oxides (magnetite and ilmenite) plus minor chromite. The sulphides are pyrrhotite (0 – 75 %), chalcopyrite (25 – 40 %), pentlandite (10 – 20 %) and pyrite (0 – 35 %). Texturally, the sulphides occur as

i) disseminations of small composite or monomineralic grains included in, or interstitial to, recrystallized silicate grains (mostly orthopyroxene), and

ii) replacements of primary silicates along cleavage planes in the form of fine disseminations intergrown with the alteration minerals.

Pyrrhotite forms micron- to millimetre-sized grains that are often intergrown with chalcopyrite and pentlandite and may carry flame-like exsolution lamellae of the latter (Fig. 8.2a). The mineral rarely forms monomineralic grains.

Chalcopyrite occurs as an interstitial phase that is internally homogenous and has irregular grain margins. It is commonly intergrown with pentlandite and pyrrhotite, in places forming lamellae in pyrrhotite (Fig. 8.2a and b). It also replaces pyrrhotite along fractures (Fig. 8.2e) and orthopyroxene along cleavage planes. Secondary minerals after plagioclase and pyroxenes (i.e. chlorite, amphibole, quartz and albite) with disseminated (a few µm sized) chalcopyrite and, in places, pyrite form an aureole around composite sulphides or monomineralic chalcopyrite (Fig. 8.2c and d). Finally, chalcopyrite may be included in plagioclase as monomineralic anhedral grains (Fig. 8.2c), or intergrown with minor pyrite (Fig. 8.2d).

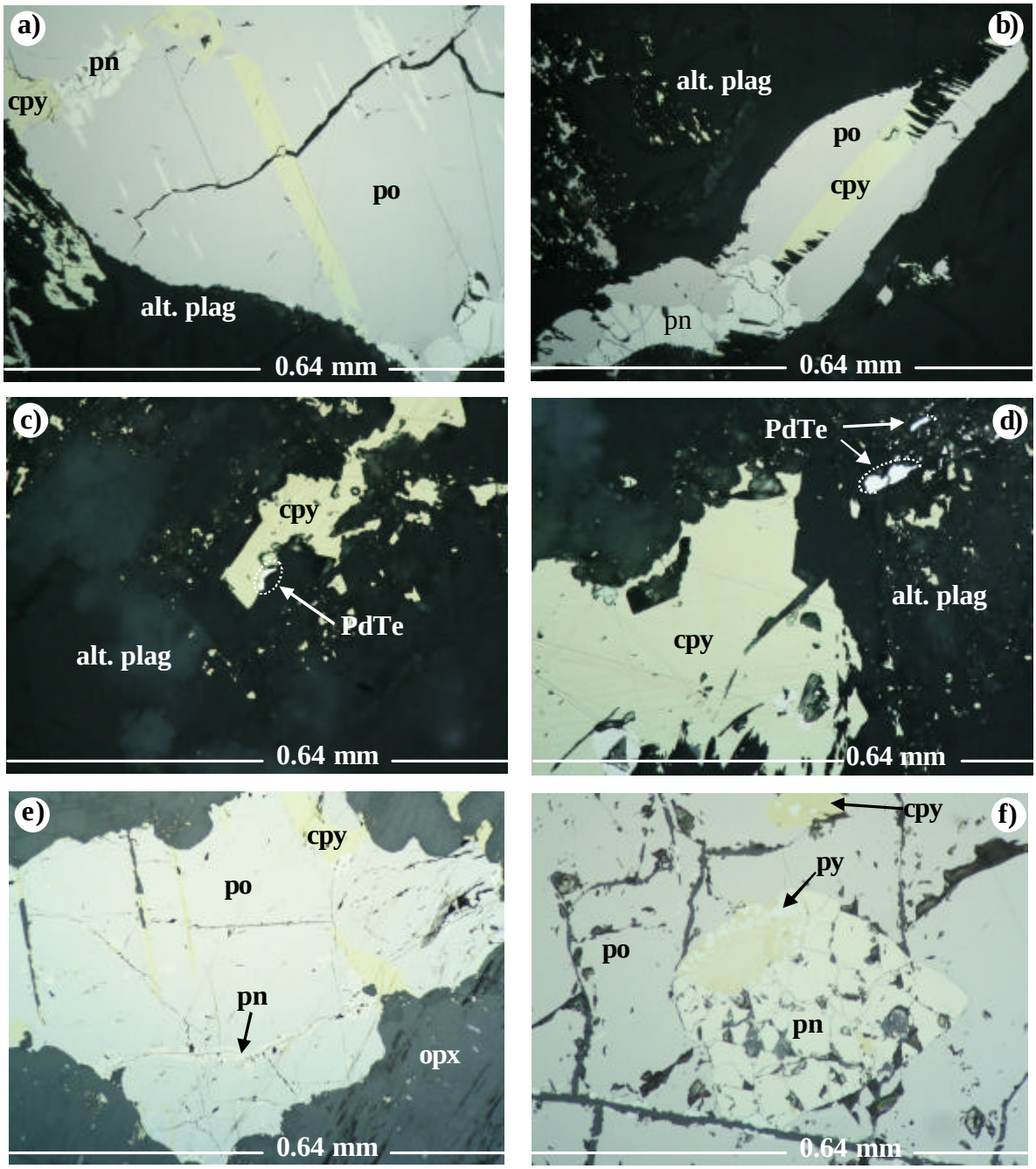

Fig. 8.2: Photomicrographs:
(a & b) Pyrrhotite (po) intergrown with minor chalcopyrite (cpy) and pentlandite (pn). Note the pentlandite and chalcopyrite lamellae in pyrrhotite (sample MOX12). (c & d) Anhedral chalcopyrite with an aureole of disseminated chalcopyrite intergrown with alteration silicate minerals (mainly chlorite after plagioclase) (sample MOX9). (e) Anhedral pyrrhotite intergrown with pentlandite along fractures and chalcopyrite along its margins (sample MOX12). (f) Fractured pyrrhotite enclosing fragmented, vaguely round pentlandite that is intergrown with pyrite (py) and chalcopyrite on its margin. Note also chalcopyrite enclosed in pyrrhotite (sample MOX10). In reflected light, plane polarised light, in oil.

Pentlandite forms flame-like exsolution lamellae and granular masses included in pyrrhotite (Fig. 8.2f) or along pyrrhotite grain margins and fractures (Figs. 8.2b and e, respectively). Pentlandite included in pyrrhotite may be intergrown with worm-like intergrowths of chalcopyrite and pyrite at its margin (Fig. 8.2f), suggesting replacement of pentlandite by chalcopyrite and pyrite. Other forms of pentlandite-chalcopyrite-pyrite intergrown are shown in Fig. 8.2g and h.

Pyrite occurs predominantly as polycrystalline fracture fillings in plagioclase (Fig. 8.2i and j) and, in places, as rims around pentlandite, in which case it may be intergrown with chalcopyrite (Fig. 8.2g).

Ilmenite (up to 400 µm) occurs interstitial to, or included in, pyroxene. The grains are anhedral, internally homogenous and often intergrown with magnetite (Fig. 8.2k). Magnetite is also interstitial and, as mentioned above, is mostly intergrown with ilmenite grains. Magnetite may be replaced by pyrrhotite along cleavage planes (Fig. 8.2k).

Notably, samples with high pyrrhotite contents contain no pyrite and vice versa. This suggests a reaction-replacement relationship between the two sulphides. The presence of pyrite may suggest increased S fugacity (fS_2) resulting in pyrrhotite being replaced by pyrite.

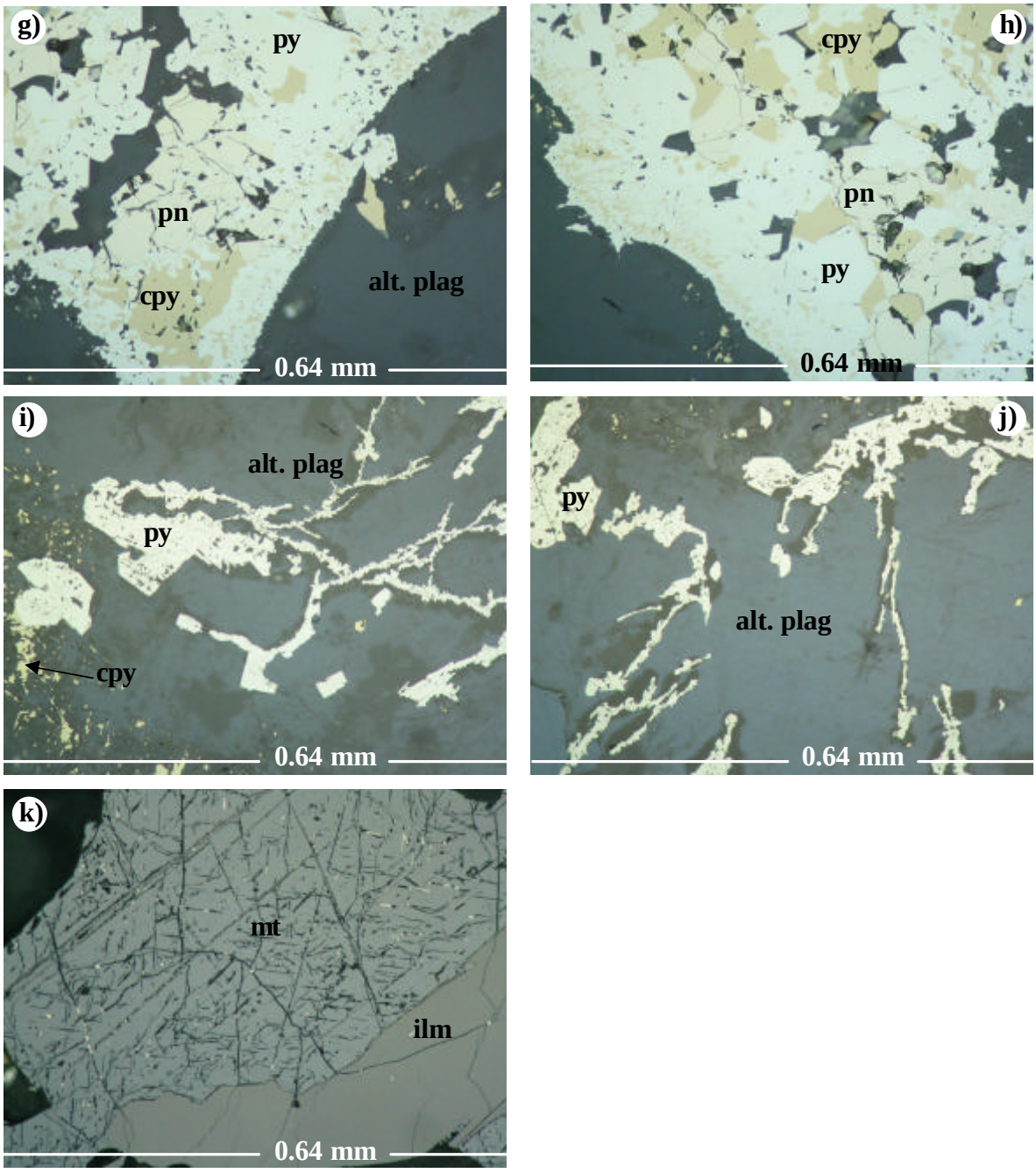

Fig. 8.2 continued. Photomicrographs:
(g & h) Pyrite enclosing fragmented pentlandite and intergrown with disseminated chalcopyrite. Note the rim of fine chalcopyrite intergrown with pyrite around the coarse, fragmented, composite sulphide (sample MOX10), (i & j) Pyrite in fractures within altered plagioclase (alt. plag). Disseminated chalcopyrite is intergrown with secondary silicates (sample MOX9 and 10, respectively). (k) Magnetite (mt) intergrown with ilmenite (ilm). Magnetite contains pyrrhotite along cleavage planes (sample MOX12). In reflected light, plane polarised light, i and j in air and g, h and k in oil.

8.1.3 Anorthosite

The anorthosites may contain up to 20 vol. % sulphides, in relative proportions: chalcopyrite 35 – 85 %, pyrrhotite 5 – 50 %, pentlandite 5 – 20 %, and pyrite 0 – 15 %. Up to 3 vol. % ilmenite with rare magnetite and chromite may also occur. The sulphides tend to be associated with felsic domains of the rock and the relative proportions of the sulphides are extremely variable ranging from chalcopyrite-dominated to pyrrhotite-dominated. Chalcopyrite-dominated samples have the highest sulphide contents. The sulphides occur as

i) aggregates of composite grains interstitial to plagioclase and clinopyroxene or included in clinopyroxene, and
ii) replacement minerals along cleavage planes of clinopyroxene, fractures in plagioclase or intergrown with secondary alteration silicates.

Two generations of chalcopyrite are present in the samples.

(1) The first occurs as irregular shaped, mostly fractured interstitial monomineralic grains that range from a few µm to mm in size. In places, the chalcopyrite grains are corroded and intergrown with secondary silicate minerals (amphiboles), mostly along grain boundaries. The chalcopyrite may include coarse (mm-sized) subhedral crystals of pyrite, small (1 – 2 µm) crystals of sphalerite and pyrrhotite as well as zircon (Fig. 8.3a), apatite and calcite. Zircon and apatite are euhedral or subhedral in shape and up to 100 µm and 1-2 µm in size, respectively.

(2) The other generation of chalcopyrite is of a secondary nature and occurs as

i) rims around pyrrhotite which in turn is rimmed by secondary pyrite (Fig. 8.3b and c), and

ii) vaguely round vermicular intergrowths of chalcopyrite and pyrite included in pyrrhotite (Fig. 8.3d and e).

Pyrrhotite mostly occurs as interstitial anhedral grains that are intergrown with chalcopyrite and pentlandite (Fig. 8.3f). Pyrrhotite also includes vaguely round vermicular intergrowths of pyrite and chalcopyrite, in places with a remnant of pentlandite (Fig. 8.3d and e, respectively). Similar textural intergrowths have been observed in recrystallized gabbronorite of the Platreef (Section 7.1.2) and in the Main Sulphide Zone of the Great Dyke of Zimbabwe (Oberthür, personal communication, 2005), where these textures were interpreted as replacements of pentlandite by pyrite and chalcopyrite.

Pentlandite occurs as fragmented interstitial grains that may be intergrown with chalcopyrite (Fig. 8.3g), as fracture fillings together with pyrite, pyrrhotite and chalcopyrite, along grain margins in pyrrhotite, or as minor flame- like exsolution lamellae and vaguely round inclusions in pyrrhotite. In places, pentlandite may be altered and replaced by coronas of violarite (Fig. 8.3h). Relict pentlandite forming islands in violarite is observed in sample MOX29 (Fig. 8.3i).

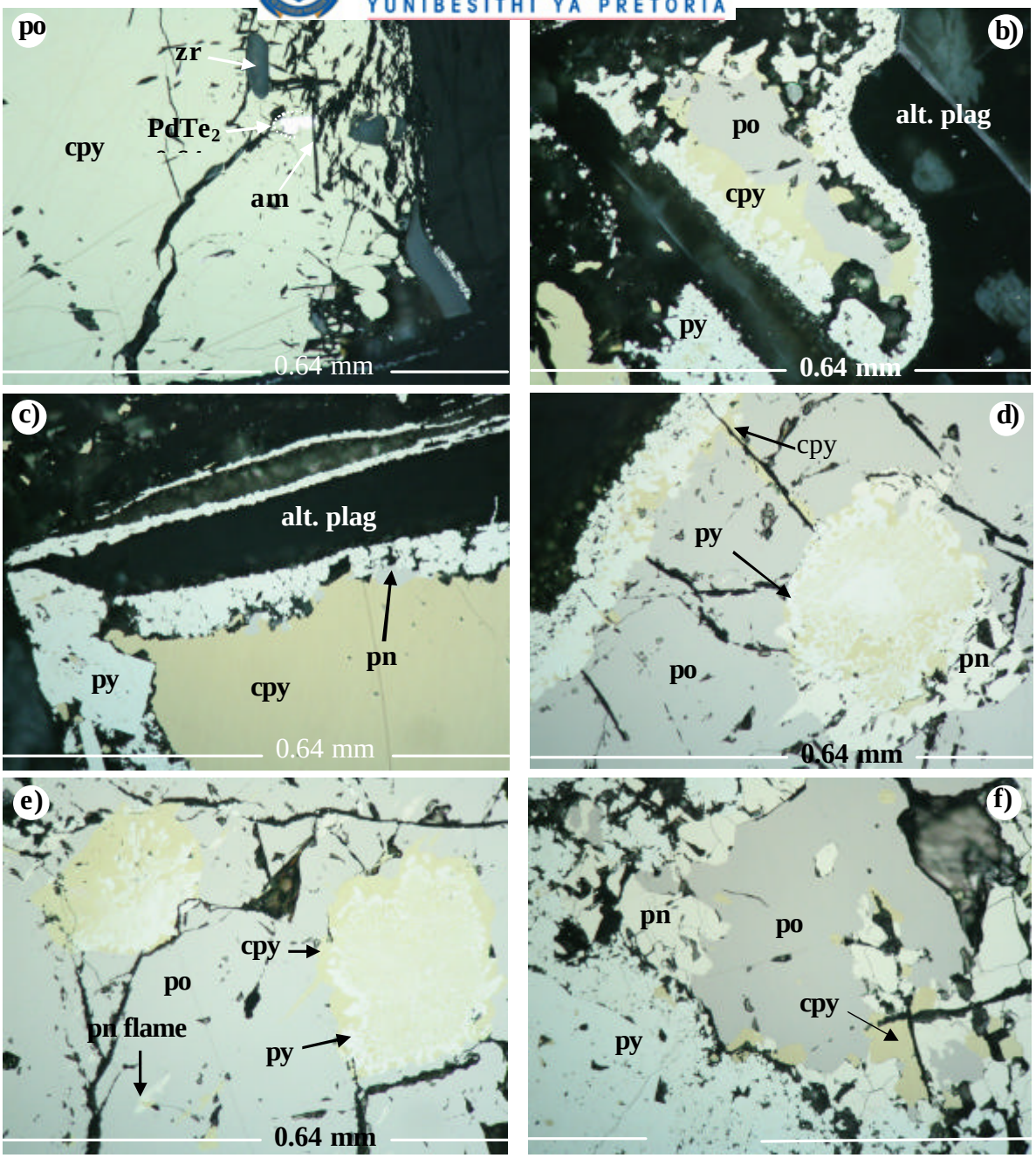

Fig. 8.3: Photomicrographs:
(a) Chalcopyrite intergrown with amphibole (am) laths along its margin, and enclosing subhedral zircon (sample MOX29). (b) Aggregate of pyrrhotite rimmed by chalcopyrite which is in turn rimmed by pyrite (sample MOX32). (c) Chalcopyrite intergrown with minor pentlandite at its margin and rimmed by pyrite. Note streaks of pyrite in adjacent altered plagioclase (Sample MOX32). (d) Pyrrhotite enclosing an intergrowth of pentlandite, pyrite and chalcopyrite. The corona around pyrrhotite consists of pyrite intergrown with minor chalcopyrite (sample MOX32). (e) Pyrrhotite enclosing vaguely round blebs of an intergrowth of pyrite and chalcopyrite. Chalcopyrite is concentrated towards the rims whereas pyrite is concentrated in the core. Pyrrhotite additionally contains flame-like exsolutions of pentlandite (sample MOX32). (f) Intergrowth of pyrrhotite (po) pyrite (py), minor chalcopyrite (cpy), and pentlandite (pn). (sample MOX27). opx = orthopyroxene. In reflected light, plane polarised light, in oil.

Pyrite exhibits a wide variety of textures. The main modes of occurrence are:

i) worm-like intergrowths with chalcopyrite and pyrrhotite (Fig. 8.3d)

ii) deuteric veinlets within plagioclase (Fig. 8.3c)

iii) replacement of clinopyroxene along cleavage planes and fractures (Fig. 8.3l).

In addition, pyrite occurs as an interstitial phase along plagioclase and clinopyroxene grain margins where, in places, it may replace the silicate minerals (Fig. 8.3j and k). It can also occur along plagioclase and clinopyroxene cleavage planes (Fig. 8.3l), or cross-cutting quartz. In the latter case it is net textured and porous and often intergrown with minor chalcopyrite.

Ilmenite is interstitial to, or enclosed in, pyroxenes. Most of the grains are altered to leucoxene suggesting fluid activity. Hematite tends to be euhedral, up to 1 mm in size, and occurs included in chalcopyrite. Rare magnetite, containing ilmenite lamellae, occurs interstitial to silicates or enclosed in altered orthopyroxene.

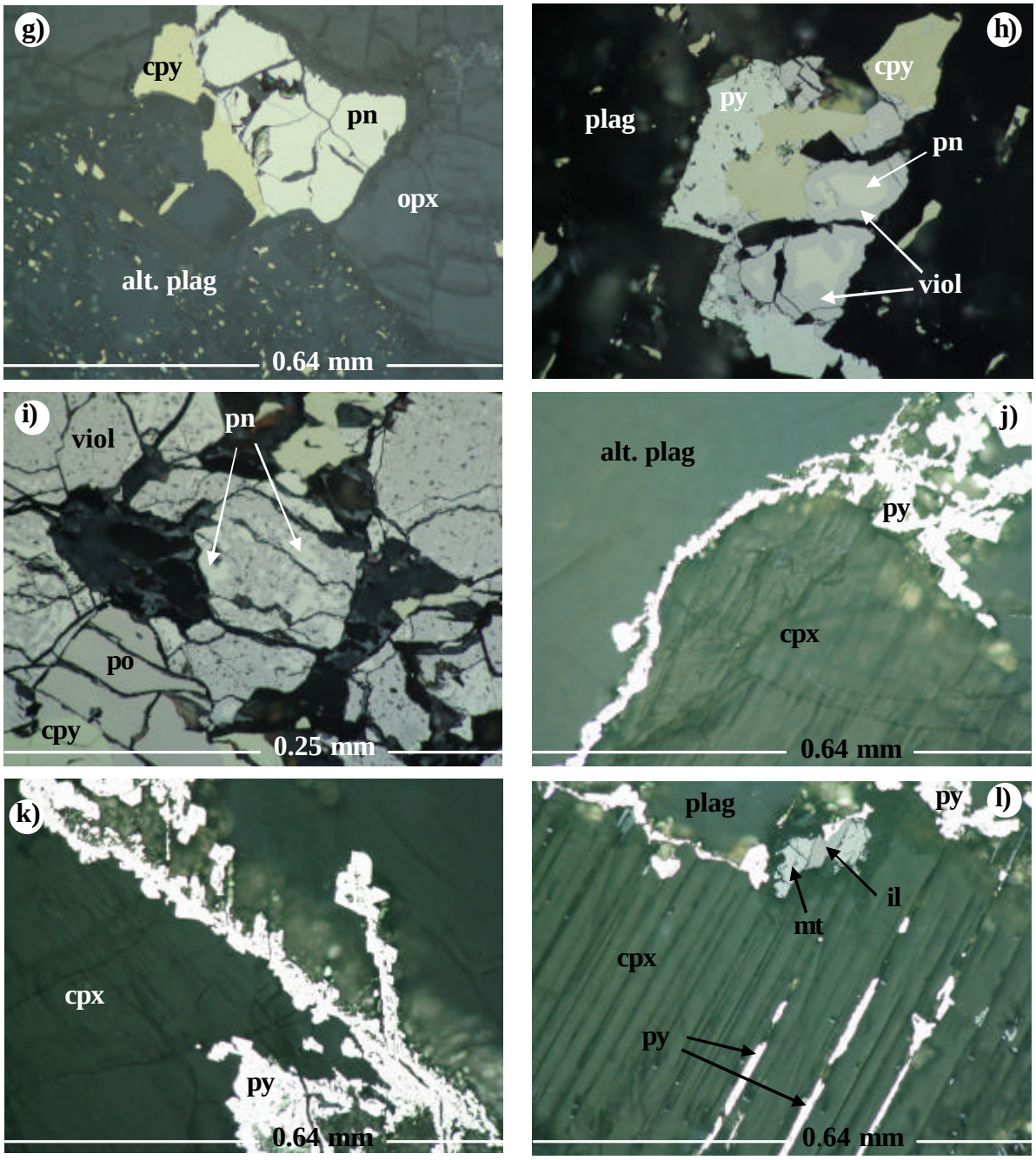

Fig. 8.3 continued:
(g) Interstitial pentlandite intergrown with chalcopyrite. Disseminated chalcopyrite replaces adjacent altered plagioclase (alt. plag) along cleavage planes (sample MOX27). (h) Violarite (viol) rimming pentlandite and intergrown with pyrite and chalcopyrite sample (MOX29). (i) Violarite with minor relictic pentlandite is intergrown with pyrrhotite and chalcopyrite (sample MOX29). (j & k) Pyrite occurs interstitial to plagioclase and clinopyroxene (cpx) and replaces the silicates along fractures (sample MOX32). (l) Interstitial pyrite replaces clinopyroxene along cleavage planes (sample MOX 32). In reflected light, plane polarised light, in oil.

8.2 Sulphide and oxide minerals on Townlands

8.2.1 Upper Platreef

The Upper Platreef is characterised by low sulphide contents (< 2 vol. %) towards the top of the Unit, and sulphide-rich rocks (up to 30 vol. %) towards the base. The latter may also contain up to 5 vol. % oxides (chromite, magnetite and ilmenite). The sulphide assemblage consists of pyrite (30 – 70 %), chalcopyrite (15 -50 %) and millerite (0 – 20 %). Pyrrhotite is rare. Only one sample (P2) contained abundant pentlandite (60 %) in addition to chalcopyrite (15 %). Minor amounts of violarite and covellite are also present in the rocks.

It is important to note that the samples with low sulphide contents have the lowest pyrite and highest chalcopyrite contents, whereas the sulphide-rich samples near the base of the Unit have high pyrite and low chalcopyrite contents and always contain millerite. The dominance of pyrite towards the basal portions of the Platreef was also reported by Iljina and Lee (2005). This was interpreted to suggest a change from S-rich to S-poor (or metal rich) environments during the crystallisation of the Platreef.

Pyrite occurs as massive, up to 10 mm-wide subhedral or anhedral grains that are mostly intergrown with chalcopyrite and secondary silicates (mainly amphiboles; (Fig. 8.4a and b). Coarse pyrite is often cut by veinlets of intergrown millerite and chalcopyrite (Fig. 8.4e and f). Locally, pyrite is intergrown with magnetite that encloses, or is intergrown with, millerite and fine chalcopyrite (Fig. 8.4c and d).

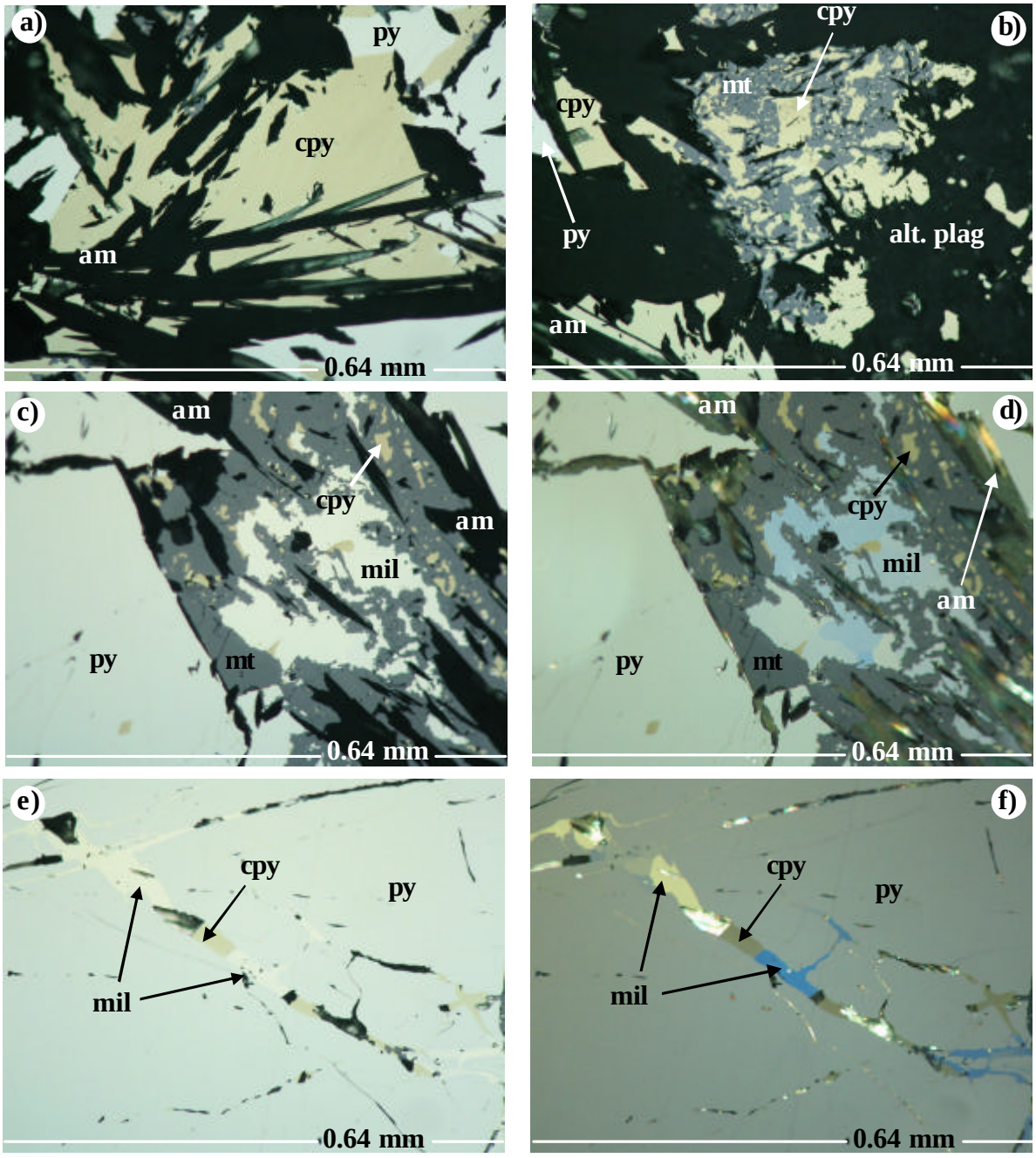

Fig. 8.4: Photomicrographs:
(a) Chalcopyrite (cpy) and pyrite (py) intergrown with acicular amphibole actinolite (am) (sample P7). (b) An aggregate of intergrown anhedral magnetite (mt) and chalcopyrite in altered plagioclase (alt. plag) (sample P7). (c & d) Coarse pyrite intergrown with magnetite that encloses millerite (mil). Magnetite is also intergrown with anhedral, disseminated chalcopyrite (sample P7). (e & f) Coarse pyrite cut by veinlets of intergrown chalcopyrite and millerite (sample P7). In reflected light, in oil, (a, b & e) plane polarised light and (d & f) cross polarised light.

Chalcopyrite exhibits a variety of textures. It occurs as coarse (up to 1.5 mm) grains that are intergrown with pyrite and acicular (up to 1.5 mm) amphibole (actinolite) (Fig. 8.4a). It also occurs as disseminated anhedral grains intergrown or enclosed in magnetite (Fig. 8.4b, c and d) and intergrown with millerite along fractures in coarse pyrite (Fig. 8.4e and f). Coarse interstitial chalcopyrite grains which may be intergrown with minor pentlandite on their margins occur in places and are cut and replaced by covellite veinlets and rimmed by magnetite (Fig. 8.4g and h). Patchy chalcopyrite grains occur along the margins of anhedral violarite masses after pentlandite (Fig. 8.4i).

Millerite is anhedral and occurs intergrown with chalcopyrite in fractures within coarse pyrite (Fig. 8.4e and f) or enclosed in magnetite (Fig. 8.4b end c).

Pentlandite tends to be intergrown with chalcopyrite and is often cut by veinlets of magnetite and minor covellite. In places, pentlandite forms minor anhedral grains at the margins of violarite (Fig. 8.4i and j).

Violarite forms anhedral, patchy masses that are intergrown with chalcopyrite and associated with magnetite along its margins (Fig. 8.4i and j). As noted earlier, minor amounts of pentlandite may occur along the margins of violarite, suggesting that the pentlandite is relictic and that most of the primary pentlandite has been replaced by violarite.

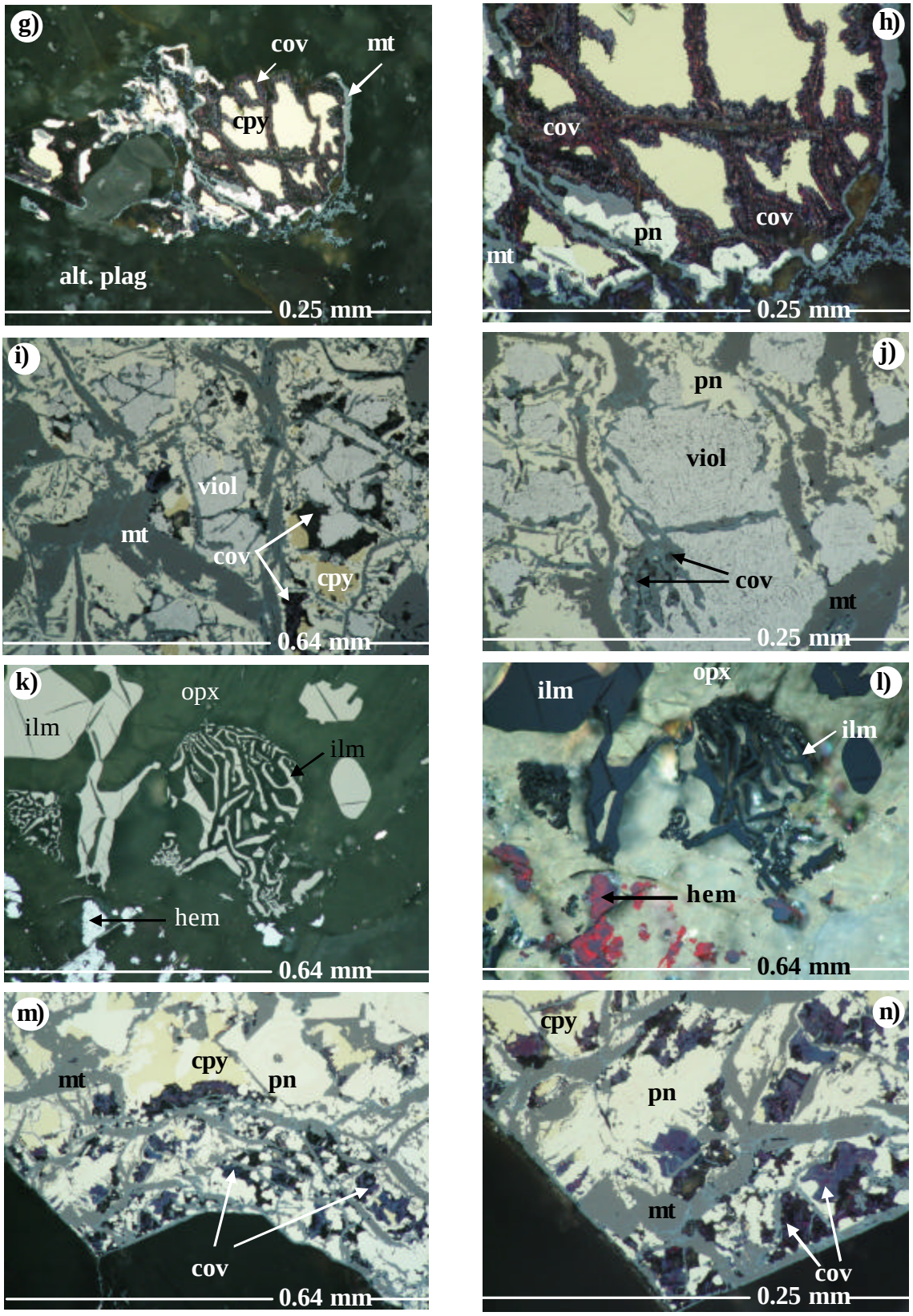

Fig. 8.4 continued: Refer to next page for explanation of the photomicrographs

Fig. 8.4 continued:
g & h) Chalcopyrite cut by covellite (cov) veins and rimmed by magnetite. Note minor pentlandite in h (sample P2). (i & j) Patches of violarite intergrown with pentlandite, minor chalcopyrite, covellite and cut by magnetite veinlets (sample P2). (k & l) Intergrowth of orthopyroxene (opx) and ilmenite, as well as granular, subhedral and anhedral ilmenite (ilm), orthopyroxene (opx) and minor anhedral hematite (hem) (sample P4). (m & n) Pentlandite and chalcopyrite show extensive alteration to covellite and magnetite along irregular fractures (sample P2). In reflected light, plane polarised light except l, in oil.

Covellite replaces chalcopyrite along fractures (Fig. 8.4g and h) or forms islands towards altered margins of composite sulphides where it is associated with magnetite (Fig. 8.4m and n).

Magnetite is anhedral and may be intergrown with anhedral disseminated chalcopyrite or it may enclose an intergrowth of anhedral millerite and chalcopyrite grains (Fig. 8.4b and d, respectively). Ilmenite is internally homogenous, forming anhedral or subhedral grains that may be included in orthopyroxene or occur as intergrowth of ilmenite and orthopyroxene (Fig. 8.4k and l). Anhedral hematite (oxidised magnetite) enclosed in plagioclase was also identified and is mostly associated with ilmenite (Fig. 8.4k and l).

8.2.2 Middle Platreef

As the Upper Platreef, the Middle Platreef is also characterised by an inhomogeneous distribution of the sulphides. The samples towards the top of the unit have 1 – 2 vol. % sulphides whereas those towards the base have 15 – 20 vol. % sulphides. The proportions of the different sulphides show significant variation especially in samples with low sulphide contents. Some samples are pyrrhotite-rich (up to 70 %) and contain no pyrite, whereas others are pyrite-rich

(up to 75 %) with only minor to trace amounts of pyrrhotite. Chalcopyrite and pentlandite occur in about equal amounts and together constitute 20 – 30 % of the sulphides. Samples with high sulphide contents are characterised by abundant pyrite (50 – 60 %), as well as millerite (10 – 20 %), chalcopyrite (10 – 20 %) and pentlandite (0 – 20 %). Trace amounts of galena and rare molybdenite are also present, but pyrrhotite is absent. Oxides reach a maximum of 4 vol. % and include magnetite, chromite and ilmenite.

Pyrite exhibits a variety of textures. It occurs as polycrystalline monomineralic grains up to 5 mm in size or as net-textured or vermicular masses in plagioclase (Fig. 8.5a and b). It may also occur as a replacement sulphide in fractures in altered pyroxene (Fig. 8.5b). In places, pyrite occurs as rims around chalcopyrite or millerite (Fig. 8.5a and e, respectively) or in millerite-bearing veinlets that transect through chalcopyrite (Fig. 8.5f and g). Pyrite may be cut by polycrystalline veinlets containing intergrown chalcopyrite and pentlandite (Fig. 8.5c and d).

Chalcopyrite occurs as optically homogenous grains with irregular grain margins, often intergrown with magnetite (Fig. 8.5h) and pyrite (Fig. 8.5i). Chalcopyrite may be interstitial to millerite (Fig. 8.5j) and in places enclosing millerite (Fig. 8.5k), or it may occur at the margin of intergrown millerite and pyrite (Fig. 8.5l and m). As noted earlier, chalcopyrite may be transected by millerite veinlets (Fig. 8.5f and g). The coarse grains of chalcopyrite occasionally display twinning (Fig. 8.5j and k). Fine disseminated chalcopyrite grains also occur around pyrite or magnetite (Fig. 8.5h), or are remobilised together with pentlandite along veinlets that cut through plagioclase (Fig. 8.5d).

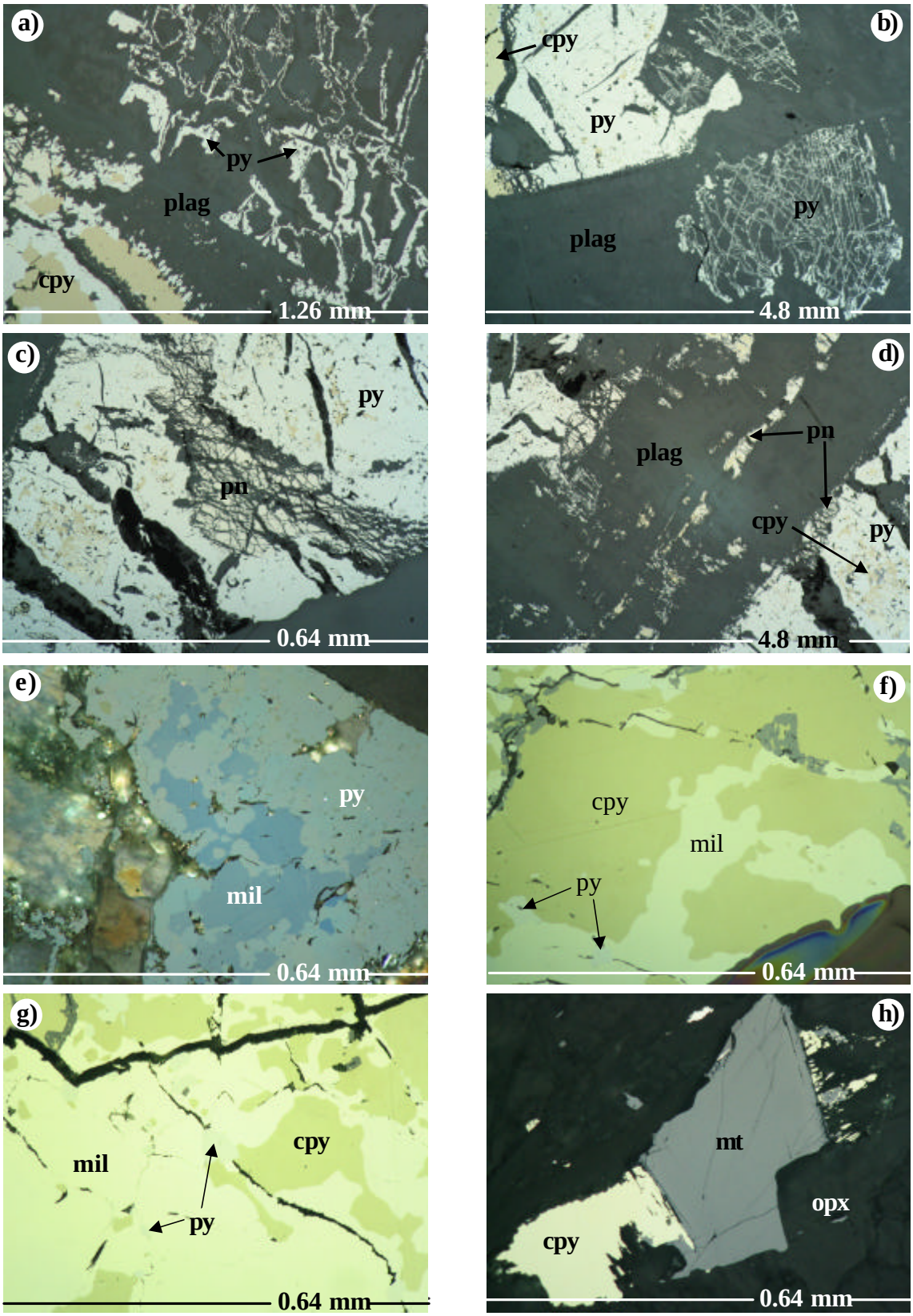

Fig. 8.5: Refer to next page for explanation of the photomicrographs.

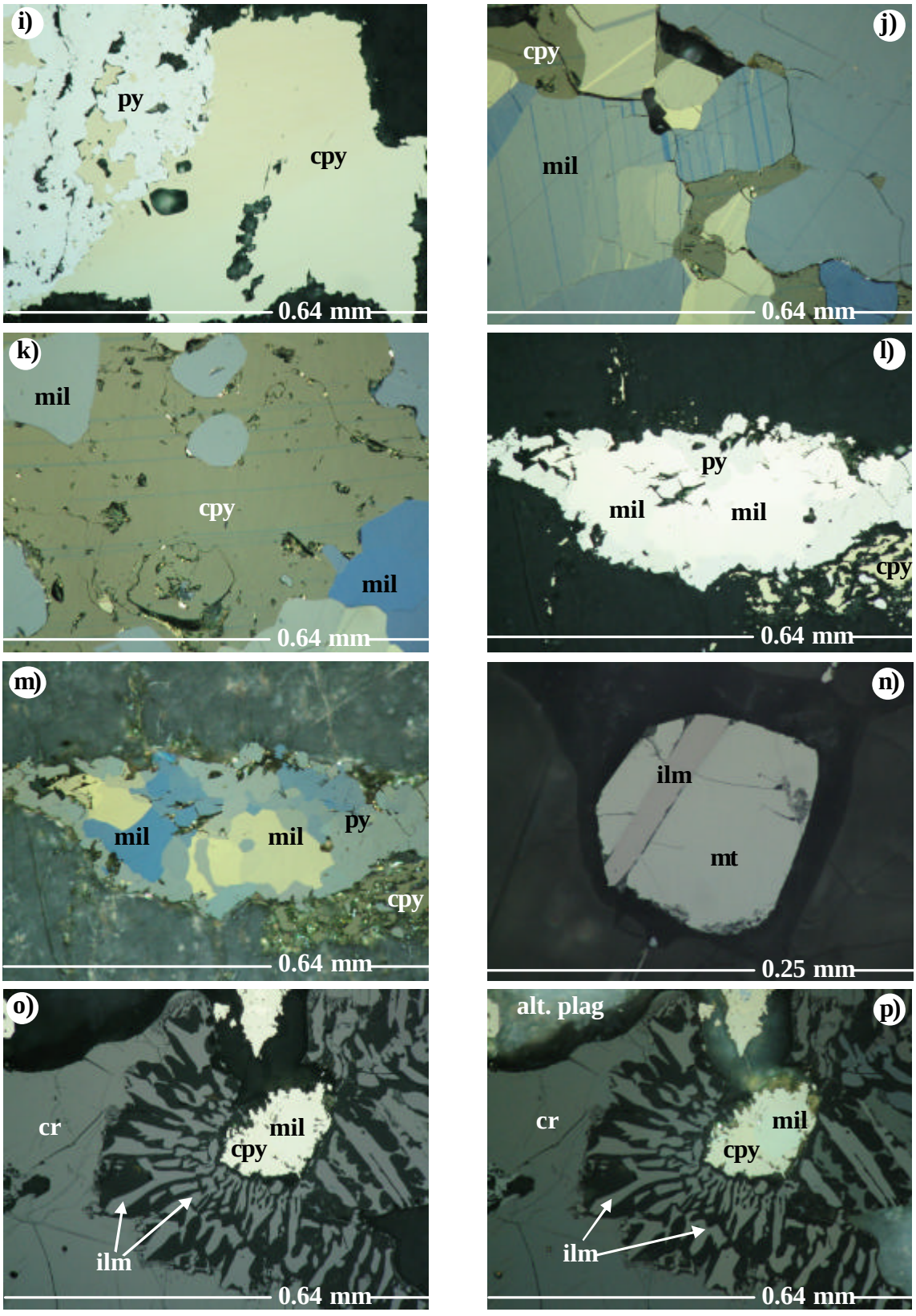

Fig. 8.5 continued: Refer to next page for explanation of the photomicrographs.

Fig. 8.5: Photomicrographs:

(a) Plagioclase (plag) containing vermicular network of pyrite. Pyrite also forms coronas around chalcopyrite (sample P19). (b) Skeletal pyrite and pyrite replacing plagioclase along cleavage planes (sample P19). (c) Pyrite cut by pentlandite-rich veins. Also note fine disseminated chalcopyrite in pyrite (sample P19). (d) Pentlandite replacing plagioclase along cleavage planes. Matrix is pyrrhotite with disseminated fine chalcopyrite (sample P19). (e) Pyrite enclosing millerite. Note fine disseminated chalcopyrite intergrown with pyrite (sample P15). (f & g) Millerite replacing chalcopyrite along fractures. Minor pyrite (py) grains occur at the contact between chalcopyrite and millerite, or are enclosed in millerite (sample P14). (h) Magnetite (mt) is intergrown with chalcopyrite, with minor chalcopyrite being remobilised into adjacent silicates (sample P11). In reflected light, cross polarised light, in oil.

Fig. 8.5 continued:

(i) Anhedral chalcopyrite intergrown with anhedral pyrite (sample P11). (j) Massive, twinned, subhedral millerite (mil) intergrown with interstitial chalcopyrite (cpy) (sample P106). (k) Anhedral, twinned chalcopyrite intergrown with, and enclosing, vaguely round millerite (sample P106). (l & m) Fragmented pyrite intergrown with millerite and chalcopyrite (sample P15). (n) Subhedral magnetite with ilmenite lamellae (sample P15). (o & p) Radiating, skeletal ilmenite vaguely round chromite (cr) and enclosing an intergrowth of chalcopyrite and millerite (sample P15). In reflected light, plane polarised light (except i, l, n and o), in oil.

Millerite occurs as massive, subhedral or anhedral grains that may form monomineralic aggregates, in places intergrown with chalcopyrite and pyrite (Fig. 8.5j, k and e), or as veins in fractured chalcopyrite (Fig. 8.5f and g). The grains show distinct pleochroism from yellowish cream to bluish grey/cream in reflected light and abundant internal lamellae. Millerite may also be rimmed by pyrite (Fig. 8.5l and m).

Magnetite is euhedral to subhedral and occurs interstitial to, or enclosed, in pyroxenes. It often contains thick lamellae of ilmenite (Fig. 8.5n).

Chromite is subhedral and optically homogenous. It may occur surrounding radiating skeletal ilmenite grains that in turn surround composite grains of chalcopyrite and millerite (Fig. 8.5o and p).

8.3 Compositions of major base metal sulphides and spinel

Pentlandite, pyrrhotite, pyrite and chalcopyrite were analyzed by microprobe, both in the "normal" analytical mode and using the TRACE program (35 kV voltage; high current, extended counting times of up to 10 minutes peak and background). The latter setup leads to detection limits of *ca.* 20 ppm Pd in pentlandite. Analytical results are given in Table 3. For the analyses, sulphides were selected from well mineralized samples of the Platreef at Nonnenwerth and Townlands, notably the recrystallized gabbronorite and anorthosite at Nonnenwerth and the Middle and Upper Platreef at Townlands.

8.3.1 Pentlandite

Pentlandite is characterised by Ni/Fe ratios close to unity (Table 3a). Cobalt contents are between 0.9 and 1.3 wt. %; only sample MOX12 has a higher Co content (1.7 to 1.8 wt. %). Notably, there is considerable variation in Co contents between samples but little intra-sample variation.

There is a dramatic difference in the Pd contents of pentlandite from Nonnenwerth and Townlands.

Up to 700 ppm Pd were analyzed in pentlandite from Nonnenwerth; samples from recrystallized gabbronorite contain the highest Pd contents (139 – 697 ppm, averaging 433 ppm) whereas samples from anorthosites have generally between 66 – 224 ppm (average 147 ppm).

In the "typical magmatic" sulphide assemblage at Nonnenwerth, no PGM enclosed in pentlandite were identified. It is well-known that pentlandite may carry even up to some % of Pd (substituting for Ni) in its crystal lattice (e.g. Gervilla et al., 2004).

In contrast, pentlandites from Townlands have Pd contents below the detection limit (20 ppm Pd) of the method. This lack of measurable Pd contents in pentlandite may find the following explanations: (i) Pd in pentlandite was analysed in one sample (P 13) only, so the results may not be representative. (ii) The Townlands sulphide assemblage differs from being "typical magmatic" and has experienced syn- to post-magmatic modification (formation of millerite and pyrite replacing the lower-S minerals pentlandite and pyrrhotite). Therefore, the relatively rare pentlandite at Townlands may either represent a second generation of pentlandite, or is a relict phase that has suffered an overprint that extracted earlier lattice-bound Pd. (iii) Pd-bearing PGM could have been mobilized during replacement of 'primary' sulphides by pyrite dominated assemblages into the surrounding silicates (Prichard *et al*., 2001).

The analytical work presented here has shown marked differences in Pd contents in pentlandites from the Platreef for the first time. It is suggested that systematic

research in this topic would be a worthwhile undertaking to further our understanding of the distribution of the PGE in Platreef ores.

Se contents vary between 200 – 500 ppm (averaging 282 ppm) in Nonnenwerth samples, and 70 – 450 ppm (averaging 173 ppm) at Townlands. Rhodium, platinum and silver are below the detection limits of the electron microprobe.

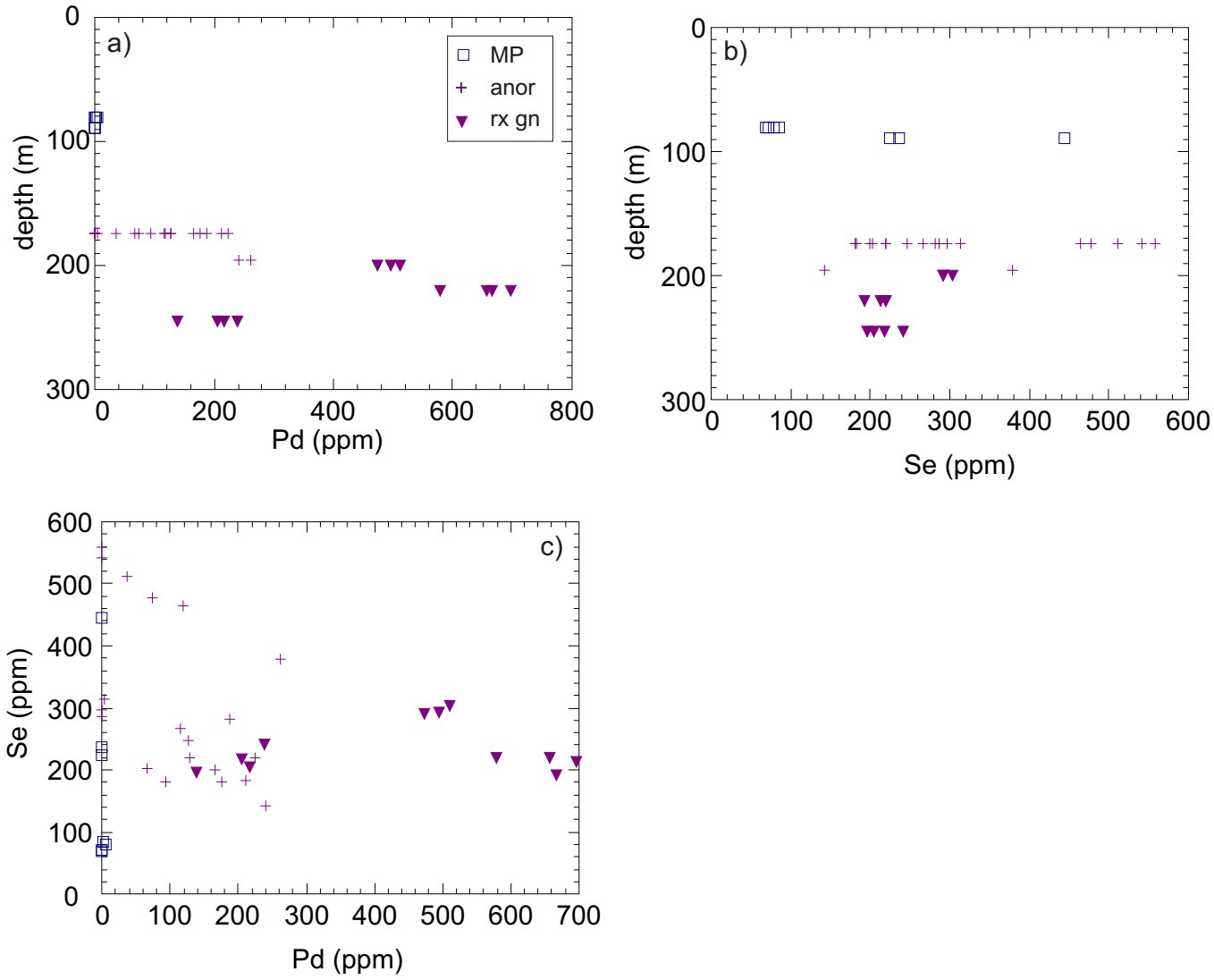

Fig. 8.6:Variation of a) Pd, b), Se with depth in pentlandite, andSe versus Pd. MP = Middle Platreef (from Townlands), anor = anorthosite, rx gn = recrystallized gabbronorite (both from Nonnenwerth).

8.3.2 Pyrrhotite

Pyrrhotite has between 47 – 48.5 atomic % Fe and 51.2 – 52.8 atomic % S indicating the presence of hexagonal/monoclinic pyrrhotite ($Fe_{1-x}S$) (Table 3b). Se contents range from 216 – 362 ppm (averaging 267 ppm) in Nonnenwerth samples and 38 – 128 ppm (averaging 98 ppm) at Townlands. Fe and S show distinct differences between samples but little within sample variation. Pyrrhotite from Nonnenwerth anorthosite has the highest Fe (48.1 – 48.4 atomic %), followed by pyrrhotite from the recrystallized gabbronorite (47.3 – 47.6 at. %), with the Townlands pyrrhotites (both from the Upper and Middle Platreef) having the lowest Fe contents (46.9 – 47.1 at. %). Pyrrhotites from recrystallized gabbronorite and anorthosite have generally similar Se contents, and no PGE were detected. Pt, Pd and Rh contents are all below the detection limits of the electron microprobe.

8.3.3 Pyrite

Platreef pyrite is characterised by stoichiometric Fe and S contents (Table 3c). Pyrite from Nonnenwerth samples carries no Co but up to 1 wt. % Ni is present in pyrite from anorthosite samples. Pyrite from Townlands is Co- and Ni- bearing, with up to 1.8 wt. % Co and 1 wt. % Ni. Pt, Pd and Rh contents are all below the detection limits of the electron microprobe. Se contents of pyrite vary from 104 – 377 ppm (average 224 ppm) in recrystallized gabbronorite, and 143 – 327 ppm (average 266 ppm) in anorthosite, with one sample (MOX29) having 720 ppm Se. Townlands pyrite has 31 to 338 ppm Se with a generally similar range for the Upper and Middle Platreef. No systematic compositional variation of pyrite with depth or lithology is visible at Townlands or Nonnenwerth.

8.3.4 Chalcopyrite

Only two analyses of chalcopyrite from Nonnenwerth recrystallized gabbronorite (sample MOX10) were obtained. Chalcopyrite has a stoichiometric composition with PGE, Ni, Au, Co, Se and Ag levels below the detection limit suggesting that none of these elements substitute significantly in chalcopyrite (Table 3d).

8.3.5 Millerite

One analysis each of millerite from the Upper Platreef and Middle Platreef on Townlands were obtained. Millerite has a stoichiometric composition with significant Fe (<1.6 wt. %).

8.3.6 Spinel

Spinel-group minerals resembling chromite in reflected light are accessory minerals in serpentinised peridotite and some high magnesian gabbronorites from Nonnenwerth. Analytical results for “chromite” (more precise: Cr-bearing magnetite; see below), corrected for Fe^{3+} content using the method of Finger (1972), are given in Table 4. However, the compositional variations and trends of the chromites are difficult to comment on because only a small number of grains were observed and analysed (8 grains altogether).

In the northern lobe, chromite distribution is sporadic and is mostly accessory except at few localities like Zwartfontein (Schürmann et al., 1998), Rooipoort (Maier et al., in preparation) and Grasvally (Hulbert, 1983). The stratiform-type chromites from the Lower and Critical Zones of the Rustenburg Layered Suite have the following characteristics: The LG6 layer has a Cr_2O_3 content of 46 - 47

wt. %, MG chromitites 44 - 46 wt. %, and the UG2 layer has around 43 wt. % Cr_2O_3 (Schürmann et al., 1998). The LG6 layer has a Cr/Fe ratio of between 1.56 and 1.60, MG chromitites are between 1.35 and 1.50 whilst the UG2 layer has a Cr/Fe ratio of between 1.26 and 1.40 (Schürmann et al., 1998). For Platreef chromites, Hatton and von Gruenewaldt (1987) reported Cr_2O_3 contents ranging from 34.5 up to 52.5 wt. %. On Zwartfontein, Cr/Fe ratios range from 1.13 to 2.2 (Schürmann et al., 1998).

The Cr-bearing spinels from **Nonnenwerth** have total combined iron contents ranging from 60 – 74 wt. % (FeO + Fe_2O_3) in high magnesian gabbronorite, and 71 – 78 wt. % (FeO + Fe_2O_3) in serpentinised peridotite. MgO and Al_2O_3 contents are low (ca. 1 – 3 wt. % MgO and 4 – 6 wt. % Al_2O_3). Cr_2O_3 contents are in the range 18 - 26, average 23 wt. % Cr_2O_3 in high magnesian gabbronorite, and 11 to 14, averaging 12 wt. % in serpentinised peridotite. Accordingly, Cr/Fe ratios are also low and range from 0.32 to 0.4 in serpentinised peridotite and 0.6 to 0.82 in high magnesian gabbronorite. The above analytical data clearly point to the fact that the spinels at Nonnenwerth are **Cr-bearing magnetites**.

Fig. 8.7a shows Cr # versus Fe^{2+} # of the analysed Cr-bearing magnetites. Clearly, the compositions plot outside the fields of ophiolitic and stratiform spinels/chromites, towards Fe-rich compositions (magnetite). The Cr # can still be seen to indicate a stratiform heritage, however, the Fe^{2+} # clearly points to the fact that the compositions of the Cr-bearing magnetites reflect secondary overprinting of probably primary magmatic chromites. It is well-known that Fe is released during serpentinization and may cause this observed Fe-upgrading of spinels. The

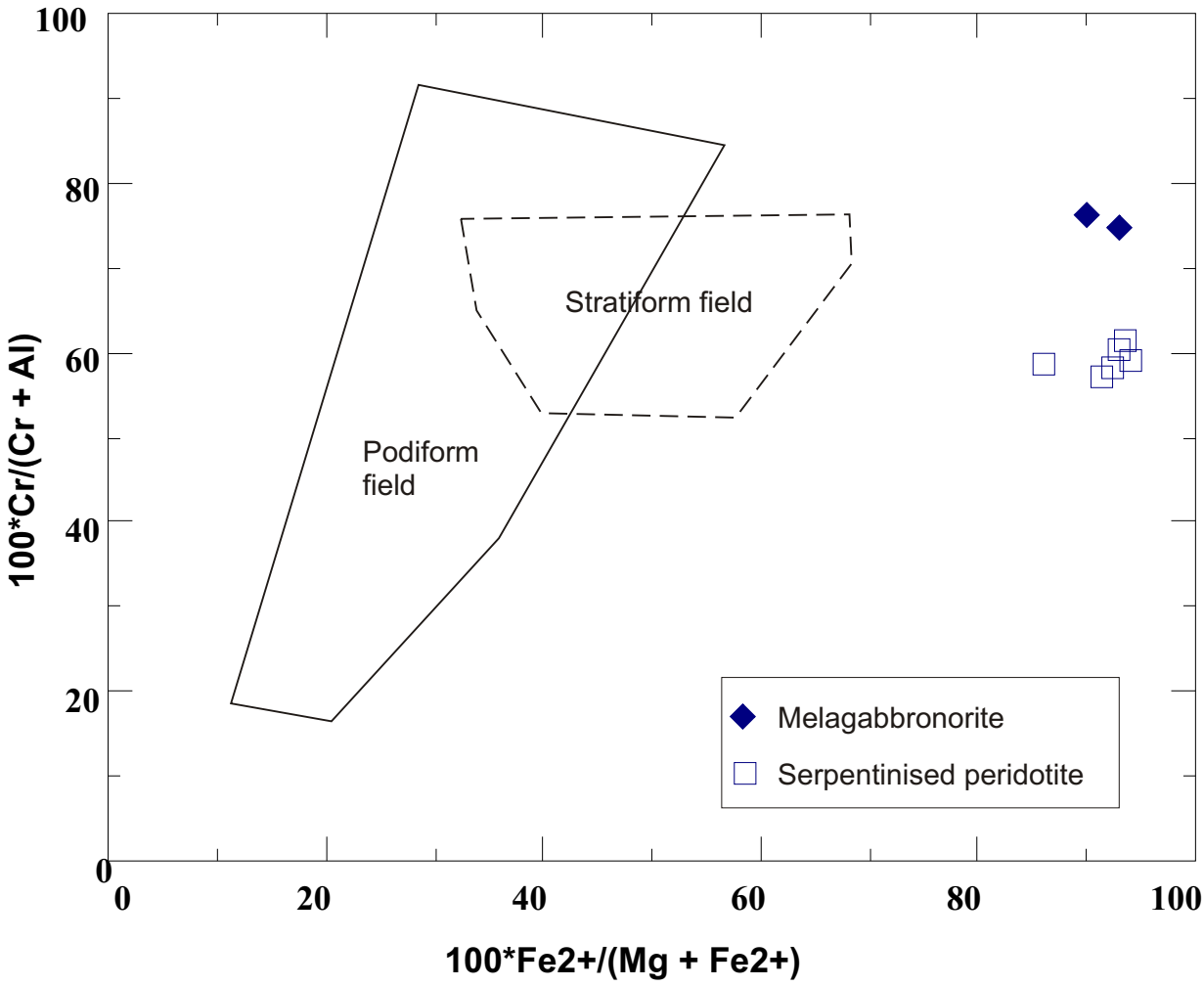

Fig. 8.7a: Cr # versus Fe # of the analysed Cr-bearing spinels from serpentinized peridotite (MO 26) and from melagabbronorites (MO 27).

compositions of Cr-bearing magnetites especially in serpentinised peridotites may be explained by subsolidus equilibration with ultramafic minerals (pyroxenes and olivines).

8.4 Summary and Discussion

The relative abundances of the sulphide minerals on Nonnenwerth are, in decreasing order, **pyrrhotite, chalcopyrite** and **pentlandite.** Textures, mineral assemblages and mineral chemistry point to a "typical magmatic" sulphide assemblage (e.g. Naldrett, 1989) that developed down-temperature from immiscible sulphide droplets in the silicate magma. Pyrite occurs locally and sphalerite, violarite and mackinawite occur in trace amounts.

In contrast, samples from Townlands are characterized by **chalcopyrite > millerite > pyrite > pentlandite**. Pyrrhotite occurs locally only and galena and molybdenite are further accessories. This sulphide assemblage differs from being "typical magmatic" and came into existence through syn- to post-magmatic modification at elevated fugacity of sulphur (fS_2).

The estimated abundance of sulphides, oxides and PGM in selected samples from Nonnenwerth and Townlands is given in Table 5 and some interrelationships are marked in colour.

Table 5: Estimated abundance of sulphides, oxides and PGM in polished thin sections from Nonnenwerth and Townlands

Sample	Sulphide abundance (%)	po	cpy	pn	py	mil	cr	mt	ilm	PGM	others
Nonnenwerth											
MOX9	1		+++	++	+++					Pd,Te Pt,Te Pt,Pd,Te	
MOX10	1	+++	++	++	+			+	+	Pt,Te Pt,Pd,S	
MOX11	2	+++	+++	+	+			+			
MOX12	2-3	+++	++	++				++	+	Pd,Te Au	
MOX14	< 1		+++	+/o	+++			++			
MOX15	1-2	+++	++	++							
MOX16	1	+++	+++	+				++	+		
MOX27	3-4	+++	+++	+++	++			++			
MOX29	20	+	+++	+	+			+		Pd,Te Pd,Pt,Bi,Te Pd,Bi,Te	hm
MOX30	10	+++	+	+	++			+			
MOX32	2	+++	+++	+	++		+		+		
MOX33	4-6	+++	+++	+				++			
Townlands											
P1	1	++	+++		+			+			
P2	5		++	+++		+		+++			viol
P4			++		++	++		++	+		hm
P7	30		++		+++	++		++		Pd,Fe,As	
P11	1-2	++	++		+++			+			
P12	5	+++	++	+++				+++			
P13		+++	++	++			++	++		Pd,Bi,Te Pd,Te,As Pt,As	moly
P14	20	+	++		+++	+++		++			ga, moly
P15	15-20	+/o	++		+++	+	+		+		
P19	20		++		+++	++		++			
P20	2-3	+	++	++	+++			++			
P26	2		+++	++	++	++		++			
P106			++		+++	++		+++		Pd,Bi,Te Pd,Te	

Estimated frequency: +++ very frequent, ++ frequent, + minor, o rare

Abbreviations: po = pyrrhotite, cpy = chalcopyrite, pn = pentlandite, py = pyrite, mil = millerite, cr = chromite, mt = magnetite, ilm = ilmenite, PGM = platinum-group mineral, hm = hematite, ga = galena, moly = molybdenite.

Nonnenwerth

The relative abundances of the sulphide minerals on Nonnenwerth are, in decreasing order, **pyrrhotite, chalcopyrite** and **pentlandite.** Textures, mineral assemblages and mineral chemistry (for example, elevated Pd contents in pentlandite) basically point to a "typical magmatic" sulphide assemblage (e.g. Naldrett, 1989) that developed down-temperature from immiscible sulphide droplets in the silicate magma. Pyrite occurs locally and sphalerite, violarite and mackinawite occur in trace amounts.

The current study distinguishes three different associations of sulphide at Nonnenwerth, i.e. (i) the "typical" magmatic sulphides, (ii) secondary sulphides replacing magmatic sulphides, and (iii) sulphides associated with secondary silicates.

(i) Magmatic sulphides are interstitial to plagioclase and orthopyroxene in essentially unaltered or slightly altered samples. They are represented by composite grains of pyrrhotite often intergrown with chalcopyrite and pentlandite, chalcopyrite and polycrystalline fragmented pentlandite grains along pyrrhotite fractures or pentlandite and chalcopyrite included in pyrrhotite towards pyrrhotite grain margins (Fig. 8.1a to e). Pentlandite may occur as flame-like exsolution lamellae in pyrrhotite. These magmatic sulphides represent fractionated blebs of sulphide. During crystallization, magmatic sulphide liquid crystallizes to a monosulphide solid solution (mss) with the residual sulphide liquid forming intermediate solid solution (iss) (Barnes *et al*., 2006). The former recrystallizes to pyrrhotite and pentlandite on cooling and the latter to chalcopyrite and some

pentlandite (Barnes *et al*., 2006) in agreement with the textures displayed by magmatic sulphides.

(ii) Secondary sulphides, as defined here, replace magmatic sulphides and lack the zoned, fractionated textures displayed by magmatic sulphides and have a 'rugged' outline. They are dominated by chalcopyrite, pyrite, and minor pentlandite. Pyrrhotite includes subrounded vermicular intergrowths of pyrite and chalcopyrite, in places with a remnant pentlandite suggesting replacement of pentlandite by the two phases (Fig. 8.3d, e and f). Pentlandite may be altered and replaced by coronas of violarite with relict pentlandite forming islands in violarite suggesting that the pentlandite is relictic and that most of the primary pentlandite has been replaced by violarite (Fig. 8.3h and i). It should be noted that recrystallized gabbronorite samples with high pyrrhotite contents have no pyrite and vice versa. The absence of pyrrhotite may suggest an increase in S fugacity (fS_2) resulting in pyrrhotite being transformed to or replaced by pyrite. Minor phases are fine, flame-like exsolutions of mackinawite and small disseminated sphalerite grains in chalcopyrite.

(iii) Sulphides associated with secondary silicate assemblages are rare in the Platreef at Nonnenwerth. They are represented by fine disseminated chalcopyrite grains intergrown with alteration minerals in replacement of primary silicates adjacent to coarse composite sulphides, deuteric veinlets of pyrite that cut through the plagioclase (Fig. 8.2i and j) or pyrite replacing clinopyroxene along cleavage planes and cracks (Fig. 8.3i). The sulphides do not display well defined sulphide zonation.

Townlands

In contrast to Nonnenwerth, samples from Townlands are characterized by **chalcopyrite > millerite > pyrite > pentlandite**. Pyrrhotite occurs locally only and galena and molybdenite are further accessories. Notably, this is the first time that such a sulphide assemblage is reported from the Platreef. This type of mineralization was detected in one drill hole only and therefore, must at this stage be regarded as exceptional and probably local only.

This sulphide assemblage differs from being "typical magmatic" and came into existence through syn- to post-magmatic modification including formation of millerite from pentlandite, and pyrite replacing pyrrhotite. It is envisaged that the sulphide assemblage at Townlands originally also developed from immiscible magmatic sulphide droplets and an association pyrrhotite – pentlandite – chalcopyrite. However, this early formation was overprinted and converted to pyrite – millerite – chalcopyrite. The observed sulphide assemblage gives evidence that the conversion took place at elevated fugacity of sulphur (fS_2) as will be shown below. This conversion was not completely pervasive, as evidenced by relict pyrrhotite – pentlandite assemblages (Table 5). Furthermore, no direct replacements (millerite after pentlandite and pyrite after pyrrhotite) were observed in situ.

The relative timing of this remobilization and replacement is hard to constrain; it probably took place early on the down-temperature path of the mineralization. Probably, syn- to post-emplacement fluids were also involved as evidenced by amphibole needles crosscutting sulphide grains (Fig. 8.4a).

An attempt is made to estimate the fO_2 and fS_2 in the Fe-Ni-S-O system under conditions of common hypogene equilibrium in altered ultramafic rocks (Eckstrand, 1975). The nature of the sulphide assemblage (pyrite, paucity of pyrrhotite, presence of millerite instead of pentlandite, presence of magnetite) suggest that its crystallisation occurred at elevated fugacities of sulphur and oxygen. The sulphides from the sulphide-poor rocks at the top of each Unit formed under moderate fS_2 and low fO_2 conditions (Eckstrand, 1975; Fig. 8.8). This is in agreement with the observed sulphide assemblages represented by assemblage 1 and 2 in Fig. 8.8b. In contrast, the sulphide-rich assemblage that occurs towards the base of each Unit probably formed under high fS_2 and fO_2 conditions (assemblage 3 in Fig. 8.8b). This model is thus in agreement with the observed sulphide assemblages and available S-isotope data (Manyeruke, 2003; Manyeruke *et al.*, 2005). Values of $d^{34}S$ increase towards the base of the Middle and Upper Platreef (Manyeruke, 2003), a phenomenon that was attributed to enhanced assimilation of crustal S towards the base of each layer, perhaps by continued degassing of the floor rocks during crystallisation of the Platreef. The high O fugacity may also be attributed to assimilation of dolomite followed by devolatization of the dolomite xenoliths and oxidation of the magma (de Waal, 1977).

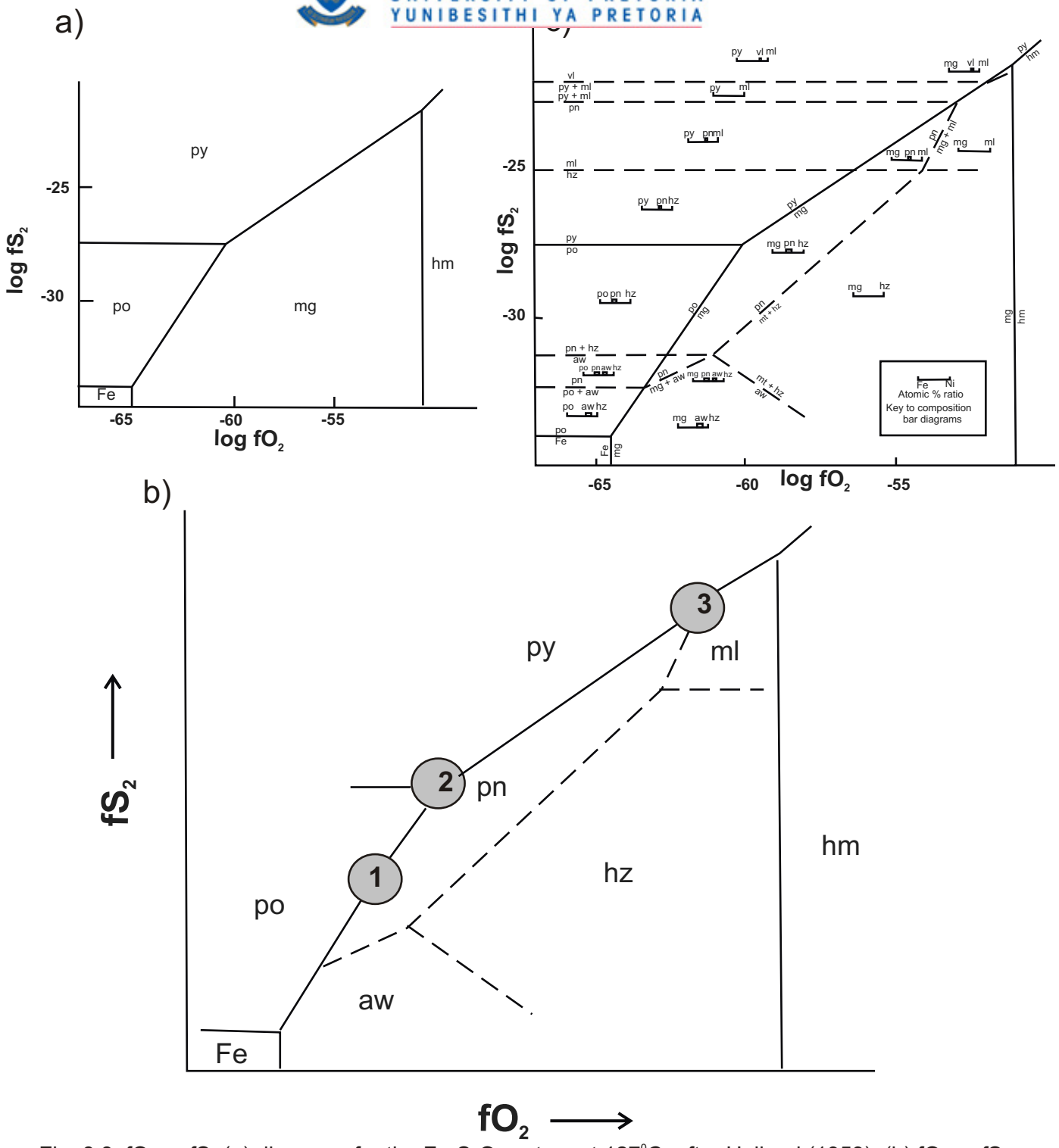

Fig. 8.8. fO_2 vs fS_2 (a) diagrams for the Fe-S-O system at 127^{0}C, after Holland (1959). (b) fO_2 vs fS_2 diagram for the Fe-Ni-S-O system at about 127^{0}C. Reaction boundaries for the Fe-S-O sub-system are shown as solid lines; others for which thermodynamic data are unavailable or unreliable are shown in dashed lines. (c) Approximate fO_2 vs fS_2 diagram for the Fe-Ni-S-O system under conditions of common hypogene equilibrium in altered ultramafic rocks, probably less than 200^{0}C. Assemblages noted in the Platreef on Townlands are shown by circled numbers on the appropriate field of the boundary. Assemblage 1 is composed of pyrrhotite, chalcopyrite, pentlandite ± magnetite, assemblage 2 is characterised by pyrite, pentlandite, chalcopyrite and minor pyrrhotite and assemblage 3 is characterized by pyrite, millerite, chalcopyrite ± pentlandite ± galena, molybdenite and magnetite. Figures modified after Eckstrand (1975).

As outlined above, the lack of a "typical "magmatic sulphide assemblage at Townlands may be the result of a number of possible processes. However, S-assimilation from the floor rocks shales is favoured here for the following reasons: Manyeruke (2003) and Manyeruke *et al.* (2005) have shown that $d^{34}S$ values in the Platreef at Townlands increase towards the base of the Middle and Upper Platreef, a phenomenon that was attributed to enhanced assimilation of crustal S towards the base of each layer, perhaps by continued degassing of the floor rocks during crystallisation of the Platreef. This is supported by the increase in the abundance of sulphides towards the base of each Unit at Townlands (Manyeruke, 2003: Manyeruke et al., 2005). The additional sedimentary sulphur probably reacted and totally modified the magmatic assemblage resulting in the paucity of "typical" magmatic sulphides at Townlands. This would suggest primary sulphide mineralization in the Platreef is of magmatic origin and contamination with floor rock sulphur. at Townlands (Manyeruke, 2003; Manyeruke *et al*., 2005) is a localised process in areas where the floor rocks are sulphur- bearing.

PGE

With the exception of pentlandite from Nonnenwerth (see below), Pd, Pt and Rh are below the detection limits of the electron microprobe in the sulphides analysed from Nonnenwerth and Townlands.

Pentlandites as part of the "typical magmatic" sulphide assemblage at Nonnenwerth constantly contain appreciable amounts of Pd (range from ~ 140 – 700 ppm). This finding is in accordance with literature data (e.g. Gervilla et al., 2004) that pentlandite may carry even up to some % of Pd (substituting for Ni) in

its crystal lattice. Accordingly, the Pd contents in Nonnenwerth pentlandite probably reflect a primary magmatic signature.

In contrast, pentlandites from Townlands have Pd contents below the detection limit (20 ppm Pd) of the method. This lack of measurable Pd contents in pentlandite may find the following explanations:

(i) Pd in pentlandite was analysed in one sample (P 13) only, and therefore, the results may not be representative.

(ii) Pd-bearing PGM could have been mobilized during replacement of 'primary' sulphides by pyrite dominated assemblages into the surrounding silicates (Prichard *et al*., 2001).

(iii) The Townlands sulphide assemblage differs from being "typical magmatic" and has experienced severe syn- to post-magmatic modification as described above. Therefore, the relatively rare pentlandite at Townlands may either represent a second generation of pentlandite, or is a relict primary phase that has suffered an overprint that extracted lattice-bound Pd. Arguments for the latter possibility are provided by the presence of abundant Pd-minerals in sample P 13 (see Table 5).

The analytical work presented here has shown marked differences in Pd contents in pentlandites from the Platreef for the first time. It is suggested that systematic research in this topic would be a worthwhile undertaking to improve our understanding of the distribution of the PGE in Platreef ores.

The nature and distribution of the PGM from Nonnenwerth and Townlands are documented in the next chapter (Chapter 9).

CHAPTER NINE: PLATINUM-GROUP MINERALS (PGM), TELLURIDES AND TRACE MINERALS

This chapter documents and compares the PGM assemblages at Nonnenwerth and Townlands, and considers the different processes of formation of these PGM.

A considerable number of platinum group minerals were identified and analysed using a CAMECA SX-100 electron microprobe at the Federal Institute for Geosciences and Natural Resources, Hannover, Germany. Analytical details are given in Appendix 1e and the results are shown in Table 6. The nomenclature followed in this work is that used by Cabri (2002).

The analysed suite of PGM comprises [Pt,Pd]-bismuthotellurides, namely merenskyite [$PdTe_2$], kotulskite [PdTe], moncheite [$PtTe_2$] and michenerite [Pd(Bi,Te)], as well as rare sperrylite [$PtAs_2$] and braggite [(Pd,Pt)S]. Other PGM include isomertieite [$Pd_{11}Sb_2As_2$], stibiopalladinite [Pd_5Sb_2] and temagamite [Pd_3HgTe]. Native gold was also found. Additional minor phases include several tellurides, e.g. tetradymite-type group minerals [Bi_2Te_2S], hessite [Ag_2Te], altaite [PbTe], and pilsenite [Bi_4Te_3]), as well as argento-pentlandite [$Ag(Fe,Ni)_8S_8$] and two unnamed minerals with calculated formulae [Bi_4Te_2Se] and [$FeBiS_2$].

9.1 Nonnenwerth

53 PGM grains were identified at Nonnenwerth. The suite of PGM is dominated by Pd-rich (69 %) and Pt-rich (27 %) bismuthotellurides, as well as one grain each (2 %) of braggite and sperrylite. The PGM occur predominantly at the contact

between sulphide (mostly chalcopyrite, minor pyrrhotite and rare pyrite) and secondary silicate (mostly chlorite and albite after plagioclase), enclosed in silicates or enclosed in sulphides (mostly chalcopyrite and minor pyrrhotite and pyrite). However, even those PGM enclosed in silicates retain a strong spatial relationship with the base metal sulphides, mostly chalcopyrite, and are associated with secondary minerals (mostly chlorite and albite which replace plagioclase, or rarely amphibole which replaces orthopyroxene and base metal sulphides).

Grain sizes of the PGM and other trace minerals range from ca. < 1 µm to 40 µm. The larger grains could thus be readily analysed. Grains < 2 µm in size were analysed qualitatively by energy dispersive spectrometry (EDS).

9.1.1 Recrystallized gabbronorite

The PGM suite (n=34) is dominated by kotulskite [PdTe] (59 %) and moncheite [$PtTe_2$] (35 %). Only one grain each of braggite [(Pd,Pt)S] and sperrylite [$PtAs_2$] were identified. Other trace minerals include hessite [Ag_2Te], native bismuth and a few grains of gold.

Kotulskite [PdTe] occurs enclosed in plagioclase in the vicinity of a chalcopyrite grain (Fig. 9.1a) where it is associated with secondary albite and chlorite, and at chalcopyrite-plagioclase or pyrrhotite-plagioclase grain boundaries. This textural relationship may indicate the partial replacement of chalcopyrite by actinolite (Li *et al.*, 2004). The kotulskite grains occur as clusters of discrete grains often closely associated with moncheite (Fig. 9.1 c to f). In places, kotulskite occurs as composite grains with sperrylite and gold (Fig. 9.1g) or hessite. In the triangular

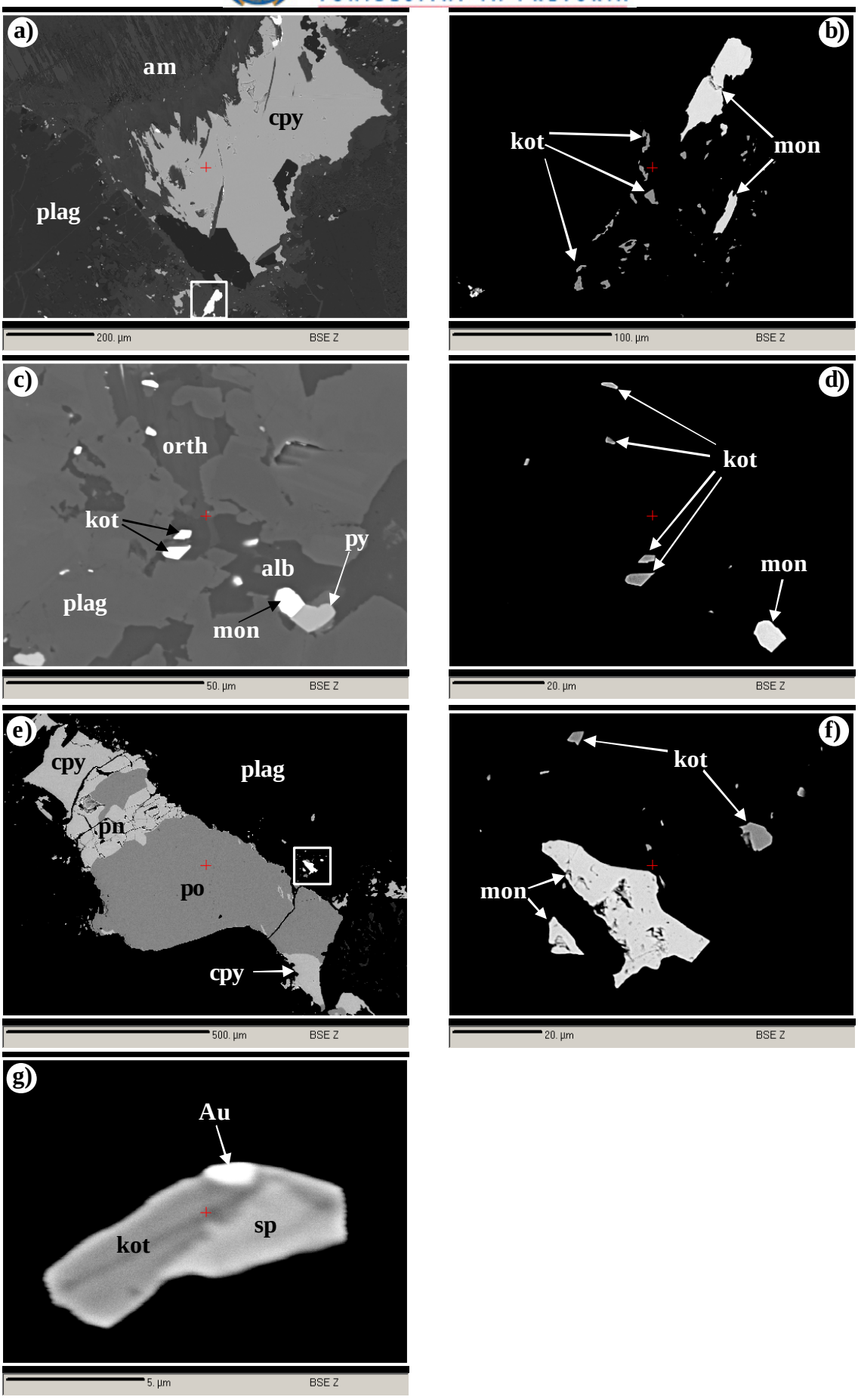

Fig. 9.1: Refer to next page for explanation of the images

plot (Pt+Pd)-(Bi+Sb)-Te for Pd-dominated (Pt,Pd)-bismuthotellurides (i.e., those with Pd > Pt atomic percent; Fig. 9.2a), most of the kotulskite compositions plot along the join kotulskite [PdTe] – sobolevskite [PdBi], suggesting significant substitution of Te by Bi, i.e., kotulskite and sobolevskite form a solid solution. Bismuth contents in kotulskite from recrystallized gabbronorite samples range from 3.84 to 13.98 wt. %.

Moncheite [$PtTe_2$] is euhedral or subhedral with grain sizes ranging from < 5 µm to 40 µm, but mostly between 5 and 20 µm. Like kotulskite, moncheite occurs mostly enclosed in plagioclase, where it is intergrown with secondary minerals (chlorite and amphibole) and generally located close to the edges of plagioclase adjacent to pyrrhotite and chalcopyrite (Fig. 9.1e, f, h & i). This could indicate replacement of sulphides by silicates, resulting in mobility of S, Fe, Cu and formation of PGM

Fig. 9.1:
Back-scattered electron images showing various textures and associations of PGM and gold. Rectangles represent area enlarged in the image to the immediate right.

(a) PGM (in rectangle) enclosed in plagioclase (plag) that has been altered to amphibole (am), in the vicinity of chalcopyrite (cpy). Sample MOX9. (b) Enlarged rectangle from a). Anhedral moncheite (mon) is associated with disseminated anhedral kotulskite (kot) in amphibole (black). Sample MOX9. (c) Kotulskite and moncheite enclosed in altered portions of plagioclase. Moncheite is in contact with pyrite. orth = orthoclase, alb = albite. Sample MOX9. (d) Euhedral to subhedral kotulskite and moncheite. Altered plagioclase is shown in black. Sample MOX9. (e) Composite grain of pyrrhotite (po), pentlandite (pn) and chalcopyrite, with PGM (in rectangle) situated in the periphery of the grain. Sample MOX10. (f) Enlarged rectangle from e). Subhedral to anhedral moncheite and associated kotulskite occur included in altered plagioclase (black background). Sample MOX10. (g) A composite grain of kotulskite, gold (Au) and sperrylite in altered plagioclase (black background). Sample MOX9.

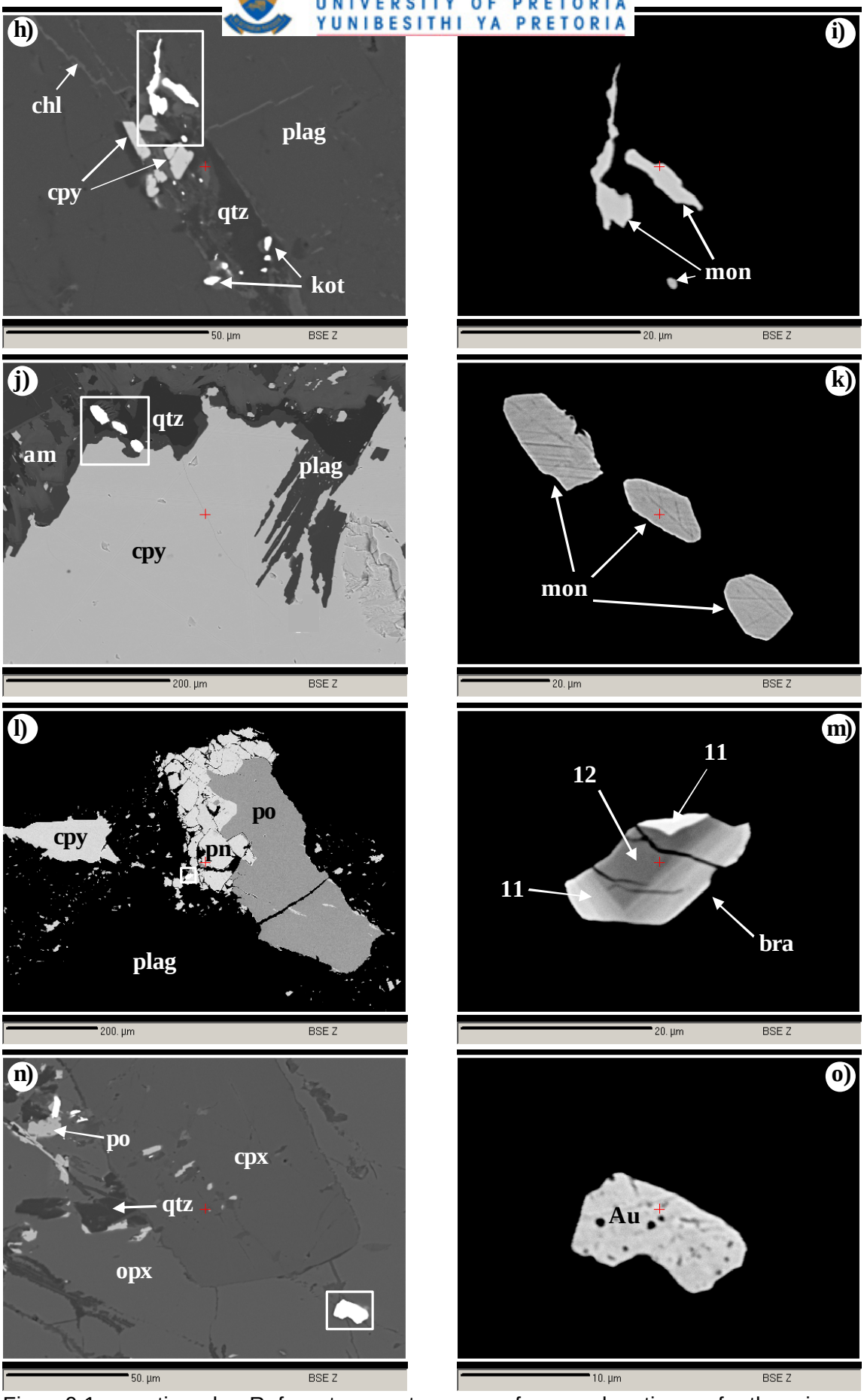

Fig. 9.1 continued: Refer to next page for explanation of the images.

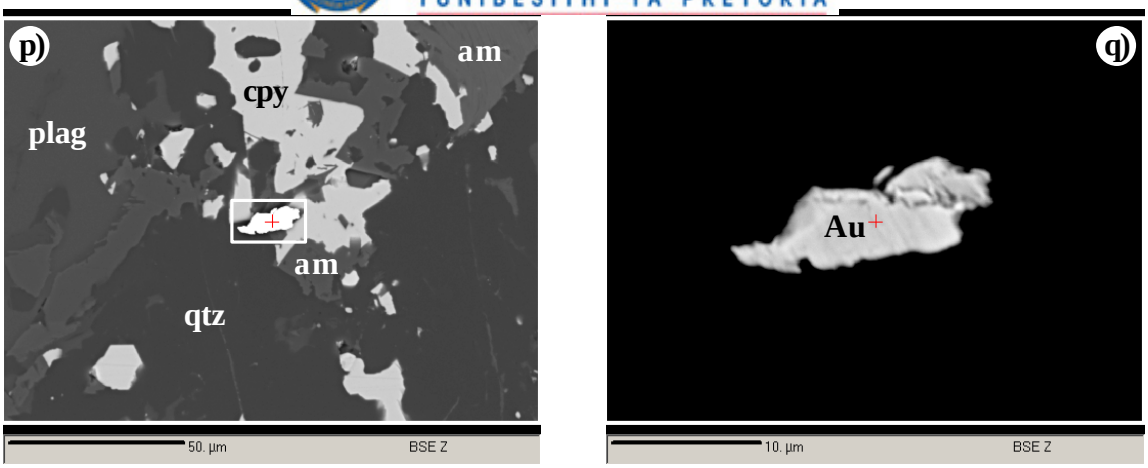

Fig. 9.1 continued:

Fig. 9.1 continued:

Back-scattered electron images showing various textures and associations of PGM and gold. Rectangle represents area enlarged for image to the immediate right.

(h) Chalcopyrite and PGM associated with quartz (qtz) and chlorite (chl), interstitial to plagioclase. Anhedral moncheite is highlighted by rectangle. The other PGM are subhedral kotulskites (kot) Sample MOX9. (i) Enlargement of rectangle from h). Anhedral moncheite is enclosed in chlorite (black background). Sample MOX9. (j) Subhedral moncheite forming a trail from the margin of chalcopyrite (cpy) into adjacent quartz and amphibole (after plagioclase). Sample MOX9. (k) Enlargement of rectangle from j. (l) Intergrown pyrrhotite and pentlandite, with braggite (in rectangle) occurring near margin of sulphide. Sample MOX10. (m) Enlargement of rectangle from l). Zoned subhedral grain of braggite. Increase in brightness corresponds to increase in Pt content. The numbers correspond to analyses e.g. 11 represents 11_MOX10 in Table 6 (Sample MOX10). (n) Grain of gold (Au) (in rectangle) located near fracture in orthopyroxene (opx). Sample MOX12. (o) Enlargement of rectangle from n). Subhedral grain of gold is partly corroded. Sample MOX12. (p) Gold (in rectangle) located at the contact between quartz (qtz) and chalcopyrite (cpy). Sample MOX9. (q) Enlargement of rectangle in p). Sample MOX9.

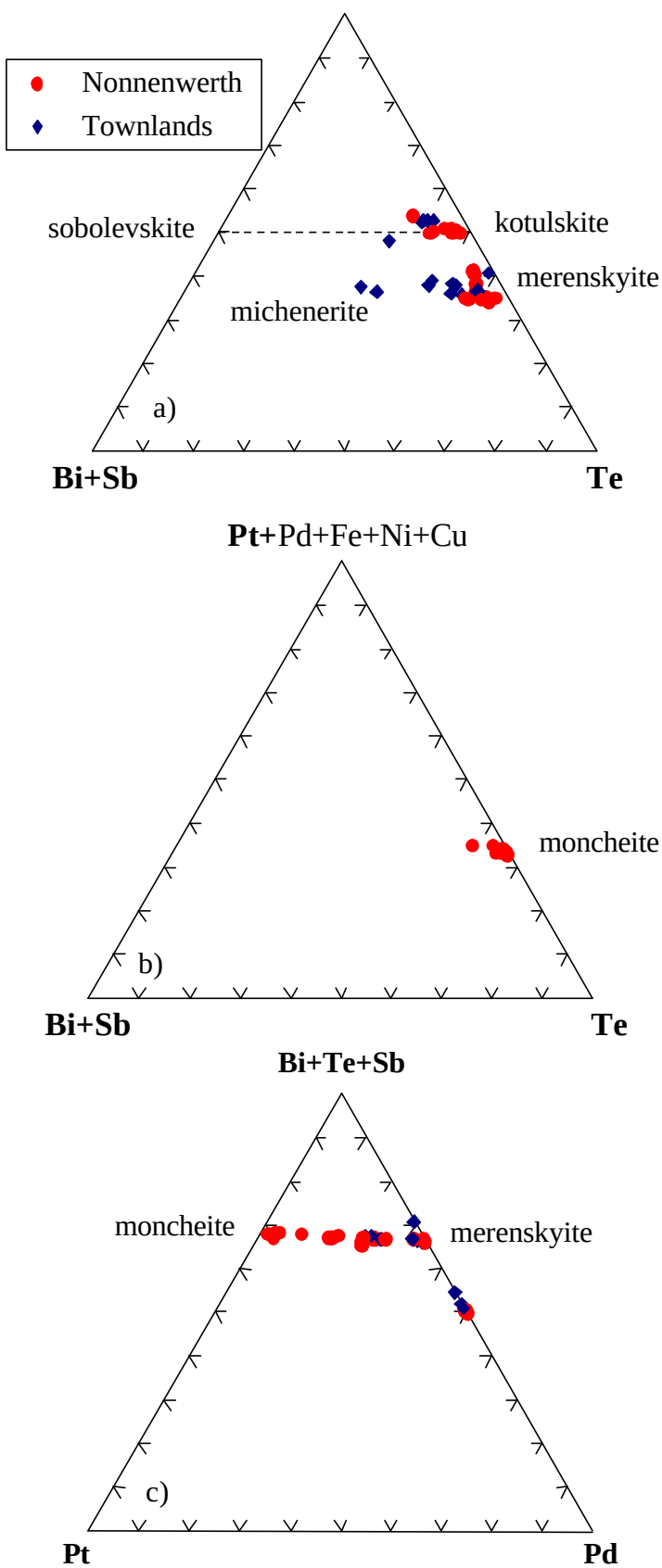

Fig. 9.2: Mineral chemistry of (Pt,Pd)-bismuthotellurides from Nonnenwerth and Townlands. a) Pd-dominated (Pt,Pd)-bismuthotellurides in the triangular plot (Pt+Pd)- (Bi+Sb)-Te (at. %). b) Pt-dominated (Pt,Pd)-bismuthotellurides in the triangular plot (Pd+Pt)-(Bi+Sb)-Te (at. %). c) (Pt,Pd)-bismuthotellurides in the triangular plot (Bi+Te+Sb)-Pt-Pd (at. %).

due to immobility of PGE (Li et al., 2004). In one instance, discrete, euhedral grains of moncheite form a linear trail emanating from the chalcopyrite-plagioclase grain boundary into plagioclase (Fig. 9.1j & k). In rare instances, moncheite may occur intergrown with pyrrhotite enclosed in plagioclase. In a plot of the Pt-dominated (Pt,Pd)-bismuthotellurides (Fig. 9.1b), moncheite analyses plot very close to the Pt+Pd+Fe+Ni+Cu – Te join. This point to only minor substitution of Te by Bi. Most grains have < 2 wt. % Bi; only one grain has a Bi content of 3.8 wt. %.

One grain each of sperrylite [$PtAs_2$] and braggite [(Pd,Pt)S] were identified. Quantitative analyses are given in Table 6a. Sperrylite is ~ 5 µm in size, and occurs as a composite grain with kotulskite and gold (Fig. 9.1g). Braggite is ~ 20 µm in size, of subhedral habit and occurs at the contact between chalcopyrite, pyrrhotite and plagioclase (Fig. 9.1l &m). The grain shows zoning defined by variation in Pd/Pt ratio. In the triangular plot Pt-Pd-Ni (Fig. 9.3), analyses of the braggite grain plot in a line parallel to the Pt-Pd join and show substantial substitution of Pd for Pt with Pd ranging from 10.70 – 31.15 at % and Ni 9.02 – 10.26 at %. The single grain of braggite clearly displays the solid solution between braggite [(Pt,Pd,Ni)S] and vysotskite [PdS] (Verryn and Merkle, 2000).

Seven grains of anhedral and rounded native gold were found in the recrystallized gabbronorite samples. Grain sizes range from < 1 µm to 15 µm. The grains occur enclosed in plagioclase (Fig. 9.1n & o) or along internal fractures in orthopyroxene altered to amphibole in the vicinity of chalcopyrite (Fig. 9.1p & q). The grain enclosed in plagioclase occurs intergrown with kotulskite and hessite. Ag contents

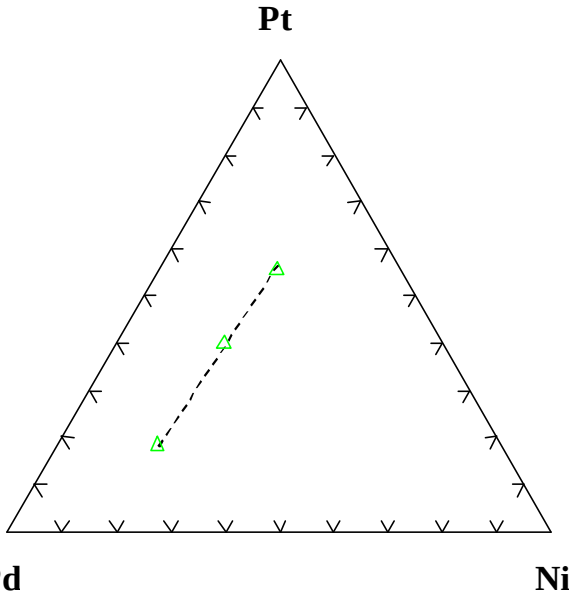

Fig. 9.3: Mineral chemistry of braggite from Nonnenwerth (sample MOX10).

of gold grains range from 12.9 to 20.62 wt. %, with the low Ag bearing gold enclosed in plagioclase. Trace contents of Pd in gold ranges from 0.36 to 0.6 wt. %.

One grain of hessite [Ag_2Te] has been identified and analysed. The grain is ~5 µm in size, and occurs intergrown with kotulskite at the chalcopyrite-plagioclase grain boundary. The chemical composition of the grain is given in Table 6a.

9.1.2 Anorthosite

The PGM suite (n=18) mainly comprises merenskyite (89 %). In addition, one grain each of kotulskite and moncheite were observed. The relative scarcity of moncheite and kotulskite in anorthosite is notable because these minerals dominate the PGM suite in recrystallized gabbronorite.

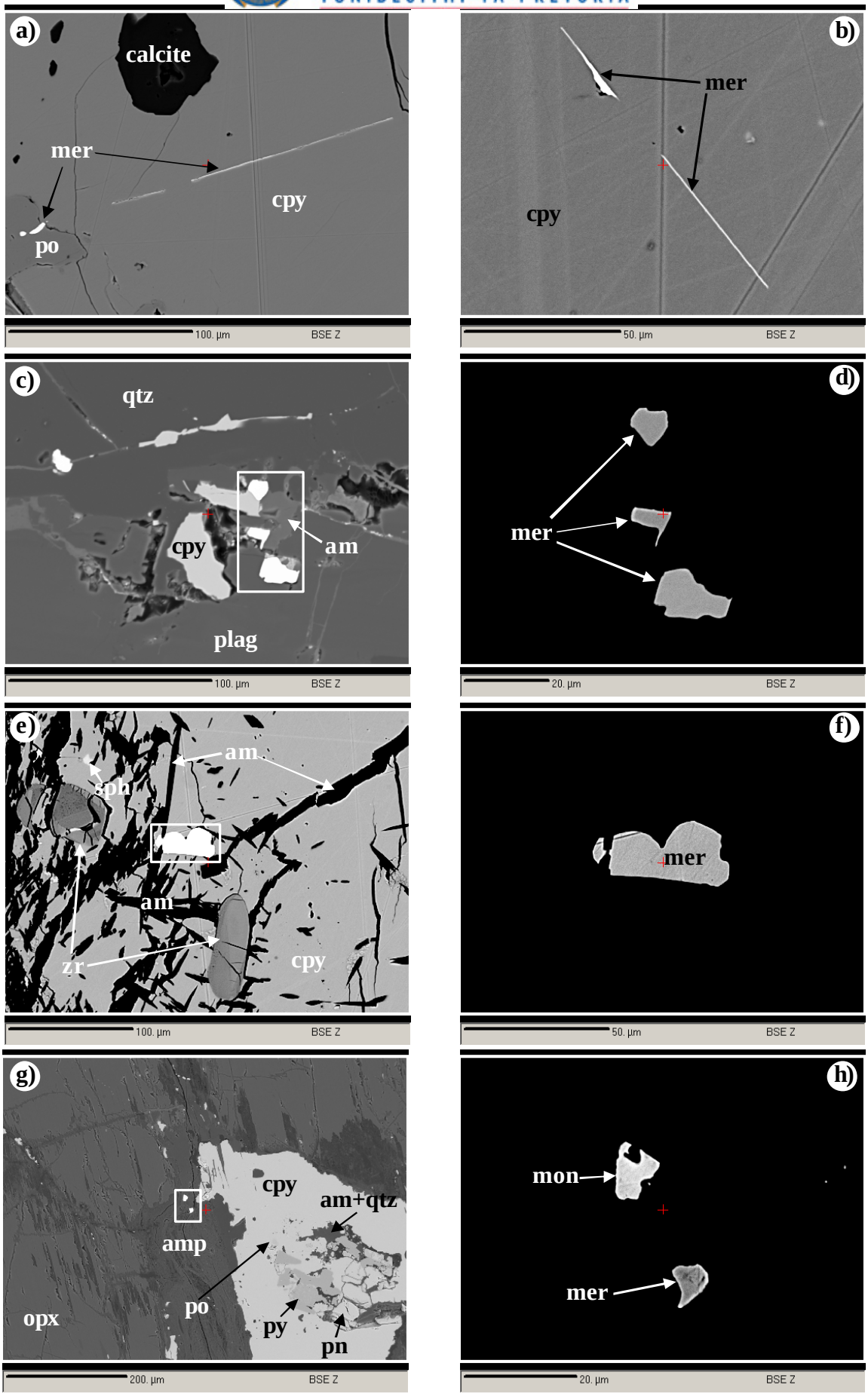

Fig. 9.4: Refer to next page for explanation of images.

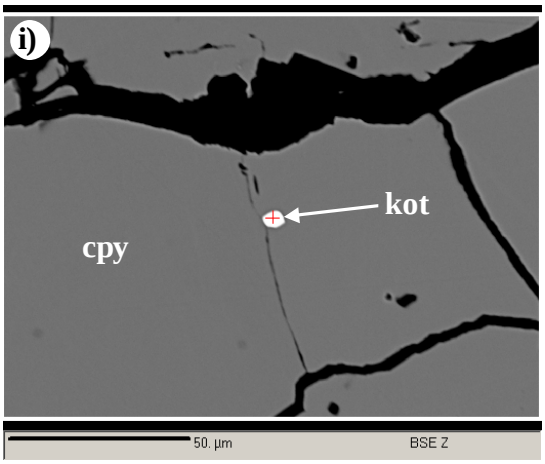

Fig. 9.4: Back-scattered electron images showing various textures and associations of PGM. (a) Merenskyite (mer) enclosed in pyrrhotite (po) and occurring as thin lamellae in chalcopyrite. Note also calcite enclosed in chalcopyrite. Sample MOX29. (b) Merenskyite lamellae in chalcopyrite. Sample MOX29. (c) Merenskyite (in rectangle) intergrown with amphibole, quartz and chalcopyrite within plagioclase. Sample MOX29. (d) Enlargement of rectangle in c). Subhedral merenskyite grains in amphibole and quartz after plagioclase. Sample MOX29. (e) Merenskyite (in rectangle) enclosed in chalcopyrite that is intergrown with acicular amphiboles (actinolite). Chalcopyrite also encloses subhedral zircons (zr). Sample MOX29. (f) Enlargement of rectangle in e). Subhedral merenskyite enclosed in chalcopyrite. Sample MOX29. (g) PGM (in rectangle) in amphibole peripheral to a composite grain of chalcopyrite, pyrrhotite and pentlandite. Sample MOX27. (h) Enlargement of rectangle in g) Anhedral moncheite and merenskyite in amphibole. Sample MOX27. (i) Kotulskite enclosed in chalcopyrite, close to a fracture. Sample MOX29.

Merenskyite [$PdTe_2$] shows grain sizes between < 1 µm to 18 µm, occasionally reaching 50 µm, but mostly around 10 µm. It occurs as lamellae in chalcopyrite (Fig. 9.4a & b) suggesting that it exsolved from the sulphide. It also occurs as subhedral to anhedral grains at the boundary between chalcopyrite and altered plagioclase or enclosed in plagioclase in the vicinity of chalcopyrite (Fig. 9.4c & d). In places, it may occur enclosed in pyrrhotite, pentlandite or chalcopyrite where

the sulphides are intergrown with amphiboles (Fig. 9.4e & f). Bismuth contents vary substantially and range from 2.17 to 14.82 wt. % (Table 6a).

One crystal of moncheite [$PtTe_2$] examined is anhedral, measuring ~12 µm in size and occurs in amphibole adjacent to a large grain of intergrown chalcopyrite-pentlandite-pyrite-pyrrhotite. It is closely associated with merenskyite (Fig. 9.4g & h). The analysed grain has relatively high Bi contents (8.72 wt. %).

The analysed grain of kotulskite [(PdTe] is ~3 µm in size, subrounded and occurs enclosed in chalcopyrite, close to a fracture (Fig. 9.4i). Quantitative analyses of this grain show that it has a relatively high Bi content (17.12 wt. %) when compared to the maximum of 13.98 wt. % in samples from the recrystallized gabbronorite.

One grain of argento-pentlandite (~2 um) intergrown with chalcopyrite was identified. Quantitative analyses of this grain are given in Table 6a.

9.2 Townlands

The PGM assemblage at Townlands is dominated by Pd-rich (75 %) bismuthotellurides, minor sperrylite (15 %), rare stibiopalladinite (5 %) and isomertieite (5 %). The PGM occur predominantly enclosed in sulphides (mostly pyrite and minor chalcopyrite and millerite) or, in places, at the contact between sulphide (mostly pyrite, minor chalcopyrite and rare galena) and secondary silicate (amphibole after orthopyroxene).

9.2.1 Upper Platreef

Only one crystal of isomertieite-I ($Pd_{11}Sb_2As_2$), was identified in the Upper Platreef. The crystal (~8 µm) is subrounded and occurs enclosed in chalcopyrite, near the contact with intergrown pyrite (Fig. 9.5a & b). The chemical composition of the grain is given in Table 6b. In addition to the stoichiometric Pd, As and Sb, isomertieite contains significant amounts of Ag (0.84 at. %).

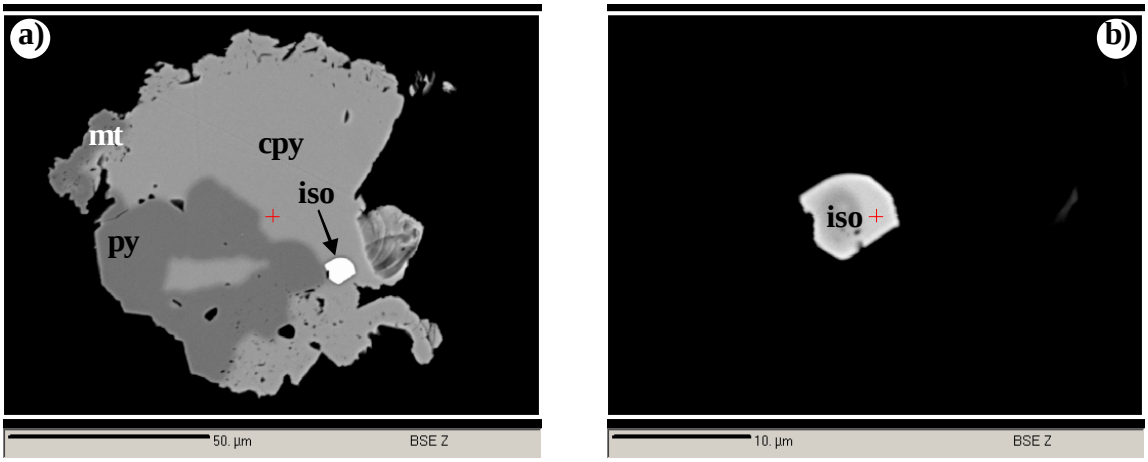

Fig. 9.5: Back-scattered electron images of isomertieite and its textural setting. (a) Isomertieite (iso) enclosed in chalcopyrite, near contact with pyrite. Sample P7. (b) Enlargement of isomertieite shown in a). Sample P7.

9.2.2 Middle Platreef

Compared to the other Platreef packages investigated, the Middle Platreef hosts the largest variety of PGM by far, including PGE-bismuthotellurides, sperrylite, stibiopalladinite as well as Bi-Te phases and gold. In the PGM suite (n=19), Pd-rich bismuthotellurides are predominant (79 %), with lower abundances of sperrylite (16 %) and stibiopalladinite (5 %).

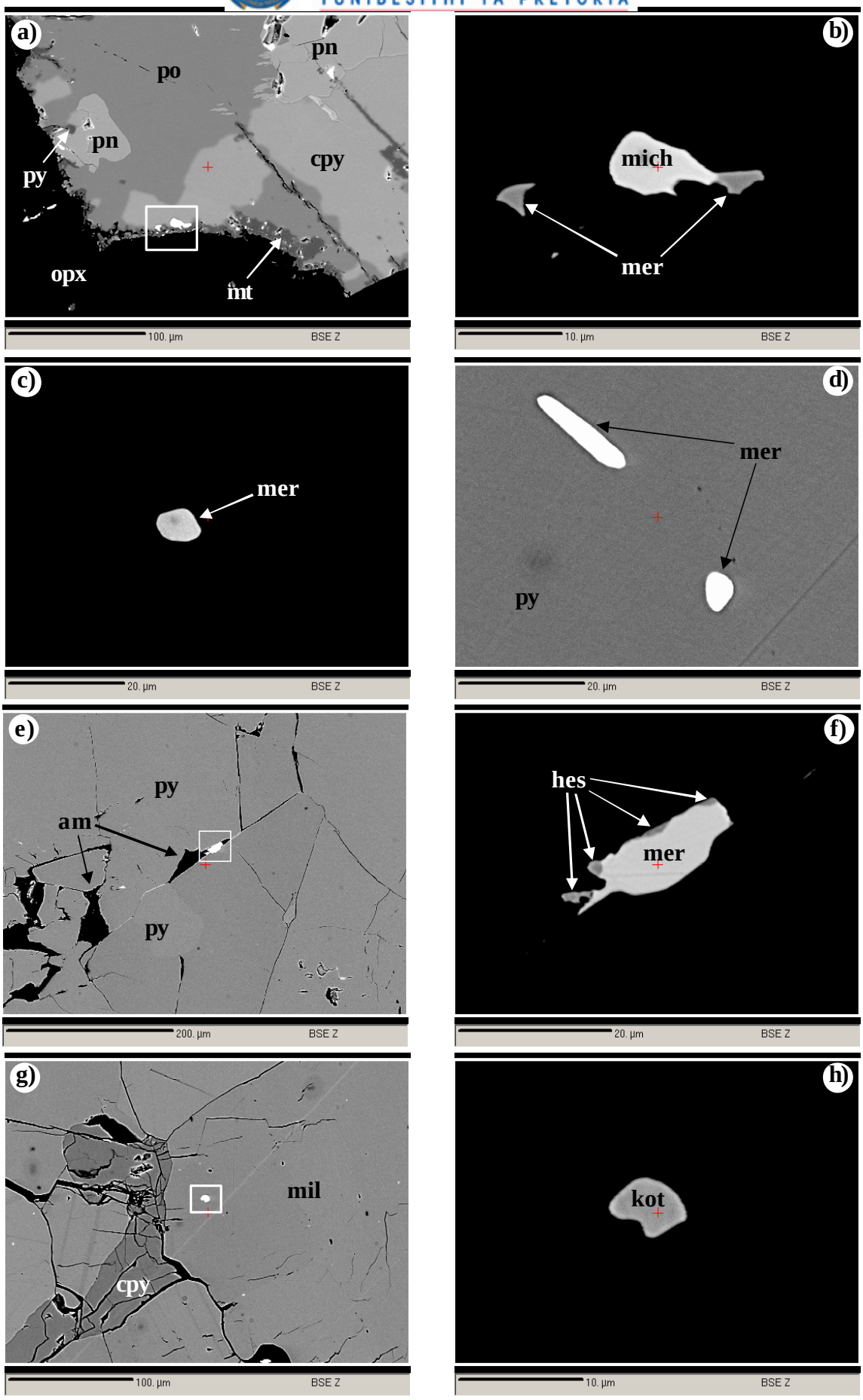

Fig. 9.6: Refer to next page for explanation of the images.

Fig. 9.6: Back-scattered electron images showing various textures and associations of PGM. Rectangle represents area enlarged for image to the immediate right. (a) PGM (in rectangle) enclosed in chalcopyrite (cpy) adjacent to the margin of the sulphide. Magnetite (mt) is also enriched in the border zone of the sulphide. po = pyrrhotite, pn = pentlandite, opx = orthopyroxene. Sample P13. (b) Enlargement of rectangle in a). Subrounded michenerite (mich) intergrown with merenskyite (mer). Sample P13. (c) Subrounded merenskyite enclosed in millerite. Sample P106. (d) A subrounded and an elongate merenskyite grain are enclosed in pyrite (py), associated with a fracture. Sample P15. (e) PGM (in rectangle) enclosed in pyrite along internal cracks. The PGM are associated with amphibole (am) that is intergrown with pyrite, also along cracks. Sample P15. (f) Enlargement of rectangle in e). Anhedral merenskyite intergrown with hessite (hes). Sample P15. (g) Kotulskite (kot) (in rectangle) enclosed in millerite (mil). Note chalcopyrite that is interstitial to millerite. Sample P106. (h) Enlargement of rectangle in g). Subrounded kotulskite enclosed in millerite. Sample P106.

Merenskyite [$PdTe_2$] is subhedral or rounded to elongate in shape with grain sizes ranging from < 2 µm to 22 µm but mostly between 5 and 10 µm. It is enclosed in chalcopyrite and, in general, located close to the margins of chalcopyrite (Fig. 9.6a & b). It may also be enclosed in pyrite (Fig. 9.6c & d) and, in places, in millerite intergrown with pyrite. In one case, several crystals of hessite were observed at the margin of merenskyite (Fig. 9.6e & f). Merenskyite from Townlands is relatively Bi- rich (1.51 to 28.58 wt. %, mostly above 14 wt. %) compared to merenskyite from anorthosite at Nonnenwerth.

Kotulskite [PdTe] occurs enclosed in pyrite, millerite or chalcopyrite (Figs. 9.6g & h). The grains are sub-rounded in shape and grain sizes range from 2 to 7 µm. Quantitative analyses of this phase are given in Table 6b. Three subhedral to anhedral grains of sperrylite [$PtAs_2$] were identified. These occur at pyrrhotite/orthopyroxene grain boundaries (Figs. 9.6i & j). One grain is ~22 µm

wide, the others are < 2 µm in size. Only one quantitative analysis was obtained on the larger grain. In addition to near-stoichiometric Pt and As contents, this grain has 2.14 at. % S, 0.55 at. % Sb, 0.5 at. % Te and 0.1 at. % Rh (Table 6b).

One grain each of michenerite [(Pd,Pt)Te] and stibiopalladinite [Pd_5Sb_2] was identified. The former is subhedral to subrounded, ~10 µm in size, and occurs enclosed in chalcopyrite, close to the margin of the sulphide (Fig. 9.6a & b). The grain is intergrown with merenskyite (Fig. 9.6a & b). Stibiopalladinite is ~1 µm in size of subhedral habit and occurs enclosed in pyrite associated with amphibole.

An unnamed phase with a calculated chemical formula **$FeBiS_2$** was also identified. It probably represents the iron end member of emplectite [$CuBiS_2$] (Wagner and Lorenz, 2002). The mineral occurs enclosed in pyrite and forms subhedral to subrounded and elongate grains with grain sizes up to 15 µm. One grain occurs attached to pyrrhotite, which is enclosed in pyrite (Fig. 9.6k & l). Quantitative analyses of this phase are given in Table 6b.

Hessite [Ag_2Te] occurs enclosed in pyrite, particularly along fractures, where it may be intergrown with amphibole. Grain sizes are < 2 µm. One grain is intergrown with merenskyite and the others form a cluster of discrete grains.

Altaite [PbTe] forms subhedral (≈5 µm), subhedral and anhedral grains that are enclosed in secondary amphibole in the vicinity of coarse base metal sulphides (Fig. 9.6m & n). One of the examined grains is intergrown with galena and the other is intergrown with magnetite (Fig. 9.6m & n).

Tetradymite-type minerals identified have calculated chemical formulae close to [Bi_2Te_2S]. Two identified crystals are subhedral, with grain sizes of 10 and 20 µm, and occur at the boundary between chalcopyrite enclosed in pyrite.

One grain each of pilsenite [Bi_4Te_3], temagamite [Pd_3HgTe_3] and an unnamed phase with a calculated chemical formula $Bi_4Te_2S_2$ were identified. Pilsenite is anhedral to subhedral, < 2 µm in size and occurs enclosed in pyrite, adjacent to chalcopyrite. Temagamite is anhedral, ~2 µm in size and also occurs enclosed in pyrite. Quantitative analyses of these two phases are given in Table 6b.

A small (< 2 µm) grain of an unnamed phase with a calculated formula Bi_4Te_2Se (close to UN 1133; Xiang-ping Gu et a., 2001) was identified. The unnamed phase occurs at the contact between pyrite and pyrrhotite and forms part of a complex composite sulphide enclosed in pyrite consisting of chalcopyrite, pyrrhotite, pilsenite, Fe-emplectite? and the unnamed phase [Bi_4Te_2Se] (Fig. 9.6l).

Three grains of gold enclosed in pyrite were identified. They occur associated with amphibole intergrown with pyrite, or along the contact between pyrite and chalcopyrite (Fig. 9.6o & p). One quantitative analyses was obtained, showing has 67.06 wt. % Au, 30.53 wt. % Ag, 0.11 wt. % Fe and 240 ppm Bi.

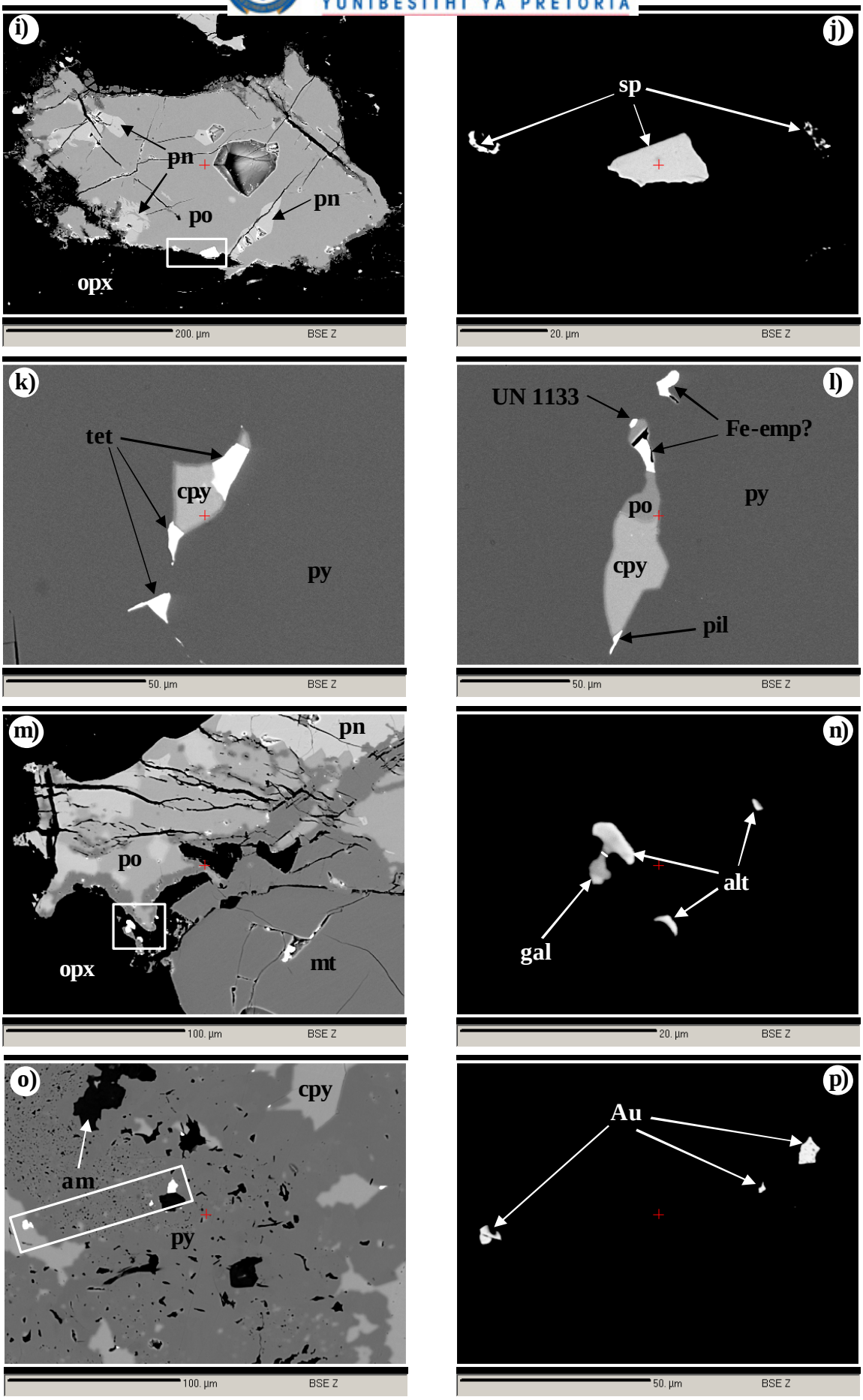

Fig. 9.6 continued: Refer to next page for explanation of the images.

Fig. 9.6 continued: Back scattered electron images showing various textures and associations of PGM and Bi-,Te- phases. Rectangle represents area enlarged for image to the immediate right.

(i) Sperrylite (sp) (in rectangle) located at the contact between pyrrhotite and orthopyroxene (opx). Pyrrhotite is intergrown with pentlandite and also contains minor flame-like exsolutions of pentlandite. Sample P13. (j) Enlargement of rectangle in c). Subhedral sperrylite and smaller anhedral sperrylite at the contact between pyrrhotite and orthopyroxene. Sample P13. (k) Pyrite enclosing intergrowths of tetradymite-type (tet) minerals and chalcopyrite. Sample P15. (l) Pyrite enclosing a composite grain of chalcopyrite, pyrrhotite, pilsenite (pil), Fe-emplectite? (Fe-emp?) and the unnamed phase UN 1133 with a calculated chemical formula [Bi_4Te_2Se]. Sample P15. (m) Altaite (alt) grains (in rectangle) are enclosed in secondary amphibole adjacent to pyrrhotite showing rims of magnetite. Sample P13. (n) Enlargement of rectangle in m). One grain of altaite is intergrown with galena (gal). Sample P13. (o) Gold (Au) grains (in rectangle) enclosed in pyrite or located near the contact between pyrite and enclosed chalcopyrite. Sample P106. (p) Enlargement of rectangle in o). Anhedral gold grains in pyrite. Sample P106.

9.3 Summary and Discussion

At Nonnenwerth, PGM are dominated by **Pd-rich *and* Pt-rich** bismuthotellurides followed by rare braggite and sperrylite. The PGM occur predominantly at the contact between sulphide (mostly chalcopyrite, minor pyrrhotite and rare pyrite) and secondary silicate (mostly chlorite and albite after plagioclase) or enclosed in sulphides. Importantly, Pd-rich PGM (Pd-bismuthotellurides) are mostly enclosed in silicates. However, even these PGM enclosed in silicates retain a strong spatial relationship with the base metal sulphides, mostly chalcopyrite, and are associated with secondary minerals (mostly chlorite and albite which replace plagioclase, or rarely amphibole which replaces orthopyroxene and base metal sulphides). The above observation may result from dissolution of the base metal sulphides hosting Pd, and leaving isolated insoluble Pd-PGM behind (Barnes *et al*., 2007), or Pd

may have been remobilized from the sulphides into the surrounding silicates. Based on textural evidence, the latter model is preferred.

At Townlands, the PGM assemblage is dominated by **Pd-rich** bismuthotellurides, minor sperrylite, rare stibiopalladinite and isomertieite. The PGM occur predominantly enclosed in sulphides (mostly pyrite and minor chalcopyrite and millerite), or locally at the contact between sulphide and secondary silicate (amphibole after orthopyroxene).

In summary, there are no dramatic differences between the PGM assemblages at Nonnenwerth and Townlands, also in comparison to descriptions from most other Platreef occurrences (e.g. Kinloch, 1982; Holwell et al., 2006). Bismuthotellurides predominate followed by rarer arsenides and antimonides. One obvious difference, however, is the wide compositional range of Pt-Pd bismuthotellurides and the presence of Pt-rich bismuthotellurides at Nonnenwerth only, whereas at Townlands, only Pd-rich bismuthotellurides are present. The significance of this finding cannot be evaluated conclusively. The variability may be related to local factors like different host rocks; footwall lithologies, down-temperature re-equilibration, activity of fluids, and other possible causes.

It is here suggested that originally, at magmatic conditions, the PGE were collected by and partitioned into an immiscible sulphide liquid (e.g Naldrett et al., 1986; Naldrett, 1989). The IPGE (Ru, Os, Ir) tend to concentrate into chromite (Lee, 1996), and the PPGE (Pt, Pd and Rh) are mainly concentrated in the sulphide fraction (Naldrett, 1989). During down-temperature crystallisation of the

magmatic sulphide liquid, pyrrhotite, pentlandite and chalcopyrite form on further cooling (Hawley, 1965; Kullerud et al., 1968; Ewers and Hudson, 1972). The PGE are either kept in solid solution in the sulfides (e.g. up to some hundred ppm of Pd in pentlandite at Nonnenwerth; see also Gervilla et al., 2005), or if incompatible with sulfide at lower temperature, PGE-compounds (PGM) are formed by reactions of the PGE with respective ligands like sulphur, arsenic, antimony, tellurium or bismuth. Accordingly, as proposed by Cawthorn et al. (2002), the primary mechanism concentrating the PGE is a first-order process (PGE collection by sulfides), and the evolution of the PGM is the result of secondary processes related to cooling, local changes in $f(S_2)$ in the crystallization environment, subsolidus re-equilibration, and probably also reactions with fluids (late-magmatic to hydrothermal) percolating in the rocks.

The remobilization and redistribution PGE may be attributed to various factors among them assimilation of crustal S where floor rocks are of Transvaal Supergroup, devolatization of dolomite xenoliths which are present along the whole strike length of the northern lobe or interaction of primary magmatic sulphides with late stage magmatic fluids. The involvement of late magmatic/hydrothermal fluids is supported by the occurrence of violarite which is probably of hydrothermal origin.

Addition of floor rock crustal S is supported by the studies of Manyeruke *et al*. (2005). The PGM are dominated by lower temperature Pd-rich bismuthotellurides and minor Bi-, Sb- and Te-bearing phases (Kim et al., 1990), as opposed to the Merensky Reef, where PGE sulphides may constitute a substantial proportion of

the overall PGM assemblage (e.g. Kinloch, 1982; Mostert et al., 1982). Therefore, the PGM assemblages at Nonnenwerth and Townlands support the suggestion that the PGM are “secondary” in the sense of Cawthorn et al. (2002).

The model of sulphide control for the PGE is supported by the broad positive correlation between Pt and Pd and between PGE and S, and abundance of magmatic sulphides at Nonnenwerth suggesting that sulphides were the primary PGE collector. Even though the base metal sulphides do not host the PPGE (Pt, Pd and Rh) – except for a certain proportion of Pd in pentlandite – the PGM that do host them maintain a close spatial relationship with the base metal sulphides, underlining the initial control of PGE by sulphides.

Thus, assimilation of external S during magma emplacement was apparently not the principal controlling factor in sulphide genesis since PGE mineralisation occur at Nonnenwerth where the Platreef over granite gneiss. Instead, significant assimilation of S may have merely modified already existing sulphide melt, essentially diluting the tenor of the sulphides, particularly in areas where the floor rocks consisted of sulphidic shales, between Townlands and Tweefontein (Manyeruke *et al.*, 2005; Hutchinson and Kinnaird, 2005) and the formation of the lower temperature semi-metal PGM e.g. (Pt,Pd)-bismuthotellurides.

CHAPTER TEN: SULPHUR-ISOTOPE GEOCHEMISTRY

The formation of magmatic Cu-Ni-(PGE) sulphide deposits is controlled by the interaction between the sulphide saturation state of mafic magmas and dynamic processes by which immiscible sulphide liquid can be concentrated into favorable locations (Ripley, 1999). In many sulphide-rich Cu-Ni deposits, addition to the magma of external S is considered important. Examples include Kambalda (Naldrett, 1989), Voisey's Bay (Li *et al.*, 2000), Noril'sk (Godlevsky and Grinenko, 1963; Gorbachev and Grienko, 1973; Naldrett *et al.*, 1996) and Pechenga (Green and Melezhik, 1999). A similar model has been proposed by Buchanan *et al.* (1981) for the Platreef on the farm Tweefontein and by Manyeruke (2003) at Townlands. Alternatively, assimilation of sulphide-poor siliceous or carbonaceous country rocks may also induce sulphide saturation (De Waal, 1977; Gain and Mostert, 1982; Naldrett *et al.*, 1986; Li and Naldrett, 1993). Sulfur isotope compositions may be used as tracers to detect the presence of external sulphur and thus can potentially constrain the ore forming process and may be used as a guide to ore. Mantle $d^{34}S$ values are in the range ~0 ± 3 ‰ (Ripley, 1999), whereas sedimentary rocks may have strongly negative or positive values. Thus, if igneous rocks show substantial deviation from the mantle values, this may indicate assimilation of crustal sulphur (Ripley, 1999). It should, however, be noted that contamination with Archean sedimentary host rocks may be difficult to detect as these rocks generally have $d^{34}S$ values in the range of mantle values (Ripley, 1999).

The available S isotopic database for the Platreef is shown in Table 7a and Fig. 10.1. Liebenberg (1968) reported sulphur isotopic values for the Northern limb of the Bushveld Complex on the farm Zwartfontein, with $d^{34}S$ values of +0.7 and +1.9 ‰ for a calc-silicate and a pegmatoidal norite, respectively. Buchanan *et al.* (1981) carried out S-isotopic analyses on 9 samples (+6.3 to +9.2 ‰) of the Platreef on the farm Tweefontein, where the floor rocks consist of calc-silicate, banded ironstone and argillaceous sediments. This was followed by the work of Hulbert (1983) on Lower Zone pyroxenites and chromitites, Critical Zone pyroxenites, chromitites, anorthosites and Platreef-type rocks on Grasvally to the south of Mokopane. $d^{34}S$ values of +0.96 to +7.54 ‰ were reported for the Platreef. Manyeruke (2003) provided S-isotopic data on 12 samples ($d^{34}S$ values of +2.6 to +10.1 ‰) covering the Platreef and its floor rocks on the farm Townlands where the floor rocks consist of metasediments of the Silverton Formation of the Transvaal Supergroup. Sharman-Harris and Kinnaird (2004) published results of $d^{34}S$ analyses on pyrrhotite and chalcopyrite on the farms Rietfontein, Turfspruit and Macalacaskop ($d^{34}S$ of +4.5 to +5.6 ‰). Tuovila (in preparation) analysed sulphide-bearing pyroxenite sills several km below the basal contact of the Bushveld, on the farm Uitloop. These yielded $d^{34}S$ values from +8 to +15 ‰. Holwell *et al.* (2005, 2007) reported magmatic signatures for S-isotopic analyses of the pyroxenites on the farm Overysel ($d^{34}S$ +1.7 to +2.0 ‰) where the floor rocks consist of granite gneisses.

In the course of the present study, a total of 7 samples from the Platreef on Nonnenwerth were analysed at Indiana University, Bloomington, U.S.A. Analytical

Farm	**$d^{34}S$ (‰ VCDT)**	**Reference**
Grasvally	+.96 to +7.54	Hulbert (1983)
Rooipoort	+2.0 to +5.0	Maier *et al*. (2007)
Townlands	+4.0 to +8.0	Manyeruke (2005)
Macalacaskop	+2.9	Sharman-Harris *et al*. (2005)
Uitloop	+8.0 to +15.0	Touvila (in preparation)
Turfspruit	+5.2	Sharman-Harris *et al*. (2005)
Rietfontein	+5.0	Sharman-Harris *et al*. (2005)
Tweefontein	+6.3 to +9.2	Buchannan *et al*. (1981)
Tweefontein Hill	+ 6.3 to 9.0	Scholtysek (2005)
Sandsloot	0 to +2.6	Holwell *et al*. (2007)
Zwartfontein	+0.7 – 1.9	Liebenberg (1968); Holwell *et al*. (2007)
Overysel	+1.7 to +2.0	Holwell *et al*. (2005)

Table 7a: S-isotopic analyses of the Platreef along strike from south to north.

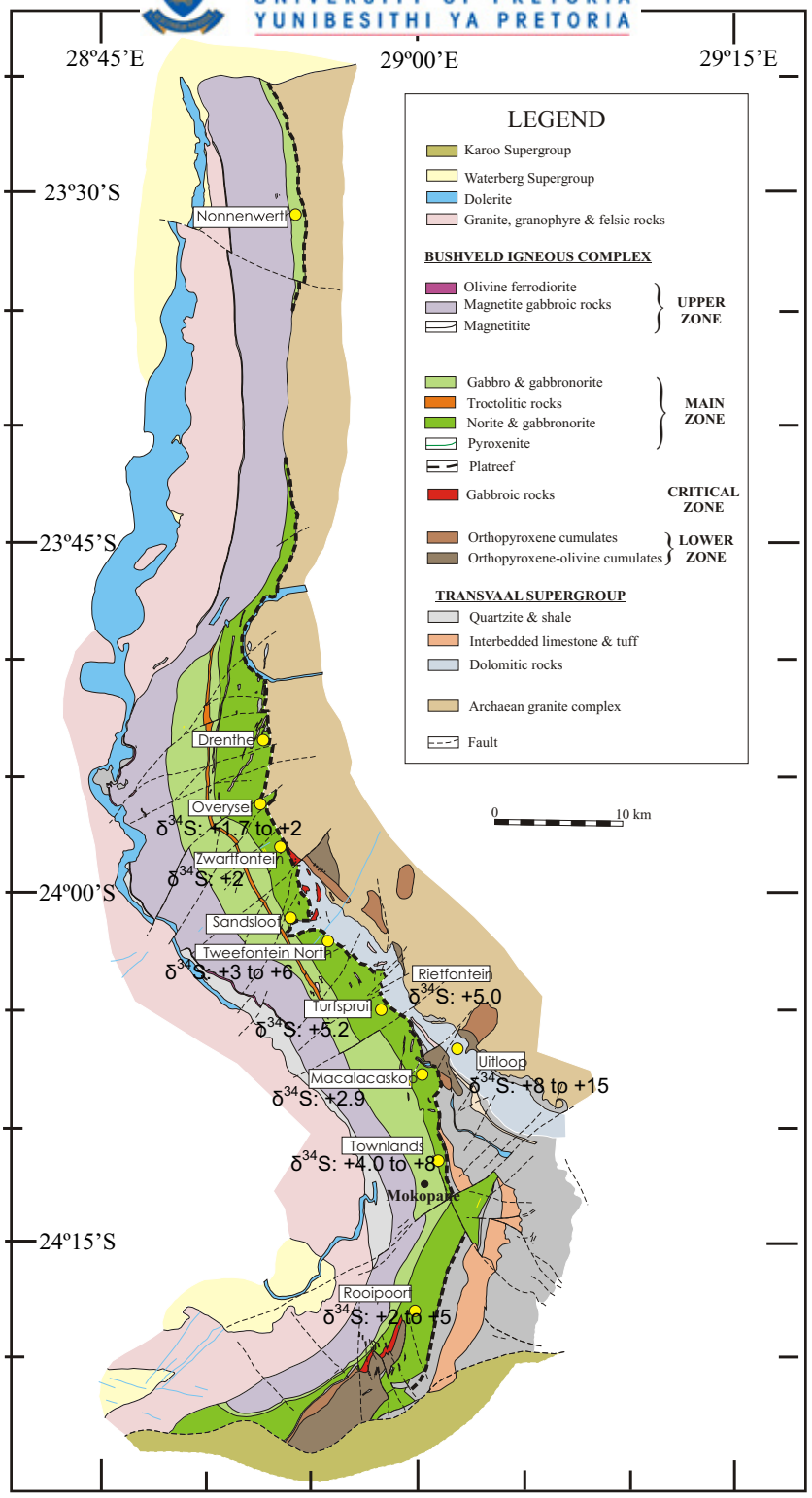

Fig. 10.1: Regional geological map of the northern limb with results of S isotope analyses superimposed. Data from Townlands are from Manyeruke et al. (2005), data from Macalakaskop, Rietfontein and Turfspruit are from Sharman-Harris et al. (2005), data from Tweefontein are from Buchannan et al. (1981), data from Rooipoort are from Maier et al. (2007), data from Uitloop are from Tuovila (in preparation), data from Overysel are from Holwell et al. (2005) and data from Zwartfontein are from Liebenberg (1968). (Map modified after Ashwal et al., 2005).

results are presented in Table 7b and analytical procedures are given in Appendix 1f. Sulphur isotopic compositions are reported in standard d notation relative to VCDT (Vienna Cañon Diablo Troilite). The analyses were performed to

(i) determine the role of crustal contamination in the formation of the Platreef,

(ii) compare the S-isotopic composition of the Platreef along strike, and thus to determine whether the high $d^{34}S$ values of the Platreef on the farms Townlands (Manyeruke, 2003), Tweefontein (Buchanan *et al.*, 1981), Rietfontein, Turfspruit and Macalacaskop (Sharman-Harris and Kinnaird, 2004) are characteristic of the entire Platreef,

(iii) determine whether regional trends in $d^{34}S$ values can be observed,

(iv) compare the $d^{34}S$ signature of the Platreef to other examples of basal Ni-Cu-PGE mineralization elsewhere in the world (Fig. 10.2) .

Most samples from Nonnenwerth have relatively homogeneous $d^{34}S$ values ranging from +0.73 to +1.87 ‰ which is within the mantle range (Ripley, 1999). This suggests minute or no recognizable addition of crustal sulphur to most of the Platreef rocks examined. One sample from the base of the Platreef (MOX36) has $d^{34}S$ of +5.24 ‰, suggesting that localized assimilation of heavy crustal sulphur may have occurred in this sample.

Notably, the Nonnenwerth data are similar to those of Holwell *et al*. (2005) in the Platreef at Overysel where $d^{34}S$ values range from +1.7 to +2.0 ‰ and where the floor rocks equally consist of granite gneiss. Broadly similar values of $d^{34}S$ are also found on Zwartfontein, where the floor rocks are constituted by dolomite. In contrast,

Sample	Borehole	Distance above base of Platreef (m)	$\mathbf{d}^{34}S$ ($^{0}/_{00}$VCDT)	Rock unit
MOX9	2121	111.32	1.33	recrystallized gabbronorite
MOX10	2121	91.10	1.22	recrystallized gabbronorite
MOX14	2121	35.77	1.87	melagabbronorite
MOX27	2199	184.95	1.33	anorthosite
MOX29	2199	163.82	0.73	pegmatoidal gabbro
MOX33	2199	88.81	1.22	norite
MOX36	2199	31.94	5.24	altered gabbronorite

Table 7b: S-isotopic analyses of samples from the Platreef at Nonnenwerth.

at the localities where the floor rocks consist of shale and quartzite, $d^{34}S$ values tend to be strongly positive. These data are generally interpreted to suggest that the Platreef magma assimilated external S from the shales and granites (Manyeruke, 2003). In contrast, the dolomitic floor rocks may have either contributed insignificant amounts of external S to the magma, or the sulphur within the dolomites and granites was unfractionated. The model is supported by the S isotopic data on metasediments of the Silverton Formation (Manyeruke, 2003; Manyeruke *et al*., 2005) that show $d^{34}S$ values of +2.6 to +10.1 ‰. Unfortunately, no data on sulphides within the dolomites underlying the northern lobe is yet available. Cameron (1982b) analysed dolomite of the Malmani sub-group in the Fochville area and found $d^{34}S$ between -8 and +10 ‰. It remains unclear whether the dolomites of the study area have similar S isotopic signatures.

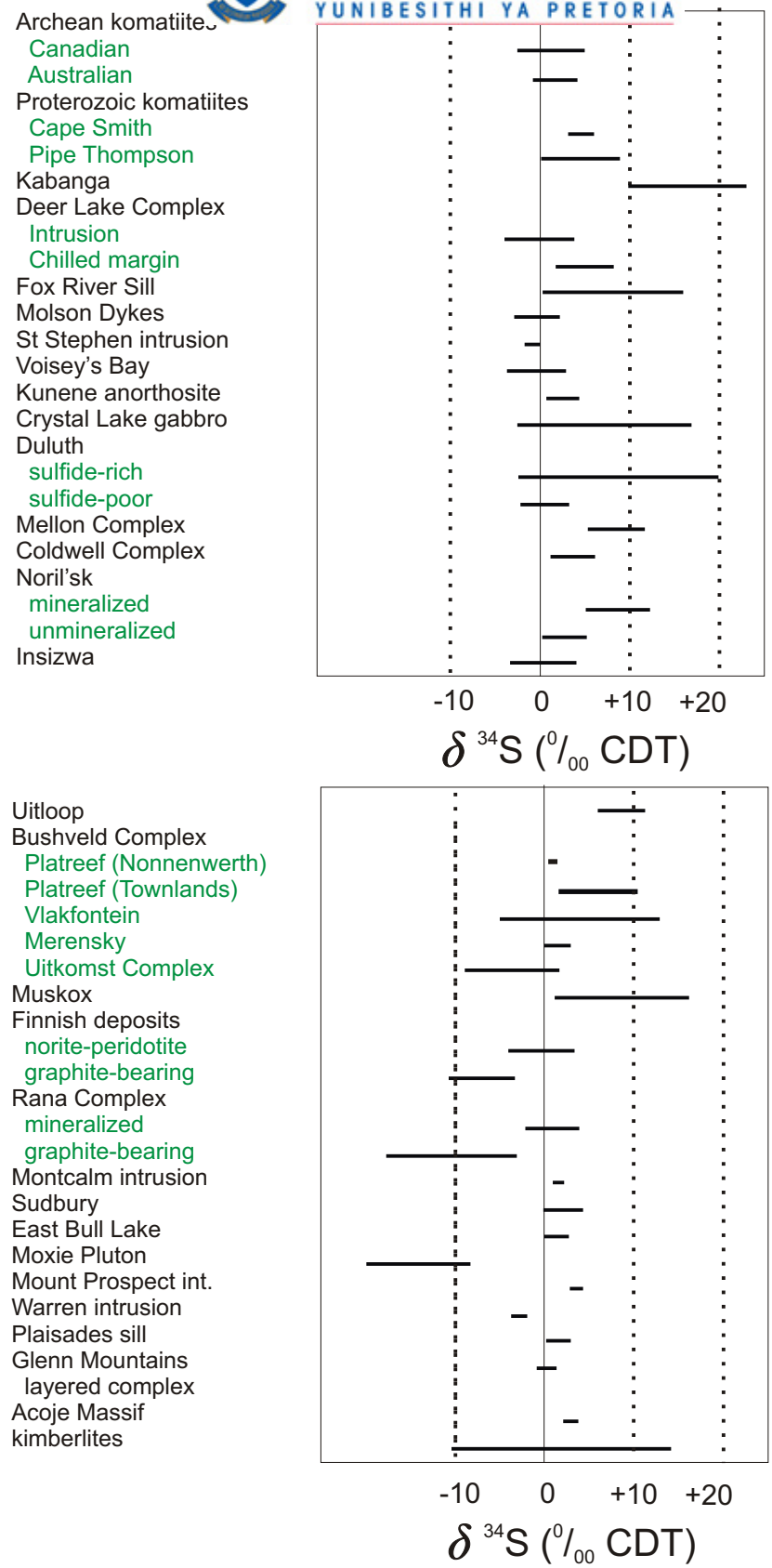

Fig. 10.2: $\delta^{34}S$ values of sulphidic rocks and sulphides in selected mafic/ultramafic intrusions (modified from Ripley, 1999). Kabanga and Kunene data from Maier (unpublished), Uitloop data from Touvila, (personal communication) and Townlands data from Manyeruke (2003).

10.1 Summary

This study has shown that the sulphur isotope compositions of the Platreef at Nonnenwerth, where floor rocks are granite gneiss, are mantle-like ($d^{34}S$ values mostly in the range from +0.73 to +1.87 ‰). At Overysel, the Platreef is also underlain by granite gneiss and $d^{34}S$ values range from +1.7 to +2.0 ‰ (Holwell *et al*, 2005). The distinct positive sulphur isotope values at Townlands (Manyeruke, 2003; Manyeruke *et al*., 2005), and in the lower parts of the Platreef on Rietfontein, Turfspruit and Macalacaskop (Sharman-Harris and Kinnaird (2004); Sharman-Harris *et al*. (2005)), indicate that the Platreef assimilated external S from the Transvaal Supergroup floor rocks underlying the areas. Therefore, the variation of the footwall along strike was critical in determining the $d^{34}S$ signature of the Platreef.

Importantly, this study and previous investigations by Holwell *et al*. (2005), Sharman-Harris and Kinnaird (2004), Sharman-Harris et al. (2005) show that the Platreef-style PGE-sulphide mineralization is associated with floor rocks containing variable S contents and S-isotopic signatures. Thus, assimilation of external S during magma emplacement was apparently not the principal controlling factor in sulphide genesis. Sulphur saturation probably occurred prior to intrusion in a deep staging chamber (Lee, 1996). Subsequently, assimilation of S may have merely modified already existing sulphide melt. This would have resulted in lowering the tenor of the sulphides by dilution due to low R-factors of assimilated sulphides, particularly in areas where the floor rocks consisted of sulphidic shales, between Townlands and Tweefontein.

CHAPTER ELEVEN: O-ISOTOPE GEOCHEMISTRY

The $d^{18}O$ of most crustal rock types are in excess of +8.0 ‰ compared to oxygen isotope values of mantle-derived mafic magmas which fall in a restricted range of +5 to +7 ‰ (Ripley, 1999). Thus oxygen isotope measurements offer a great potential as a tracer of crustal contamination of mantle-derived basaltic melts.

Pristine, mantle-derived tholeiitic melts are characterised by $d^{18}O$ values of +5.7 to +6.0 ‰ (Ripley, 1999). Mafic igneous rocks crystallizing from such magmas should thus also show the same range of oxygen isotopic values. Deviations from the above oxygen isotopic range require explanation that may include hydrothermal alteration and exchange with a fluid phase, derivation from anomalous ^{18}O-zones in the mantle related to crustal recycling, or assimilation of crustal material (Ripley, 1999).

The magma that gave rise to the eastern and western Bushveld Complex has been found to have $d^{18}O$ values of +6.9 ‰ (Schiffries and Rye, 1989 and Reid *et al*., 1993, respectively), approximately 1 % higher than values expected for rocks crystallizing from mantle-derived basaltic magma. Furthermore, the oxygen isotopes do not display any systemic variation with stratigraphic height and the authors attributed this and the higher $d^{18}O$ values to contamination and well mixing in a staging chamber before emplacement. The model was supported by Harris *et al*. (2005) who also found slightly elevated $d^{18}O$ values and no stratigraphic variation.

Orthopyroxene $d^{18}O$ values for the eastern Bushveld Complex range from +6.12 to +6.97 ‰ (average +6.6 ‰) and for the western Bushveld Complex +6.2 to +6.8 ‰ (average +6.5 ‰) (Schiffries and Rye, 1989).

Harris and Chaumba (2001) carried out oxygen isotope analyses on plagioclase and pyroxene separates for Upper Zone and Main Zone from the Bellevue core and the Platreef. The Upper Zone and Main Zone from Bellevue core show a restricted range in $d^{18}O$ values, from +7.0 to +8.3 ‰ and +6.1 to +7.6 ‰, respectively, indicating crystallisation from a well-mixed, already contaminated, magma having $d^{18}O$ values of +7.5 ‰, whereas Platreef samples have generally higher and more variable $d^{18}O$ values (+7.4 to +10.3 ‰ in plagioclase and +6.0 to +8.9 ‰ in pyroxene) indicating assimilation of a crustal component, probably Transvaal Supergroup rocks. The authors also noted that some Platreef samples have plagioclase and pyroxene not in oxygen isotope equilibrium at magmatic temperatures, suggesting the Platreef fluid was a mixture of predominantly magmatic water with a minor component derived from the footwall.

Harris et al. (2005) showed that plagioclase, pyroxene and olivine of the Rustenburg Layered Suite have $d^{18}O$ values indicating that the magmas from which they crystallized had $d^{18}O$ values that were about 7.1‰, that is, 1.4‰ higher than expected for mantle-derived magmas, suggesting extensive crustal contamination. The authors also found no systematic change in $d^{18}O$ value with stratigraphic height and interpreted this to suggest that contamination occurred in a ‘staging chamber’ before emplacement of the magma(s) into the present chamber.

This was followed by isotopic studies by Sharman-Harris *et al*. (2005) on samples from the southern Platreef at Turfspruit, Macalacaskop and Rietfontein, where floor rocks are Duitschland Formation metasediments. The authors reported $d^{18}O$ values of +6.5 to +8.5 ‰ for plagioclase, +6·5 to +8·5 ‰ for pyroxene and slightly higher $d^{18}O$ values (maximum values of +11.5 ‰) for cordierite from hornfels rafts. However, a calc–silicate from the direct footwall displayed a similar $d^{18}O$ values as that of the Platreef itself (+8 ‰).

For the present study, oxygen isotope analyses were carried out on orthopyroxene separates and whole rock samples from Platreef gabbronorites and a dolomite xenolith, at Indian University, Bloomington, U.S.A. Only three rock samples were analysed, therefore the data and interpretations thereof should be treated with caution. Analytical results are presented in Table 8 and analytical procedures are given in Appendix 1g. This was done to document the $d^{18}O$ values of orthopyroxene separates from the Platreef at Townlands and Nonnenwerth and to compare the data to available oxygen isotope data on the Platreef (Harris and Chaumba, 2001; Harris *et al.,* 2005; Sharman-Harris *et al*., 2005), and the eastern and western Bushveld Complex (e.g. Schiffries and Rye, 1989).

The gabbronorites and pyroxene separates from the Platreef on Nonnenwerth show $d^{18}O$ values that vary from +6.3 to +7.2 ‰ and +4.4 to +5.2 ‰, respectively. These values are within the range for mantle-derived mafic magmas (+5 to +7 ‰) (Ripley, 1999) suggesting little or no contamination in Nonnenwerth rocks. However, the Platreef on Townlands has generally higher $d^{18}O$ values (+8.0 to +8.3 ‰ in whole

Sample	Borehole	Distance above base of Platreef (m)	?^{18}O ($^{0}/_{00}$V-SMOW)	Rock unit
MOX9 bulk	2121	111.32	7.2	recrystallized gabbronorite
MOX9 (PYX)	2121	111.32	5.2	recrystallized gabbronorite
MOX10 bulk	2121	91.1	6.4	recrystallized gabbronorite
MOX10 (PYX)	2121	91.1	4.4	recrystallized gabbronorite
MOX14 bulk	2121	35.77	6.3	melagabbronorite
MOX14 (PYX)	2121	35.77	4.8	melagabbronorite
P15 bulk	TL1-03	57.45	8.1	Middle Platreef gabbronorite
P15 (PYX)	TL1-03	57.45	7.2	Middle Platreef gabbronorite
P19 bulk	TL1-03	44.65	8.0	Middle Platreef gabbronorite
P19 (PYX)	TL1-03	44.65	11.2	Middle Platreef gabbronorite
P25 bulk	TL1-03	8.62	8.3	Lower Platreef gabbronorite
P25 (PYX)	TL1-03	8.62	5.4	Lower Platreef gabbronorite

Table 8: S-isotopic analyses of samples from the Platreef at Nonnenwerth and Townlands. SMOW = standard mean ocean water.

rock samples and +5.4 to +11.2 ‰ in pyroxene) indicating assimilation of a crustal component, probably Transvaal Supergroup rocks. It should be noted that the pyroxene separates and whole rock give different d^{18}O values probably resulting from post-crystallisation processes. The above would generally be investigated by evaluating the degree of oxygen-isotope equilibrium between coexisting minerals and/or whole rocks, using so-called d–d plots (Gregory and Criss, 1986; Gregory *et al.,* 1989), but unfortunately, only pyroxene separates were analyzed for O-isotopic composition in this study.

This study also shows that $d^{18}O$ values on Nonnenwerth are lower and uncontaminated compared to $d^{18}O$ values of the Main Zone and Upper Zone from the Bellevue borehole (Harris *et al.,* 2005), eastern and western Bushveld Complex has (Schiffries and Rye, 1989 and Reid *et al*., 1993, respectively). However the data on both Townlands and Nonnenwerth is in agreement with the trace element and S-isotope data which showed that the Platreef on Nonnenwerth experienced little or no contamination compared to Platreef on Townlands which interacted and was contaminated by floor rock shales. Finally, the data on Townlands is in agreement with previous published O-isotope data on the Platreef (e.g. Harris and Chaumba, 2001; Sharman-Harris *et al*., 2005; Harris *et al.,* 2005).

11.1 Summary

The present study has established that $d^{18}O$ values on Nonnenwerth are lower and uncontaminated compared to $d^{18}O$ values of the Platreef at Townlands, Sandsloot (Harris and Chaumba, 2001), Main Zone and Upper Zone from the Bellevue core (Harris *et al.,* 2005), eastern and western Bushveld Complex has (Schiffries and Rye, 1989 and Reid *et al*., 1993, respectively). This may suggest that local contamination with dolomite did not play a role in the mineralization process at Nonnenwerth. Thus, the occurrence of mineralization close to the dolomite xenoliths at Nonnenwerth may be due to the dolomite forming an impermeable layer that forced the magma below into sulphide saturation. Dolomite assimilation may however have played part in other parts of the Platreef e.g. at Sandsloot.

CHAPTER TWELVE: DISCUSSION AND CONCLUSIONS

12.1 Compositional and lithological variation of the Platreef in the northern lobe

PGE-sulphide mineralization has been known to occur in the Platreef since ca. 80 years. Much of the publicly available data has been generated on localities in the southern and south central portions of the northern lobe, between Grassvally and Drenthe (e.g. Buchanan *et al.*, 1981; Gain and Mostert, 1982; Hulbert, 1983; Barton *et al.*, 1986). Additional data was generated by mining companies in the form of drilling and analyses, but much of these data remained unavailable to the public until recently. Thus, there was a perception that the Platreef occurs only in the south and that it consists of heterogeneous rocks dominated by pyroxenites enriched in xenoliths, as seen at Sandsloot (McDonald *et al.*, 2005), Tweefontein, Turfspruit, and adjacent localities (e.g., Kinnaird, 2005). This has influenced models on the origin of the mineralization during the last decades. The present study describes for the first time the occurrence of the Platreef in the north, and provides a detailed lithological and chemical description. This allows making comparisons of the Platreef along strike, to establish how the reef changes along strike, and ultimately constrains how the mineralization has formed.

12.1.1 Nature of the floor rocks to the Platreef

Along the nearly 100 km separating the southernmost portions of the northern lobe from its northernmost portions, the Bushveld Complex has transgressed through several kilometers of Transvaal sedimentary rocks. Thus, in the south the floor consists largely of shales of the Timeball Hill Formation on Townlands and Macalacaskop (Manyeruke *et al.*, 2005; Kinnaird *et al.*, 2005), sulphidic shales and limestone of the Duitschland Formation on Turfspruit and Tweefontein (Kinnaird *et al.*, 2005), and Penge iron formation in the northern parts of Tweefontein (Buchanan *et al.*, 1981). From northern Tweefontein through Sandsloot to Zwartfontein, the Platreef rests on dolomite of the Malmani sub-group (White, 1994; Harris and Chaumba, 2001). Interestingly, this is where the peak mineralization occurs at Sandsloot. Some authors e.g., De Waal (1977) proposed that devolatization of dolomite may increase the O fugacity of the magma, thereby decreasing the activity of Fe^{2+} and the S solubility. Finally, from Overysel to Nonnenwerth and adjoining farms, the floor to the Bushveld consists of granite-gneiss basement rocks (Stevens, 2004; Manyeruke, in preparation). Dolomite may have been present based on abundant and occasionally very large and laterally persistent dolomite layers (e.g., at Nonnenwerth and Drenthe), but if so has been largely ingested by the magma.

12.1.2 Platreef Lithologies

Previous studies in the south have shown that the Platreef consists of a variety of rock types, including fine-, medium- to coarse grained gabbronorites, norites, anorthosites, pyroxenites, peridotites and chromitites (Kinnaird *et al.*, 2005, and references therein). At several localities, ultramafic rocks appear to be dominant (e.g., Turfspruit; Kinnaird, 2005). The present study documents that at Nonnenwerth, the

Platreef is essentially gabbronoritic, with very minor quantities of ultramafic rocks. The lithologies at Nonnenwerth are similar to those at Drenthe (Stevens, 2004). The available data thus suggests that there is significant lithological variation along strike, and that the rocks become less ultramafic towards the north. The observed lithological changes are most likely reflecting increased differentiation of the Platreef magma from south to north, possibly reflecting a feeder zone in the south.

12.1.3 Nature of xenoliths

The xenoliths population in the Platreef includes shales, hornfels, quartzite, ironstone, dolomites of the Transvaal Supergroup and granite gneisses of the Archean granite gneiss basement. Their distribution along Platreef strike seems to be controlled by the nature of the floor rocks immediately underlying the Platreef at different localities. In the south, the xenolith population is variable whereas the northern portions of the northern lobe from Tweefontein and Nonnenwerth have dolomite and calc-silicate xenoliths (e.g., Cawthorn *et al.*, 1985; Buchanan and Rouse, 1984; Holwell and McDonald, 2006) except at Drenthe which additionally has granite gneiss xenoliths (Stevens, 2004). From Rooipoort to Tweefontein, xenoliths present are dominated by hornfels, quartzite, ironstone and calc-silicate (Manyeruke, 2003; Kinnaird *et al.*, 2005) and minor dolomites (e.g., at Macalacaskop and Turfspruit; Kinnaird, 2005). Notably, dolomite xenoliths are present everywhere along the strike of the Platreef even in areas where the Platreef overlies stratigraphically more elevated sedimentary rocks of the Pretoria Group. The along strike variation of the xenoliths in the Platreef suggests the Platreef was contaminated with variable material. However, which one, if any was responsible for the sulphide segregation is unclear.

12.1.4 Mineral compositions

Silicate minerals reveal a compositional break between the Platreef and Main Zone. Although the composition of the two intervals overlap, the Platreef is more heterogeneous, with several samples having high Ni, Cr and Mg# in pyroxenes and An in plagioclase. Furthermore, the Platreef pyroxenes and plagioclase become more primitive with height, whereas in the Main Zone, the silicates become more evolved with height. These compositional differences between the Platreef and the Main Zone suggest that the two units represent distinct influxes of magma.

The orthopyroxenes from the Platreef at Nonnenwerth are more difficult to correlate with other sequences in the northern lobe or elsewhere, partly because of their compositional variations. The orthopyroxenes are markedly less magnesian ($Mg\#_{57-72}$) than orthopyroxenes in the Platreef on the farms Townlands ($Mg\#_{68-82}$; Manyeruke, 2003), Tweefontein ($Mg\#_{74-78}$; Buchanan *et al.*, 1981) and Sandsloot ($Mg\#_{76-80}$ for the primary reef, McDonald *et al.*, 2005). Plagioclase in the Platreef at Townlands (An_{54-84}, average 71; Manyeruke *et al.*, 2005) is also more An-rich than plagioclase at Nonnewerth (An_{47-75}, average 63). The former has a composition similar to plagioclase in the Upper Critical Zone (An_{68-85}; Cameron, 1982a; Naldrett *et al.*, 1986; Kruger and Marsh, 1985; Maier and Eales, 1997).

Past studies from south have shown that the Platreef shows important similarities to the Upper Critical Zone (e.g., Wagner, 1929; Hulbert, 1983; Maier *et al.,* 2007). Platreef orthopyroxenes on Nonnenwerth have broadly similar maximum values of Mg# as orthopyroxenes on Drenthe and Overysel ($Mg\#_{65-77}$; Gain and Mostert, 1982;

Cawthorn *et al.*, 1985), where the reef is equally underlain by granite-gneiss and dolomite. These compositions are less magnesian than those of Upper Critical Zone orthopyroxenes ($Mg\#_{78 - 84}$; Cameron, 1982a; Naldrett *et al.*, 1986; Eales *et al.*, 1993; Cawthorn, 2002). The closest compositional match exists with the central Main Zone and the lower Main Zone seems to be missing. Thus there is trend of reef becoming more differentiated towards the north.

12.1.5 Lithophile whole rock data

The Nonnenwerth Platreef shows unfractionated trace element patterns, with similarities to the Main Zone at Union Section. Major element data also overlap with central Main Zone. This suggests the Platreef has a B2/B3 magmatic lineage with little contamination or some dolomite contamination. Dolomite contamination is not easily detectable by using major and trace elements due to the paucity of the Transvaal dolomite in most trace elements (Klein and Beukes, 1989). In the south, trace elements are more fractionated, more similar to Upper Critical Zone, and probably also contain some crustal contaminant because the concentrations of the REE are too high to be explained by a trapped melt component of either B1 or B2 Bushveld lineage. Thus, the data shows again that there is a systematic variation along strike, partly due to contamination with variable footwall rocks and possibly because the magma from which the Platreef crystallised became more differentiated from the south northwards along the Platreef strike.

12.1.6 Sulphides and chalcophile elements

Firstly, the Nonnenwerth Platreef contains broadly similar amounts of sulphides than elsewhere along the Platreef, but the PGE are more fractionated, with higher Pd/Ir ratios. This is in agreement with a more differentiated magma, suggested by the mineral and major elements chemistry and the absence of pyroxenite and chromitite. In addition, laurite is present at Townlands, but not in the northern portions of the northern lobe. Secondly, the present study has established a broad positive correlation amongst those PGE that could behave in a mobile manner (in particular Pd, Hsu *et al*. 1991) and those that are believed to be immobile under most conditions (e.g., Pt and Ir; Fig. 6.9b and e) and between individual PGE and S (for samples with > 0.1 % S), suggesting that magmatic sulphides were the primary PGE collector and that PGE are largely hosted by sulphides. However, there is also considerable scatter, notably in samples from borehole 2199, suggesting some localized secondary mobility of S, Cu, Pt and Pd. Textural evidence for the mobility of these elements is shown by discrete, euhedral grains of moncheite forming a linear trail emanating from the chalcopyrite-plagioclase grain boundary into plagioclase (Fig. 9.1j & k). A similar pattern has been observed at Overysel (Holwell, *et al.*, 2005), Drenthe (Gain and Mostert, 1982) and at Townlands (Manyeruke, 2003; Manyeruke *et al.*, 2005).

At Sandsloot and Turfspruit, sulphides and platinum-group elements are decoupled and the PGE appear to be largely controlled by PGM (Armitage, *et al.*, 2002). Here, the floor rocks consist of dolomite and shale, respectively, which may release fluids in response to heating by the intrusives (e.g. Wallmach *et al.*, 1989). The fluids could potentially have resorbed the sulphides and remobilised S resulting in the formation of

secondary sulphides (chalcopyrite, pyrite and millerite) and PGM. Pd also seems to have locally behaved in a mobile manner, as indicated by the fact that Pt/Pd ratios at Sandsloot and Turfspruit are significantly higher than at Nonnenwerth.

At Townlands, where floor rocks are quartzites and shales, magmatic sulphide assemblages were not identified. The sulphide assemblage is characterized by chalcopyrite > millerite > pyrite > pentlandite. Pyrrhotite occurs locally only and galena and molybdenite are further accessories. Notably, this is the first time that such a sulphide assemblage is reported from the Platreef. This type of mineralization was detected in one drill hole only and therefore, must at this stage be regarded as exceptional and probably local only. This sulphide assemblage differs from being "typical magmatic" and came into existence through syn- to post-magmatic modification including formation of millerite from pentlandite, and pyrite replacing pyrrhotite. It is envisaged that the sulphide assemblage at Townlands originally also developed from immiscible magmatic sulphide droplets and an association pyrrhotite – pentlandite – chalcopyrite. However, this early formation was overprinted and converted to pyrite – millerite – chalcopyrite. The observed sulphide assemblage gives evidence that the conversion took place at elevated fugacity of sulphur (fS_2) as will be shown below. This conversion was not completely pervasive, as evidenced by relict pyrrhotite – pentlandite assemblages (Table 3). Furthermore, no direct replacements (millerite after pentlandite and pyrite after pyrrhotite) were observed in situ.

The relative timing of this remobilization and replacement is hard to constrain; it probably took place early on the down-temperature path of the mineralization. Probably, syn- to post-emplacement fluids were also involved as evidenced by amphibole needles crosscutting sulphide grains (Fig. 8.4a).

Sulphide contents in any Unit increase towards the base from disseminated (< 2 vol. %) to semi-massive and disseminated (up to 30 vol. %.) The disseminated sulphides towards the top of each Unit probably formed under moderate fS_2 and low fO_2 conditions whereas those towards the floor probably formed under high fS_2 and fO_2 conditions. The gradients in the S-fugacity in Platreef rocks from Townlands are in agreement with the S-isotope study of the Platreef on Townlands (Manyeruke, 2003; Manyeruke *et al.*, 2005). The authors showed that $d^{34}S$ values from Townlands are distinctively heavier (+2.6 to +10.1 ‰) and increase towards the base of the Middle and Upper Platreef, a phenomenon they attributed to enhanced assimilation of crustal S towards the floor of each layer, perhaps by continued degassing of the floor rocks during crystallisation of the Platreef or by S loss towards the top of each Unit.

The current study distinguishes three different associations of sulphide at Nonnenwerth i.e. the magmatic sulphides, secondary sulphides replacing magmatic sulphides and sulphides associated with secondary silicates. Magmatic sulphides represent the dominant sulphide assemblage. They are represented by composite grains of pyrrhotite often intergrown with chalcopyrite and pentlandite, chalcopyrite and polycrystalline fragmented pentlandite grains along pyrrhotite fractures or pentlandite and chalcopyrite included in pyrrhotite towards pyrrhotite grain margins.

Pentlandite may occur as flame-like exsolution lamellae in pyrrhotite. These magmatic sulphides represent fractionated blebs of sulphide. During crystallization, magmatic sulphide liquid crystallizes to a monosulphide solid solution (mss) with the residual sulphide liquid forming intermediate solid solution (iss) (Barnes *et al*., 2006). The former recrystallizes to pyrrhotite and pentlandite on cooling and the latter to chalcopyrite and some pentlandite (Barnes *et al*., 2006) in agreement with the textures displayed by magmatic sulphides.

Secondary sulphides, as defined here, replace magmatic sulphides and lack the zoned, fractionated textures displayed by magmatic sulphides and have a 'rugged' outline. They are dominated by chalcopyrite, pyrite, and minor pentlandite. Pyrrhotite includes subrounded vermicular intergrowths of pyrite and chalcopyrite, in places with a remnant pentlandite suggesting replacement of pentlandite by the two phases. Pentlandite may be altered and replaced by coronas of violarite with relict pentlandite forming islands in violarite suggesting that the pentlandite is relictic and that most of the primary pentlandite has been replaced by violarite. It should be noted that recrystallized gabbronorite samples with high pyrrhotite contents have no pyrite and vice versa. The absence of pyrrhotite may suggest an increase in S fugacity (fS_2) resulting in pyrrhotite being transformed to or replaced by pyrite. Minor phases are fine, flame-like exsolutions of mackinawite and small disseminated sphalerite grains in chalcopyrite.

Sulphides associated with secondary silicate assemblages are rare in the Platreef at Nonnenwerth. They are represented by fine disseminated chalcopyrite grains

intergrown with alteration minerals in replacement of primary silicates adjacent to coarse composite sulphides, deuteric veinlets of pyrite that cut through the plagioclase or pyrite replacing clinopyroxene along cleavage planes and cracks. The sulphides do not display well defined sulphide zonation.

Platinum-group elements and S display good correlation, a pattern also observed at Overysel (Holwell, *et al.*, 2005; Holwell and McDonald, 2006) and Drenthe (Gain and Mostert, 1982) suggesting the mineralization at these localities is magmatic. Thus the degree of S-mobility is dependant on the nature of the floor rocks to the Platreef. Where the floor rocks consist largely of relatively unreactive granite e.g., at Nonnenwerth, the platinum-group elements are controlled by sulphides and decoupling of base metal sulphides and platinum-group elements is prevalent were floor rocks are reactive e.g., at Sandsloot and Turfspruit.

With the exception of pentlandite from Nonnenwerth (see below), Pd, Pt and Rh are below the detection limits of the electron microprobe in the sulphides analysed from Nonnenwerth and Townlands. Pentlandites as part of the “typical magmatic” sulphide assemblage at Nonnenwerth constantly contain appreciable amounts of Pd (range from ~ 140 – 700 ppm). This finding is in accordance with literature data (e.g. Gervilla et al., 2004) that pentlandite may carry even up to some % of Pd (substituting for Ni) in its crystal lattice. Accordingly, the Pd contents in Nonnenwerth pentlandite probably reflect a primary magmatic signature.

In contrast, pentlandites from Townlands have Pd contents below the detection limit (20 ppm Pd) of the method. This lack of measurable Pd contents in pentlandite may find the following explanations: (i) Pd in pentlandite was analysed in one sample (P 13) only, and therefore, the results may not be representative. (ii) Pd-bearing PGM could have been mobilized during replacement of 'primary' sulphides by pyrite dominated assemblages into the surrounding silicates (Prichard *et al*., 2001). (iii) The Townlands sulphide assemblage differs from being "typical magmatic" and has experienced severe syn- to post-magmatic modification as described above. Therefore, the relatively rare pentlandite at Townlands may either represent a second generation of pentlandite, or is a relict primary phase that has suffered an overprint that extracted lattice-bound Pd. Arguments for the latter possibility are provided by the presence of abundant Pd-minerals in sample P 13 (see Table 3).

The analytical work presented here has shown marked differences in Pd contents in pentlandites from the Platreef for the first time. It is suggested that systematic research in this topic would be a worthwhile undertaking to improve our understanding of the distribution of the PGE in Platreef ores. The nature and distribution of the PGM from Nonnenwerth and Townlands are discussed below in section 12.1.7.

12.1.7 Platinum-group mineral, tellurides and trace minerals

The present study has established that Pd-rich phases account for approximately 70 and 76 % of the PGE-bearing phases at Nonnenwerth and Townlands, respectively and IPGE-bearing phases predominantly occur in the south. The Pd-bearing PGM are

dominated by merenskyite and kotulskite which range in size from <5 to 40 µm in size, averaging 20 µm. Three subhedral to anhedral grains of sperrylite were identified at Townlands.

At Nonnenwerth, The PGM occur predominantly at the contact between sulphide (mostly chalcopyrite, minor pyrrhotite and rare pyrite) and secondary silicate (mostly chlorite and albite after plagioclase) or enclosed in sulphides. Importantly, Pd-rich PGM (Pd-bismuthotellurides) are mostly enclosed in silicates. However, even these PGM enclosed in silicates retain a strong spatial relationship with the base metal sulphides, mostly chalcopyrite, and are associated with secondary minerals (mostly chlorite and albite which replace plagioclase, or rarely amphibole which replaces orthopyroxene and base metal sulphides). The above observation may result from dissolution of the base metal sulphides hosting Pd, and leaving isolated insoluble Pd-PGM behind (Barnes *et al*., 2007), or Pd may have been remobilized from the sulphides into the surrounding silicates. Based on textural evidence, the latter model is preferred. In contrast, at Townlands, the PGM assemblage is dominated by **Pd-rich** bismuthotellurides, minor sperrylite, rare stibiopalladinite and isomertieite. The PGM occur predominantly enclosed in sulphides (mostly pyrite and minor chalcopyrite and millerite), or locally at the contact between sulphide and secondary silicate (amphibole after orthopyroxene).

In general, there are no dramatic differences between the PGM assemblages at Nonnenwerth and Townlands, also in comparison to descriptions from most other Platreef occurrences (e.g. Kinloch, 1982; Holwell et al., 2006). Bismuthotellurides

predominate followed by rarer arsenides and antimonides. One obvious difference, however, is the wide compositional range of Pt-Pd bismuthotellurides and the presence of Pt-rich bismuthotellurides at Nonnenwerth only, whereas at Townlands, only Pd-rich bismuthotellurides are present. The significance of this finding cannot be evaluated conclusively. The variability may be related to local factors like different host rocks; footwall lithologies, down-temperature re-equilibration, activity of fluids, and other possible causes.

The observation that most of the PGM at the studied Platreef intersections occur mostly intergrown with secondary silicate minerals close to sulphides suggests the PGM formed or re-equilibrated at moderately low temperature conditions. The above is in agreement with the observed resorption of primary sulphides and the occurrence of secondary sulphides e.g. violarite. Low temperature conditions for PGM formation are also supported by the abundance of Pd-rich and Pt-rich bismuthotellurides, the significant substitution of Te by Bi, which are in agreement with the low thermal stability of Merenskyite (Kim *et al.*, 1990) and michenerite (Hoffman and MacLean, 1976). The above data indicate that the (Pt,Pd)-bismuthotellurides formed at temperatures below 500^0C (Hoffman and MacLean, 1976), which is consistent with their textural sitting in the ore. The above model finds support in the studies on Sandsloot, north of Townlands and south of Nonnenwerth (Holwell *et al.*, 2006) and Turfspruit, north of Townlands and south of Nonnenwerth (Hutchinson *et al.*, 2004). The authors of these previous studies suggest the PGM formed in response to considerable S and chalcophile metals in metasomatic fluids and felsic melts, leading

to the formation of a non-sulphide assemblage dominated by chalcopyrite particularly near the floor contact.

At Sandsloot, the PGM assemblage is dominated by PGE-alloys and tellurides and no PGE-sulphides were identified (Armitage *et al.*, 2002). The abundance of PGE-alloys here is notable as there scarce in the north and south of the northern lobe. In the latter, PGM are dominated by tellurides, bismuthotellurides and antimonides (e.g., Kinloch, 1982; Viljoen and Schürmann, 1998; Holwell *et al.*, 2006; Hutchinson and Kinnaird, 2005). This may indicate considerable sulphide resorption or hydrothermal remobilization where floor rocks are fusible dolomite.

Thus the PGE were most likely initially scavenged by immiscible sulphide liquid within the Platreef magma. During crystallisation of the magmatic sulphide liquid, Pd, Pt, Cu, Ag and Au are incompatible in the mss (Barnes and Maier, 1999) and thus are partitioned into the fractionated Cu-rich liquid in solid solution or exsolved from the sulphide melt. The exsolved PGE may then form PGM on the margins of the crystallised pyrrhotite and pentlandite or when retained in solid solution in the Cu-rich melt, are exsolved and form thin merenskyite lamellae in chalcopyrite, explaining the observed occurrence of merenskyite laths in chalcopyrite. However, on Townlands, the merenskyite exsolution is thicker and occurs in pyrite. The thin nature of the merenskyite lamellae in chalcopyrite may be due to low temperature exsolution and due to lower diffusion speeds in low-S sulphides (chalcopyrite) when compared to high-S sulphides (pyrite) (Peregoedova, *et al.*, 2004). The coarser grains of PGM on the margins of sulphides may suggest preferential distribution of the PGE into the

metal phase (Peregoedova, *et al.*, 2004). The occurrence of the bismuthotellurides close to each other together with silver tellurides and lead tellurides may indicate that these minerals crystallised almost at the same time. This was followed by variable remobilization and secondary redistribution of the PGE in secondary silicates close to partially resorbed sulphides. The remobilization and redistribution PGE may be attributed to various factors among them assimilation of crustal S where floor rocks are of Transvaal Supergroup, devolatization of dolomite xenoliths which are present along the whole strike length of the northern lobe or interaction of primary magmatic sulphides with late stage magmatic fluids. The involvement of late magmatic/hydrothermal fluids is supported by the occurrence of violarite which is probably of hydrothermal origin.

Addition of floor rock crustal S is supported by the studies of Manyeruke *et al*. (2005). The PGM are dominated by lower temperature Pd-rich bismuthotellurides and minor Bi-, Sb- and Te-bearing phases (Kim et al., 1990), as opposed to the Merensky Reef, where PGE sulphides may constitute a substantial proportion of the overall PGM assemblage (e.g. Kinloch, 1982; Mostert et al., 1982). Therefore, the PGM assemblages at Nonnenwerth and Townlands support the suggestion that the PGM are “secondary” in the sense of Cawthorn et al. (2002).

The model of sulphide control for the PGE is supported by the broad positive correlation between Pt and Pd and between PGE and S, and abundance of magmatic sulphides at Nonnenwerth suggesting that sulphides were the primary PGE collector. Even though the base metal sulphides do not host the PPGE (Pt, Pd and Rh) –

except for a certain proportion of Pd in pentlandite – the PGM that do host them maintain a close spatial relationship with the base metal sulphides, underlining the initial control of PGE by sulphides.

12.1.8 S and O- isotopes

S isotopes in the northern sections of the northern limb were floor rocks are granite gneiss are mantellic e.g., at Nonnenwerth ($d^{34}S$ values from +0.73 to +1.87 ‰) and Overysel ($d^{34}S$ values from +1.7 to +2.0 ‰; Holwell et al, 2005). This suggests little assimilation of external S at Nonnenwerth, which is in agreement with the available Nd isotopic data from Drenthe (eNd –6.9 to -7.7; Stevens, 2004). In contrast, in the south where the floor rocks consist of shale and quartzite, $d^{34}S$ values are strongly positive suggesting significant assimilation of external S. The observations are supported by the S-isotopic composition of the floor rocks e.g. $d^{34}S$ values of –12 to –18 ‰ for the Timeball Hill shale (Cameron, 1982b) and $d^{34}S$ values of +2.6 to +10.1 ‰ for metasediments of the Silverton Formation (Manyeruke, 2003; Manyeruke *et al.*, 2005).

The data indicate that Platreef-style PGE-sulphide mineralization may be associated with floor rocks containing variable S contents and S-isotopic signatures. Thus, assimilation of external S during magma emplacement was apparently not the principal controlling factor in sulphide genesis since PGE mineralisation occur at Nonnenwerth where the Platreef over granite gneiss. Instead, significant assimilation of S may have merely modified already existing sulphide melt, essentially diluting the tenor of the sulphides, particularly in areas where the floor rocks consisted of

sulphidic shales, between Townlands and Tweefontein (Manyeruke *et al.*, 2005; Hutchinson and Kinnaird, 2005) and the formation of the lower temperature semi-metal PGM e.g. (Pt,Pd)-bismuthotellurides.

$d^{18}O$ values on Nonnenwerth are lower and uncontaminated compared to $d^{18}O$ values of the Platreef at Townlands, Sandsloot (Harris and Chaumba, 2001), Main Zone and Upper Zone from the Bellevue core (Harris *et al.,* 2005), eastern and western Bushveld Complex has (Schiffries and Rye, 1989 and Reid *et al*., 1993, respectively). This may suggest that local contamination with dolomite did not play a role in the mineralization process at Nonnenwerth. Thus, the occurrence of mineralization close to the dolomite xenoliths at Nonnenwerth may be due to the dolomite forming an impermeable layer that forced the magma below into sulphide saturation. Dolomite assimilation may however have played part in other parts of the Platreef e.g. at Sandsloot. The data on both Townlands and Nonnenwerth is in agreement with the trace element and S-isotope data which showed that the Platreef on Nonnenwerth experienced little or no contamination compared to Platreef on Townlands which interacted and was contaminated by floor rock shales. Finally, the data on Townlands is in agreement with previous published O-isotope data of the Platreef (e.g. Harris and Chaumba, 2001; Sharman-Harris *et al*., 2005; Harris *et al.,* 2005).

12.2. Magmatic lineage of the Platreef

The data summarized in the preceding section suggest that the Platreef is very variable along strike, probably due to processes including contamination and

differentiation. The question thus is whether there is a specific magmatic lineage of the Platreef. Or does the Platreef represent magmas of variable composition that were variably contaminated with variable floor rocks?

The Nonnenwerth data clearly indicate overlap with Main Zone, in terms of the lithologies, mineral and whole rock compositions. Thus, the rocks are gabbronorites, orthopyroxene has Mg# mostly 60 - 70, and plagioclase has An mostly 50 – 75, REE patterns are relatively unfractionated, with Ce/Sm ratios between 5.7 and 10.6 (averaging 8) i.e., a B2 signature. This is in agreement with the data of Stevens (2004) who provided Nd isotopic data on the Platreef at Drenthe which indicate crustal values very similar to the Main Zone of the western Bushveld Complex (eNd – 6.9 to -7.7). But even at Nonnenwerth, the Platreef is more variable, more PGE enriched, more S enriched, and contains more xenoliths than the Main Zone. Thus one could propose a model of contamination of an initial surge of B2/B3 Bushveld parental magma with dolomite, followed by more B2/B3 magma that was less contaminated with dolomite and formed the Main Zone.

In the south, the Platreef is more variable than in north. At Sandsloot (McDonald *et al.*, 2005) and Drenthe (Maier *et al.,* 2007), there are similarities to Nonnenwerth in terms of the trace element (average Ce/Sm 8 at Nonnenwerth, 9.03 at Drenthe, 7.51 at Sandsloot) and REE patterns, with relatively lower La/Yb_N (Fig. 9.5) and low total element abundances. At Townlands (Manyeruke *et al.*, 2005) and Rooipoort (Maier *et al.*, 2007), the data indicate mixed B1-B2 signature i.e., higher and more fractionated REE contents (average Ce/Sm 12.6 at Townlands) with relatively higher La/Yb_N.

Moreover, the high concentration of the trace elements in some samples clearly indicates contamination with shale. It is possible that the entire crustal component is due to contamination with shale, and thus the importance of B1 is uncertain. On the other hand, the presence of dunites, harzburgites and orthopyroxenites below Platreef at Rooipoort (de Klerk 2005) could suggest some B1 influence in Platreef. Magmatic serpentinites are also present at Nonnenwerth, Turfspruit and south of Tweefontein (Hutchinson and Kinnaird, 2005) which could suggest that some B1 magma surges may have reached the north, but this is uncertain as the rock is altered. Alternatively, the serpentinite could also be a cumulate of B2 Bushveld parental magma.

In summary, the Platreef seems predominantly B2 related. This model is supported by close spatial association of the Platreef with the Main Zone. Compositional variation of the Platreef is partly due to variable contamination with various floor rocks, and also to variable state of differentiation of the Platreef and Main Zone magma. The latter is shown by Mg# and Cr content of orthopyroxene, An of plag and variation in Pd/Ir which indicate significantly more differentiation of the Platreef and Main Zone magma towards the northern portions of the northern lobe of the Bushveld Complex. This could reflect distance to a feeder zone in the south. Some localized influence of B1 magma is possible, notably at Turfspruit where Kinnaird reports abundance of peridotite.

12.3 Origin of the Mineralization

Basal sulphides are common in layered intrusions underlain by various floor rocks e.g., Portimo, Finland (Alapieti and Lahtinen, 2002) and East Bull Lake, Canada (Peck *et al.*, 2002). This could suggest that local contamination does play some role in the mineralization process. However, my data show that Platreef is present above variable floor rocks and assimilates variable floor. S isotopes are mantellic in places, trace elements unfractionated. This could suggest that the presence of mineralization is not controlled by assimilation of any specific lithology, or external sulphides. The only common factor at all localities is the presence of dolomite xenoliths. Calc-silicate xenoliths are found at all Platreef localities throughout the northern lobe, suggesting that dolomites formed part of the country rock assemblage during intrusion of the Platreef magma. Thus, the magma may have reached S-saturation in response to assimilation of dolomite which may have lowered the S solubility of the magma in response to devolatization and oxidation (e.g. de Waal, 1975), which could be supported by the peak mineralization at Sandsloot where floor is dolomite. The importance of dolomite assimilation in causing sulfide saturation in the Nonnenwerth contact rocks is highlighted by the concomitant paucity of sulfides in most other Main Zone rocks elsewhere in the Bushveld. The presence of a dolomite component in the magma is difficult to detect using major and trace element geochemistry, due to the paucity of the Transvaal dolomite in most trace elements (Klein and Beukes, 1989). However, O isotope data from Sandsloot (Harris and Chaumba, 2001) clearly indicate significant assimilated dolomite. At Nonnenwerth, dolomite is absent as floor rocks probably due to effective erosion and assimilation of much of the dolomitic floor rocks at this locality. However, the dolomite xenoliths present have mantellic $d^{18}O$ values, possibly ruling out assimilation of dolomite as a trigger to mineralization here.

Additional factors could be enhanced cooling rate along base of intrusions (suggested by occurrence of fine grained contact phases), and perhaps differentiation (differentiated magmas are more close to S saturation, and it is also notable that most basal sulphide reefs are associated with gabbroic rather than ultramafic rocks). Finally, some authors (Lee, 1996) have suggested that sulphides were entrained based on the tenor of Cu and Ni in the sulphides and the concentration of PGE in the Platreef which is difficult to reconcile with local floor-derived sulphur source. Sulphide saturation could have been triggered by mixing of compositionally contrasting magmas (e.g. Naldrett and von Gruenewaldt, 1989; Li and Ripley, 2005). I consider this model unlikely because at Nonnenwerth, Ce/Sm ratios of the rocks are relatively constant, indicating the predominance of one type of magma, namely the tholeiitic B2/B3 Bushveld type.

Where floor rocks were assimilated, devolatization of the host rocks and xenoliths possibly occurred during or prior to the assimilation process. The resulting fluids, which may have introduced some S as indicated by crustal S-isotopes at some localities, percolated through the semi-consolidated Platreef rocks and would separate as a separate phase once they reach saturation. Ultimately, hydrous phases such as amphibole and chlorite crystallized from this hydrous component, generally in association with sulphides (see Fig. 8.4a). With the cooling of the sulphide- and volatile-saturated Platreef portion of the magma, a sulphide/volatile phase separated from the magma (first boliling). As saturation is approached, coarse/pegmatitic textures start to proliferate. This is followed by precipitation of sulphides and hydrous silicates from the hydrothermal fluid. Where the floor rocks are pelitic e.g., at

Townlands (Manyeruke, 2003; Manyeruke et al., 2005), Macalacaskop and Turfspruit (Hutchinson and Kinnaird, 2005), H_2O-rich fluids would dominate and hydrous silicates would be common. Where carbonate rocks occur in the floor, CO_2-rich fluids would dominate e.g. at Sandsloot (Armitage *et al*., 2002; Holwell *et al*., 2006). Where the floor rocks are granitic e.g., at Nonnenwerth, Drenthe (Stevens, 2004) and Overysel (Holwell, 2005) the volatile phase would be less prevalent than further south.

References

Alapieti, T.T. and Lahtinen, J.J. (2002). Platinum-group element mineralization in layered intrusions of northern Finland and the Kola Peninsula, Russia. *In:* L.J. Cabri (Editor), *The geology, geochemistry, mineralogy and mineral beneficiation of platinum-group elements. Canadian Institute of Mining and Metallurgy*. Special Volume **54**, 507-546.

Armitage, P.E.B., McDonald, I., Edwards, J.S. and Manby, G.M. (2002). Platinum-group element mineralisation in the Platreef and calc-silicate footwall at Sandsloot, Potgietersrus District, South Africa. *Transactions of the Institute of Mining and Metallurgy* **111** (reprinted from Applied Earth Science, January-April 2002), B36-45.

Ashwal, L.D., Webb, S.J. and Knoper, M.W. (2005). Magmatic stratigraphy in the Bushveld northern lobe: continuous geophysical and mineralogical data from the 2950 m Bellevue drillcore. *South African Journal of Geology* **108**, v. 2, 199-232.

Bailie, R.H. and Robb, L.J. (2004). Polymetallic mineralization in the granites of the Bushveld Complex - examples from the central southeastern lobe. *South African Journal of Geology* **107,** v. 4, 633 - 652.

Barnes, S-J. and Francis, D. (1995). The distribution of platinum-group elements, nickel, copper, and gold in the Muskox Layered Intrusion, northwest territories, Canada. *Economic Geology* **90**, 135-154.

Barnes, S-J. and Maier, W.D. (1999). The fractionation of Ni, Cu and the noble metals in silicate and sulphide liquids. *In:* R.R. Keays, C.M. Lesher, P.C. Lightfoot and C.E.G. Farrow (Editors), *Dynamic processes in magmatic ore deposits and their application to mineral exploration. Geological Association of Canada, Short Course Notes* **13**, 69-106.

Barnes, S-J. and Maier, W.D. (2002a). Platinum-group elements and microstructures of normal Merensky Reef from Impala Platinum Mines, Bushveld Complex. *Journal of Petrology* **43**, 103-128.

Barnes, S-J. and Maier, W.D. (2002b). Platinum-group element distributions in the Rustenburg Layered Suite of the Bushveld Complex, South Africa. *In:* L. Cabri (Editor), *The geology, geochemistry, mineralogy and mineral benefication of the platinum-group elements. Canadian Institute of Mining and Metallurgy Special Volume* **54,** 431-458.

Barnes, S-J. and Naldrett, A.J. (1987). Fractionation of the platinum-group elements and gold in some komatiities of the Abitibi Greenstone Belt, Northern Ontario. *Economic Geology* **82**, 165-183.

Barnes, S-J., Maier, W.D. and Ashwal, L.D. (2004). Platinum-group element distribution in the Main Zone and Upper Zone of the Bushveld Complex, South Africa. Chemical Geology **208,** 293– 317.

Barnes, S.-J., Prichard, H.M., Cox, R.A., Fisher, P.C. and Godel, B. (2007). The location of the chalcophile and siderophile elements in platinum-group element ore deposits (a textural, microbeam and whole rock geochemical study): Implications for formation of the deposits. *Chemical Geology*, doi:10.1016/j.chemgeo.2007.08.004

Barton, J.M., Cawthorn, R.G. and White, J. (1986). The role of contamination in the evolution of the Platreef of the Bushveld Complex. *Economic Geology* **81**, 1096-1104.

Bédard, L.P. and Barnes, S-J. (2002). A comparison of the capacity of FA-ICP-MS and FA-INAA to determine platinum-group elements and gold in geological samples. *Journal of Radioanalytical and Nuclear Chemistry* **254**, 319-329.

Bennett, H. and Oliver, G. (1992). *XRF analysis of Ceramics, Minerals and Applied Materials*. John Wiley and Sons, 67-93.

Boudreau, A. (1998). Chromatographic separation of the platinum-group elements during gegassing of a compacting, solidifying cumulate pile. *In: 8th International Platinum Symposium, Rustenburg. South African Institute Mining Metallurgy Symposium Series* **S18**, 41-44.

Boudreau, A.E., Mathez, E.A. and McCallum, I. (1986). Halogen geochemistry of the Stillwater and Bushveld Complexes: Evidence for transport of the platinum-group elements by Cl-rich fluids. *Journal of Petrology* **27**, 967-986.

Buchanan, D.L. (1975). The petrography of the Bushveld Complex intersected by boreholes in the Bethal area. *Transactions of the Geological Society of South Africa* **78,** 335–348.

Buchanan, D.L. (1979). *Bureau for Mineral studies*: *Report*, *University of the Witwatersrand*, **4**.

Buchanan, D.L. (1988). *Platinum-group element exploration*. Elsevier: Amsterdam, 185p.

Buchanan, D.L. and Rouse, J.E. (1984). Role of contamination in the precipitation of sulphides in the Platreef of the Bushveld Complex. *In*: D.L. Buchanan and M.J. Jones (Editors), *Sulphide deposits in mafic and ultramafic rocks. Institute of Mining and Metallurgy*, *London*, 141-146.

Buchanan, D.L., Nolan, J., Suddaby, P., Rouse, M.J. and Davenport, J.W.J. (1981). The genesis of sulphide mineralisation in a portion of the Potgietersrus limb of the Bushveld Complex. *Economic Geology* **76**, 568-579.

Buick, I.S., Maas, R. and Gibson, R. (2001). Precise U-Pb titanite age constraints on the emplacement of the Bushveld Complex, South Africa. *Journal of the Geological Society, London* ***158****,* 3-6.

Cabri, J.L. (2002). The Platinum-Group Minerals. *In* The Geology, Geochemistry, Mineralogy and Mineral Beneficiation of Platinum-Group Elements. Edited by L.J. Cabri. *Canadian Institute of Mining, Metallurgy and Petroleum* Volume **54**, 13-129.

Cameron, E.N. (1975). Postcumulus and subsolidus equilibration of chromite and coexisting silicates in the Eastern Bushveld Complex. *Geochimica et Cosmochimica Acta* **39**, 1021-1033.

Cameron, E. N. (1978). The Lower Zone of the eastern Bushveld Complex in the Olifants River Trough. *Journal of Petrology* **19**, 437-462.

Cameron, E.N. (1980). Evolution of the Lower Critical Zone, central sector, Eastern Bushveld Complex and its economic deposits. *Economic Geology* **75**, 845-871.

Cameron, E.N. (1982a). The Upper Critical Zone of the Eastern Bushveld Complex – Precursor of the Merensky Reef. *Economic Geology* **77**, 1307-1327.

Cameron, E.M. (1982b). Sulphate and sulphate reduction in early Precambrian oceans. *Nature* **296**, 145-148.

Cawthorn, R.G. (2002). Delayed accumulation of plagioclase in the Bushveld Complex. *Mineralogical Magazine* **66,** 881–893.

Cawthorn, R.G. and Webb, S.J. (2001). Connectivity between the western and eastern limbs of the Bushveld Complex. *Tectonophysics* **330,** Elsevier, 195-209.

Cawthorn, R.G., Barton, J.M., Jr. and Viljoen, M.J. (1985). Interaction of floor rocks with the Platreef on Overysel, Potgietersrus, northern Transvaal. *Economic Geology* **80**, 988-1006.

Cawthorn, R.G., Lee, C.A., Schouwstra, R.P. and Mellowship, P. (2002). Relationship between PGE and PGM in the Bushveld Complex. *The Canadian Mineralogist* **40**, 311-328.

Coertze, F.J. (1974). The geology of the basic portion of the Western Bushveld Igneous Complex. *Geological Society of South Africa Memoir* **66**.

Cousins, C.A. (1959). The structure of the mafic portion of the Bushveld Igneous Complex. *Transactions of the Geological Society of South Africa* **62**, 174-189.

Curl, E.A. (2001). Parental magmas of the Bushveld Complex, South Africa. *Unpublished PhD thesis, Department of Earth Sciences, Monash University, Australia,* 140p.

Davies, G. and Tredoux, M. (1985). The platinum-group element and gold contents of the marginal rocks and sills of the Bushveld Complex. *Economic Geology* **80**, 838-848.

De Klerk, L. (2005). Bushveld stratigraphy on Rooipoort, Potgietersrus limb. *2nd Platreef workshop, University of the Witwatersrand, South Africa.*

de Waal, S.A. (1977). Carbon dioxide and water from metamorphic reactions as agents for sulphide and spinel precipitation in mafic magmas. *Transactions of the Geological Society of South Africa* **80**, 193-196.

Eales, H.V. and Cawthorn, R.G.C. (1996). The Bushveld Complex. *In*: Cawthorn R.G. (editor) *Layered Intrusion*: Elsevier, Amsterdam, 181-228.

Eales, H.V., De Klerk, W.J., Teigler, B. and Maier, W.D. (1994). Nature and origin of orthopyroxenites in the Western Bushveld Complex, in the light of compositional data. *South African Journal of Geology* **97**, 399-407.

Eales, H.V., Marsh, J.S., Mitchell, A.A., De Klerk, W.J., Kruger, F.J. and Field, M. (1986). Some geochemical constraints upon models for the crystallisation of the Upper Critical zone – main zone interval, northwestern Bushveld Complex. *Mineralogical Magazine* **50**, 567-582.

Eales, H.V., Teigler, B. and Maier, W.D. (1993). Cryptic variations of minor elements Al, Cr, Ti and Mn in Lower and Critical Zone orthopyroxenes of the Western Bushveld Complex. *Mineralogical Magazine* **57**, 257-264.

Eckstrand, O.R. (1975). The Dumont serpentinite: A model for control of nickeliferous opaque mineral assemblages by alteration reactions in ultramafic rocks. *Economic Geology* **70**, 183-201.

Eriksson, P.G., Schreiber, U.M. and Van der Neut, M. (1991). A review of the sedimentology of the early Proterozoic Pretoria Group, South Africa: Implications for tectonic setting. *Journal of African Earth Science* **13**, 107-119.

Finger, L.W. (1972). The uncertainty in the calculated ferric iron content of a microprobe analysis. *Year Book*, Carnegie Institution of Washington **71**, 600-603.

Francis, R.D. (1990). Sulphide globules in mid-ocean ridge basalts (MORB) and the effect of oxygen abundances in Fe-S-O liquids on the ability of those liquids to partition metals from MORB and komatiitic magmas. *Chemical Geology* **85**, 199-213.

Gain, S.B. (1985). The geological setting of the Platiniferous UG2 chromitite layer on Maandagshoek, eastern Bushveld Complex. *Economic Geology* **80**, 925-943.

Gain, S.B. and Mostert, A.B. (1982). The geological setting of the platinoid and base metal sulphide mineralisation in the Platreef of the Bushveld Complex on Drenthe, north of Potgietersrus. *Economic Geology* **77**, 1395-1404.

Gervilla, F., Proenza, J.A., Frei, R., Gonzalez-Jimenez, J.M., Garrido, C.J.,Melgarejo, J.C., Meibom, A., Diaz-Martinez, R. And Lavaut, W. (2005). Distribution of platinum-group elements and Os isotopes in chromite ores from Mayari-Baracoa Ophiolitic Belt (eastern Cuba). *Contributions to Mineralogy and Petrology* **150**, 589-607.

Green., A.H. and Melezhik, V.A. (1999). Geology of the Pechenga ore deposit – A review with comments on ore forming processes, *In:* R.R. Keays, C.M. Lesher, P.C. Lightfoot and C.E.G. Farrow (Editors), *Dynamic processes in magmatic ore deposits and their application to mineral exploration. Geological Association of Canada, Short Course Notes* **13**, 287-328.

Gregory, R. T. and Criss, R. E. (1986). Isotopic exchange in open and closed systems. In: Valley, J. W., Taylor, H. P., Jr and O'Neil, J. R. (eds) Stable Isotopes in High Temperature Geological Processes. Mineralogical Society of America, Reviews in Mineralogy **16**, 91 - 127.

Gregory, R. T., Criss, R. E. and Taylor, H. P., Jr (1989). Oxygen isotope exchange kinetics of mineral pairs in closed and open systems: applications to problems of hydrothermal alteration of igneous rocks and Precambrian iron formations.

Chemical Geology **75**, 1 - 42.

Gorbachev, N.S. and Grienko, L.N. (1973). The sulphur isotope ratios of sulphides and sulfates of the Oktyabv'sk sulphide deposit, Noril'sk region, and the problem of its origin. *Geokhimiya* **8**, 1127-1136.

Godolevsky, M.N. and Grienko, L.N. (1963). Some data on the isotopic composition of sulphur in the sulphides of the Noril'sk deposit. *Geochemistry* **1**, 335-341.

Hall, A.L. (1932). The Bushveld Igneous Complex of the central Transvaal. *Memoir. Geological Survey of South Africa* **28**, 560.

Hamlyn, P.R. and Keays, R.R. (1979). Origin of chromite compositional variations in the Panton sill, Western Australia. *Contributions to Mineralogy and Petrology*, **69**, 75-82.

Harmer, R.E. and Armstrong, R.A. (2000). Duration of Bushveld Complex (senso lato) magmatism: Constraints from new SHRIMP zircon chronology. *Abstracts and program*, *Workshop on the Bushveld Complex*, Gethane Lodge, Burgersfort.

Harris, C. and Chaumba, J.B. (2001). Crustal contamination and fluid-rock interaction during the formation of the Platreef, northern limb of the Bushveld Complex, South Africa. *Journal of Petrology* **42**, 1321-1347.

Harris, C., Pronost, J.J.M., Ashwal, L.D. and Cawthorn, R.G. (2005). Oxygen and hydrogen isotope stratigraphy of the Rustenburg Layered Suite, Bushveld Complex: Constraints on crustal contamination'. *Journal of Petrology* **40**, 579-601.

Hatton, C.J. and von Gruenewaldt, G. (1985). Chromite from the Swartkop Chrome Mine-An estimate of the effects of subsolidus re-equilibration. *Economic Geology*, **80**, 911-924.

Henderson, P. (1975). Reaction trends shown by chrome-spinels of the Rhum layered intrusion. *Geochimica et Cosmochimica Acta*, **39**, 1035-1044.

Henderson, P., and Wood, R.J. (1981). Reaction relationships of chrome- spinels in igneous rocks-Further evidence from the layered intrusions of Rhum and Mull, Inner Hebrides, Scotland. *Contributions to Mineralogy and Petrology*, **78**, 225-229.

Hiemstra, S. A. (1985). "The distribution of some platinum group elements in the UG-2 chromitite layer of the Bushveld Complex." *Economic Geology* **80,** 944-957.

Hiemstra, S.A. (1986). The distribution of chalcophile and platinum-group elements in the UG2 chromitite layer of the Bushveld Complex. *Economic Geology* **81**, 1080-1086.

Hoffman, E. and MacLean, W.H. (1976). Phase relations of michenerite and merenskyite in the Pd-Bi-Te system. *Economic Geology* **71**, 1461-1468.

Holwell, D.A. and McDonald, I. (2006). Petrology, geochemistry and the mechanisms determining the distribution of platinum-group element and base metal sulphide mineralisation in the Platreef at Overysel, northern Bushveld Complex, South Africa. *Mineralium Deposita* **41**, number 6, 575-598.

Holwell, D.A., Boyce, A.J. and McDonald, I. (2007). Sulphur Isotope Variations within the Platreef Ni-Cu-PGE Deposit: Genetic Implications for the Origin of Sulphide Mineralization. *Economic Geology* **102,** 1091-1110.

Holwell, D.A., Armitage, P.E.B. and McDonald, I. (2005). Observations on the relationship between the Platreef and its hangingwall. *Applied Earth Science (Transactions of the Institute of Mining and Metallurgy B)* **114,** B199-207.

Holwell, D.A., McDonald, I. and Armitage, P.E.B. (2006). Platinum-group mineral assemblages in the Platreef at the Sandsloot Mine, northern Bushveld Complex, South Africa. *Mineralogical Magazine* **70(1)**, 83-101.

Holwell, D.A., McDonald, I., and Boyce, A.J. (2005). Platreef mineralisation at Overysel, northern Bushveld Complex, South Africa. *2nd Platreef workshop, University of the Witwatersrand, South Africa.*

Holland, H.D. (1959). Some applications of thermochemical data to problems of ore deposits. I. Stability relations among the oxides, sulphides, sulphates and carbonates of ore and gangue metals: *Economic Geology* **54**, 184-233.

Hsu, L.C., Lechler, P.J. and Nelson, J.H. (1991). Hydrothermal solubility of palladium in chloride solutions from 300°C to 700°C: Preliminary experimental results. *Economic Geology* **86,** 422–427

Hulbert, L.J. (1983). A petrographical investigation of the Rustenburg Layered Suite and associated mineralization south of Potgietersrus. *Unpublished DSc dissertation, University of Pretoria,* 511p.

Hutchinson, D. and Kinnaird, J.A. (2005). Complex multistage genesis for the Ni–Cu–PGE mineralisation in the southern region of the Platreef, Bushveld Complex, South Africa. *Applied Earth Science* (*Transactions of the Institute of Mining and Metallurgy B*) **114**, B208-B224.

Hutchinson, D., Kinnaird, J.A. and Schürmann L.W. (2004). Complex multi-stage mineralisation history in the southern sector of the Platreef, Bushveld Complex, South Africa. *Abstract Volume Geoscience Africa, July 2004*.

Iljina, M.J. and Lee, C.A. (2005). PGE Deposits in the marginal series of layered intrusions. *In:* J.E. Mungall (Editor), *Exploration for Platinum-group Element Deposits. Mineralogical Association of Canada, Short Course* ***35,*** 75 – 96*.*

Irvine, T.N. and Sharpe, M.R. (1986). Magma mixing and the origin of stratiform oxide ore zones in the Bushveld and Stillwater Complexes. *In*: *Metallogeny of Basic and Ultrabasic Rocks, Conference Proceedings, Edinburgh*, **1985**, 183-198.

James, D.E., Boyd, F.R., Schutt, D., Bell, D.R. and Carlson, R.W. (2004). Xenolith constraints on seismic velocities in the upper mantle beneath southern Africa. *Geochemistry Geophysics Geosystemes* **5**, 1002-1029.

Keays, R.R. and Campbell, I.H. (1981). Precious metals in the Jimberlana Intrusion, Western Australia: Implications for the genesis of platiniferous ores in layered intrusions. *Economic Geology* **76**, 1118-1141.

Kim, Won-Sa, Chao, G.Y. and Cabri, L.J. (1990). Phase relations in the Pd-Te system. *Journal of Less-Common Metals* **162**, 61-74.

Kinloch, E.D. (1982). Regional trends in platinum-group mineralogy of the Critical Zone of the Bushveld Complex, South Africa. *Economic Geology* **85**, 1328-1347.

Kinnaird, J.A. (2004). What are the questions we need to ask about the Platreef? Platreef Workshop field guide, Mokopane 16-19July, 2004, *Geoscience Africa*, University of Witwatersrand.

Kinnaird, J.A. (2005). Geochemical evidence for multiphase emplacement in the southern Platreef. *Applied Earth Science* (*Transactions of the Institute of Mining and Metallurgy B*) **114**, B225-B242.

Kinnaird, J.A., Hutchinson, D., Schürmann, L.W., Nex, P.A.M. and de Lange, R. (2005). Petrology and mineralisation of the southern Platreef: northern limb of the Bushveld Complex, South Africa. *Mineralium Deposita* **40**, 576-597.

Kleeman, G. J. and Twist D. (1989). The compositionally-zoned sheet-like granite pluton of the Bushveld Complex: Evidence bearing on the nature of A-type magmatism. *Journal of Petrology* **30** 1383-1414.

Klein, C. and Beukes, N.J. (1989). Geochemistry and sedimentology of a facies transition from limestone to iron-formation deposition in the Early Proterozoic Transvaal Supergroup, South Africa. *Economic Geology* **84**, 1733-1774.

Klemm, D.D., Ketterer, S., Reichhardt, F., Steindl, J. and Weber-Diefenbach, K. (1985). Implications of vertical and lateral compositional variations across the Pyroxenite Marker and its associated rocks in the upper part of the Main Zone in the Eastern Bushveld Complex. *Economic Geology* **80**, 1075-1088.

Kruger, F.J. (1990). The stratigraphy of the Bushveld Complex: a reappraisal and relocation of the Main Zone boundaries. *South African Journal of Geology* **93**, 376-381.

Kruger, F.J. and Marsh, J.S. (1985). The mineralogy, petrology and origin of the Merensky cyclic unit in the western Bushveld Complex. *Economic Geology* **80**, 958-974.

Kullerud, G., Yund, R.A., and Moh, G.H. (1969). Phase relations in the Cu-Fe-S, Cu-Ni-S and Fe-Ni-S systems. *Economic Geology*, *monograph* **4**, 323 282.

Lee, C.A. (1983). Trace and platinum-group element chemistry and the development of the Merensky unit of the Western Bushveld Complex. *Mineralium Deposita* **18**, 173-190.

Lee, C.A. (1996). A review of mineralisation in the Bushveld Complex and some other layered mafic intrusions. *In*: R.G. Cawthorn (Editor), *Layered Intrusions*. Elsevier, Amsterdam, 103-145.

Lee, C.A. and Parry, S.J. (1988). Platinum-group element geochemistry of the Lower and Middle Group chromitites of the Eastern Bushveld Complex. *Economic Geology* **83**, 1127-1139.

Li, C. and Naldrett, A.J. (1993). Sulphide capacity of magma: A quantitative model and its application to the formation of the sulphide ores at Sudbury. *Economic Geology* **88**, 1253-1260.

Li, C. and Ripley, E.M. (2005). Empirical equations to predict the sulfur content of

mafic magmas at sulfide saturation and applications to magmatic sulfide deposits. *Mineralium Deposita* **40**, 218-230

Li, C., Lightfoot, P.C., Amelin, Y. and Naldrett, A.J. (2000). Contrasting petrological and geochemical relationships in the Voisey's Bay and Mushuau Intrusions, Labrador, Canada: implications for ore genesis, *Economic Geology* **95**, 771-800.

Li, C., Maier, W.D. and de Waal, S.A. (2001a). The role of magma mixing in the genesis of PGE mineralisation of the Bushveld Complex: Thermodynamic calculation and new interpretations. *Economic Geology* **96**, 653-662.

Li, C., Ripley, E.M., Merino, E. and Maier, W.D. (2004). Replacement of base metal sulphides by actinolite, epidote, calcite and magnetite in the UG2 and Merensky Reef of the Bushveld Complex, South Africa. *Economic Geology* **99,** 173-184.

Liebenberg, L. (1968). The sulfides in the layered sequence of the Bushveld igneous complex. *Unpublished DSc thesis, University of Pretoria*, 260 p.

Maier, W.D. and Barnes, S-J. (1998). Concentrations of rare earth elements in silicate rocks of the Lower, Critical and Main Zones of the Bushveld Complex. *Chemical Geology* **150**, 85-103.

Maier, W.D. and Barnes, S-J, (1999). Platinum-group elements in silicate rocks of the

lower, critical, and main zones at Union Section, western Bushveld Complex. *Journal of Petrology* **40**, 1647-1671.

Maier, W.D and Eales, H.V. (1994). A facies model for the interval between the UG2 chromitite and Merensky Reef, western Bushveld Complex. *Applied Earth Science (Transactions of the Institute of Mining and Metallurgy B)* **103**, B22-B30.

Maier, W.D. and Eales, H.V. (1997). Correlation within the UG2-Merensky Reef interval of the Western Bushveld Complex, based on geochemical, mineralogical and petrological data. *Council for Geosciences, Bulletin of the Geological Survey of South Africa* **120**, 56pp.

Maier, W. D., de Klerk, L., Blaine, J., Manyeruke, T., Barnes, S-J., Stevens, M. V. A. and Mavrogenes, J. A. (2007). Petrogenesis of contact-style PGE mineralization in the northern lobe of the Bushveld Complex: comparison of data from the farms Rooipoort, Townlands, Drenthe and Nonnenwerth. *Mineralium Deposita*, DOI 10.1007/s00126-007-0145-3.

Manyeruke, T.D. (2003). The petrography and geochemistry of the Platreef on the farm Townlands, near Potgietersrus, northern Bushveld Complex. *Unpublished MSc thesis, University of Pretoria, South Africa*, 107pp.

Manyeruke, T.D, Maier, W.D. and Barnes, S.-J. (2005). Major and Trace Element Geochemistry of the Platreef on the farm Townlands, northern Bushveld Complex. *South African Journal of Geology* **108**, no. 3, 381-396.

Mathez, E.A. and Peach, C. (1997). Fractionation and behaviour of the platinum-group elements as inferred from experiments in sulphide-bearing systems and analysis of rocks. *In*: *The origin and fractionation of highly siderophile elements in the earth's mantle. EAG- Workshop 1997, Mainz Plank Institute*, 51-52.

McDonald, I., Holwell, D.A. and Armitage, P.E.B. (2005b). Geochemistry and Mineralogy of the Platreef and "Critical Zone" of the Northern Lobe of the Bushveld Complex, South Africa: Implications for Bushveld Stratigraphy and the development of PGE Mineralization. *Mineralium Deposita* **40**, 526-549.

Mitchell, A.A. (1986). The petrology, mineralogy and geochemistry of the Main Zone of the Bushveld Complex at Rustenburg Platinum Mines, Union Section. *Unpublished PhD thesis, Rhodes University*, 122pp.

Mitchell, A.A. (1990). The stratigraphy, petrology and mineralogy of the Main Zone of the northwestern Bushveld Complex. *South African Journal of Geology* **93**, 818-831.

Mitchell, R.H. and Keays, R.R. (1981). Abundance and distribution of gold, palladium and iridium in some spinel and garnet lherzolites: Implications for the nature and

origin of precious metal-rich intergranular components in the upper mantle. *Geochimica et Cosmochimica Acta* **45**, 2425-2442.

Mitchell, A.A. and Scoon, R.N. (1991). Discussion on 'The stratigraphy of the Bushveld Complex: a reappraisal and the relocation of the Main Zone boundaries'. *South African Journal of Geology* **94**, 183-187.

Morrissey, C.J. (1988). Exploration for platinum. *In*: H.M. Prichard, J. Potts, J.F.W. Bowles and S.J. Cribb (Editors), *Geo-platinum* **87**. Amsterdam: Elsevier, 1-12.

Naldrett, A.J. (1989). *Magmatic sulphide deposits*. Oxford, Oxford University Press, 186p.

Naldrett, A.J. and Lehmann, J. (1988). Spinel non-stoichiometry as the explanation as the explanation for Ni-, Cu-, and PGE-enriched sulphides in chromitites. *In*: H.M. Prichard, P.J. Potts, J.F.W. Bowles and S.J. Cribb (Editors), *Geo-Platinum* **87,** Amsterdam: Elsevier, 113-143.

Naldrett, A.J. and von Gruenewaldt, G. (1989). Association of platinum-group elements with chromitite in layered intrusions and ophiolite complexes. *Economic Geology* **84**, 180-187.

Naldrett, A.J., Fredorenko, V.A., Asif, M., Shushen, L., Kunilov, V.E., Stekhin, A.I., Lightfoot, P.C. and Gorbachev, N.S. (1996). Controls of the composition of Ni-

Cu-sulphide deposits as illustrated by those at Noril'sk, Siberia. *Economic Geology* **91**, 751-773.

Naldrett, A.J., Gasparini, E.C., Barnes, S.J., Von Gruenewaldt, G. and Sharpe, M.R. (1986). The Upper Critical Zone of the Bushveld Complex and the origin of the Merensky-type ores. *Economic Geology* **81**, 1105-1117.

Naldrett, A.J., Rao, B.V. and Evensen, N.M. (1986). Contamination at Sudbury and its role in ore formation. *In*: M.J. Gallagher, R.A. Ixer, C.R. Neary and Pritchard, H.M. (Editors), *Metallogeny of basic and ultrabasic rocks: London Institute of Mining and Metallurgy,* 75-91.

Nelson, D.R., Trendall, A.F. and Altermann, W. (1999). Chronological correlations between Pilbara and Kaapvaal Cratons*. Precambrian Research* **97**, 165-189.

Nex, P.A.M. (2005). The structural setting of mineralisation on Tweefontein Hill, northern limb of the Bushveld Complex, South Africa. *Applied Earth Science (Transactions of the Institute of Mining and Metallurgy B)* **114**, B243-B251.

Peck, D.C., Scoates, R.E.J., Theyer, P., Desharnais, G., Hulbert, L.J. and Huminicki, M.A.E. (2002). Stratiform and contact-type PGE-Cu-Ni mineralization in the Fox River Sill and the Bird River Belt, Manitoba. *In:* L.J. Cabri (Editor), *The geology, geochemistry, mineralogy and mineral beneficiation of platinum-group elements. Canadian Institute of Mining and Metallurgy*. Special Volume **54**, 367-387.

Peregoedova, A., Barnes, S.-J. and Baker, D.R. (2004). The formation of Pt-Ir alloys and Cu-Pd rich sulphide melts by partial desulphurization of Fe-Ni-Cu sulphides: Results of experiments and implications for natural systems. *Chemical Geology* **208**, 247-264.

Prichard, H.M., Sa, J.H.S. and Fisher, P.C. (2001). Platinum-group mineral assemblages and chromite composition in the altered and deformed Bacuri complex, Amapa, northeastern Brazil. *Canadian Mineralogist* **39**, 377-396.

Reczko, B.F.F., Oberholzer, J.D., Res, M., Erikson, P.G. and Schreiber, U.M. (1995). A re-evaluation of the volcanism of the Palaeoproterozoic Pretoria Group (Kaapvaal craton) and a hypothesis on basin development. *Journal of African Earth Sciences* **21**, 505-519.

Reid, D.L., Cawthom, R G., Kruger, F.J. and Tredoux, M. (1993). Isotope and trace-element patterns below the Merensky Reef, Bushveld complex, South Africa: evidence for fluids? *Chemical Geology* **106**, 171-186.

Ripley, E.M. (1999). Systematics of sulphur and oxygen isotopes in mafic igneous rocks and related Cu-Ni-PGE mineralisation. *In:* R.R. Keays, C.M. Lesher, P.C. Lightfoot and C.E.G. Farrow (Editors), *Dynamic processes in magmatic ore deposits and their application in mineral exploration. Geological association of Canada, Short Course* **13**, 133-158.

Rollinson, H.R. (1993). *Using Geochemical Data: Evaluation, Presentation, Interpretation*. Longman/Wyllie. Harlow/New York, 352pp.

Ruiz, J., Barra, F., Ashwal, L.D. and Le Grange, M. (2004). Re-Os systematics on sulphides from the Platreef, Bushveld Complex. *Geoscience Africa 2004. University of the Witwatersrand, Abstracts volume*, p564.

SACS (South African Committee on Stratigraphy). (1980). Stratigraphy of South Africa. *Geological Survey of South Africa. Handbook* **8**, 690pp.

Schiffries, C.M. and Rye, D.M. (1989). Stable isotope systematics of the Bushveld Complex, I. Constraints on magmatic processes in layered intrusions. *American Journal of Science* **289,** 841-873.

Schürmann, L.W., Grabe, P-J. and Steenkamp, C.J. (1998). Chromium. *In* M.G.C. Wilson and C.R. Anhaeusser (Editors), *The mineral resources of South Africa*: Handbook, Council for Geoscience **16**, 740pp

Scoon, R.N. and Mitchell, A.A. (1994). Discordant iron-rich pegmatites in the Bushveld Complex and their relationship to iron-rich intercumulus residual liquids. *Journal of Petrology* **35**, 881-917.

Scoon, R.N. and Teigler, B. (1994). Platinum-group mineralisation in the Critical Zone of the Western Bushveld Complex: I. Sulfide poor chromitites below the UG2. *Economic Geology* **89**, 1094-1121.

Sharman-Harris, E.R. and Kinnaird, J.A. (2004). Into the new millennium: Sulphur isotope studies of the southern Platreef, Northern limb, Bushveld igneous complex. *Abstract volume Geoscience Africa*, July 2004, 589-590.

Sharman-Harris, E.R., Kinnaird, J.A., Harris, C. and Horstmann, U.E. (2005). A new look at sulphide mineralisation of the northern limb, Bushveld Complex: a stable isotope study. *Applied Earth Science* (*Transactions of the Institute of Mining and Metallurgy B*) **114**, B252-B263.

Stevens, M. (2004). Constraining Platreef petrogenesis, northern limb of the Bushveld Complex, South Africa. *Unpublished BSc Hns thesis, Australian National University, Canberra,* 98p.

Stumpfl, E.F. (1993). Fluids: A prerequisite for Pt metals mineralisation. *In:* P.F.Haeh-Alf, J. Torres-Ruiz and F. Gervilla (Editors), *Current Research in Geology Applied to Ore Deposits*. *Proceedings, 2nd Biennial SGA Meeting*, 15-21.

Taylor, S.R. and McLennan, S.M. (1985). *The Continental Crust: Its Composition and Evolution.* Blackwell Scientific, Oxford, 312pp.

Teigler, B. (1990a). Mineralogy, petrology and geochemistry of the Lower and Lower Critical Zones, northwest Bushveld Complex. *Unpublished Ph.D. thesis. Rhodes University, Grahamstown, South Africa*.

Teigler, B. (1990b). Platinum-group element distribution in the Lower and Middle chromitites in the Western Bushveld Complex. *Mineralogy and Petrology* **42**, 165-179.

Tredoux, M., Lindsay, N.M., Davies, G. and McDonald, I. (1995). The fractionation of platinum-group elements in magmatic systems, with the suggestion to a novel causal mechanism. *South African Journal of Geology* **98**, 157-167.

Van der Merwe, M.J. (1976). The layered sequence of the Potgietersrus limb of the Bushveld Complex. *Economic Geology* **71**, 1337-1351.

Verryn, S,M,C. and Merkle, R.K.W. (2000). Stability fields and Ni-content in synthetic cooperate, braggite and vysotskite between 1.200^{0}C and 700^{0}C. *In:* D. Rammllmair, J. Mederer, T. Oberthür, R.B. Heimann and H. Pentinghaus (Editors), *Applied mineralogy*. Balkema, Rotterdam, 451-454.

Viljoen, M.J. and Schürmann, L.W. (1998). Platinum-group metals. *In*: M.G.C. Wilson and C.R Anhaeusser (Editors), *The Mineral Resources of South Africa, Council for Geoscience, Pretoria*, 532-568.

Von Gruenewaldt, G. (1973). The Main and Upper Zones of the Bushveld Complex in the Roossenekal area, eastern Transvaal. *Transactions of the Geological Society of South Africa* **76**, 207-227.

Von Gruenewaldt, G. (1976). Sulphides in the Upper Zone of the Bushveld Complex. *Economic Geology* **71**, 1337-1351.

Von Gruenewaldt, G., Hatton, C.J., Merkle, R.K.W. and Gain, S.B. (1986). Platinum-group element – chromitite associations in the Bushveld Complex. *Mineral Petrology* **42**, 71-95.

Von Gruenewaldt, G., Hulbert, L.J. and Naldrett, A.J. (1989). Contrasting platinum-group concentration patterns in cumulates of the Bushveld Complex. *Mineralium Deposita* **24**, 219-229.

Wagner, A. (1929). *The Platinum Deposits and Mines of South Africa.* Oliver and Boyd, 366p.

Wager, L.R. and Brown, G.M. (1968). *Layered igneous rocks*. Edinburgh and London. Oliver and Boyd, 58p.

Wagner, T. and Lorenz, J. (2002). Mineralogy of complex Co-Ni-Bi vein mineralization, Bieber deposit, Spessart, Germany. *Mineralogical Magazine* **63** (3), 385-407.

Wallmach, T., Hatton, C.J. and Droop, G.T.R. (1989). Extreme facies of contact metamorphism developed in calc-silicate xenoliths in the eastern Bushveld Complex. *Canadian Mineralogist* **27**, 509–523.

Walraven, F., Armstrong, R.A. and Kruger, F.J. (1990). A chronostratigraphic framework for the north-central Kaapvaal craton, the Bushveld Complex and the Vredefort structure. *Tectonophysics* **171**, 23-48.

Watson, J. S. (1996). *Fast,* Simple Method of Powder Pellet Preparation for X-Ray Fluorescence Analysis. *X-Ray Spectrometry* **25**, 173-174.

Webb, S. J., Cawthorn, R. G. Nguuri, T. and James, D. (2004). Gravity modeling of Bushveld Complex connectivity supported by Southern African Seismic Experiment results. *South African Journal of Geology* **107**, 207-218.

White, J.A. (1994). The Potgietersrus project geology and exploration history: *Proceedings, 15th CMMI Congress, South African Institute of Mining and Metallurgy*, 173-182.

Xiang-ping Gu, X., Watanabe, M., Hoshino, K. and Shibata, Y. (2001). Mineral chemistry and associations of Bi-Te(S,Se) minerals from China. *Neues Jahrbuch für Mineralogie* **7**, 289-336.

www.panpalladium.com

Appendix I

Analytical Methods

Appendix Ia: **Sample preparation**

Appendix Ib: **X-Ray fluorescence analysis**

Appendix Ic: **Silicate mineral microprobe analysis**

Appendix Id: **PGE analysis**

Appendix Ie: **Platinum group mineral analyses**

Appendix If: **S-Isotope analyses**

Appendix Ia: Sample preparation

Quarter-core samples were crushed in a jaw crusher before being milled in a C-steel mill. The samples were milled to a particle size of <63 µm. To minimize possible cross contamination, the mill was cleaned after every sample by milling clean quartz, washing the mill pots, and drying with acetone.

Appendix Ib: X-Ray Fluorescence Analysis

APPARATUS: ARL 9400XP+ Wavelength dispersive XRF Spectrometer

SAMPLE PREPARATION: 3 grams of each sample powder were weighed and dried at 100^0C overnight before being roasted at 1000^0C overnight to determine the absorbed (H_2O^-) and the percentage loss on ignition, respectively.

Major elements were determined on fused beads, prepared following the standard method used in the XRD and XRF laboratory of the University of Pretoria, as adapted from Bennett and Oliver (1992). One gram of pre-roasted sample powder and 6 grams of flux (Lithium tetra borate) mixed in a Au crucible was fused at 1050^0C for 15 minutes in a muffle furnace with occasional swirling. The fusion mixture was poured into a pre-heated Pt/Au mould and left to cool at room temperature. The bottom surface of the glass disk was analysed by XRF.

Trace elements were determined on pressed powder briquettes prepared following the method of Watson (1996). Approximately 16-20ml of sample powder mixed with less than 1 volume % of a liquid binder (Mowiol: polyvinyl alcohol) was loaded into aluminum cups to increase the stability and strength before being pressed at ± 7 tons/in^2.

CALIBRATION: The XRF Spectrometer was calibrated with certified reference materials. The NBSGSC fundamental parameter program was used for matrix correction of major elements as well as Cl, Co, Cr, V, Sc and S. The Rh compton peak ratio method was used for the other trace elements.

Standard deviations and detection limits are listed in the Table below.

STANDARD DEVIATIONS AND LOWER LIMIT OF DETECTION OF THE XRF METHOD

	Std dev. (%)	LOD (wt. %)
SiO_2	0.4	0.02
TiO_2	0.03	0.0032
Al_2O_3	0.3	0.01
Fe_2O_3	0.3	0.0097
MnO	0.0065	0.0013
MgO	0.1	0.0118
CaO	0.07	0.01
Na_2O	0.11	0.0265
K2O	0.06	0.005
P_2O_5	0.08	0.01
Cr_2O_3	0.0053	0.0006
NiO	0.01	0.0013
V_2O_5	0.0018	0.0008
ZrO_2	0.005	0.0009
CuO	0.0037	0.0003

	Std dev. (ppm)	LOD (ppm)
Cu	3	2
Ga	2	2
Mo	1	1
Nb	3	2
Ni	6	3
Pb	3	3
Rb	4	2
Sr	4	3
Th	2	3
U	2	3
Y	4	3
Zn	4	4
Zr	6	10
Ba	14	5
Ce	14	6
Co	6	3
Cr	40	15
Sc	5	1
V	10	1

LOD = Limit of Detection, std dev = standard deviation, ppm = parts per million.

Appendix Ic: Silicate mineral microprobe analyses

Quantitative electron microprobe analyses were performed using a CAMECA SX 100 Electron Microprobe. The acceleration voltage was 20 kV and the beam current was 20 nA with a defocused beam while analyzing the plagioclases. Counting times were 20 seconds on peak position and 10 seconds on each background.

The following X-ray lines, spectrometer crystals and standards (in brackets) were used:

SiKa, TAP (Wollastonite);

CaKa, PET (Wollastonite);

AlKa, TAP (Almandine);

MgKa, TAP (Periclase);

NaKa, LTAP (Albite);

FeKa, LLIF (Almandine);

MnKa, LLIF (Rhodonite);

CrKa, PET (Cr_2O_3);

TiKa, PET (Rutile);

KKa, PET (Orthoclase).

Appendix Id. **PGE analysis**

The platinum-group elements, Re and Au were determined by instrumental neutron activation analysis (INAA) at the University of Quebec at Chicoutimi (UQAC), after pre-concentration in a Ni-sulphide bead from 50g of rock powder. Sample irradiation was carried out at the Ecole Polytechnique in Montreal in a SLOWPOKE ll reactor.

Five determinations of five different NiS beads of the CANMET standard WGB-1 (Table below) can be used to estimate the precision and accuracy of the analyses. For all the elements except Au the relative standard deviations are 9–17 %.

For Au, Pt and Pd the accuracy of the analyses may be assessed by comparing the results obtained at UQAC for standards UTM-1 and WGB-1 with the certified values. The results are in good agreement with both the high- and low-level standard. For Rh, Ru and Ir certified values are available only for UTM-1. The UQAC analysed results agree with CANMET results. For the low-level standard WGB-1 only informational values are available for Rh, Ru, Ir and Re. The results agree with these when the standard deviation on the CANMET informational value ic considered.

No noble metals were detected in the blank, except Ir and Au. These were present at 0.02 and 0.1 ppb, respectively. As both values are far lower than the levels present in the samples, no significant contamination is believed to have occurred in preparing the samples, and no blank correction was made on the samples.

Precision and accuracy of the PGE analyses

	UTM-1				WGB-1			
	UQAC*	s	CANMET	error	UQAC*	s	CANMET	error
	ppb	+/-	ppb	+/-	ppb	+/-	ppb	+/-
Os ppb	7.10	0.57	*8.00*	*2.1*	0.48	0.08	n.v.	
Ir	10.00	0.40	8.80	0.60	0.25	0.04	*0.33*	*0.27*
Ru	10.90	0.98	10.90	1.50	<1.20	0.33	*0.30*	*0.20*
Rh	10.80	0.43	9.50	1.10	0.46	0.08	*0.32*	*0.19*
Pt	131.00	7.90	129.00	5.00	5.98	0.55	6.10	1.60
Pd	110.00	4.40	106.00	3.00	13.20	1.94	13.9	2.10
Au	47.90	4.30	48.00	2.00	1.34	0.59	2.90	1.10

* = average of five NiS beads all fused, dissolved and irradiated in the same batch,

s = 1 sigma of the five values, CANMET Certificate of Analysis (1996). Note that the figures in italics are informational values only, i.e. there are as yet no certified values for these elements in these standards, the error in these cases are the standard deviation of the values submitted in the round robin tests.

n.v. = no values

Appendix Ie: Platinum-group mineral analyses

Quantitative electron microprobe analyses were performed using a CAMECA SX 100. Three programs were applied:

1) Platinum-group minerals: 20 kV acceleration voltage and 30 nA sample current (on brass). Counting times were 10 seconds on peak and 5 seconds on each background. The following X-ray lines, spectrometer crystals and standards (in brackets) were used: S Ka, PET (sphalerite), Fe Ka, LLIF (Fe); Co Ka, LLIF (Co); Ni Ka, LLIF (Ni); Cu Ka, LLIF (Cu); As La, TAP (AsGa); Se La, TAP (Se); Ru La, PET (Ru); Rh La, LPET (Rh); Pd La, LPET (Pd, merenskyite); Ag Lß, LPET (Ag); Sn La, PET (Sn); Sb La, PET (Sb); Te La, LPET (merenskyite); Os Ma, TAP (Os); Ir La, LLIF(Ir); Pt La, LLIF (Pt); Au La, LLIF (Au); Hg La, LLIF (HgS); Pb Ma, PET (PbS); Bi Ma, PET (Bi). Background positions were carefully selected to avoid interferences. All elements were measured in differential mode to minimize interference problems by overlapping lines of higher than first order. Off-line interference corrections were performed in cases where element concentrations were enhanced by first-order secondary lines by more than 0.1%.

2) Base metal sulphides: 20 kV acceleration voltage and 20 nA sample current (on brass). Counting times were 10 seconds on peak for S, Fe, Ni, Si, and 30 seconds for Co, As and Pd. The following X-ray lines, spectrometer crystals and standards (in brackets) were used: S Ka, PET (pentlandite, pyrite), Fe Ka, LLIF (pentlandite, pyrite); Co Ka, LLIF (cobaltite); Ni Ka, LLIF (pentlandite); Cu Ka, LLIF (Cu); As La, TAP (AsGa); Pd La, LPET (Pd); Si Ka, TAP (kaersutite).

3) Trace element analyses in sulphides: 35 kV acceleration voltage and 300 nA sample

current (on brass). Counting times were 600 seconds on peak and 300 seconds on each background. The following X-ray lines, spectrometer crystals and standards (in brackets) were used: Se La, TAP (Se); Pd La, LPET (Pd); Rh La, LPET (Rh); Pt La, LLIF (Pt). Background offsets were ±300 steps for each element. Detection limits thus achieved were 35 ppm (Se), 18 ppm (Pd), 19 ppm (Rh) and 34 ppm (Pt).

Appendix If: S-Isotope analyses

APPARATUS: Finnigan MAT252 isotope ratio mass spectrometer

SAMPLE PREPARATION: Sulphide powders and a small amount of V_2O_5 were loaded into tin capsules and analysed using Elemental Analyser-Continuous Flow Isotope Ratio Mass Spectrometry on a Finnigan MAT252 isotope ratio mass spectrometer.

ANALYTICAL PRECISION: better than ± 0.05 per mil.

SAMPLE REPRODUCIBILITY: ± 0.1 per mil.

Appendix II

POLISHED THIN SECTION SAMPLE LIST

Borehole 2121

Sample	Depth (m)	Rock name
MO50	38.84	Main Zone meso-gabbronorite
MO51	52.44	Main Zone meso-gabbronorite
MO52	74.02	Main Zone meso-gabbronorite
MO53	93.69	Main Zone meso-gabbronorite
MO54	116.4	Main Zone meso-gabbronorite
MO55	136.68	Main Zone meso-gabbronorite
MO56	149.11	Main Zone meso-gabbronorite
MO57A	161.06	Main Zone meso-gabbronorite
MO58	172.65	amphibolised and chloritised pyroxenite in contact with anorthosite
MO59	183.01	carbonated and altered calcsilicate
MO60	186.7	mylonitised and altered calsilicate
MO61	189.32	carbonated and chloritised calcsilicate
MO62	197.47	Platreef anorthosite
MO63	199.89	Platreef leuco-gabbronorite
MO64	207.38	Platreef anorthosite
MO65	211.82	Platreef leuco-gabbronorite
MO66	220.02	Platreef recrystallised gabbronorite (in contact with coarse gabbronorite)
MO67	221.54	Platreef clinopyroxene-bearing norite
MO68	236.25	Platreef leuco-gabbronorite
MO69	236.5	Platreef mela-gabbronorite
MO70	244.35	Platreef recrystallised gabbronorite
MO71	245.88	Platreef mela-gabbronorite
MO72	251.31	Platreef mela-gabbronorite (highly amphibolised)
MO73	255.31	Platreef anorthosite
MO74	265.33	Platreef mela-gabbronorite
MO75	271.12	Platreef biotite bearing norite
MO76	275.34	Platreef leuco-gabbronorite
MO77	284.34	Platreef mela-gabbronorite
MO78	285.46	Platreef mela-gabbronorite
MO79	288.25	Platreef fine grained mela-gabbronorite (chilled?)
MO80	289.59	Platreef fine grained norite (chilled) in contact with altered coarse gabbronorite
MO81	290.67	Platreef fine grained norite (chilled) in contact with altered coarse gabbronorite
MO82	292.3	Platreef quartz gabbro
MO83	299.04	Platreef clinopyroxene-bearing norite (hydrothermally altered)
MO84	309.11	Platreef chilled norite with coarse gabbronorite bands
MO85	316.23	hydrothermally altered norite in contact with granitic material
MO86	333.98	amphibolised and sericitised pyroxenite
MO87	342.6	granite gneiss

Borehole 2199

Sample	Depth (m)	Rock name
MO1	44.71	Main Zone meso-gabbronorite
MO2	57.97	Main Zone meso-gabbronorite
MO3	68.54	Main Zone meso-gabbronorite
MO4	107.15	Main Zone meso-gabbronorite
MO5	139.36	Main Zone meso-gabbronorite
MO6	151.6	Main Zone anorthosite
MO8	174.19	Platreef anorthosite
MO9	182.82	Platreef gabbronorite
MO10	195.26	Platreef pegmatoidal gabbro
MO11	200.81	Biotite-rich gabbronorite
MO12	203.30	Biotite-rich gabbronorite
MO13	208.80	Platreef recrystallised gabbronorite
MO15	223.72	Platreef pegmatoidal norite
MO16	241.25	Platreef anorthosite
MO17	255.78	Platreef norite in contact with gabbronorite
MO18	270.2	Platreef norite
MO19	277.48	Platreef medium grained norite in contact with coarse anorthosite
MO20A	292.42	Platreef gabbronorite
MO20B	292.22	Platreef norite
MO21	299	Platreef norite in contact with recrystallised anorthosite
MO22	301.62	Platreef norite
MO23	306.08	Platreef coarse grained, altered norite in contact with medium grained gabbro
MO24	315.45	Platreef gabbronorite
MO25	326.94	Platreef altered gabbronorite
MO26	338.85	Serpentinite peridotite
MO27	342.81	Platreef gabbronorite (partially recrystallised)
MO28	355.76	Platreef gabbronorite (partially recrystallised)
MO29	362.42	Platreef carbonated granitic gneiss
MO30	370.13	Platreef carbonated granitic gneiss

Appendix III

XRF SAMPLE LIST

Nonnenwerth Borehole 2121

Sample	Depth (m)	S-isotopes	PGE analyses	Description
MOX1	38.58		∨	Main Zone gabbronorite
MOX2	52.58		∨	Main Zone gabbronorite
MOX3	74.21		∨	Main Zone gabbronorite
MOX4	93.83		∨	Main Zone gabbronorite
MOX5	116.18		∨	Main Zone gabbronorite
MOX6	136.82		∨	Main Zone gabbronorite
MOX7	149.25		∨	Main Zone gabbronorite
MOX8	165.05		∨	Main Zone gabbronorite
MOX9	199.68	∨	∨	Platreef recrystallised gabbronorite
MOX10	219.9	∨	∨	Platreef recrystallised gabbronorite
MOX11	236.69		∨	Platreef mela-gabbronorite
MOX12	244.55		∨	Platreef recrystallised gabbronorite
MOX13	265.16		∨	Platreef mela-gabbronorite
MOX14	275.23	∨	∨	Platreef mela-gabbronorite
MOX15	284.48		∨	Platreef mela-gabbronorite
MOX16	288.37		∨	Platreef mela-gabbronorite
MOX17	300.16		∨	Platreef norite

Nonnenwerth Borehole 2199

Sample	Depth (m)	S-isotopes	PGE analyses	Description
MOX20	44.88		∨	Main Zone gabbronorite
MOX21	58.09		∨	Main Zone gabbronorite
MOX22	68.65		∨	Main Zone gabbronorite
MOX23	106.97		∨	Main Zone gabbronorite
MOX24	129.15		∨	Main Zone anorthosite
MOX25	139.51		∨	Main Zone anorthosite
MOX26	151.42		∨	Main Zone anorthosite
MOX27	173.94	∨	∨	Platreef anorthosite
MOX28	183.07		∨	Platreef gabbronorite
MOX29	195.07	∨	∨	Platreef gabbro
MOX31	208.55		∨	Platreef gabbronorite
MOX32	241.65		∨	Platreef anorthosite
MOX33	270.08	∨	∨	Platreef norite
MOX34	283.55		∨	Platreef norite
MOX35	306.05		∨	Platreef norite in contact with recrystallised gabbro
MOX36	326.95	∨	∨	Platreef altered gabbronorite
MOX37	342.56		∨	Platreef gabbronorite (partially recrystallised)
MOX38	355.65		∨	Platreef gabbronorite (partially recrystallised)
MOX39	339.00			Serpentinized peridotite

NB. The depth on polished thin section refers to bottom measurements of the core.

Townlands

Sample	Depth(m)	S-isotopes	PGE analyses	Description
P1	30.4		V	U- Platreef gabbronorite
P2	32.69	v	V	U- Platreef sulphide bearing gabbronorite
P4	38.85		V	U- Platreef gabbronorite with minor disseminated sulphides
P6	55.8	v	V	fine-med grained norite sill
P7	57.7		V	U- Platreef sulphide bearing pegmatoidal gabbronorite
P11	76.99	v	V	M- Platreef sulphide bearing gabbronorite
P12	78.74		V	M- Platreef sulphide bearing gabbronorite
P13	80.75		V	M- Platreef sulphide bearing gabbronorite
P14	86.42		V	M- Platreef sulphide bearing gabbronorite
P15	89.55	v	V	M- Platreef sulphide bearing pegmatoidal gabbronorite
P19	102.35	v	V	M- Platreef sulphide bearing pegmatoidal gabbronorite
P106	106	v	V	M- Platreef sulphide bearing gabbronorite
P20	109.82		V	M- Platreef sulphide bearing pegmatoidal gabbronorite
P26	145.6	v	V	M- Platreef sulphide bearing norite

NB. The depth on polished thin section refers to bottom measurements of the core.

U- Platreef = Upper Platreef

M- Platreef = Middle Platreef

L- Platreef = Lower Platreef

Appendix IV

Analytical results on mineral chemistry, whole rock major elements, trace elements, PGE, sulphides and PGM.

An = cationic ratio of 100 * Ca/(Ca + Na + K)

Mg # = cationic ratio of 100 * Mg/(Mg + Fe^{2+})

Table 1: Whole rock major, trace element and PGE contents in Nonnenwerth rocks from borehole 2121.

Sample	MOX1	MOX2	MOX3	MOX4	MOX5	MOX6	MOX7	MOX8	MOX 9	MOX 10	MOX 11	MOX 12	MOX13	MOX14	MOX 15	MOX 16	MOX 17
Borehole	2121	2121	2121	2121	2121	2121	2121	2121	2121	2121	2121	2121	2121	2121	2121	2121	2121
Depth (m)	38.58	52.58	74.21	93.83	116.18	136.82	149.25	165.05	199.68	219.9	236.69	244.55	265.16	275.23	284.48	288.37	300.16
Rock Type	MZ GN	MZ GN	MZ GN	MZ GN	MZ GN	MZ GN	MZ GN	MZ GN	PR rx GN	PR rx GN	PR mela-GN	PR rx GN	PR mela-GN	PR mela-GN	PR mela-GN	PR mela-GN	PR Nor
wt. %																	
SiO_2	49.70	50.35	50.14	50.04	50.20	51.15	50.98	50.49	44.86	45.87	49.67	46.97	50.12	50.19	48.10	48.00	48.34
TiO_2	0.42	0.34	0.36	0.23	0.25	0.23	0.25	0.26	0.11	0.22	0.20	0.16	0.19	0.18	0.27	0.27	0.41
Al_2O_3	18.00	13.04	9.76	17.53	17.38	15.29	9.31	11.58	20.50	14.31	9.41	14.98	15.41	15.36	7.84	16.65	10.56
Fe_2O_3	10.20	13.63	14.75	10.20	9.83	11.53	15.84	12.63	9.74	14.28	16.77	14.19	9.84	9.28	19.28	12.83	20.56
MnO	0.17	0.23	0.26	0.17	0.18	0.21	0.26	0.22	0.17	0.23	0.30	0.24	0.19	0.18	0.38	0.23	0.35
MgO	6.59	9.56	11.47	7.68	7.54	9.35	14.89	12.34	8.40	10.98	13.72	10.87	8.70	8.70	13.97	7.08	10.48
CaO	11.50	10.12	11.07	10.51	10.38	9.75	7.24	9.47	10.54	9.46	6.16	9.34	11.75	12.62	7.50	10.21	5.93
Na_2O	2.69	1.56	0.96	2.14	2.15	1.87	0.90	1.13	1.90	1.47	1.20	1.52	1.77	1.79	0.99	3.01	1.80
K_2O	0.23	0.13	0.07	0.17	0.17	0.19	0.09	0.12	0.32	0.12	0.12	0.15	0.24	0.17	0.11	0.28	0.22
P_2O_5	0.02	0.04	0.04	0.04	0.04	0.04	0.04	0.04	0.04	0.05	0.05	0.03	0.04	0.03	0.03	0.06	0.09
Cr_2O_3	0.02	0.03	0.04	0.02	0.02	0.02	0.05	0.04	0.05	0.03	0.05	0.01	0.03	0.02	0.03	0.03	0.04
NiO	0.02	0.01	0.02	0.01	0.01	0.02	0.03	0.02	0.32	0.40	0.15	0.25	0.03	0.04	0.09	0.04	0.08
LOI	0.26	0.79	1.07	0.95	0.36	0.35	-0.03	1.38	1.36	0.01	1.06	0.10	1.41	0.67	-0.35	0.15	-0.11
TOTAL	99.82	99.84	99.99	99.69	98.51	99.99	99.84	99.73	98.31	97.43	98.86	98.81	99.70	99.23	98.58	98.83	98.86
Trace elements (ppm)																	
Cu	76	101	103	86	93	101	94	112	5275	5581	2427	3253	234	273	1066	986	789
Ga	17	13	10	15	16	14	10	12	12	11	9	12	14	13	8	16	13
Ni	102	149	183	133	128	152	271	203	2010	2523	887	1694	226	346	523	252	602
Pb	3	3	3	3	3	3	3	6	11	9	6	14	3	5	9	10	5
Rb	4	3	3	2	4	5	3	5	6	2	4	3	5	4	4	8	4
Sr	232	155	105	205	218	197	104	116	211	139	95	159	217	228	80	213	141
Y	8	10	12	6	6	7	8	8	4	6	8	5	6	6	9	8	12
Zn	26	31	48	76	45	66	73	85	68	40	60	78	36	37	88	87	121
Zr	12	12	15	11	11	12	11	16	10	10	49	10	11	10	12	17	23
Cl	139	208	184	203	166	208	194	291	231	342	1230	191	566	288	237	409	348
Co	45	65	76	51	49	59	87	65	85	132	94	104	53	60	111	66	118
Cr	119	187	252	129	143	132	282	262	241	133	184	130	156	113	206	125	190
S	168	250	282	151	198	231	554	258	8551	17018	6557	10809	387	1752	2929	2864	8723
Sc	26	41	56	29	28	31	43	41	20	38	38	35	39	40	52	38	36
Th	0.16	<0.03	<0.02	<0.02	0.06	0.07	<0.03	0.05	0.09	0.09	2.01	0.15	0.21	0.03	0.23	0.46	0.80
V	148	175	242	131	134	128	177	174	82	148	135	129	159	153	201	173	163
Ba	88	45	30	61	79	87	37	59	52	47	53	59	86	73	34	116	80
REE (ppm)																	
La	2.42	1.62	1.59	1.90	2.06	2.03	1.59	2.24	1.38	1.36	2.13	1.58	1.92	1.32	1.67	3.75	5.40
Ce	6.49	5.15	5.58	4.93	5.37	5.34	4.60	6.84	3.03	3.28	4.97	3.60	4.67	3.82	4.40	9.14	12.33
Nd	2.11	1.70	1.59	2.09	1.60	1.40	1.46	2.93	0.55	1.21	1.28	1.48	1.74	1.52	1.54	4.02	4.18
Sm	0.77	0.99	1.06	0.62	0.70	0.67	0.67	0.86	0.31	0.57	0.67	0.49	0.67	0.63	0.74	1.18	1.36
Eu	0.51	0.42	0.39	0.44	0.46	0.40	0.32	0.39	0.28	0.30	0.26	0.30	0.34	0.37	0.27	0.54	0.46
Ho	0.29	0.37	0.38	0.28	0.31	0.26	0.34	0.39	0.16	0.18	1.51	0.27	0.27	0.22	0.39	0.46	0.68
Tb	0.18	0.23	0.25	0.12	0.14	0.13	0.14	0.17	0.06	0.13	0.18	0.09	0.14	0.15	0.18	0.23	0.26
Yb	0.82	1.14	1.24	0.75	0.77	0.77	0.89	1.01	0.37	0.72	0.93	0.64	0.74	0.68	1.13	1.10	1.25
Lu	0.12	0.18	0.20	0.12	0.12	0.12	0.15	0.16	0.06	0.12	0.17	0.11	0.12	0.11	0.18	0.18	0.21
PGE (ppb)																	
Os	<0.5	<0.5	<0.5	<0.5	<0.5	<0.5	<0.5	<0.5	16	18	<0.5	15	<0.5	1	2	<0.5	< 1.12
Ir	0.0	0.1	0.1	0.1	0.2	0.2	0.1	0.1	12.5	20.2	0.7	7.4	0.2	0.4	0.2	0.2	0.2
Ru	<5	<5	<5	<5	<5	<5	<5	<5	15	15	<5	<5	<5	<5	<5	<5	< 3.17
Rh	<0.1	<0.1	1	1	<0.1	1	<0.1	<0.1	45	90	2	31	1	1	1	1	
Pt	<2	<2	1	41	3	7	2	3	3134	2480	477	1457	110	176	32	23	19
Pd	<2	<2	<2	2	<2	2	2	<2	5731	4677	597	2431	16	116	35	37	33
Au	1	1	1	3	1	1	0	1	952	347	333	363	14	20	27	24	25

< = below detection limit

MZ GN = Main Zone gabbronorite, PR mela-GN = Platreef mela-gabbronorite, PR Nor = Platreef norite, PR rx GN = Platreef recrystallised gabbronorite.

Table 1: contd. Whole rock major, trace element and PGE contents in Townlands rocks.

sample	P1	P2	P3	P4	P5	P6	P7	P8	P9	P10	P11	P12	P13	P14	P15	P16	P17	P18	P19	P20	P21
Borehole	TL1-03	TL1-03	TL1-03	TL1-03	TL1-03	TL1-03	TL1-03	TL1-03	TL1-03	TL1-03	TL1-03	TL1-03	TL1-03	TL1-03	TL1-03	TL1-03	TL1-03	TL1-03	TL1-03	TL1-03	TL1-03
depth (m)	30.4	32.69	34.91	38.85	44.77	44.77	57.7	62.65	63.65	68.3	76.99	78.74	80.75	86.42	89.55	94.3	96.6	100.05	102.35	109.82	110.95
Rock type	UP	UP	UP	UP	Gabbro	Norite	UP	Gabbro	hornfels	hornfels	MP	MP	MP	MP	MP	MP	skarn	MP	MP	MP	MP
wt %																					
SiO_2	52.37	43.74	52.19	46.79	52.03	52.06	43.18	52.65	28.11	50.35	49.49	42.09	39.37	45.26	45.55	51.49	39.12	47.75	43.49	47.58	48.11
TiO_2	0.15	0.25	0.16	0.18	0.30	0.30	0.23	0.16	1.75	0.34	0.29	0.17	0.22	0.30	0.19	0.37	0.32	0.45	0.19	0.18	0.33
Al_2O_3	7.43	6.73	7.20	7.40	10.38	10.38	5.56	22.57	18.98	12.23	4.40	5.04	4.43	7.24	7.88	4.92	10.10	10.31	7.52	16.08	7.97
Fe_2O_3	10.94	14.19	11.77	14.91	6.93	6.93	19.15	5.70	40.31	14.52	16.56	17.49	21.67	11.10	18.17	9.20	12.35	8.82	19.00	13.44	9.44
MnO	0.21	0.20	0.24	0.21	0.14	0.14	0.21	0.09	0.20	0.23	0.27	0.28	0.18	0.14	0.18	0.14	0.14	0.13	0.18	0.16	0.17
MgO	21.31	18.92	20.97	20.98	10.05	10.05	21.58	5.48	7.24	16.39	22.00	27.05	19.71	23.59	18.83	19.79	35.93	21.63	21.14	16.64	21.15
CaO	6.65	13.53	6.52	7.80	18.24	18.25	3.24	9.21	1.97	3.83	4.29	6.01	6.82	10.35	3.60	13.75	1.01	10.34	4.77	3.58	11.96
Na_2O	0.13	0.01	0.04	0.01	1.07	1.07	0.01	3.41	1.07	1.65	0.01	0.01	0.01	0.01	0.01	0.01	0.01	0.01	0.01	0.53	0.01
K_2O	0.27	0.33	0.29	0.48	0.68	0.68	0.34	0.47	0.18	0.15	0.37	0.13	0.14	0.35	0.49	0.22	0.07	0.47	0.43	0.35	0.35
P_2O_5	0.01	0.03	0.01	0.02	0.04	0.04	0.05	0.03	0.01	0.02	0.03	0.03	0.02	0.03	0.03	0.02	0.01	0.07	0.03	0.07	0.03
Cr_2O_3	0.42	0.04	0.46	0.33	0.04	0.03	0.30	0.07	0.15	0.23	0.21	0.11	0.20	0.04	0.10	0.05	0.03	0.01	0.07	0.06	0.04
Ni	0.06	0.37	0.06	0.16	0.03	0.03	0.73	0.01	0.03	0.03	0.48	0.38	1.42	0.28	0.76	0.02	0.15	0.01	0.43	0.23	0.08
S	0.04	1.42	0.07	0.71	0.08	0.03	4.98	0.13	0.00	0.01	1.38	1.01	5.45	1.16	3.37	0.01	0.63	0.00	2.29	0.90	0.30
Cu	0.02	0.26	0.01	0.01	0.00	0.00	0.43	0.00	0.00	0.00	0.25	0.25	0.35	0.15	0.85	0.00	0.16	0.00	0.46	0.22	0.06
TOTAL	100.00	100.02	100.00	100.00	100.00	100.00	100.00	100.00	100.00	100.00	100.02	100.04	100.00	100.00	100.00	100.01	100.03	100.00	100.00	100.01	100.00
LOI	0.43	3.20	1.13	2.60	1.58	1.54	4.27	1.44	*	*	1.18	6.19	4.78	5.60	3.35	1.95	11.53	5.70	4.88	2.21	2.80
Trace elements (ppm)																					
Cu	152.89	2543.63	134.78	143.00	14.32	14.33	4273.74	9.25	24.25	4.03	2472.73	2319.51	3533.46	1470.88	8509.66	17.66	1448.37	24.59	4647.70	2173.29	609.28
Ga	8.15	9.29	8.23	8.00	12.28	12.29	9.08	21.59	64.67	14.12	7.20	7.52	8.05	8.41	11.24	8.31	13.63	13.90	10.44	17.33	10.42
Ni	583.01	3563.98	628.63	1535.00	281.38	281.53	7346.43	120.27	286.98	301.54	4664.54	3501.29	14166.04	2817.70	7567.66	209.78	1302.96	62.01	4291.55	2230.38	774.88
Pb	6.12	47.51	13.38	24.00	17.39	17.40	31.26	16.45	11.12	9.08	19.55	16.12	37.25	33.64	27.59	4.15	13.63	3.21	10.44	16.31	21.87
Rb	12.23	17.56	12.35	26.00	31.72	31.74	19.16	16.45	11.12	3.03	21.61	7.52	10.07	16.82	26.56	13.50	5.68	24.59	24.02	24.46	15.62
Sr	148.81	160.07	105.97	214.00	169.85	169.94	174.46	649.64	482.01	354.99	59.68	75.20	74.49	107.24	230.90	117.35	15.90	248.02	155.62	209.99	201.01
Y	6.12	13.43	7.20	10.00	30.70	30.71	9.08	7.20	5.05	11.09	10.29	7.52	11.07	12.62	11.24	22.85	5.68	12.83	10.44	8.15	18.75
Zn	82.56	108.44	112.15	109.00	69.58	69.62	144.21	55.51	409.26	128.08	128.63	124.62	110.74	77.80	144.06	64.39	191.98	80.18	120.11	120.29	70.82
Zr	19.37	36.15	19.55	30.00	54.23	54.26	33.28	20.56	27.28	31.26	29.84	25.78	35.23	57.83	67.43	55.04	44.30	51.31	42.82	36.70	60.41
Co	88.67	116.70	92.60	124.00	40.93	40.95	307.57	24.67	158.65	89.76	170.82	146.11	293.95	95.68	173.69	56.08	81.79	48.11	176.51	125.38	67.70
Cr	2876.32	259.22	3116.42	2361.00	256.83	256.96	2080.40	462.56	1015.56	1576.29	1605.27	758.49	1391.24	260.74	660.01	406.07	207.88	60.94	445.97	453.62	293.70
S	377.12	14188.78	699.63	7136.20	777.64	303.03	49816.59	1295.17	16.17	80.68	13765.18	10059.09	54521.95	11554.66	33705.55	129.82	6286.49	17.10	22852.06	8966.36	3030.77
Sc	19.37	12.39	21.61	12.00	40.93	40.95	12.10	2.06	16.17	40.34	19.55	5.37	7.05	7.36	11.24	10.39	17.04	13.90	8.36	17.33	8.33
Th	0.33	0.58	0.49	1.15	2.02	0.97	1.00	0.58	0.22	0.32	0.79	0.53	0.75	1.18	1.48	1.05	na	na	2.40	1.19	2.16
Cs	0.86	2.44	1.23	1.88	2.05	1.37	1.64	1.41	1.73	0.52	1.17	1.23	1.63	1.44	2.10	1.45	na	na	3.03	5.81	1.20
V	99.89	115.67	101.86	78.00	79.81	79.85	65.55	32.89	450.69	107.91	122.45	70.91	82.55	79.90	66.41	114.24	54.53	102.63	61.62	67.28	91.65
Ba	162.71	232.93	90.18	216.92	159.73	270.02	124.50	275.43	140.42	106.76	101.80	60.64	74.41	114.33	164.44	47.05	na	na	143.18	204.30	118.61
Hf	0.18	0.84	0.30	0.59	1.64	0.64	0.69	0.29	0.56	0.86	0.44	0.45	0.62	1.56	1.51	1.44	na	na	0.94	0.70	1.48
REE (ppm)																					
La	1.84	4.20	1.87	4.67	10.20	9.34	7.43	11.86	8.41	9.27	4.24	3.16	4.24	5.55	6.94	8.87	na	na	6.25	7.10	9.47
Ce	4.41	12.45	3.98	12.43	38.65	20.43	14.17	22.06	12.28	16.78	8.51	7.85	10.04	13.87	13.30	30.93	na	na	13.66	13.26	26.01
Nd	2.72	4.58	1.59	4.14	20.11	5.69	4.57	7.09	3.66	4.62	3.41	2.95	4.02	6.51	4.46	16.08	na	na	5.55	3.12	10.96
Sm	0.49	1.29	0.50	1.20	5.27	1.10	1.09	0.99	0.50	0.84	0.93	0.76	1.18	1.44	0.99	3.31	na	na	1.17	0.93	2.48
Eu	0.20	0.46	0.20	0.38	0.99	0.70	0.50	0.89	0.49	0.56	0.39	0.30	0.60	0.47	0.55	0.85	na	na	0.45	0.58	0.63
Tb	0.06	0.22	0.09	0.17	0.92	0.17	0.09	0.11	0.05	0.14	0.12	0.14	0.11	0.24	0.17	0.54	na	na	0.18	0.10	0.44
Yb	0.48	0.66	0.54	0.64	2.32	0.71	0.67	0.40	0.16	1.26	0.75	0.46	0.66	0.73	0.90	1.64	na	na	0.73	0.83	1.27
Lu	0.09	0.12	0.08	0.11	0.33	0.13	0.11	0.06	0.03	0.23	0.13	0.07	0.11	0.12	0.15	0.25	na	na	0.13	0.17	0.21
PGE (ppb)																					
Os	8.35	4.64	1.45	3.17	<1.1	1.41	20.09	<1.5	1.10	0.87	7.28	4.73	21.60	2.52	6.31	1.30	na	na	4.41	3.09	1.01
Ir	7.49	4.43	2.01	3.00	0.14	1.44	21.85	0.14	0.31	0.58	8.66	5.28	24.75	1.07	10.22	0.05	na	na	6.21	3.35	0.24
Ru	57.98	23.12	11.86	11.68	<4	3.59	106.14	<5.9	7.60	2.36	33.62	24.81	35.22	<7.3	<9.3	3.90	na	na	18.02	14.27	<4.6
Rh	21.56	23.20	4.24	12.26	0.30	7.91	86.43	0.43	0.47	1.39	37.35	20.63	107.69	7.11	34.94	0.53	na	na	28.63	14.31	1.82
Pt	319.10	361.56	64.31	227.34	8.07	95.77	1592.47	7.89	6.23	20.53	427.74	244.74	726.53	633.35	310.85	9.50	na	na	253.05	237.85	125.17
Pd	111.79	770.84	44.01	347.55	3.91	277.29	1664.87	<6	4.85	<6	962.29	422.89	3409.14	1141.88	953.31	8.30	na	na	723.68	491.38	307.06
Au	6.95	65.26	7.73	35.88	0.52	161.00	190.98	0.47	0.36	0.64	143.78	60.96	142.60	79.14	185.96	0.41	na	na	99.36	64.41	21.72
Re	0.26	3.82	<0.3	0.17	<0.1	0.37	13.34	<0.4	0.26	<0.4	8.79	2.60	28.22	4.18	<0.6	0.20	na	na	4.95	0.38	<0.3

Notes: All data are normalised to 100% LOI free
* = not detected, < = below detection limit and na = not analysed, Merensky Reef estimates from Barnes and Maier, 2002.

Table 1: contd. Whole rock major, trace element and PGE contents in Townlands rocks.

sample	P22	P23	P24	P25	P26	P28	P29	P30	P31	P32	P33
Borehole	TL1-03	TL1-03	TL1-03	TL1-03	TL1-03	TL1-03	TL1-03	TL1-03	TL1-03	TL1-03	TL1-03
depth (m)	112.75	118.95	126.9	138.38	145.6	170.4	174.95	189.95	197.37	205.18	213
Rock type	hornfels	hornfels	LP	LP	LP	hornfels	hornfels	dolomite	hornfels	hornfels	hornfels
wt %											
SiO_2	38.01	56.16	50.97	48.73	50.97	63.09	55.58	35.55	39.90	53.40	20.02
TiO_2	1.04	0.30	0.19	0.45	0.38	1.01	0.22	0.18	1.81	0.26	0.21
Al_2O_3	24.67	11.92	14.16	8.58	9.76	13.59	10.52	7.96	16.74	3.67	3.75
Fe_2O_3	23.41	11.36	10.28	11.66	14.17	12.72	11.78	4.55	27.74	17.46	2.12
MnO	0.16	0.20	0.18	0.23	0.21	0.09	0.20	0.17	0.13	0.29	0.07
MgO	6.52	12.59	14.05	17.11	15.81	2.97	15.45	42.66	5.45	16.11	28.43
CaO	3.85	5.99	8.15	12.55	6.19	3.26	5.01	7.88	3.80	3.94	45.31
Na_2O	1.55	0.07	1.06	0.03	0.01	2.36	0.53	0.01	3.27	0.69	0.00
K_2O	0.34	1.15	0.58	0.32	0.78	0.31	0.37	0.02	0.62	2.03	0.01
P_2O_5	0.03	0.05	0.20	0.08	0.06	0.05	0.05	0.01	0.03	1.56	0.08
Cr_2O_3	0.07	0.18	0.10	0.10	0.36	0.03	0.24	0.01	0.10	0.05	0.00
Ni	0.01	0.02	0.03	0.04	0.20	0.01	0.04	0.00	0.02	0.02	0.00
S	0.33	0.01	0.02	0.09	0.72	0.50	0.00	0.98	0.37	0.49	0.00
Cu	0.00	0.00	0.00	0.02	0.36	0.00	0.00	0.00	0.01	0.03	0.00
TOTAL	100.00	100.00	100.00	100.00	100.00	100.00	100.00	100.00	100.00	100.00	100.00
LOI	1.31	1.07	1.16	1.52	1.83	1.69	0.28	13.85	*	*	37.41
Trace elements (ppm)											
Cu	39.10	5.14	46.97	202.53	3608.95	6.14	5.07	4.54	125.20	342.71	2.77
Ga	43.22	11.30	14.30	12.34	12.31	22.50	10.14	11.34	40.39	7.04	6.92
Ni	122.45	237.34	343.09	436.93	2038.82	63.41	407.67	27.23	241.32	177.89	15.22
Pb	16.46	5.14	36.76	22.62	11.28	9.20	5.07	3.40	13.13	12.06	5.53
Rb	19.55	42.13	22.46	17.48	34.87	11.25	21.30	5.67	21.20	93.47	4.15
Sr	755.25	344.20	308.37	283.75	417.40	438.75	110.54	14.75	640.15	112.56	157.71
Y	7.20	11.30	13.27	19.53	14.36	21.48	10.14	6.81	8.08	50.25	13.83
Zn	186.24	196.25	87.81	85.33	83.07	73.64	103.44	74.87	199.92	180.90	26.29
Zr	55.56	35.96	36.76	77.10	42.05	211.70	41.58	21.55	39.38	70.35	80.24
Co	95.69	71.92	67.39	82.25	114.86	53.18	79.10	19.28	112.08	91.46	2.77
Cr	453.77	1210.36	697.41	734.04	2469.55	238.29	1745.26	71.47	700.74	392.96	17.98
S	3251.49	113.02	163.38	867.69	7230.21	4990.85	16.23	9778.34	3746.01	4895.48	0.00
Sc	7.20	32.88	16.34	13.36	21.54	11.25	33.47	2.27	18.17	17.09	1.38
Th	0.56	0.95	1.62	3.07	1.14	4.34	na	na	11.08	0.26	na
Cs	3.03	1.16	1.61	1.57	1.04	2.38	na	na	10.66	2.33	na
V	212.99	147.96	70.46	135.70	115.89	151.36	153.13	6.81	376.62	49.25	16.60
Ba	166.42	306.90	233.52	170.61	369.20	350.91	na	na	2.11	0.81	na
Hf	1.38	0.65	0.68	1.73	0.83	5.59	na	na	0.67	0.07	na
REE (ppm)											
La	18.44	7.82	8.66	12.68	7.22	40.21	na	na	232.08	38.04	na
Ce	33.97	17.22	19.55	31.97	17.65	86.86	na	na	97.94	11.94	na
Nd	11.99	6.61	6.95	14.22	6.22	33.56	na	na	17.17	1.36	na
Sm	1.71	1.21	1.57	2.79	1.39	5.39	na	na	2.09	1.55	na
Eu	1.11	0.50	0.64	0.77	0.48	1.68	na	na	1.99	0.08	na
Tb	0.14	0.19	0.26	0.46	0.22	0.65	na	na	4.62	0.57	na
Yb	0.24	0.83	1.04	1.44	0.86	1.28	na	na	0.71	0.10	na
Lu	0.04	0.14	0.18	0.24	0.14	0.21	na	na	4.45	< 0,36	na
PGE (ppb)											
Os	<1.1	0.72	1.86	0.80	1.87	<1.0	na	na	<0.9	1.01	na
Ir	0.48	0.60	2.05	0.32	2.11	0.15	na	na	0.17	0.12	na
Ru	<4.0	4.26	8.42	3.35	6.84	<3.2	na	na	2.78	4.51	na
Rh	0.86	1.61	5.34	1.86	8.57	<0.6	na	na	0.68	0.44	na
Pt	4.64	22.71	72.42	29.60	176.56	2.54	na	na	6.14	5.75	na
Pd	4.08	5.16	34.18	16.59	246.89	<6.8	na	na	4.96	2.30	na
Au	1.33	0.97	3.01	4.72	49.06	0.42	na	na	1.02	6.12	na
Re	0.12	0.07	0.31	0.34	0.77	<0.23	na	na	<0.2	0.40	na

Notes: All data are normalised to 100% LOI free
* = not detected, < = below detection limit and na = not analysed, Merensky Reef estimates from Barnes and Maier, 2002.

Table 1: contd. Whole rock major, trace element and PGE contents in Nonnenwerth rocks from borehole 2199.

Sample	MOX20	MOX21	MOX22	MOX23	MOX24	MOX25	MOX26	MOX27	MOX28	MOX29	MOX31	MOX32	MOX33	MOX34	MOX35	MOX36	MOX37	MOX38	MOX39
Borehole	2199	2199	2199	2199	2199	2199	2199	2199	2199	2199	2199	2199	2199	2199	2199	2199	2199	2199	2199
Depth (m)	44.88	58.09	68.65	106.97	129.15	139.51	151.42	173.94	183.07	195.07	208.55	241.65	270.08	283.55	306.05	326.95	342.56	355.65	339.00
Rock Type	MZ GN	MZ GN	MZ GN	MZ GN	MZ GN	MZ Anor	MZ Anor	PR Anor	PR Gabbro	PR Gabbro	PR rx GN	PR Anor	PR Nor	PR rx GN	PR Nor	PR mela-GN	PR mela-GN	PR mela-GN	Serp peridotite
wt. %																			
SiO_2	50.57	51.15	50.99	51.31	48.56	48.88	49.61	45.16	50.65	45.30	51.20	46.32	45.74	48.27	47.21	54.05	53.14	53.17	32.22
TiO_2	0.32	0.24	0.30	0.27	0.10	0.12	0.14	0.15	0.21	0.69	0.10	0.15	0.31	0.24	0.69	0.21	0.32	0.33	0.43
Al_2O_3	20.31	17.61	16.86	16.00	27.77	24.45	25.00	23.77	14.98	12.18	17.52	22.47	8.26	14.14	17.90	9.33	8.06	9.56	1.72
Fe_2O_3	8.05	10.10	10.75	11.14	2.96	5.06	4.79	7.22	9.33	14.04	9.34	8.60	23.45	15.19	12.59	11.93	10.44	11.18	22.63
MnO	0.14	0.18	0.18	0.20	0.05	0.09	0.08	0.10	0.17	0.22	0.18	0.15	0.37	0.24	0.20	0.13	0.14	0.14	0.12
MgO	5.34	7.46	7.70	8.43	1.69	4.17	3.59	4.82	9.56	9.60	9.26	6.38	12.69	12.11	6.38	13.37	18.52	14.81	26.12
CaO	11.57	10.80	10.66	10.28	14.43	13.23	13.89	13.47	12.35	14.61	9.68	11.43	6.37	6.87	10.07	8.44	6.55	6.80	1.64
Na_2O	2.65	2.17	2.13	2.01	2.50	2.16	2.23	2.61	1.60	1.27	1.90	2.29	0.92	1.71	2.61	1.56	1.14	1.75	1.06
K_2O	0.22	0.18	0.15	0.12	0.21	0.39	0.13	0.19	0.11	0.19	0.09	0.23	0.14	0.14	0.21	0.26	0.41	0.20	0.19
P_2O_5	0.05	0.04	0.05	0.04	0.05	0.04	0.04	0.04	0.05	0.10	0.03	0.03	0.03	0.01	0.02	0.05	0.05	0.23	0.03
Cr_2O_3	0.01	0.02	0.02	0.02	0.01	0.02	0.01	0.01	0.02	0.03	0.03	0.02	0.03	0.12	0.02	0.19	0.29	0.21	0.78
NiO	0.01	0.01	0.01	0.01	0.00	0.01	0.01	0.22	0.04	0.38	0.03	0.08	0.16	0.06	0.04	0.08	0.10	0.07	0.46
LOI	0.26	-0.03	0.00	0.07	0.63	1.12	0.47	0.99	0.71	0.33	0.40	0.59	-0.39	-0.06	0.90	0.28	0.48	1.53	9.02
TOTAL	99.50	99.95	99.81	99.90	98.95	99.73	99.98	98.75	99.78	98.94	99.74	98.74	98.08	99.04	98.84	99.87	99.64	99.98	98.21
Trace elements (ppm)																			
Cu	31	94	91	121	57	73	59	3119	478	2476	160	808	3280	526	366	171	45	56	2089
Ga	17	15	15	14	18	16	16	15	13	11	13	15	9	13	17	12	10	12	6
Ni	68	118	123	143	40	88	69	1593	314	2488	211	467	1052	452	300	605	734	588	2463
Pb	3	3	3	3	3	3	3	3	3	3	3	6	14	4	8	9	3	3	9
Rb	3	3	4	2	5	11	2	4	3	9	2	5	3	2	4	5	9	4	6
Sr	245	218	202	192	302	365	243	231	168	109	204	270	105	197	340	137	186	271	38
Y	7	7	9	6	4	4	5	4	9	13	4	4	8	4	12	8	9	15	8
Zn	42	63	72	74	24	36	38	51	61	61	69	60	173	129	88	66	62	88	101
Zr	15	15	14	15	11	13	10	11	16	20	10	10	16	10	19	18	24	30	19
Cl	130	113	117	132	136	241	137	172	206	260	179	209	297	165	255	308	236	431	
Co	35	47	52	54	10	22	23	70	56	124	57	50	147	92	67	68	67	60	82
Cr	74	108	122	126	50	110	67	86	140	165	182	151	192	825	195	1251	1813	1372	3605
S	52	221	333	195	16	82	16	8713	585	8046	132	3012	14978	2643	1369	413	277	120	2629
Sc	23	27	31	32	8	15	17	27	42	66	24	24	44	32	37	36	23	25	7
Th	0.33	0.20	0.17	0.15	0.50	0.32	0.25	0.19	0.40	0.51		0.12	0.36	0.07	0.18	0.19	0.53	0.32	3
V	130	122	143	158	40	67	71	98	157	336	82	99	183	144	452	130	113	113	125
Ba	100	73	69	59	75	122	55	68	38	37	27	82	55	55	129	199	280	152	39
REE (ppm)																			
La	3.20	2.60	2.53	2.21	3.37	2.51	2.19	2.35	2.25	4.76	0.82	1.52	2.14	1.34	3.79	3.83	3.98	5.68	9.69
Ce	7.97	6.38	7.00	5.81	6.87	5.52	5.97	6.10	6.08	13.03	1.65	3.88	5.71	2.83	11.61	13.51	13.05	20.99	4.88
Nd	3.22	2.27	2.53	2.38	2.22	2.03	1.88	2.21	2.01	5.19	0.36	1.19	1.87	1.00	3.93	5.05	5.03	8.28	
Sm	0.93	0.76	0.86	0.68	0.54	0.55	0.51	0.62	0.75	1.50	0.16	0.42	0.75	0.37	1.34	1.51	1.59	2.44	
Eu	0.54	0.45	0.48	0.41	0.41	0.36	0.40	0.43	0.33	0.38	0.21	0.36	0.30	0.29	0.58	0.47	0.55	0.68	
Ho	0.18	0.23	0.32	0.24	0.15	0.18	0.14	0.45	0.25	0.00	0.07	0.18	0.44	0.21	0.38	0.28	0.28	0.48	
Tb	0.21	0.18	0.19	0.16	0.11	0.12	0.10	0.18	0.21	0.40	0.06	0.03	0.17	0.10	0.28	0.29	0.26	0.47	
Yb	0.79	0.75	0.87	0.80	0.32	0.46	0.46	0.61	0.78	1.24	0.35	0.45	1.12	0.63	1.09	0.83	0.81	1.30	
Lu	0.12	0.12	0.15	0.13	0.06	0.08	0.07	0.10	0.12	0.19	0.06	0.07	0.19	0.11	0.17	0.12	0.12	0.21	
PGE (ppb)																			
Os	<0.5	<0.5	<0.5	<0.5	1	<0.5	1	7	<0.5	<0.5	<0.5	<0.5	<0.5	<0.5	<0.5	<0.5	<0.5	1	
Ir	0.0	0.0	0.1	0.1	0.2	0.1	0.4	4.2	0.1	0.2	0.1	0.6	0.7	0.3	0.1	0.9	1.1	0.7	
Ru	<5	<5	<5	<5	<5	<5	<5	<5	<5	<5	<5	<5	<5	<5	<5	<5	<5	<5	
Rh	<0.1	<0.1	<0.1	<0.1	1	<0.1	1	11	<0.1	3	1	2	2	1	<0.1	2	2	1	
Pt	2	2	<2	<2	79	17	59	1049	39	623	16	115	89	34	2	37	12	12	
Pd	<2	<2	<2	<2	36	9	34	1284	51	3201	14	194	112	65	<2	36	10	10	
Au	1	1	2	1	21	5	6	346	33	3232	1	30	89	14	3	5	3	3	

< = below detection limit

MZ GN = Main Zone gabbronorite, PR mela-GN = Platreef mela-gabbronorite, PR Nor = Platreef norite, PR rx GN = Platreef recrystallised gabbronorite.

Table 2a. Selected Plagioclase Analyses from Nonnenwerth

Sample	MO50	MO52	MO55	MO57	MO62	MO63	MO65	MO66	MO67	MO68	MO69	MO70	MO71	MO73	MO74	MO78	MO79	MO80	MO83	MO84
Borehole	2121	2121	2121	2121	2121	2121	2121	2121	2121	2121	2121	2121	2121	2121	2121	2121	2121	2121	2121	2121
depth (m)	38.84	74.02	136.68	161.06	197.47	199.89	211.82	220.02	221.54	236.25	236.5	244.35	245.88	255.31	265.33	285.46	288.25	289.59	299.04	309.11
Rock Type	MZ GN	MZ GN	MZ GN	MZ GN	PR anor	PR leuco-GN	PR leuco-GN	PR rx GN	PR Nor	PR leuco-GN	PR mela-GN	PR rx GN	PR mela-GN	PR anor	PR mela-GN	PR mela-GN	PR mela-GN	PR nor	PR nor	PR nor
wt. %																				
Na_2O	3.74	3.87	4.15	3.71	3.35	3.09	2.91	4.38	3.34	3.46	3.51	4.26	4.49	4.36	4.30	2.85	4.93	3.31	5.37	4.82
SiO_2	51.66	51.78	52.43	51.10	50.54	49.89	48.89	52.93	50.50	50.63	51.12	52.57	53.05	53.15	52.77	49.45	54.17	50.37	54.78	53.43
Al_2O_3	29.64	29.45	29.24	29.49	30.15	30.54	30.71	28.92	30.14	30.00	30.41	28.79	28.45	28.76	28.66	31.21	27.82	30.75	26.95	28.19
CaO	13.58	13.28	12.82	13.54	14.21	14.64	15.01	12.44	14.23	14.05	14.00	12.50	12.02	12.40	12.37	15.21	11.27	14.53	10.54	11.79
K_2O	0.29	0.28	0.22	0.26	0.22	0.20	0.16	0.29	0.21	0.21	0.24	0.27	0.36	0.34	0.33	0.12	0.34	0.17	0.43	0.25
FeO	0.29	0.29	0.28	0.32	0.40	0.38	0.28	0.34	0.36	0.38	0.34	0.32	0.37	0.40	0.31	0.30	0.27	0.27	0.31	0.26
Total	99.34	99.03	99.26	98.55	99.02	98.85	98.08	99.40	98.92	98.87	99.73	98.82	98.83	99.53	98.84	99.27	98.93	99.50	98.52	98.90
Cations (based on 32 oxygens)																				
Na	1.33	1.38	1.47	1.33	1.20	1.11	1.05	1.55	1.19	1.24	1.25	1.52	1.60	1.54	1.53	1.02	1.75	1.18	1.91	1.71
Si	9.48	9.52	9.60	9.45	9.32	9.23	9.13	9.67	9.32	9.35	9.35	9.66	9.74	9.70	9.69	9.12	9.91	9.25	10.05	9.80
Al	6.41	6.38	6.31	6.43	6.56	6.66	6.76	6.23	6.56	6.53	6.56	6.24	6.16	6.19	6.21	6.78	6.00	6.65	5.83	6.09
Ca	2.67	2.62	2.51	2.68	2.81	2.90	3.00	2.43	2.82	2.78	2.74	2.46	2.36	2.42	2.44	3.01	2.21	2.86	2.07	2.32
K	0.07	0.07	0.05	0.06	0.05	0.05	0.04	0.07	0.05	0.05	0.06	0.06	0.08	0.08	0.08	0.03	0.08	0.04	0.10	0.06
Fe	0.04	0.04	0.04	0.05	0.06	0.06	0.04	0.05	0.06	0.06	0.05	0.05	0.06	0.06	0.05	0.05	0.04	0.04	0.05	0.04
Total	20.01	20.01	20.00	20.02	20.02	20.01	20.04	20.02	20.01	20.02	20.02	20.00	20.02	20.01	20.00	20.01	20.00	20.03	20.03	20.04
An	65.61	64.40	62.24	65.84	69.15	71.55	73.35	60.06	69.37	68.32	67.83	60.88	58.44	59.92	60.23	74.13	54.72	70.10	50.79	56.67
Ab	32.72	33.97	36.45	32.64	29.53	27.29	25.74	38.29	29.42	30.43	30.80	37.57	39.48	38.16	37.89	25.15	43.31	28.90	46.78	41.90
Or	1.67	1.63	1.30	1.52	1.31	1.15	0.91	1.65	1.21	1.25	1.37	1.55	2.07	1.92	1.89	0.72	1.97	1.01	2.44	1.43

MZ GN = Main Zone gabbronorite, PR mela-GN = Platreef mela-gabbronorite, PR anor = Platreef anorthosite, PR Nor = Platreef norite, PR rx GN = Platreef recrystallised gabbronorite.

Table 2a. Contd:Selected Plagioclase Analyses from Nonnenwerth

Sample	MO1	MO2	MO3	MO4	MO5	MO6	MO8	MO9	MO10	MO13	MO15	MO17	MO19	MO20	MO20#	MO21	MO22	MO22#	MO23	MO24	MO25	MO27
Borehole	2199	2199	2199	2199	2199	2199	2199	2199	2199	2199	2199	2199	2199	2199	2199	2199	2199	2199	2199	2199	2199	2199
depth (m)	44.71	57.97	68.54	107.15	139.36	151.6	174.19	182.82	195.26	208.8	223.72	255.78	277.48	292.42	292.42	299	301.62	301.62	306.08	315.45	326.94	342.81
Rock Type	MZ GN	MZ GN	MZ GN	MZ GN	MZ GN	MZ GN	PR anor	PR Gabbro	PR Gabbro	PR rx GN	PR Nor	PR Nor	PR Nor	PR mela-GN	PR mela-GN	PR Nor	PR Nor	PR mela-GN	PR Nor	PR mela-GN	PR mela-GN	PR mela-GN
wt. %																						
Na_2O	3.63	3.84	4.12	4.04	2.71	2.67	3.12	3.37	3.78	3.81	4.56	4.00	4.42	4.12	3.36	4.47	4.13	3.46	5.00	5.28	4.95	5.55
SiO_2	51.82	52.17	52.63	52.90	49.05	47.10	50.25	51.01	51.90	51.88	53.48	52.27	52.76	52.51	50.77	53.39	53.06	51.27	54.85	55.19	54.28	56.65
Al_2O_3	30.47	30.02	29.49	29.60	31.70	30.91	30.89	30.77	29.76	30.36	28.83	30.20	29.25	29.83	30.98	29.44	29.76	30.91	28.53	28.28	29.11	27.43
CaO	13.51	13.15	12.60	12.70	15.35	15.28	14.38	14.04	13.21	13.17	11.84	13.03	12.27	12.41	13.57	11.87	12.14	13.37	10.88	10.52	11.36	9.20
K_2O	0.24	0.27	0.32	0.32	0.15	0.15	0.21	0.23	0.26	0.21	0.34	0.24	0.29	0.28	0.19	0.26	0.25	0.20	0.34	0.33	0.25	0.40
FeO	0.37	0.31	0.34	0.32	0.38	0.35	0.38	0.31	0.46	0.29	0.43	0.29	0.31	0.38	0.59	0.27	0.29	0.33	0.27	0.25	0.25	0.16
Total	100.19	99.90	99.61	99.96	99.44	96.55	99.39	99.82	99.54	99.82	99.65	100.15	99.41	99.65	99.73	99.85	99.78	99.65	100.02	99.94	100.28	99.47
Cations (based on 32 oxygens)																						
Na	1.28	1.35	1.46	1.42	0.97	0.99	1.11	1.19	1.34	1.35	1.61	1.41	1.57	1.45	1.19	1.57	1.45	1.22	1.75	1.85	1.73	1.94
Si	9.41	9.50	9.60	9.61	9.03	8.96	9.23	9.32	9.49	9.45	9.73	9.49	9.64	9.57	9.28	9.69	9.63	9.35	9.91	9.96	9.79	10.21
Al	6.53	6.44	6.34	6.34	6.88	6.93	6.69	6.62	6.41	6.52	6.18	6.46	6.30	6.40	6.67	6.29	6.37	6.65	6.07	6.02	6.19	5.83
Ca	2.63	2.57	2.46	2.47	3.03	3.11	2.83	2.75	2.59	2.57	2.31	2.53	2.40	2.42	2.66	2.31	2.36	2.62	2.11	2.03	2.19	1.78
K	0.06	0.06	0.07	0.07	0.04	0.04	0.05	0.05	0.06	0.05	0.08	0.05	0.07	0.07	0.05	0.06	0.06	0.05	0.08	0.08	0.06	0.09
Fe	0.06	0.05	0.05	0.05	0.06	0.06	0.06	0.05	0.07	0.04	0.07	0.04	0.05	0.06	0.09	0.04	0.04	0.05	0.04	0.04	0.04	0.02
Total	19.98	19.99	19.99	19.97	20.02	20.09	20.00	19.99	19.99	19.99	20.01	20.01	20.03	19.99	20.00	19.98	19.93	19.95	19.97	19.99	20.01	19.88
An	66.36	64.40	61.63	62.28	75.13	75.31	70.93	68.79	64.91	64.80	57.74	63.37	59.51	61.44	68.29	58.58	60.98	67.30	53.52	51.41	55.13	46.76
Ab	32.22	34.01	36.50	35.85	23.99	23.84	27.83	29.88	33.57	33.95	40.26	35.26	38.82	36.90	30.54	39.92	37.53	31.50	44.50	46.66	43.45	50.83
Or	1.42	1.60	1.87	1.87	0.87	0.85	1.23	1.33	1.53	1.25	1.99	1.37	1.66	1.66	1.16	1.50	1.50	1.20	1.98	1.93	1.43	2.41

refers to plagioclase enclosed in orthopyroxene

MZ GN = Main Zone gabbronorite, PR mela-GN = Platreef mela-gabbronorite, PR anor = Platreef anorthosite, PR Nor = Platreef norite, PR rx GN = Platreef recrystallised gabbronorite.

Table 2b. Selected Orthopyroxene Analyses from Nonnenwerth

sample	MO50	MO52	MO55	MO57	MO62	MO63	MO66	MO67	MO68	MO69	MO70	MO71	MO73	MO74	MO79	MO80	MO83	MO84
Borehole	2121	2121	2121	2121	2121	2121	2121	2121	2121	2121	2121	2121	2121	2121	2121	2121	2121	2121
Depth (m)	38.84	74.02	136.68	161.06	197.47	199.89	220.02	221.54	236.25	236.5	244.35	245.88	255.31	265.33	288.25	289.59	299.04	309.11
Rock Type	MZ GN	MZ GN	MZ GN	MZ GN	PR anor	PR leuco-GN	PR rx GN	PR Nor	PR leuco-GN	PR mela-GN	PR rx GN	PR mela-GN	PR anor	PR mela-GN	PR mela-GN	PR Nor	PR Nor	PR Nor
wt. %																		
Na_2O	0.05	0.03	0.03	0.02	0.02	0.02	0.02	0.02	0.01	0.03	0.01	0.03	0.02	0.01	0.03	0.04	0.02	0.01
SiO_2	52.50	52.54	52.21	52.63	52.91	52.80	52.21	53.20	53.16	53.14	52.44	51.47	52.23	52.89	51.42	52.44	52.11	53.68
Al_2O_3	1.14	1.15	1.18	1.08	1.36	1.18	1.22	1.15	1.18	1.35	0.88	1.14	1.26	1.17	0.70	1.15	0.60	1.03
MgO	20.30	20.57	21.11	21.80	23.03	23.62	21.66	22.45	23.75	23.51	21.87	20.51	20.56	22.59	19.14	22.30	19.70	24.10
Cr_2O_3	0.01	0.04	0.05	0.03	0.04	0.12	0.02	0.05	0.03	0.06	0.01	0.01	0.00	0.05	0.00	0.12	0.03	0.11
TiO_2	0.23	0.28	0.25	0.20	0.14	0.17	0.20	0.22	0.17	0.14	0.19	0.19	0.22	0.13	0.20	0.21	0.22	0.25
CaO	1.29	1.65	1.78	1.59	1.85	1.71	1.11	1.84	1.54	2.04	0.77	1.24	2.11	1.34	0.93	1.63	1.40	0.88
NiO	0.03	0.04	0.05	0.04	0.09	0.12	0.09	0.09	0.08	0.08	0.05	0.08	0.10	0.06	0.03	0.05	0.03	0.08
FeO	23.87	23.13	22.08	21.40	19.57	18.52	21.99	20.27	18.86	18.60	22.17	23.33	22.50	20.58	25.34	20.64	24.41	19.35
MnO	0.50	0.49	0.48	0.45	0.41	0.36	0.50	0.42	0.39	0.39	0.52	0.49	0.50	0.43	0.56	0.41	0.58	0.40
Total	99.74	99.98	99.27	99.30	99.41	98.68	99.27	99.80	99.20	99.40	98.97	98.54	99.49	99.31	98.42	99.06	99.12	99.97
Cations (based on 6 oxygens)																		
Na	0.00	0.00	0.00	0.00	0.00	0.00	0.00	0.00	0.00	0.00	0.00	0.00	0.00	0.00	0.00	0.00	0.00	0.00
Si	1.98	1.97	1.97	1.97	1.96	1.97	1.97	1.97	1.97	1.97	1.98	1.97	1.97	1.97	1.98	1.97	1.99	1.97
Al	0.05	0.05	0.05	0.05	0.06	0.05	0.05	0.05	0.05	0.06	0.04	0.05	0.06	0.05	0.03	0.05	0.03	0.04
Mg	1.14	1.15	1.19	1.22	1.27	1.31	1.22	1.24	1.31	1.30	1.23	1.17	1.16	1.26	1.10	1.25	1.12	1.32
Cr	0.00	0.00	0.00	0.00	0.00	0.00	0.00	0.00	0.00	0.00	0.00	0.00	0.00	0.00	0.00	0.00	0.00	0.00
Ti	0.01	0.01	0.01	0.01	0.00	0.00	0.01	0.01	0.00	0.00	0.01	0.01	0.01	0.00	0.01	0.01	0.01	0.01
Ca	0.05	0.07	0.07	0.06	0.07	0.07	0.04	0.07	0.06	0.08	0.03	0.05	0.09	0.05	0.04	0.07	0.06	0.03
Ni	0.00	0.00	0.00	0.00	0.00	0.00	0.00	0.00	0.00	0.00	0.00	0.00	0.00	0.00	0.00	0.00	0.00	0.00
Fe	0.75	0.73	0.70	0.67	0.61	0.58	0.69	0.63	0.58	0.58	0.70	0.75	0.71	0.64	0.82	0.65	0.78	0.60
Mn	0.02	0.02	0.02	0.01	0.01	0.01	0.02	0.01	0.01	0.01	0.02	0.02	0.02	0.01	0.02	0.01	0.02	0.01
Total	4.00	4.00	4.01	4.00	4.00	4.00	4.00	4.00	4.00	4.01	4.00	4.01	4.00	4.00	4.00	4.01	4.00	4.00
Mg#	60.26	61.32	63.02	64.50	67.71	69.45	63.71	66.38	69.17	69.26	63.74	61.04	61.96	66.18	57.39	65.83	58.99	68.94

MZ GN = Unit 2 gabbronorite, PR mela-GN = Platreef mela-gabbronorite, PR anor = Platreef anorthosite, PR Nor = Platreef norite, PR rx GN = Platreef recrystallised gabbronorite.

Table 2b. Contd: Selected Orthopyroxene Analyses from Nonnenwerth

sample	MO1	MO2	MO3	MO4	MO6	MO8	MO9	MO10	MO13	MO15	MO17	MO19	MO20	MO21	MO22	MO23	MO24	MO25
Borehole	2199	2199	2199	2199	2199	2199	2199	2199	2199	2199	2199	2199	2199	2199	2199	2199	2199	2199
Depth (m)	44.71	57.97	68.54	107.15	151.6	174.19	182.82	195.26	208.8	223.72	255.78	277.48	292.42	299	301.62	306.08	315.45	326.94
Rock type	MZ GN	MZ GN	MZ GN	MZ GN	MZ GN	PR anor	PR gabbro	PR gabbro	PR rx-GN	PR Nor	PR Nor	PR Nor	PR mela-GN	PR Nor	PR Nor	PR Nor	PR mela-GN	PR mela-GN
wt. %																		
Na_2O	0.02	0.03	0.02	0.03	0.02	0.01	0.02	0.03	0.02	0.02	0.02	0.01	0.03	0.01	0.02	0.02	0.02	0.02
SiO_2	52.60	52.57	52.11	52.58	52.20	53.96	52.94	52.32	53.31	52.28	53.77	52.13	53.12	53.73	53.91	52.70	52.80	54.30
Al_2O_3	1.03	1.09	0.67	1.06	1.39	1.46	1.54	1.18	1.15	0.70	1.33	0.87	0.96	1.02	0.99	0.94	0.77	0.71
MgO	20.63	21.04	19.60	21.51	21.06	24.87	21.89	20.95	22.83	19.83	24.25	20.11	21.78	23.94	24.16	20.81	21.38	24.09
Cr_2O_3	0.02	0.04	0.02	0.04	0.03	0.08	0.02	0.02	0.07	0.02	0.18	0.04	0.08	0.10	0.06	0.02	0.04	0.14
TiO_2	0.24	0.24	0.17	0.18	0.17	0.16	0.15	0.32	0.16	0.23	0.17	0.23	0.19	0.24	0.19	0.21	0.20	0.22
CaO	1.02	1.13	0.73	0.96	0.65	1.34	1.63	1.13	1.17	1.26	1.07	0.96	1.55	0.93	0.99	1.27	1.18	1.24
NiO	0.03	0.03	0.05	0.04	0.03	0.14	0.08	0.07	0.05	0.08	0.08	0.06	0.07	0.07	0.07	0.04	0.03	0.11
FeO	23.70	23.09	24.90	22.54	23.36	17.35	20.64	22.86	20.17	24.08	18.61	24.16	21.32	19.30	18.87	22.92	22.75	19.31
MnO	0.52	0.52	0.56	0.49	0.49	0.40	0.47	0.53	0.45	0.58	0.40	0.55	0.46	0.38	0.38	0.48	0.49	0.23
Total	99.89	99.81	98.91	99.52	99.48	99.80	99.43	99.94	99.43	99.10	99.90	99.15	99.59	99.80	99.73	99.49	99.70	100.43
Cations (based on 6 oxygens)																		
Na	0.00	0.00	0.00	0.00	0.00	0.00	0.00	0.00	0.00	0.00	0.00	0.00	0.00	0.00	0.00	0.00	0.00	0.00
Si	1.98	1.97	1.99	1.98	1.97	1.97	1.97	1.97	1.98	1.99	1.97	1.98	1.98	1.98	1.98	1.98	1.98	1.99
Al	0.05	0.05	0.03	0.05	0.06	0.06	0.07	0.05	0.05	0.03	0.06	0.04	0.04	0.04	0.04	0.04	0.03	0.03
Mg	1.16	1.18	1.12	1.21	1.18	1.35	1.21	1.18	1.26	1.12	1.33	1.14	1.21	1.31	1.32	1.17	1.20	1.31
Cr	0.00	0.00	0.00	0.00	0.00	0.00	0.00	0.00	0.00	0.00	0.01	0.00	0.00	0.00	0.00	0.00	0.00	0.00
Ti	0.01	0.01	0.01	0.01	0.00	0.00	0.00	0.01	0.00	0.01	0.00	0.01	0.01	0.01	0.01	0.01	0.01	0.01
Ca	0.04	0.05	0.03	0.04	0.03	0.05	0.07	0.05	0.05	0.05	0.04	0.04	0.06	0.04	0.04	0.05	0.05	0.05
Ni	0.00	0.00	0.00	0.00	0.00	0.00	0.00	0.00	0.00	0.00	0.00	0.00	0.00	0.00	0.00	0.00	0.00	0.00
Fe	0.75	0.72	0.80	0.71	0.74	0.53	0.64	0.72	0.63	0.77	0.57	0.77	0.67	0.59	0.58	0.72	0.71	0.59
Mn	0.02	0.02	0.02	0.02	0.02	0.01	0.01	0.02	0.01	0.02	0.01	0.02	0.01	0.01	0.01	0.02	0.02	0.01
Total	4.00	4.00	4.00	4.01	4.01	4.00	3.99	3.99	4.00	3.99	4.00	4.00	3.99	4.00	4.00	4.00	4.00	4.00
Mg#	60.83	61.90	58.39	62.98	61.64	71.87	65.35	62.64	66.86	59.49	69.90	59.75	64.56	68.85	69.54	61.80	62.62	68.97

MZ GN = Unit 2 gabbronorite, PR mela-GN = Platreef mela-gabbronorite, PR anor = Platreef anorthosite, PR Nor = Platreef norite, PR rx GN = Platreef recrystallised gabbronorite.

Table 2c. Selected Clinopyroxene Analyses from Nonnenwerth

sample	MO50	MO52	MO55	MO57	MO62	MO63	MO65	MO66	MO67	MO68	MO69	MO70	MO71	MO72	MO74	MO79	MO80	MO83	MO84
Borehole	2121	2121	2121	2121	2121	2121	2121	2121	2121	2121	2121	2121	2121	2121	2121	2121	2121	2121	2121
Depth (m)	38.84	74.02	136.68	161.06	197.47	199.89	211.82	220.02	221.54	236.25	236.5	244.35	245.88	251.31	265.33	288.25	289.59	299.04	309.11
Rock Type	MZ GN	MZ GN	MZ GN	MZ GN	PR anor	PR leuco-GN	PR leuco-GN	PR rx GN	PR Nor	PR leuco-GN	PR mela-GN	PR rx GN	PR mela-GN	PR mela-GN	PR mela-GN	PR mela-GN	PR nor	PR nor	PR nor
wt. %																			
Na_2O	0.29	0.30	0.30	0.35	0.30	0.27	0.26	0.24	0.29	0.26	0.61	0.33	0.35	0.27	0.29	0.31	0.37	0.42	0.36
SiO_2	51.35	51.17	51.80	51.38	51.48	51.03	52.76	52.73	51.41	52.06	52.91	51.64	51.59	52.21	51.49	51.51	51.77	51.11	51.25
Al_2O_3	2.20	2.62	1.96	2.26	2.21	2.23	1.82	1.07	2.45	2.13	3.82	1.90	1.86	1.63	2.03	1.51	2.18	1.87	2.50
MgO	13.00	13.49	13.65	13.28	12.72	13.95	15.49	14.20	14.15	15.02	17.22	13.92	12.70	13.91	13.61	12.94	14.13	12.87	14.26
Cr_2O_3	0.04	0.08	0.05	0.11	0.01	0.07	0.09	0.04	0.08	0.06	0.04	0.04	0.03	0.02	0.08	0.05	0.31	0.04	0.16
TiO_2	0.55	0.49	0.49	0.48	0.46	0.62	0.31	0.18	0.42	0.22	0.27	0.44	0.41	0.35	0.39	0.32	0.47	0.43	0.51
CaO	21.70	19.93	21.96	21.91	21.84	21.68	21.64	22.47	21.73	20.88	12.14	20.74	21.37	20.55	21.71	21.31	21.11	20.00	21.39
NiO	0.01	0.02	0.02	0.02	0.06	0.08	0.04	0.05	0.05	0.05	0.12	0.03	0.06	0.06	0.03	0.02	0.04	0.02	0.04
FeO	10.39	11.33	9.28	9.27	10.50	8.85	7.44	8.65	8.73	8.54	10.17	10.10	10.87	10.54	9.58	10.89	9.08	12.25	8.55
MnO	0.27	0.28	0.21	0.23	0.31	0.22	0.20	0.26	0.22	0.23	0.14	0.28	0.27	0.29	0.25	0.28	0.23	0.31	0.20
Total	99.84	99.79	99.76	99.31	99.94	99.04	100.13	99.98	99.58	99.50	98.04	99.48	99.54	99.83	99.52	99.18	99.71	99.36	99.28
Cations (based on 6 oxygens)																			
Na	0.02	0.02	0.02	0.03	0.02	0.02	0.02	0.02	0.02	0.02	0.04	0.02	0.03	0.02	0.02	0.02	0.03	0.03	0.03
Si	1.93	1.93	1.94	1.94	1.94	1.93	1.95	1.97	1.93	1.94	1.97	1.95	1.95	1.96	1.94	1.96	1.94	1.94	1.92
Al	0.10	0.12	0.09	0.10	0.10	0.10	0.08	0.05	0.11	0.09	0.17	0.08	0.08	0.07	0.09	0.07	0.10	0.08	0.11
Mg	0.73	0.76	0.76	0.75	0.71	0.79	0.85	0.79	0.79	0.84	0.96	0.78	0.72	0.78	0.76	0.73	0.79	0.73	0.80
Cr	0.00	0.00	0.00	0.00	0.00	0.00	0.00	0.00	0.00	0.00	0.00	0.00	0.00	0.00	0.00	0.00	0.01	0.00	0.00
Ti	0.02	0.01	0.01	0.01	0.01	0.02	0.01	0.01	0.01	0.01	0.01	0.01	0.01	0.01	0.01	0.01	0.01	0.01	0.01
Ca	0.88	0.81	0.88	0.89	0.88	0.88	0.86	0.90	0.87	0.84	0.49	0.84	0.87	0.83	0.88	0.87	0.85	0.81	0.86
Ni	0.00	0.00	0.00	0.00	0.00	0.00	0.00	0.00	0.00	0.00	0.00	0.00	0.00	0.00	0.00	0.00	0.00	0.00	0.00
Fe	0.33	0.36	0.29	0.29	0.33	0.28	0.23	0.27	0.27	0.27	0.32	0.32	0.34	0.33	0.30	0.35	0.28	0.39	0.27
Mn	0.01	0.01	0.01	0.01	0.01	0.01	0.01	0.01	0.01	0.01	0.00	0.01	0.01	0.01	0.01	0.01	0.01	0.01	0.01
Total	4.02	4.02	4.02	4.01	4.01	4.02	4.02	4.03	4.02	4.02	4.00	4.02	4.01	4.01	4.02	4.02	4.01	4.02	4.02
Mg#	69.06	68.05	72.38	71.85	68.34	73.76	78.78	74.54	74.30	75.88	75.11	71.13	67.57	70.19	71.70	67.94	73.51	65.33	74.86

MZ GN = Main Zone gabbronorite, PR mela-GN = Platreef mala-gabbronorite, PR anor = Platreef anorthosite, PR Nor = Platreef norite, PR rx GN = Platreef recrystallised gabbronorite.

Table 2c.contd: Selected Clinopyroxene Analyses from Nonnenwerth

sample	MO1	MO2	MO3	MO4	MO5	MO6	MO8	MO9	MO10	MO13	MO15	MO17	MO19	MO20	MO22	MO23	MO24	MO25
Borehole	2199	2199	2199	2199	2199	2199	2199	2199	2199	2199	2199	2199	2199	2199	2199	2199	2199	2199
Depth (m)	44.71	57.97	68.54	107.15	139.36	151.6	174.19	182.82	195.26	208.8	223.72	255.78	277.48	292.42	301.62	306.08	315.45	326.94
Rock Type	MZ GN	MZ GN	MZ GN	MZ GN	MZ GN	MZ GN	PR anor	PR Gabbro	PR Gabbro	PR rx GN	PR Nor	PR rx GN	PR Nor	PR mela-GN	PR Nor	PR Nor	PR mela-GN	PR mela-GN
wt. %																		
Na_2O	0.17	0.31	0.31	0.27	0.23	0.25	0.20	0.27	0.28	0.29	0.38	0.38	0.31	0.45	0.27	0.29	0.31	0.40
SiO_2	53.10	51.66	51.51	51.68	51.33	50.54	50.13	51.72	51.72	52.29	52.15	52.23	51.52	51.84	52.86	52.23	52.01	53.41
Al_2O_3	0.64	2.15	1.92	1.67	1.57	1.98	1.55	2.28	2.23	1.86	1.41	2.15	1.88	2.20	1.68	1.47	1.69	1.93
MgO	13.48	13.22	13.34	13.55	12.48	12.40	13.80	14.01	14.04	14.29	12.96	14.72	13.21	13.21	14.92	13.40	14.02	15.98
Cr_2O_3	0.01	0.07	0.08	0.03	0.00	0.02	-0.01	0.06	0.04	0.13	0.03	0.50	0.09	0.06	0.09	0.01	0.08	0.27
TiO_2	0.09	0.47	0.42	0.43	0.38	0.44	0.35	0.43	0.34	0.33	0.33	0.36	0.44	0.40	0.32	0.27	0.35	0.31
CaO	22.67	21.43	21.34	22.10	21.80	20.28	17.49	21.06	21.40	21.58	21.67	21.87	21.72	20.82	21.26	21.53	19.34	18.00
NiO	0.01	0.02	0.02	0.05	0.04	0.03	0.08	0.05	0.04	0.05	0.04	0.04	0.03	0.05	0.05	0.03	0.02	0.08
FeO	9.48	10.09	10.29	9.49	11.29	12.56	13.66	9.31	9.14	8.23	10.11	7.14	9.74	9.67	7.01	9.70	10.93	8.67
MnO	0.27	0.29	0.26	0.24	0.30	0.34	0.34	0.26	0.25	0.21	0.28	0.19	0.22	0.26	0.17	0.27	0.26	0.12
Total	99.94	99.82	99.52	99.59	99.49	98.88	97.64	99.48	99.52	99.29	99.41	99.62	99.21	99.01	98.67	99.27	99.08	99.33
Cations (based on 6 oxygens)																		
Na	0.01	0.02	0.02	0.02	0.02	0.02	0.02	0.02	0.02	0.02	0.03	0.03	0.02	0.03	0.02	0.02	0.02	0.03
Si	1.99	1.94	1.94	1.95	1.95	1.94	1.94	1.94	1.94	1.96	1.97	1.94	1.95	1.96	1.98	1.97	1.96	1.98
Al	0.03	0.10	0.09	0.07	0.07	0.09	0.07	0.10	0.10	0.08	0.06	0.09	0.08	0.10	0.07	0.07	0.08	0.08
Mg	0.75	0.74	0.75	0.76	0.71	0.71	0.80	0.78	0.79	0.80	0.73	0.82	0.74	0.74	0.83	0.75	0.79	0.88
Cr	0.00	0.00	0.00	0.00	0.00	0.00	0.00	0.00	0.00	0.00	0.00	0.01	0.00	0.00	0.00	0.00	0.00	0.01
Ti	0.00	0.01	0.01	0.01	0.01	0.01	0.01	0.01	0.01	0.01	0.01	0.01	0.01	0.01	0.01	0.01	0.01	0.01
Ca	0.91	0.86	0.86	0.89	0.89	0.83	0.73	0.85	0.86	0.87	0.88	0.87	0.88	0.84	0.85	0.87	0.78	0.72
Ni	0.00	0.00	0.00	0.00	0.00	0.00	0.00	0.00	0.00	0.00	0.00	0.00	0.00	0.00	0.00	0.00	0.00	0.00
Fe	0.30	0.32	0.32	0.30	0.36	0.40	0.44	0.29	0.29	0.26	0.32	0.22	0.31	0.31	0.22	0.31	0.35	0.27
Mn	0.01	0.01	0.01	0.01	0.01	0.01	0.01	0.01	0.01	0.01	0.01	0.01	0.01	0.01	0.01	0.01	0.01	0.00
Total	4.00	4.02	4.02	4.02	4.02	4.02	4.03	4.01	4.01	4.01	4.01	4.01	4.01	4.01	3.99	4.01	4.01	4.00
Mg#	71.71	70.06	69.81	71.77	66.34	63.75	64.33	72.90	73.32	75.61	69.56	78.63	70.73	70.88	79.15	71.15	70.03	76.64

MZ GN = Main Zone gabbronorite, PR mela-GN = Platreef mala-gabbronorite, PR anor = Platreef anorthosite, PR Nor = Platreef norite, PR rx GN = Platreef recrystallised gabbronorite.

Table 3a: Selected electron microprobe analyses of pentlandite on Nonnenwerth and Townlands

Table 3a cc

Sample	M0X9	M0X9	M0X9	M0X10	M0X10	M0X10	M0X10	M0X12	M0X12	M0X12	M0X12	M0X27	M0X27	M0X27	M0X27	M0X27	M0X27	M0X27	Sample
Analyses	10_F4	11_F4	12_F4	1_BSE2a	2_BSE2a	3_BSE2a	4_BSE2a	1_BSE2a	2_BSE2a	3_BSE2a	10_BSE2a	7_BSE1c	8_BSE1c	10_BSE1c	11_BSE2a	12_BSE2a	17_BSE2a	13_BSE2a	Analyses
Borehole	2121	2121	2121	2121	2121	2121	2121	2121	2121	2121	2121	2199	2199	2199	2199	2199	2199	2199	Borehole
Depth (m)	199.68	199.68	199.68	219.9	219.9	219.9	219.9	244.55	244.55	244.55	244.55	173.94	173.94	173.94	173.94	173.94	173.94	173.94	Depth (m)
Rock Type	PR rx GN	PR rx GN	PR rx GN	PR rx GN	PR rx GN	PR rx GN	PR rx GN	PR rx GN	PR rx GN	PR rx GN	PR rx GN	PR Anor	PR Anor	PR Anor	PR Anor	PR Anor	PR Anor	PR Anor	Rock Type
	Weight per cent																		
S	32.73	32.73	32.59	32.93	32.81	32.62	32.56	32.59	32.76	32.64	33.00	33.29	32.94	33.01	33.00	32.83	53.52	32.97	S
Ni	36.68	36.49	36.45	34.88	34.75	34.75	34.79	34.42	34.58	34.61	35.00	34.13	34.48	34.57	35.17	34.99	0.24	34.87	Ni
Fe	29.78	29.99	29.60	30.54	30.80	30.77	30.66	30.56	30.77	30.69	30.50	31.76	31.21	31.45	31.40	31.30	43.46	31.25	Fe
Co	0.91	0.92	0.94	1.20	1.16	1.16	1.13	1.76	1.73	1.75	1.00	1.13	1.13	1.16	0.55	0.61	2.71	0.57	Co
Cu	<0.04	<0.04	<0.04	<0.04	<0.04	<0.04	<0.04	<0.04	<0.04	<0.04	<0.04	0.286	0.221	0.110	<0.04	<0.04	<0.04	<0.04	Cu
As	<0.05	<0.05	<0.05	<0.05	<0.05	<0.05	<0.05	<0.05	<0.05	<0.05	<0.05	<0.05	<0.05	<0.05	<0.05	<0.05	<0.05	<0.05	As
Se	0.030	0.029	0.029	0.019	0.021	0.022	0.022	0.022	0.024	0.021	0.020	0.047	0.028	0.020	0.025	0.022	0.056	0.027	Se
Rh	<0.002	<0.002	<0.002	<0.002	0.0038	<0.002	<0.002	<0.002	<0.002	0.0034	<0.002	<0.002	<0.002	<0.002	<0.002	<0.002	<0.002	<0.002	Rh
Pd	0.051	0.050	0.047	0.067	0.070	0.058	0.066	0.021	0.024	0.022	0.014	0.012	0.019	0.017	0.013	0.013	<0.002	0.012	Pd
Pt	<0.003	<0.003	<0.003	<0.003	<0.003	<0.003	<0.003	<0.003	<0.003	<0.003	<0.003	<0.003	<0.003	<0.003	<0.003	<0.003	<0.003	<0.003	Pt
Ag	<0.004	<0.004	<0.004	<0.004	<0.004	<0.004	<0.004	<0.004	<0.004	<0.004	<0.004	<0.004	<0.004	<0.004	<0.004	<0.004	<0.004	<0.004	Ag
Total	100.18	100.18	99.68	99.59	99.70	99.48	99.29	99.44	99.95	99.75	99.53	100.66	99.95	100.44	100.44	100.44	100.46	100.44	Total
	Atomic concentration																		
S	46.525	46.508	46.549	46.911	46.791	46.671	46.645	46.624	46.646	46.556	47.0	46.942	46.771	46.730	46.807	46.744	66.844	46.920	S
Ni	28.468	28.312	28.430	27.139	27.063	27.146	27.216	26.889	26.890	26.958	27.2	26.282	26.728	26.720	27.239	27.205	0.166	27.098	Ni
Fe	24.297	24.463	24.271	24.980	25.216	25.273	25.217	25.098	25.149	25.133	24.9	25.712	25.436	25.557	25.569	25.578	31.159	25.527	Fe
Co	0.703	0.709	0.732	0.932	0.900	0.899	0.879	1.372	1.337	1.358	0.8	0.866	0.876	0.895	0.427	0.471	1.843	0.439	Co
Cu	0.023	0.004	0.002	-0.003	0.014	0.004	-0.002	0.013	-0.010	-0.004		0.203	0.158	0.078	-0.003	-0.004	-0.004	-0.005	Cu
Se	0.018	0.017	0.017	0.011	0.012	0.013	0.013	0.013	0.014	0.012	0.011	0.027	0.016	0.012	0.014	0.013	0.032	0.015	Se
Pd	0.022	0.021	0.020	0.029	0.030	0.025	0.028	0.009	0.010	0.009	0.006	0.005	0.008	0.007	0.005	0.006	0.000	0.005	Pd

Detection limits : 20 ppm (Rh, Pd), 35 ppm (Se, Pt), 45 ppm (Ag), 300 ppm (S), 330 ppm (Co), 370 ppm (Cu), 510 ppm (As), 640 ppm (Ni), 900 ppm (Fe)

Detection lir

MOX = Nonnenwerth samples and P = Townlands samples, MP GN = Middle Platreef gabbronorite, PR Anor = Platreef anorthosite, PR rx GN = Platreef recrystallised gabbronorite

MOX = Nor

ontd: Selected electron microprobe analyses of pentlandite on Nonnenwerth and Townlands

M0X27 14_BSE2a 2199 173.94 PR Anor	M0X27 15_BSE2a 2199 173.94 PR Anor	M0X27 18_BSE2a 2199 173.94 PR Anor	M0X27 19_BSE3a 2199 173.94 PR Anor	M0X27 20_BSE3a 2199 173.94 PR Anor	M0X27 23_BSE3a 2199 173.94 PR Anor	M0X27 24_BSE3a 2199 173.94 PR Anor	M0X27 25_BSE3a 2199 173.94 PR Anor	M0X27 26_F4 2199 173.94 PR Anor	P13 8_BSE1b TL1-03 80.75 MP GN	P13 9_BSE4b TL1-03 80.75 MP GN	P13 10_BSE4b TL1-03 80.75 MP GN	P13 11_BSE4b TL1-03 80.75 MP GN
Weight per cent												
32.95	38.89	53.59	39.19	39.07	33.07	33.09	33.04	33.10	32.89	32.79	32.88	32.74
35.01	0.49	0.09	0.34	0.38	34.88	34.85	35.35	35.20	36.52	36.60	36.67	36.68
31.11	60.90	46.00	61.10	60.96	31.40	31.58	31.56	31.46	29.95	29.78	29.70	29.63
0.56	-0.01	0.10	-0.01	-0.01	0.45	0.43	0.46	0.52	1.07	1.28	1.06	1.10
<0.04	<0.04	<0.04	<0.04	<0.04	<0.04	<0.04	<0.04	<0.04	0.156	<0.04	0.138	0.086
<0.05	<0.05	<0.05	<0.05	<0.05	<0.05	<0.05	<0.05	<0.05	<0.05	<0.05	<0.05	<0.05
0.020	0.031	0.054	0.030	0.029	0.018	0.018	0.022	0.018	0.007	0.008	0.009	0.007
<0.002	<0.002	<0.002	<0.002	<0.002	<0.002	<0.002	<0.002	<0.002	<0.002	<0.002	<0.002	<0.002
0.007	<0.002	<0.002	<0.002	<0.002	0.018	0.021	0.022	0.009	<0.002	<0.002	<0.002	<0.002
<0.003	<0.003	<0.003	<0.003	<0.003	<0.003	<0.003	<0.003	<0.003	<0.003	<0.003	<0.003	<0.003
<0.004	<0.004	<0.004	<0.004	<0.004	<0.004	<0.004	<0.004	<0.004	<0.004	<0.004	<0.004	<0.004
100.43	100.43	100.46	100.43	100.43	100.44	100.44	100.45	100.43	100.71	100.51	100.51	100.21
Atomic concentration												
46.909	52.469	66.889	52.631	52.590	46.966	46.926	46.719	46.837	46.518	46.475	46.570	46.482
27.219	0.361	0.058	0.247	0.279	27.049	26.981	27.292	27.196	28.204	28.329	28.358	28.435
25.422	47.166	32.963	47.106	47.106	25.606	25.709	25.615	25.556	24.319	24.226	24.147	24.150
0.434	-0.008	0.065	-0.008	-0.007	0.348	0.333	0.351	0.400	0.821	0.984	0.819	0.849
-0.004	0.003	0.005	0.012	0.005	0.018	0.022	0.001	0.007	0.111	0.005	0.099	0.061
0.012	0.018	0.031	0.017	0.017	0.010	0.011	0.013	0.010	0.004	0.005	0.005	0.004
0.003	0.000	0.000	0.000	0.000	0.008	0.009	0.010	0.004	0.000	0.000	0.000	0.000

nits : 20 ppm (Rh, Pd), 35 ppm (Se, Pt), 45 ppm (Ag), 300 ppm (S), 330 ppm (Co), 370 ppm (Cu), 510 ppm (As), 640 ppm (Ni), 900 ppm (Fe)
nnenwerth samples and P = Townlands samples, MP GN = Middle Platreef gabbronorite, PR Anor = Platreef anorthosite, PR rx GN = Platreef recrystallised gabbronorite

Table 3b: Selected electron microprobe analyses of pyrrhotite on Nonnenwerth and Townlands

Sample	M0X10	M0X10	M0X10	M0X12	M0X12	M0X12	M0X27	M0X27	M0X29	M0X29	M0X29	P13	P13	P13	P13	P15
Analysis	5_BSE2a	6_BSE2a	7_BSE2a	4_BSE2a	5_BSE2a	6_BSE2a	16_BSE2a	27_F4	11_F1	12_BSE3b	13_F3	6_BSE1b	7_BSE1b	12_BSE4b	13_BSE4b	28_BSE3e
Borehole	2121	2121	2121	2121	2121	2121	2199	2199	2199	2199	2199	TL1-03	TL1-03	TL1-03	TL1-03	TL1-03
Depth (m)	219.9	219.9	219.9	244.55	244.55	244.55	173.94	173.94	195.07	195.07	195.07	80.75	80.75	80.75	80.75	89.55
Rock Type	PR rx GN	PR rx GN	PR rx GN	PR rx GN	PR rx GN	PR rx GN	PR Anor	PR Anor	PR Gabbro	PR Gabbro	PR Gabbro	MP GN	MP GN	MP GN	MP GN	MP GN
	Weight per cent															
S	38.45	38.45	38.49	38.51	38.79	38.75	38.88	39.04	37.89	37.50	37.61	38.66	38.71	38.71	38.67	38.35
Ni	0.46	0.49	0.52	0.49	0.48	0.42	0.49	0.41	0.12	0.35	0.18	0.93	0.87	0.91	0.91	0.13
Fe	61.10	60.75	60.81	61.26	61.26	61.11	60.98	60.75	61.57	61.87	62.04	60.52	60.55	60.66	60.62	61.98
Co	<0.03	<0.03	<0.03	<0.03	<0.03	<0.03	<0.03	<0.03	<0.03	<0.03	<0.03	<0.03	<0.03	<0.03	<0.03	0.033
Cu	<0.04	<0.04	<0.04	<0.04	<0.04	<0.04	<0.04	<0.04	<0.04	<0.04	0.246	<0.04	<0.04	<0.04	<0.04	0.122
As	<0.05	<0.05	<0.05	<0.05	<0.05	<0.05	<0.05	<0.05	<0.05	<0.05	<0.05	<0.05	<0.05	<0.05	<0.05	<0.05
Se	0.025	0.027	0.026	0.024	0.022	0.022	0.027	0.023	0.030	0.031	0.036	0.013	0.013	0.011	0.009	0.004
Rh	<0.002	<0.002	<0.002	<0.002	<0.002	<0.002	<0.002	<0.002	<0.002	<0.002	<0.002	<0.002	<0.002	<0.002	<0.002	<0.002
Pd	<0.002	<0.002	<0.002	<0.002	<0.002	<0.002	<0.002	<0.002	<0.002	<0.002	<0.002	<0.002	<0.002	<0.002	<0.002	<0.002
Pt	<0.003	<0.003	<0.003	<0.003	<0.003	<0.003	<0.003	<0.003	<0.003	<0.003	<0.003	<0.003	<0.003	<0.003	<0.003	<0.003
Ag	<0.004	<0.004	<0.004	<0.004	<0.004	<0.004	<0.004	<0.004	<0.004	<0.004	<0.004	<0.004	<0.004	<0.004	<0.004	<0.004
Total	100.13	99.83	99.83	100.33	100.62	100.32	99.93	99.82	99.93	99.83	100.14	100.11	100.21	100.31	99.81	100.41
	Atomic concentration															
S	52.118	52.238	52.229	52.085	52.267	52.299	52.417	52.660	51.575	51.225	51.197	52.315	52.332	52.273	52.269	51.759
Ni	0.340	0.362	0.387	0.359	0.353	0.310	0.362	0.304	0.089	0.264	0.133	0.688	0.644	0.673	0.674	0.095
Fe	47.548	47.384	47.367	47.562	47.384	47.349	47.204	47.050	48.110	48.516	48.476	47.017	46.993	47.030	47.042	48.024
Cu											0.169					0.083
Se	0.014	0.015	0.014	0.013	0.012	0.012	0.015	0.013	0.016	0.017	0.020	0.007	0.007	0.006	0.005	0.002

Detection limits : 20 ppm (Rh, Pd), 35 ppm (Se, Pt), 45 ppm (Ag), 300 ppm (S), 330 ppm (Co), 370 ppm (Cu), 510 ppm (As), 640 ppm (Ni), 900 ppm (Fe)
MOX = Nonnenwerth samples and P = Townlands samples, MP GN = Middle Platreef gabbronorite, PR Anor = Platreef anorthosite, PR rx GN = Platreef recrystallised gabbronorite

Table 3c: Selected electron microprobe analyses of pyrite on Nonnenwerth and Townlands

Sample	**M0X9**	**M0X9**	**M0X9**	**M0X10**	**M0X10**	**M0X10**	**M0X10**	**M0X27**	**M0X27**	**M0X27**	**M0X27**	**M0X29**	**M0X29**	**M0X29**
Analysis	**13_BSE6a**	**14_BSE6a**	**15_BSE6a**	**16_Camera3a**	**17_Camera3a**	**18_Camera3a**	**19_Camera4a**	**5_BSE1c**	**21_BSE3a**	**22_BSE3a**	**28_F4**	**8_BSE2a**	**9_BSE2a**	**10_BSE2a**
Borehole	**2121**	**2121**	**2121**	**2121**	**2121**	**2121**	**2121**	**2199**	**2199**	**2199**	**2199**	**2199**	**2199**	**2199**
Depth (m)	**199.68**	**199.68**	**199.68**	**219.9**	**219.9**	**219.9**	**219.9**	**173.94**	**173.94**	**173.94**	**173.94**	**195.07**	**195.07**	**195.07**
Rock Type	**PR rx GN**	**PR rx GN**	**PR rx GN**	**PR rx GN**	**PR rx GN**	**PR rx GN**	**PR rx GN**	**PR Anor**	**PR Anor**	**PR Anor**	**PR Anor**	**PR Gabbro**	**PR Gabbro**	**PR Gabbro**
	Weight per cent													
S	52.80	52.81	53.21	53.40	53.40	53.40	53.40	53.47	53.64	53.63	53.66	52.74	53.22	53.27
Ni	<0.06	<0.06	0.03	<0.06	<0.06	<0.06	<0.06	0.06	1.06	<0.06	0.11	<0.06	0.08	<0.06
Fe	46.20	46.39	46.65	46.60	46.60	46.60	46.60	46.22	45.06	46.38	45.92	46.14	46.87	46.64
Co	<0.03	<0.03	<0.03	<0.03	<0.03	<0.03	<0.03	<0.03	<0.03	<0.03	0.03	<0.03	<0.03	<0.03
Cu	<0.04	<0.04	<0.04	<0.04	<0.04	<0.04	<0.04	0.220	<0.04	<0.04	<0.04	0.084	0.061	0.091
As	<0.05	<0.05	<0.05	<0.05	<0.05	<0.05	<0.05	<0.05	<0.05	<0.05	<0.05	<0.05	<0.05	<0.05
Se	0.021	0.038	0.017	0.024	0.034	0.014	0.010	0.031	0.033	0.014	0.029	0.005	<0.004	0.008
Rh	<0.002	<0.002	<0.002	<0.002	<0.002	<0.002	<0.002	<0.002	<0.002	<0.002	<0.002	<0.002	0.0023	<0.002
Pd	<0.002	<0.002	<0.002	<0.002	<0.002	<0.002	<0.002	<0.002	<0.002	<0.002	<0.002	<0.002	<0.002	<0.002
Pt	<0.003	<0.003	<0.003	<0.003	<0.003	<0.003	<0.003	<0.003	<0.003	<0.003	<0.003	<0.003	<0.003	<0.003
Ag	<0.004	<0.004	<0.004	<0.004	<0.004	<0.004	<0.004	<0.004	<0.004	<0.004	<0.004	<0.004	<0.004	<0.004
Total	99.02	99.24	99.92	100.03	100.04	100.02	100.01	100.03	99.64	99.92	99.63	98.91	100.31	100.01
	Atomic concentration													
S	66.565	66.466	66.509	66.6	66.6	66.6	66.6	66.723	66.968	66.811	66.982	66.490	66.345	66.501
Ni	0.011	-0.001	0.021	0.0	0.0	0.0	0.0	0.041	0.725	0.021	0.073	0.022	0.053	0.027
Fe	33.436	33.515	33.476	33.4	33.4	33.4	33.4	33.110	32.292	33.171	32.906	33.396	33.539	33.424
Cu								0.138				0.053	0.039	0.057
Se	0.011	0.019	0.009	0.012	0.017	0.007	0.005	0.015	0.017	0.007	0.015	0.003		0.004

Detection limits : 20 ppm (Rh, Pd), 35 ppm (Se, Pt), 45 ppm (Ag), 300 ppm (S), 330 ppm (Co), 370 ppm (Cu), 510 ppm (As), 640 ppm (Ni), 900 ppm (Fe)

MOX = Nonnenwerth samples and P = Townlands samples, MP GN = Middle Platreef gabbronorite, PR Anor = Platreef anorthosite, PR rx GN = Platreef recrystallised gabbronorite

Table 3c contd: Selected electron microprobe analyses of pyrite on Nonnenwerth and Townlands

Sample	M0X29	P7	P7	P7	P15	P15	P15	P15	P15	P15	P15	P106	P106	P106
Analysis	14_BSE6a	2_BSE1d	5_BSE1f	6_BSE1f	21_BSE1b	22_BSE2b	23_BSE2d	24_BSE3b	25_BSE4a	26_BSE4a	27_BSE5a	3_BSE1b	5_BSE1b	7_BSE2b
Borehole	2199	TL1-03	TL1-03	TL1-03	TL1-03	TL1-03	TL1-03	TL1-03	TL1-03	TL1-03	TL1-03	TL1-03	TL1-03	TL1-03
Depth (m)	195.07	57.7	57.7	57.7	89.55	89.55	89.55	89.55	89.55	89.55	89.55	106	106	106
Rock Type	PR Gabbro	UP GN	UP GN	UP GN	MP GN	MP GN	MP GN	MP GN	MP GN	MP GN	MP GN	MP GN	MP GN	MP GN
	Weight per cent													
S	51.79	53.91	53.80	53.78	53.82	53.70	53.80	54.09	53.67	53.51	53.82	52.59	53.45	53.44
Ni	0.34	0.30	0.53	0.30	0.07	0.17	0.11	0.09	0.14	0.17	0.15	1.02	<0.06	0.35
Fe	48.32	46.56	45.91	46.18	44.74	44.76	44.92	45.28	44.83	44.41	44.94	43.35	46.59	46.53
Co	<0.03	0.04	0.26	0.26	1.45	1.38	1.36	0.89	1.39	1.76	1.22	1.67	<0.03	0.07
Cu	<0.04	0.160	<0.04	<0.04	<0.04	<0.04	<0.04	<0.04	<0.04	<0.04	<0.04	2.225	<0.04	<0.04
As	<0.05	<0.05	<0.05	<0.05	<0.05	<0.05	<0.05	<0.05	<0.05	<0.05	<0.05	<0.05	<0.05	<0.05
Se	0.072	0.034	0.009	<0.004	0.024	0.045	0.022	0.008	0.015	0.010	0.023	0.006	0.010	0.025
Rh	<0.002	<0.002	<0.002	0.0024	<0.002	<0.002	<0.002	<0.002	0.0155	<0.002	<0.002	<0.002	<0.002	<0.002
Pd	<0.002	<0.002	<0.002	<0.002	<0.002	<0.002	<0.002	<0.002	0.0031	<0.002	<0.002	<0.002	<0.002	<0.002
Pt	<0.003	<0.003	0.0036	<0.003	<0.003	0.0035	<0.003	<0.003	<0.003	<0.003	<0.003	<0.003	<0.003	<0.003
Ag	<0.004	<0.004	<0.004	<0.004	<0.004	<0.004	<0.004	<0.004	<0.004	<0.004	<0.004	<0.004	<0.004	<0.004
Total	100.47	101.04	100.51	100.61	100.43	100.45	100.42	100.41	100.03	99.91	100.13	100.81	100.11	100.43
	Atomic concentration													
S	64.948	66.624	66.755	66.725	66.992	66.929	66.922	67.079	66.884	66.846	66.977	65.669	66.644	66.479
Ni	0.232	0.204	0.361	0.206	0.045	0.114	0.076	0.059	0.095	0.113	0.099	0.697	0.008	0.239
Fe	34.782	33.035	32.698	32.892	31.968	32.023	32.075	32.238	32.074	31.845	32.106	31.075	33.346	33.225
Cu		0.100										1.402		
Se		0.017	0.005		0.014	0.026	0.013	0.004	0.008	0.005	0.012	0.003	0.005	0.012

Detection limits : 20 ppm (Rh, Pd), 35 ppm (Se, Pt), 45 ppm (Ag), 300 ppm (S), 330 ppm (Co), 370 ppm (Cu), 510 ppm (As), 640 ppm (Ni), 900 ppm (Fe)

MOX = Nonnenwerth samples and P = Townlands samples, MP GN = Middle Platreef gabbronorite, PR Anor = Platreef anorthosite, PR rx GN = Platreef recrystallised gabbronorite

Table 3d: Electron microprobe analyses of chalcopyrite on Nonnenwerth

Sample	**M0X10**	**M0X10**
Analysis	**14_BSE2a**	**15_BSE2a**
Borehole	**2121**	**2121**
Depth (m)	**219.9**	**219.9**
Rock Type	**PR rx GN**	**PR rx GN**
	Weight per cent	
S	34.90	34.90
Ni	<0.06	<0.06
Fe	30.40	30.40
Co	<0.03	<0.03
Cu	34.60	34.60
As	<0.05	<0.05
Se	0.018	0.017
Rh	<0.002	<0.002
Pd	<0.002	<0.002
Pt	<0.003	<0.003
Total	99.92	99.92
	Atomic concentration	
S	49.997	49.996
Fe	25.001	25.001
Cu	25.007	25.007
Se	0.0106	0.0101

Detection limits : 20 ppm (Rh, Pd), 35 ppm (Se, Pt), 45 ppm (Ag), 300 ppm (S), 330 ppm (Co), 370 ppm (Cu), 510 ppm (As), 640 ppm (Ni), 900 ppm (Fe)
MOX = Nonnenwerth samples, PR rx GN = Platreef recrystallised gabbronorite

Table 4: Cr-bearing magnetites Analyses on samples from Nonnenwerth

Sample	MO26						MO27	
Analysis	1	2	3	4	5	6	1	2
Borehole	2199	2199	2199	2199	2199	2199	2199	2199
depth (m)	338.85	338.85	338.85	338.85	338.85	338.85	342.81	342.81
Rock Type	Peridotite	Peridotite	Peridotite	Peridotite	Peridotite	Peridotite	PR mela-GN	PR mela-GN
wt. %								
MgO	1.24	1.49	1.34	1.26	2.91	1.80	1.89	1.26
Al2O3	5.84	5.87	5.12	4.81	6.49	5.94	5.60	4.29
SiO2	0.04	0.02	0.03	0.03	0.04	0.02	0.02	0.03
TiO2	6.37	2.11	2.18	2.89	5.19	6.12	1.88	0.22
Cr2O3	12.43	12.15	11.53	11.44	13.61	11.78	26.30	18.69
MnO	1.09	0.26	0.20	0.26	0.40	0.51	0.26	0.23
Fe2O3	36.58	45.65	46.83	45.87	38.41	38.43	31.90	43.88
FeO	34.74	31.35	31.62	32.30	32.28	34.42	30.52	29.72
ZnO	0.16	0.10	0.07	0.05	0.06	0.05	0.08	0.12
Total	98.47	98.99	98.90	98.89	99.37	99.07	98.45	98.43
Cations (based on 32 oxygens)								
Si	0.01	0.01	0.01	0.01	0.01	0.01	0.01	0.01
Ti	1.42	0.47	0.49	0.65	1.13	1.35	0.42	0.05
Al	2.04	2.04	1.79	1.69	2.21	2.05	1.94	1.51
Cr	2.91	2.84	2.71	2.69	3.11	2.73	6.13	4.43
Fe3+	8.19	10.17	10.50	10.31	8.39	8.50	7.08	9.94
Fe2+	8.58	7.73	7.84	8.02	7.78	8.43	7.51	7.41
Mn	0.27	0.07	0.05	0.07	0.10	0.13	0.06	0.06
Mg	0.55	0.66	0.59	0.56	1.25	0.79	0.83	0.56
Zn	0.03	0.02	0.01	0.01	0.01	0.01	0.02	0.03
Al#	41.2	41.9	39.8	38.5	41.6	42.9	24.1	25.5
Mg#	6.0	7.8	7.0	6.5	13.9	8.6	9.9	7.0

PR mela-GN = Platreef mela-gabbronorite, peridotite = serpentinized peridotite.
Al# = 100*Al/(Cr+Al); Mg-no. = 100Mg/(Mg+Fe^{2+})

Table 6a. Composition (wt. %) of PGE-bismuthotellurides, Bi- and Te-phases, Au and trace minerals in samples from Nonnenwerth

	kotulskite										moncheite							
Sample	**MOX9**	**MOX9**	**MOX9**	**MOX9**	**MOX9**	**MOX9**	**MOX9**	**MOX10**	**MOX29**	**MOX29**	**MOX9**	**MOX9**	**MOX9**	**MOX9**	**MOX9**	**MOX9**	**MOX9**	**MOX9**
Analysis	**1_BSE1a**	**3_BSE1a**	**4_BSE2a**	**16_BSE7a**	**22_BSE9c**	**23_BSE10b**	**26_BSE14a**	**10_BSE1c**	**1_BSE1a**	**1b_BSE1a**	**5_BSE2b**	**6_BSE2b**	**7_BSE3b**	**8_BSE3b**	**9_BSE3b**	**21_BSE9b**	**25_BSE14a**	**27_BSE15b**
Borehole	**2121**	**2121**	**2121**	**2121**	**2121**	**2121**	**2121**	**2121**	**2199**	**2199**	**2121**	**2121**	**2121**	**2121**	**2121**	**2121**	**2121**	**2121**
Depth (m)	**199.68**	**199.68**	**199.68**	**199.68**	**199.68**	**199.68**	**199.68**	**219.9**	**195.07**	**195.07**	**199.68**	**199.68**	**199.68**	**199.68**	**199.68**	**199.68**	**199.68**	**199.68**
Lithology	**Rx Gn**	**Rx Gn**	**Rx Gn**	**Rx Gn**	**Rx Gn**	**Rx Gn**	**Rx Gn**	**Rx Gn**	**Anor**	**Anor**	**Rx Gn**	**Rx Gn**	**Rx Gn**	**Rx Gn**	**Rx Gn**	**Rx Gn**	**Rx Gn**	**Rx Gn**
	Weight per cent																	
S	0.01	0.02	0.01	-	-	-	0.01	-	0.14	0.17	0.04	0.03	0.02	0.03	0.03	0.04	0.03	0.05
Fe	0.44	0.47	0.57	0.48	0.67	0.17	0.26	0.31	1.92	1.95	0.24	0.25	0.36	0.40	0.37	0.56	0.34	1.64
Co	0.01	-	0.01	0.03	0.01	-	-	0.03	0.02	0.01	0.01	0.01	-	-	0.01	-	-	0.02
Ni	-	0.01	0.02	0.03	-	0.02	0.04	0.03	0.02	-	0.03	0.04	0.07	0.07	0.06	0.02	0.11	0.05
Cu	0.65	0.69	0.08	0.19	0.04	0.02	0.12	0.07	2.39	2.47	0.05	0.01	0.09	0.25	0.56	0.14	0.08	0.20
As	-	-	-	-	-	-	0.03	-	-	-	0.03	-	-	-	-	-	-	-
Se	0.01	0.01	-	-0.02	0.01	0.05	-	-	0.03	-	-	-	-	0.02	0.02	0.06	0.03	0.02
Ru	-	-	-	-	-	-	-	-	-	-	-	-	-	-	-	-	-	-
Rh	-	-	-	-	-	-	-	-	-	-	0.15	0.08	0.06	0.05	0.10	0.12	0.04	0.10
Pd	44.57	44.41	43.23	43.98	43.70	44.02	44.45	43.25	42.95	42.81	2.14	2.19	11.44	11.56	10.98	2.05	12.32	2.69
Ag	0.19	0.21	0.26	0.17	0.17	0.13	0.20	0.28	0.24	0.30	0.03	0.05	0.05	0.04	-	0.12	0.07	0.07
Sn	0.01	0.01	-	-	-	0.02	-	-	0.01	-	0.02	-	0.01	-	-	0.02	0.01	-
Sb	0.16	0.18	0.17	0.21	0.21	0.28	0.32	0.17	0.15	0.13	0.45	0.51	0.54	0.44	0.50	0.51	0.48	0.46
Te	51.08	50.73	45.92	47.31	50.54	50.59	52.67	44.55	41.87	41.84	58.10	56.60	61.48	62.07	62.58	57.52	63.10	56.49
Os	0.13	0.16	0.20	0.17	0.04	0.06	0.06	0.23	0.25	0.24	0.18	0.23	0.19	0.10	0.09	0.21	0.21	0.29
Ir	0.30	0.35	0.29	0.42	0.19	0.34	0.37	0.33	0.33	0.40	0.40	0.36	0.29	0.43	0.52	0.42	0.23	0.38
Pt	-	-	0.30	0.03	0.21	0.22	0.10	0.48	0.30	0.31	38.93	38.96	25.22	25.70	26.22	37.33	23.78	36.18
Au	0.01	-	-	-	-	-	-	-	-	-	-	-	-	-	-	-	-	-
Hg	-	-	-	-	-	-	-	-	-	-	-	-	-	-	-	-	-	-
Pb	-	-	-	-	-	-	-	-	-	-	-	-	-	-	-	-	-	-
Bi	6.01	6.25	12.62	8.05	4.47	6.30	3.88	14.14	17.14	17.32	1.91	3.51	1.91	1.86	1.27	1.75	0.99	3.06
Total	103.61	103.53	103.71	101.25	100.83	102.35	102.62	103.91	107.79	107.96	102.71	102.84	101.74	103.03	103.34	100.99	101.85	101.87
	Atomic concentration																	
S	0.05	0.07	0.03	-	-	-	0.03	-	0.49	0.58	0.19	0.13	0.08	0.11	0.10	0.17	0.13	0.21
Fe	0.91	0.97	1.21	1.02	1.40	0.36	0.54	0.67	3.85	3.90	0.63	0.64	0.86	0.94	0.88	1.43	0.80	4.11
Co	0.02	-	0.02	0.05	0.02	-	-	0.07	0.04	0.02	0.02	0.01	-	-	0.02	-	0.01	0.06
Ni	-	0.02	0.05	0.07	-	0.03	0.09	0.06	0.04	-	0.07	0.09	0.15	0.15	0.13	0.05	0.25	0.11
Cu	1.18	1.25	0.16	0.36	0.08	0.04	0.21	0.14	4.21	4.35	0.10	0.03	0.19	0.52	1.16	0.31	0.16	0.44
As	-	-	-	-	-	-	0.05	-	-	-	0.06	-	-	-	-	-	-	-
Se	0.02	-	-	-	0.02	0.07	-	-	0.04	-	-	0.01	-	0.03	0.03	0.11	0.06	0.03
Ru	-	-	-	-	-	-	-	-	-	-	-	-	-	-	-	-	-	-
Rh	-	-	-	-	-	-	-	-	-	-	0.21	0.11	0.08	0.07	0.13	0.17	0.05	0.13
Pd	48.19	48.12	48.20	48.98	47.58	48.54	48.32	48.66	45.18	44.99	2.89	2.97	14.45	14.41	13.61	2.77	15.37	3.54
Ag	0.21	0.22	0.28	0.19	0.18	0.14	0.22	0.31	0.25	0.31	0.04	0.06	0.06	0.04	-	0.16	0.08	0.09
Sn	0.01	0.01	-	-	-	0.02	-	-	0.01	-	0.02	-	0.01	-	-	0.03	0.01	-
Sb	0.15	0.17	0.16	0.20	0.20	0.27	0.30	0.17	0.14	0.12	0.53	0.60	0.60	0.48	0.54	0.60	0.53	0.53
Te	46.06	45.83	42.68	43.93	45.88	46.52	47.75	41.79	36.73	36.66	65.27	63.99	64.76	64.54	64.65	64.83	65.64	61.92
Os	0.08	0.10	0.13	0.10	0.03	0.04	0.03	0.14	0.15	0.14	0.13	0.17	0.13	0.07	0.06	0.16	0.14	0.21
Ir	0.18	0.21	0.18	0.26	0.12	0.21	0.22	0.21	0.19	0.23	0.30	0.27	0.21	0.30	0.36	0.31	0.16	0.28
Pt	-	-	0.18	0.02	0.12	0.13	0.06	0.29	0.17	0.18	28.60	28.81	17.38	17.48	17.72	27.52	16.18	25.94
Au	0.01	0.00	-	-	-	-	-	-	-	-	-	-	-	-	-	-	-	-
Hg	-	-	-	-	-	-	-	-	-	-	-	-	-	-	-	-	-	-
Pb	-	-	-	-	-	-	-	-	-	-	-	-	-	-	-	-	-	-
Bi	3.31	3.45	7.16	4.56	2.48	3.54	2.15	8.10	9.18	9.27	1.31	2.42	1.23	1.18	0.80	1.20	0.63	2.05
Total	100.42	100.52	100.55	100.47	100.40	100.46	100.40	100.78	100.71	100.76	100.42	100.41	100.25	100.46	100.28	100.47	100.39	100.52

Rx GN = recystallised gabbronorite, Anor = anorthosite
- = below detection limit

Table 6a. Contd: Composition (wt. %) of PGE-bismuthotellurides, Bi- and Te-complexes, Au and trace minerals in samples from Nonnenwerth

				merenskyite			merenskyite								gold				
MOX10 8_BSE1c 2121 219.9 Rx Gn	MOX10 9_BSE1c 2121 219.9 Rx Gn	Sample Analysis Borehole Depth (m) Lithology	MOX27 1_BSE1b 2199 173.94 Anor	MOX27 2_BSE1b 2199 173.94 Anor	MOX27 4_BSE2a 2199 173.94 Anor	MOX29 2_BSE2c 2199 195.07 Anor	MOX29 3_BSE2d 2199 195.07 Anor	MOX29 4_BSE2d 2199 195.07 Anor	MOX29 5_BSE2d 2199 195.07 Anor	MOX29 6_BSE3c 2199 195.07 Anor	MOX29 7_BSE4b 2199 195.07 Anor	MOX29 17_BSE8a 2199 195.07 Anor	MOX29 18_BSE9a 2199 195.07 Anor	MOX29 19_BSE10a 2199 195.07 Anor	MOX9 18_BSE8a 2121 199.68 Rx Gn	MOX9 19_BSE11a 2121 199.68 Rx Gn	MOX9 20_BSE13b 2121 199.68 Rx Gn	MOX12 7_BSE3b 2121 244.55 Rx Gn	MOX12 8_BSE3b 2121 244.55 Rx Gn
						Weight per cent													
0.06	0.04	**S**	0.03	0.04	0.21	0.06	0.02	0.02	0.03	2.14	0.02	0.85	7.35	5.60	5.88	0.02	0.03	0.01	0.02
0.36	0.52	**Fe**	0.93	1.04	1.59	1.05	0.68	0.30	0.45	4.60	0.37	2.36	10.80	6.24	9.09	0.18	0.86	1.48	1.68
0.02	-	**Co**	-	-	0.04	0.03	-	-	-	-	0.03	0.02	-	-	0.01	0.32	0.28	-	0.01
0.01	0.01	**Ni**	0.37	0.11	1.97	0.06	0.08	0.19	0.10	0.03	0.03	0.03	0.10	0.02	0.03	-	-	0.01	-
-	0.02	**Cu**	0.35	0.46	0.01	1.13	0.67	0.34	0.41	0.95	0.56	2.92	10.78	5.49	6.59	-	1.12	0.06	0.01
0.03	-	**As**	-	-	-	-	-	-	-	-	-	-	-	-	-	-	-	0.03	-
0.04	0.01	**Se**	-	-	0.01	-	-	-	-	0.03	0.01	-	-	0.06	0.01	0.04	0.03	-	0.02
0.02	0.01	**Ru**	-	-	-	-	-	-	-	-	-	-	-	-	-	-	-	-	-
0.13	0.18	**Rh**	0.06	0.11	-	-	-	-	-	-	-	-	-	0.02	-	-	-	-	-
1.38	1.36	**Pd**	6.12	18.62	28.28	19.17	28.48	26.03	28.59	16.14	20.90	18.34	9.80	14.56	-	-	-	0.51	0.45
0.05	0.10	**Ag**	0.18	0.09	0.15	0.10	0.26	0.28	0.23	0.10	0.19	0.14	0.15	0.09	24.29	0.78	1.54	12.95	13.26
-	-	**Sn**	0.03	0.01	-	0.02	-	-	0.03	0.01	-	0.01	-	-	-	-	-	0.01	0.02
0.46	0.51	**Sb**	0.77	0.38	0.35	0.56	0.26	0.31	0.36	0.43	0.44	0.36	0.18	0.45	-	0.08	0.08	-	-
58.77	58.25	**Te**	53.85	60.56	63.32	59.43	58.42	58.60	58.98	57.92	60.09	59.77	34.73	51.34	0.04	-	-	0.02	0.02
0.25	0.21	**Os**	0.32	0.21	0.13	0.23	0.31	0.21	0.25	0.21	0.22	0.15	0.09	0.23	0.09	-	0.04	0.02	0.04
0.44	0.27	**Ir**	0.48	0.43	0.34	0.19	0.42	0.13	0.42	0.38	0.28	0.38	0.35	0.40	0.29	0.35	0.36	0.31	0.43
40.22	40.27	**Pt**	31.51	14.04	0.49	14.19	0.36	3.30	0.39	16.56	11.47	14.51	10.99	16.09	-	-	-	-	-
-	-	**Au**	-	-	-	-	-	-	-	-	-	-	-	-	50.79	89.98	92.11	84.67	82.11
-	-	**Hg**	-	-	-	-	-	-	-	-	-	-	-	-	-	-	-	-	-
-	-	**Pb**	-	-	-	-	-	-	-	-	-	-	-	-	-	-	-	-	-
0.64	0.94	**Bi**	8.81	7.31	8.85	9.12	14.99	13.89	14.52	6.47	9.14	7.13	2.20	5.76	0.06	-	-	0.13	0.12
102.85	102.68	**Total**	103.81	103.44	105.75	105.35	104.97	103.63	104.81	105.98	103.84	106.99	88.28	106.37	98.97	92.32	96.61	100.24	98.23
						Atomic concentration													
0.26	0.16	**S**	0.14	0.14	0.76	0.23	0.07	0.09	0.12	7.48	0.08	3.06	21.75	17.00	18.43	0.12	0.20	0.06	0.11
0.91	1.33	**Fe**	2.31	2.35	3.24	2.32	1.48	0.67	0.98	9.25	0.83	4.86	18.34	10.86	16.35	0.67	2.96	4.55	5.21
0.04	-	**Co**	-	-	0.08	0.06	0.01	0.01	0.01	-	0.07	0.03	-	-	0.02	1.09	0.91	-	0.02
0.01	0.03	**Ni**	0.88	0.23	3.81	0.13	0.16	0.41	0.20	0.06	0.06	0.05	0.16	0.04	0.05	-	0.01	0.03	-
-	0.05	**Cu**	0.77	0.91	0.01	2.21	1.27	0.66	0.79	1.69	1.11	5.29	16.09	8.40	10.41	-	3.38	0.16	0.04
0.06	-	**As**	-	-	-	-	-	-	-	-	0.12	-	-	-	-	-	-	0.07	-
0.07	0.01	**Se**	-	-	0.01	-	-	-	-	0.05	0.01	-	-	0.08	0.01	0.09	0.08	-	0.04
0.02	0.01	**Ru**	-	-	-	-	-	-	-	-	-	-	-	-	-	-	-	-	-
0.18	0.24	**Rh**	0.08	0.14	-	-	-	-	-	-	-	-	-	0.02	-	-	-	-	-
1.85	1.83	**Pd**	7.98	22.10	30.24	22.35	32.38	30.39	32.60	17.03	24.77	19.85	8.73	13.31	-	-	-	0.82	0.74
0.07	0.13	**Ag**	0.23	0.10	0.16	0.11	0.29	0.32	0.26	0.11	0.22	0.15	0.13	0.08	22.61	1.47	2.73	20.55	21.33
-	-	**Sn**	0.03	0.01	-	0.02	-	-	0.03	0.01	-	0.01	-	-	-	-	-	0.01	0.03
0.54	0.60	**Sb**	0.87	0.40	0.33	0.57	0.25	0.31	0.35	0.39	0.46	0.35	0.14	0.36	-	0.13	0.13	-	-
65.87	65.39	**Te**	58.56	59.93	56.46	57.76	55.38	57.05	56.08	50.96	59.37	53.95	25.81	39.12	0.03	-	-	0.02	0.03
0.19	0.16	**Os**	0.23	0.14	0.08	0.15	0.20	0.14	0.16	0.13	0.15	0.09	0.04	0.12	0.05	-	0.04	0.01	0.03
0.32	0.20	**Ir**	0.35	0.28	0.20	0.12	0.26	0.09	0.26	0.22	0.19	0.23	0.17	0.20	0.15	0.38	0.36	0.28	0.38
29.48	29.57	**Pt**	22.41	9.09	0.29	9.02	0.22	2.10	0.24	9.53	7.41	8.57	5.34	8.02	-	-	-	-	-
-	-	**Au**	-	-	-	-	-	-	-	-	-	-	-	-	25.90	93.16	89.64	73.61	72.29
-	-	**Hg**	-	-	-	-	-	-	-	-	-	-	-	-	-	-	-	-	-
-	-	**Pb**	-	-	-	-	-	-	-	-	-	-	-	-	-	-	-	-	-
0.44	0.64	**Bi**	5.85	4.42	4.82	5.41	8.68	8.25	8.43	3.47	5.52	3.93	1.00	2.68	0.03	-	-	0.10	0.10
100.32	100.40	**Total**	100.76	100.43	100.51	100.53	100.77	100.57	100.67	100.43	100.41	100.52	100.26	100.31	100.46	101.30	101.41	100.53	100.64

Rx GN = recystallised gabbronorite, Anor = anorthosite
- = below detection limit

Table 6a. Contd: Composition (wt. %) of PGE-bismuthotellurides, Bi- and Te-complexes, Au and trace minerals in samples from Nonnenwerth

	braggite				sperrylite	hessite	Ag-pentla-ite	bismuth?
MOX12	MOX10	MOX10	Sample	MOX10	MOX9	MOX9	MOX27	MOX9
9_BSE3c	11_BSE2b	12_BSE2b	Analysis	13_BSE2b	17_BSE7a	2_BSE1a	3_BSE1c	24_BSE12a
2121	2121	2121	Borehole	2121	2121	2121	2199	2121
244.55	219.9	219.9	Depth (m)	219.9	199.68	199.68	173.94	199.68
Rx Gn	Rx Gn	Rx Gn	Lithology	Rx Gn	Rx Gn	Rx Gn	Anor	Rx Gn
0.01	18.25	21.57	**S**	19.23	1.17	0.10	31.31	0.02
1.73	2.64	1.49	**Fe**	1.71	0.76	0.51	36.23	0.12
0.01	0.02	0.03	**Co**	0.03	0.02	-	-	0.03
0.05	7.09	7.36	**Ni**	6.88	0.06	0.02	20.56	-
0.16	0.01	0.01	**Cu**	0.07	0.23	0.74	1.25	-
-	0.01	-	**As**	-	39.45	-	0.02	-
-	0.01	0.06	**Se**	0.04	0.53	0.03	-	0.01
-	-	-	**Ru**	-	-	-	-	-
-	0.25	0.01	**Rh**	0.18	0.29	-	-	-
0.87	13.39	46.04	**Pd**	25.43	1.44	4.19	-	-
15.20	0.03	0.12	**Ag**	0.11	0.07	56.68	12.55	0.93
-	-	0.03	**Sn**	-	0.54	-	0.02	-
-	-	-	**Sb**	-	0.13	0.22	-	0.02
0.03	-	-	**Te**	-	2.93	43.85	-	-
-	0.20	0.14	**Os**	0.22	0.23	0.08	-	1.11
0.38	0.47	0.35	**Ir**	0.37	0.29	0.20	0.17	0.22
-	60.94	25.08	**Pt**	46.94	52.03	0.10	-	1.49
81.56	-	-	**Au**	-	-	-	-	-
-	-	-	**Hg**	-	-	-	-	-
-	-	-	**Pb**	-	-	-	-	-
0.04	0.04	0.10	**Bi**	0.08	0.37	0.48	0.09	84.85
100.11	103.35	102.40	**Total**	101.28	100.69	107.24	102.28	91.94
0.07	48.31	48.50	**S**	48.71	4.02	0.34	46.17	0.09
5.18	4.02	1.92	**Fe**	2.48	1.50	0.98	30.67	0.40
0.01	0.02	0.04	**Co**	0.04	0.03	-	-	0.11
0.15	10.25	9.03	**Ni**	9.52	0.11	0.04	16.56	-
0.42	0.01	0.01	**Cu**	0.09	0.40	1.24	0.93	-
-	0.01	-	**As**	-	57.94	-	0.01	-
-	0.02	0.05	**Se**	0.04	0.74	0.04	-	0.02
-	-	-	**Ru**	-	-	-	-	-
-	0.21	0.01	**Rh**	0.14	0.31	-	-	-
1.37	10.68	31.18	**Pd**	19.41	1.48	4.19	-	-
23.52	0.02	0.08	**Ag**	0.08	0.07	55.94	5.50	1.65
-	-	0.02	**Sn**	-	0.50	-	0.01	-
-	-	-	**Sb**	-	0.12	0.19	-	0.04
0.04	-	-	**Te**	-	2.53	36.58	-	-
-	0.09	0.05	**Os**	0.09	0.13	0.04	-	1.12
0.33	0.21	0.13	**Ir**	0.15	0.17	0.11	0.04	0.22
-	26.52	9.26	**Pt**	19.54	29.34	0.05	-	1.46
69.09	-	-	**Au**	-	-	-	-	-
-	-	-	**Hg**	-	-	-	-	-
-	-	-	**Pb**	-	-	-	-	-
0.03	0.02	0.04	**Bi**	0.03	0.20	0.25	0.02	77.49
100.60	100.38	100.34	**Total**	100.36	100.18	100.19	100.03	103.93

Rx GN = recystallised gabbronorite, Anor = anorthosite
- = below detection limit

Table 6b. Composition (wt. %) of PGE-bismuthotellurides, Bi- a- Te-phases, Au a- trace minerals in samples from Townlands

	merenskyite											isomertieite	michenerite	sperrylite	altaite	kotulskite			Fe emplectite?	
Sample	**P13**	**P13**	**P15**	**P15**	**P15**	**P15**	**P15**	**P15**	**P15**	**P106**	**P106**	**P7**	**P13**	**P13**	**P13**	**P106**	**P106**	**P106**	**P15**	**P15**
Analysis	**2_BSE2b**	**3_BSE2b**	**1_BSE1b**	**2_BSE1d**	**3_BSE1a**	**4_BSE2b**	**5_BSE2b**	**6_BSE2a**	**17_BSE4b**	**9_BSE3b**	**12_BSE5a**	**1_BSE1e**	**1_BSE2b**	**4_BSE4c**	**5_BSE3c**	**14_BSE6a**	**15_BSE7a**	**1_BSE2c**	**7_BSE2g**	**8_BSE2g**
Borehole	**TL1-03**	**TL1-03**	**TL1-03**	**TL1-03**	**TL1-03**	**TL1-03**	**TL1-03**	**TL1-03**	**TL1-03**	**TL1-03**	**TL1-03**	**TL1-03**	**TL1-03**	**TL1-03**	**TL1-03**	**TL1-03**	**TL1-03**	**TL1-03**	**TL1-03**	**TL1-03**
Depth (m)	**80.75**	**80.75**	**89.55**	**89.55**	**89.55**	**89.55**	**89.55**	**89.55**	**89.55**	**106**	**106**	**57.7**	**80.75**	**80.75**	**80.75**	**106**	**106**	**106**	**89.55**	**89.55**
Lithology	**MP**	**MP**	**MP**	**MP**	**MP**	**MP**	**MP**	**MP**	**MP**	**MP**	**MP**	**UP**	**MP**	**MP**	**MP**	**MP**	**MP**	**MP**	**MP**	**MP**
	Weight per cent																			
S	0.18	0.09	0.62	0.12	1.04	0.29	0.27	0.21	0.05	0.05	0.09	0.14	0.03	0.62	1.08	0.08	0.27	1.26	18.54	18.31
Fe	2.35	2.24	2.59	1.87	3.44	2.17	2.51	1.84	1.62	0.11	5.10	1.46	1.52	2.36	2.79	0.09	1.90	2.92	16.65	16.35
Co	-	-	0.05	0.06	0.08	0.08	0.09	0.09	0.06	0.01	-	-	-	-	-	-	-	0.07	0.10	0.03
Ni	0.02	0.05	0.06	0.05	-	0.35	0.37	0.14	0.01	3.72	1.89	0.02	-	0.05	0.01	3.58	0.10	0.04	0.39	0.35
Cu	1.18	0.88	-	0.01	-	-	-	-	0.01	0.01	-	1.52	0.91	0.12	0.05	0.03	2.42	0.02	0.02	-
As	-	-	-	-	-	-	-	-	-	-	0.03	8.93	-	41.54	-	-	-	0.01	-	-
Se	0.01	-	0.03	0.01	0.04	0.01	0.09	0.01	0.04	0.02	0.05	0.06	0.06	0.20	0.06	0.03	-	-	0.14	0.14
Ru	-	-	-	-	-	-	-	-	-	-	-	-	-	0.04	-	-	-	-	-	-
Rh	-	-	-	-	-	-	-	-	-	-	-	-	-	0.33	-	-	-	-	-	-
Pd	18.85	19.52	26.57	37.30	26.76	17.48	16.49	25.14	25.96	42.67	19.79	73.31	23.43	0.02	-	43.07	41.23	43.79	-	-
Ag	0.20	0.23	0.21	0.38	0.29	0.15	0.18	0.17	0.46	0.22	0.12	0.91	0.60	0.04	-	0.18	0.26	0.08	0.71	0.61
Sn	0.01	-	-	-	-	0.01	0.01	-	0.01	-	-	0.08	-	-	-	-	-	-	-	-
Sb	0.36	0.32	0.26	0.21	0.23	0.44	0.42	0.32	0.21	0.39	0.34	14.46	0.23	0.62	0.26	0.66	0.64	2.06	0.10	0.08
Te	52.96	54.03	49.15	36.16	50.36	59.02	58.64	54.63	37.14	44.88	57.11	0.83	32.55	0.59	36.80	45.70	44.96	47.07	0.01	-
Os	0.29	0.26	0.40	0.42	0.36	0.21	0.25	0.26	0.58	0.29	0.01	0.10	0.54	0.24	-	0.16	0.23	0.17	0.88	0.77
Ir	0.26	0.43	0.30	0.33	0.25	0.16	0.41	0.46	0.16	0.13	0.21	0.38	0.40	0.42	1.99	0.24	0.19	0.36	0.32	0.28
Pt	12.48	12.05	1.70	0.57	1.33	14.81	16.14	3.83	0.90	0.43	0.10	-	3.21	53.88	0.18	0.22	0.17	0.20	1.07	1.04
Au	-	-	-	-	-	-	-	-	-	0.04	-	-	-	-	-	-	-	-	-	-
Hg	-	-	-	-	-	-	-	-	-	-	-	-	-	-	-	-	-	-	-	-
Pb	-	-	-	-	-	-	-	-	-	-	-	-	-	-	62.02	-	-	-	-	-
Bi	15.74	15.05	24.01	28.91	22.77	8.86	8.34	18.05	40.14	14.41	1.53	0.03	42.70	0.02	0.76	12.82	14.84	7.68	58.10	59.20
Total	104.90	105.19	105.98	106.40	106.95	104.04	104.21	105.16	107.36	107.39	89.01	102.26	106.23	101.08	106.02	106.88	107.23	105.83	97.02	97.16
	Atomic concentration																			
S	0.70	0.36	2.33	0.47	3.78	1.12	1.03	0.82	0.21	0.18	0.31	0.44	0.13	2.13	4.96	0.29	0.95	4.24	49.55	49.43
Fe	5.25	5.00	5.62	4.11	7.18	4.84	5.59	4.04	3.81	0.22	10.52	2.61	3.69	4.64	7.36	0.18	3.79	5.61	25.56	25.33
Co	-	0.01	0.10	0.13	0.16	0.16	0.20	0.19	0.14	0.03	-	-	-	-	0.01	-	-	0.12	0.14	0.04
Ni	0.04	0.11	0.12	0.10	-	0.73	0.78	0.29	0.03	7.08	3.70	0.04	-	0.09	0.02	6.82	0.19	0.07	0.57	0.51
Cu	2.32	1.72	0.01	0.02	-	-	0.00	0.00	0.02	0.01	-	2.40	1.95	0.21	0.12	0.05	4.23	0.03	0.02	-
As	-	-	-	-	-	-	-	-	-	-	0.04	11.94	-	60.90	-	-	-	0.02	-	-
Se	0.02	-	0.05	0.02	0.05	0.01	0.15	0.02	0.07	0.02	0.07	0.08	0.10	0.28	0.11	0.05	-	-	0.15	0.16
Ru	-	-	-	-	-	-	-	-	-	-	-	-	-	0.04	-	-	-	-	-	-
Rh	-	-	-	-	-	-	-	-	-	-	-	-	-	0.36	-	-	-	-	-	-
Pd	22.09	22.84	30.20	43.12	29.32	20.42	19.28	28.96	32.00	44.85	21.45	69.00	29.79	0.02	-	45.27	43.15	44.21	-	-
Ag	0.23	0.27	0.24	0.43	0.31	0.18	0.21	0.20	0.55	0.23	0.13	0.84	0.76	0.04	-	0.19	0.27	0.08	0.57	0.49
Sn	0.01	-	-	-	-	0.01	0.01	-	0.01	-	-	0.07	-	-	-	-	-	-	-	-
Sb	0.37	0.33	0.26	0.21	0.22	0.45	0.43	0.32	0.22	0.36	0.33	11.90	0.26	0.56	0.32	0.60	0.58	1.82	0.07	0.06
Te	51.78	52.72	46.58	34.85	46.01	57.50	57.16	52.47	38.17	39.34	51.61	0.65	34.51	0.50	42.55	40.05	39.24	39.63	0.01	-
Os	0.19	0.17	0.26	0.27	0.22	0.14	0.16	0.17	0.40	0.17	-	0.05	0.39	0.14	-	0.09	0.14	0.10	0.40	0.35
Ir	0.17	0.28	0.19	0.21	0.15	0.10	0.26	0.29	0.11	0.08	0.12	0.20	0.28	0.24	1.53	0.14	0.11	0.20	0.14	0.12
Pt	7.98	7.69	1.06	0.36	0.80	9.44	10.29	2.40	0.60	0.24	0.06	-	2.23	30.33	0.14	0.13	0.10	0.11	0.47	0.46
Au	-	-	-	-	-	-	-	-	-	0.02	-	-	-	-	-	-	-	-	-	-
Hg	-	-	-	-	-	-	-	-	-	-	-	-	-	-	-	-	-	-	-	-
Pb	-	-	-	-	-	-	-	-	-	-	-	-	-	-	44.15	-	-	-	-	-
Bi	9.39	8.97	13.89	17.02	12.70	5.27	4.96	10.58	25.19	7.71	0.84	0.01	27.64	0.01	0.53	6.86	7.91	3.95	23.83	24.51
Total	100.57	100.56	100.92	101.33	100.91	100.39	100.51	100.77	101.54	100.62	100.13	100.31	101.82	100.47	101.93	100.74	100.68	100.49	101.47	101.47

MP = Middle Platreef, UP = Upper Platreef
- = below detection limit

Table 6b contd: Composition (wt. %) of PGE-bismuthotellurides, Bi- a- Te-complexes, Au a- trace minerals in samples from Townlands

							tetradymite-type?		Pilsenite	UN 1133	hessite		temagamite	electrum	stibiopalladinite
Sample	**P15**	**P15**	**P15**	**P13**	**P15**	**P15**	**P15**	**P15**	**P15**	**P15**	**P15**	**P106**	**P106**	**P106**	**P106**
Analysis	**9_BSE2f**	**10_BSE2e**	**12_BSE3e**	**13_BSE3e**	**15_BSE3c**	**16_BSE3c**	**19_BSE5b**	**20_BSE5b**	**14_BSE3e**	**11_BSE3e**	**18_BSE4b**	**11_BSE5a**	**2_BSE2e**	**10_BSE4a**	**13_BSE5a**
Borehole	**TL1-03**	**TL1-03**	**TL1-03**	**TL1-03**	**TL1-03**	**TL1-03**	**TL1-03**	**TL1-03**	**TL1-03**	**TL1-03**	**TL1-03**	**TL1-03**	**TL1-03**	**TL1-03**	**TL1-03**
Depth (m)	**89.55**	**89.55**	**89.55**	**80.75**	**89.55**	**89.55**	**89.55**	**89.55**	**89.55**	**89.55**	**89.55**	**106**	**106**	**106**	**106**
Lithology	**MP**	**MP**	**MP**	**MP**	**MP**	**MP**	**MP**	**MP**	**MP**	**MP**	**MP**	**MP**	**MP**	**MP**	**MP**
	Weight per cent														
S	18.07	18.15	18.29	18.30	18.28	18.30	3.96	4.13	1.75	2.18	1.05	0.27	-	0.11	0.40
Fe	16.26	16.31	16.93	16.90	16.23	16.51	1.51	2.67	4.21	4.50	2.18	2.63	3.36	1.83	11.15
Co	0.08	0.06	0.05	0.08	0.07	0.06	0.02	0.03	0.06	0.13	0.06	0.02	-	0.06	-
Ni	0.41	0.34	0.01	0.02	0.09	0.08	-	-	-	0.01	-	0.01	0.20	-	0.01
Cu	0.02	0.02	0.01	-	-	-	0.14	0.62	1.01	0.02	0.02	0.01	0.12	0.07	0.01
As	-	-	-	-	-	-	-	-	-	-	-	0.01	-	-	2.80
Se	0.13	0.12	0.11	0.09	0.03	0.05	1.78	1.71	1.67	5.41	0.04	0.06	0.01	-	0.02
Ru	-	-	-	-	-	-	-	-	-	-	-	-	-	-	-
Rh	-	-	-	-	-	-	-	-	-	-	-	-	-	-	-
Pd	-	-	-	-	-	-	-	-	-	-	0.56	0.16	36.08	-	60.47
Ag	0.63	0.70	0.74	-	0.57	0.58	0.80	0.71	0.81	0.82	60.41	63.14	0.87	30.61	0.22
Sn	-	-	0.03	0.01	0.01	-	-	-	-	-	-	-	-	-	0.06
Sb	0.13	0.09	0.06	0.11	0.08	0.11	0.29	0.27	0.25	0.19	0.19	0.25	0.39	-	21.91
Te	0.01	-	-	0.01	-	0.01	36.64	36.53	28.36	21.81	37.89	37.37	43.62	0.04	-
Os	0.87	0.81	0.82	0.80	0.80	0.84	0.83	0.95	0.97	1.01	0.04	0.10	0.03	0.02	0.09
Ir	0.29	0.24	0.35	0.35	0.29	0.37	0.45	0.38	0.30	0.35	0.30	0.34	0.06	0.34	0.22
Pt	0.98	0.94	1.00	1.09	1.08	1.05	1.27	1.15	1.20	1.46	0.10	0.11	-	-	0.14
Au	-	0.09	-	-	-	-	-	-	-	-	-	-	-	67.06	-
Hg	-	-	-	-	-	-	-	-	-	-	-	-	18.50	-	-
Pb	-	-	-	-	-	-	-	-	-	-	-	-	-	-	-
Bi	58.95	58.65	58.43	58.59	59.05	59.01	59.33	59.44	69.02	71.52	1.13	0.05	0.44	0.02	0.05
Total	96.83	96.52	96.84	97.04	96.61	96.96	107.02	108.60	109.63	109.42	104.07	104.62	103.68	100.20	97.60
	Atomic concentration														
S	49.04	49.28	49.31	49.30	49.77	49.58	16.40	16.47	7.54	9.24	3.46	0.88	-	0.50	1.24
Fe	25.33	25.42	26.19	26.13	25.37	25.67	3.58	6.11	10.41	10.94	4.12	4.98	7.46	4.94	19.92
Co	0.11	0.08	0.08	0.12	0.11	0.09	0.05	0.06	0.15	0.30	0.12	0.03	0.00	0.14	-
Ni	0.61	0.50	0.01	0.03	0.13	0.11	-	-	0.01	0.02	-	0.01	0.42	0.01	0.02
Cu	0.03	0.03	0.01	0.01	0.00	0.01	0.30	1.25	2.20	0.05	0.03	0.02	0.24	0.17	0.02
As	-	-	-	-	-	-	-	-	-	-	-	-	-	0.01	3.73
Se	0.14	0.14	0.12	0.10	0.04	0.06	2.99	2.77	2.93	9.31	0.06	0.07	0.01	-	0.02
Ru	-	-	-	-	-	-	-	-	-	-	-	-	-	0.01	-
Rh	-	-	-	-	-	-	-	-	-	-	-	-	-	-	-
Pd	-	-	-	-	-	-	-	-	-	-	0.55	0.16	42.04	-	56.71
Ag	0.51	0.56	0.59	0.52	0.46	0.47	0.98	0.84	1.03	1.03	59.14	62.04	1.00	42.90	0.20
Sn	-	-	0.02	0.01	0.01	-	-	-	-	-	-	-	-	-	0.05
Sb	0.09	0.07	0.04	0.08	0.06	0.08	0.32	0.29	0.28	0.21	0.17	0.22	0.40	-	17.95
Te	0.01	-	-	0.01	-	0.01	38.11	36.56	30.68	23.20	31.35	31.04	42.39	0.05	-
Os	0.40	0.37	0.37	0.36	0.37	0.38	0.58	0.64	0.71	0.72	0.02	0.06	0.02	0.02	0.05
Ir	0.13	0.11	0.16	0.16	0.13	0.17	0.31	0.25	0.22	0.25	0.16	0.19	0.04	0.26	0.11
Pt	0.44	0.42	0.44	0.48	0.48	0.47	0.86	0.75	0.85	1.01	0.05	0.06	-	-	0.07
Au	-	0.04	-	-	-	-	-	-	-	-	-	-	0.00	51.46	-
Hg	-	-	-	-	-	-	-	-	-	-	-	-	11.43	-	-
Pb	-	-	-	-	-	-	-	-	-	-	-	-	-	-	-
Bi	24.54	24.44	24.16	24.21	24.66	24.52	37.69	36.32	45.59	46.46	0.57	0.02	0.26	0.02	0.02
Total	101.39	101.49	101.55	101.54	101.63	101.59	102.20	102.29	102.61	102.79	100.21	100.15	105.75	100.64	100.29

- = not detected, MP = Middle Platreef, UP = Upper Platreef
- = below detection limit